Title

Pharmacologic Neuromodulation Targeting Neuroinflammation as a Novel Therapeutic Strategy for Experimental Pulmonary Hypertension

Author

Razee, Asif Al

Publication Date

2023

Peer reviewed|Thesis/dissertation

UNIVERSITY OF CALIFORNIA

Los Angeles

Pharmacologic Neuromodulation Targeting Neuroinflammation as a Novel Therapeutic Strategy for Experimental Pulmonary Hypertension

A dissertation submitted in partial satisfaction of the
requirements for the degree of Doctor of Philosophy
in Molecular, Cellular & Integrative Physiology

by

Asif Al Razee

2023

ABSTRACT OF THE DISSERTATION

Pharmacologic Neuromodulation Targeting Neuroinflammation as a Novel Therapeutic Strategy for Experimental Pulmonary Hypertension

by

Asif Al Razee

Doctor of Philosophy in Molecular, Cellular & Integrative Physiology

University of California, Los Angeles, 2023

Professor Soban Umar, Chair

Pulmonary hypertension (PH) is a rare, progressive and debilitating disease characterized by elevated pressure in the pulmonary circulation coupled with right ventricular hypertrophy and failure. Microglial and astrocytic activation mediated neuroinflammation in the brain and spinal cord has been implicated in the sympathetic nervous system (SNS) hyperactivity in experimental PH, however, the role and precise mechanism of the intricate interplay between neuroinflammation and SNS activation in PH is still unknown.

In **Chapter 2**, we discovered that cardiopulmonary afferent signaling to the thoracic DRG and dorsal horn is mediated via TRPV1 and substance P in PH. Our first-ever transcriptomic analysis on the TSC of 2 clinically relevant rat models (MCT and SuHx) of severe PH and RVF delineated common dysregulated genes and pathways highlighting

neuroinflammation and apoptosis. We observed microgliosis, astrogliosis and increased fractalkine expression in the TSC of both rat models and in human PAH. Elevated plasma norepinephrine in both rat models confirmed increased sympathoexcitation. Finally, intrathecal minocycline decreased TSC microglial count, activation, and expression of proinflammatory cytokines, and reduced sympathoexcitation resulting in rescue of PH-RVF. In **Chapter 3**, we demonstrated that intrathecal RTX administration abolished TRPV1 expression in the TSC and attenuated PH-RVF by decreasing cardiac sympathetic tone in MCT and SuHx rats. We also revealed that mechanistically, NMDAR-NOS1 mediated neuroinflammation and neuronal apoptosis in the TSC in PH is dependent on TRPV1 activation. Lung and RV RNASeq from RTX-treated MCT rats demonstrated reversal of fibrosis, inflammation and apoptosis. In **Chapter 4**, we expanded on our findings by investigating downstream of TRPV1 gene and found increased signature of glutamatergic and NOS1 signaling in the TSC of MCT and SuHx rats and patients with PAH. We demonstrated that NMDAR inhibition decreased TSC NOS1 expression, neuroinflammation, neuronal apoptosis and associated sympathoexcitation and rescued PH-RVF in MCT rats. Finally, pharmacological inhibition of NOS1 attenuated PH-RVF by reducing TSC neuroinflammation, neuronal apoptosis and sympathoexcitation. Moreover, lung and RV RNA-Seq from SMTC-treated MCT rats demonstrated reversal fibrosis, inflammation and apoptosis. Invitro analysis indicated that norepinephrine and SP may play major role in lung and RV reversal of EndMT and fibrosis in SMTC-treated MCT Rats.

Taken together, this dissertation is a compilation of the first work investigating the mechanistic evidence of TSC neuroinflammation and its role in SNS hyperactivity in PH.

The dissertation of Asif Al Razee is approved.

Olujimi A Ajijola

Mansoureh Eghbali

Michela Ottolia

Soban Umar, Committee Chair

University of California, Los Angeles

2023

This dissertation is dedicated to my family whose love and support are unconditional and unwavering.

TABLE OF CONTENTS

LIST OF FIGURES AND TABLES xi

ACKNOWLEDGEMENTS xvii

VITA xix

CHAPTER 1: Introduction 1

Abstract 2

Overview 2

Cardiovascular autonomic neural circuits 6

CNS control of sympathetic activity 6

Sensory Input 6

Sympathetic output 7

Cardiovascular reflexes 9

Hypothalamus 10

Rostral ventrolateral medulla 11

Nucleus of the Solitary Tract 11

Insular Cortex 11

Anterior cingulate cortex 12

Central nucleus of the amygdala 12

SPGN and their role in controlling cardiovascular function 12

Involvement of spinal neurons in the maintenance of sympathoexcitation 13

Inflammation 14

Inflammation in PH 14
Neuroinflammation: The CNS immune response 15
Microglia: Resident immune cells of the CNS 16
Astrocytes: The non-immune glial cells 20
Evidence of neuroinflammation in experimental PH 25
Mechanisms of CNS neuroinflammation and sympathoexcitation 26
Role of RAS in neuroinflammation and sympathoexcitation 26
Role of RAS in neuroinflammation 26
Role of RAS in sympathoexcitation 27
Role of RAS in neuroinflammation mediated sympathoexcitation in PH 29
Role of TRPV1 in neuroinflammation and sympathoexcitation 29
Role of TRPV1 in neurological inflammation in the brain 29
Role of TRPV1 mediated SP and CGRP release in neuroinflammation 31
Role of TRPV1 in sensory afferent transmission in the spinal dorsal horn 31
Role of TRPV1 in microglial activation 32
Role of TRPV1 in astrocytic activation 33
Role of TRPV1 in sympathoexcitation 33
Role of TRPV1 in PH 35
Role of Glutamate-induced excitotoxicity in neuroinflammation and

sympathoexcitation 36

Role of Glutamate-induced excitotoxicity in neuroinflammation 36

Role of Glutamate-induced excitotoxicity in sympathoexcitation 40

Role of Cx3Cl1/Cx3Cr1 in neuroinflammation and sympathoexcitation ... 42

Role of Cx3Cl1/Cx3Cr1 in neuroinflammation..... 42

Role of Cx3Cl1/Cx3Cr1 in sympathoexcitation 43

Role of Cx3Cl1/Cx3Cr1 in PH 44

Role of microglia mediated neuroinflammation in sympathoexcitation 45

Conclusion..... 47

References 48

CHAPTER 2: Thoracic Spinal Cord Neuroinflammation as a Novel Therapeutic Target in Pulmonary Hypertension 94

Abstract..... 95

Nonstandard Abbreviations and Acronyms..... 96

Graphical Abstract 97

Introduction 98

Materials and Methods..... 100

Results..... 104

Discussion..... 118

Supplementary Materials and Methods..... 125

Supplementary Results..... 130

Supplementary Figures..... 132

Supplementary Tables 142

References 144

CHAPTER 3: Chemo-ablation of Cardiopulmonary Afferents by Intrathecal RTX Prevents PH and RV Failure by Decreasing Thoracic Spinal Cord NOS1 and Neuroinflammation 152

Abstract 153

Introduction 155

Materials and Methods 157

Results 161

Discussion 175

Supplementary Figures 181

Supplementary Tables 183

References 186

CHAPTER 4: Pharmacologic Neuromodulation Targeting NMDAR-NOS1 Axis Mediated Neuroinflammation and Apoptosis in the Thoracic Spinal Cord as a Novel Therapeutic Strategy for Pulmonary Hypertension and Right Ventricular Failure 199

Abstract 200

Introduction 202

Materials and Methods 203

Results 207

Discussion 222

Supplementary Figures 228

Supplementary Tables 233

References 236

CHAPTER 5: Conclusions and Future Directions 246

Conclusions 247

Future directions 256

Final remarks from the author 260

References 261

LIST OF FIGURES AND TABLES

CHAPTER 1: Introduction

Figure 1.1: Overview of normal pulmonary circulation compared to pulmonary hypertension 4

Figure 1.2: Afferent and efferent control of the cardiac function 8

Figure 1.3: Schematic representation of the interactions between neurons, microglia and astrocytes mediated by CX3CL1/CX3CR1 19

Figure 1.4: Schematic representation of TRPV1-mdiated NOS1 activation and regulation of neuroinflammation in the thoracic dorsal horn..... 39

CHAPTER 2: Thoracic Spinal Cord Neuroinflammation as a Novel Therapeutic Target in Pulmonary Hypertension

Figure 2.1: Increased cardiopulmonary afferent signaling in the thoracic spinal dorsal horn of MCT and SuHx rats and PAH patients..... 105

Figure 2.2: RNA-Seq based analysis of DEG's and pathway enrichment from thoracic spinal cords of MCT and SuHx rats..... 107

Figure 2.3: Validation of RNA-Seq based DEGs in thoracic and lumbar spinal cord of MCT and SuHx rats and in TSC of PAH patients…….…… 108

Figure 2.4: Increased microglial activation and astrogliosis in the TSC of MCT, SuHx rats and human PAH. Increased apoptosis in the TSC of MCT and SuHx rats..... 112

Figure 2.5: Minocycline attenuates MCT induced PH and RVF by attenuating TSC neuroinflammation and associated sympathoexcitation..... 116

Figure 2.6: Hypothetical scheme showing transcriptomic remodeling of thoracic spinal cord characterized by neuroinflammation and apoptosis leading to sympathoexcitation in PH 117

Supplemental Figure S1: Experimental models of severe PH and RV failure in rats..... 132

Supplemental Figure S2: Volcano plot of log fold change vs. mean expression for all genes from TSC for comparing MCT vs. Control groups 133

Supplemental Figure S3: Volcano plot of log fold change vs. mean expression for all genes from TSC for comparing SuHx vs. Control groups 134

Supplemental Figure S4: Bar plot showing normalized enrichment scores (NES) for Hallmark pathways derived from Gene Set Enrichment Analysis (GSEA)...135

Supplemental Figure S5: Bar plot showing normalized enrichment scores (NES) for Hallmark pathways derived from Gene Set Enrichment Analysis (GSEA)...136

Supplemental Figure S6: Time dependent increase of PH, TSC neuroinflammation, apoptosis and associated sympathoexcitation in MCT-induced PH rats..... 137

Supplemental Figure S7: Increased NPY in the ventral horn of TSC and circulating catecholamines as markers of sympathoexcitation in MCT- and SuHx-induced PH 139

Supplemental Figure S8: RNA-Seq based pathway enrichment analysis from TSC, right ventricles and lungs of MCT and SuHx rats..... 140

Supplemental Figure S9: Increased neuronal apoptosis in the TSC of MCT and SuHx rats 141

Supplemental Figure S10: Hypoxia or Sugen alone do not induce TSC NOS1 and Neuroinflammation..... 142

Supplemental Table S1: Leading edge upregulated genes from MCT vs. Control..... 142

Supplemental Table S2: Leading edge downregulated genes from MCT vs. Control..... 142

Supplemental Table S3: Leading edge upregulated genes from SuHx vs. Control..... 143

Supplemental Table S4: Leading edge downregulated genes from SuHx vs. Control..... 143

CHAPTER 3: Chemo-ablation of Cardiopulmonary Afferents by Intrathecal RTX Prevents PH and RV Failure by Decreasing Thoracic Spinal Cord NOS1 and Neuroinflammation

Figure 3.1: Lumbar intrathecal RTX administration prevents PH and RVF in MCT rats..... 162

Figure 3.2: Lumbar intrathecal RTX administration prevents PH and RVF in SuHx rats..... 163

Figure 3.3: Thoracic intrathecal RTX administration prevents PH and RVF in MCT rats..... 165

Figure 3.4: TRPV1 ablation attenuates TSC NMDAR and NOS1 expression..167

Figure 3.5: TRPV1 ablation attenuates TSC astrocytic and microglial activation……...168

Figure 3.6: TRPV1 ablation attenuates neuronal apoptosis in the TSC……....169

Figure 3.7: TRPV1 ablation results in reversal of RV transcriptomic signature in MCT rats ……...171

Figure 3.8: TRPV1 ablation results in reversal of lung transcriptomic signature in MCT rats……..……..172

Supplemental Figure S1: Intrathecal RTX administration prevents PH and RVF in MCT and SuHx rats 181

Supplemental Figure S2: Timecourse of TRPV1 expression in the thoracic dorsal horn of MCT rats 182

Supplemental Figure S3: Lumbar intrathecal RTX administration reduces TRPV1 expression in the thoracic DRG in PBS and MCT rats……...182

Supplemental Table S1: Leading edge down-regulated RV genes from RTX-treated MCT vs. PBS-treated MCT rats 183

Supplemental Table S2: Leading edge down-regulated lung genes from RTX-treated MCT vs. PBS-treated MCT rats……184

CHAPTER 4: Pharmacologic Neuromodulation Targeting NMDAR-NOS1 Axis Mediated Neuroinflammation and Apoptosis in the Thoracic Spinal Cord as a Novel Therapeutic Strategy for Pulmonary Hypertension and Right Ventricular Failure

Figure 4.1: Increased Signature of Glutamatergic and NOS1 Signaling in the TSC of MCT and SuHx Rats and PAH patients 208

Figure 4.2: AP5 attenuates MCT induced PH and RVF by reducing TSC NOS1, neuroinflammation and associated sympathoexcitation..... 210

Figure 4.3: NOS1 inhibition attenuates MCT induced PH and RVF..... 211

Figure 4.4: NOS1 inhibition attenuates TSC neuroinflammation and decreases sympathoexcitation in MCT induced PH rats 213

Figure 4.5: NOS1 inhibition attenuates neuronal apoptosis in the TSC of MCT induced PH rats 214

Figure 4.6: NOS1 inhibition results in reversal of RV transcriptomic signature in MCT-induced PH rats 217

Figure 4.7: NOS1 inhibition results in reversal of lung transcriptomic signature in MCT-induced PH rats 220

Figure 4.8: Hypothetical scheme..... 221

Supplemental Figure S1: Increased NOS1 Expression in the TSC of MCT and SuHx Rats and PAH patients..... 228

Supplemental Figure S2: AP-5 reduced Cx3Cl1 expression in the TSC of MCT Rats 231

Supplemental Figure S3: Substance P and Norepinephrine induce EndMT in HCAECs and HPAECs and Myofibroblast Transition in HCF *in vitro*……..232

Supplemental Table S1: Leading edge down-regulated RV genes from SMTC-treated MCT vs. PBS-treated MCT rats 233

Supplemental Table S2: Leading edge down-regulated lung genes from SMTC-treated MCT vs. PBS-treated MCT rats 235

CHAPTER 5: Conclusion and Future Directions

Figure 5.1: Schematic of proposed mechanism of TSC neuroinflammation

through TRPV1 activation and downstream NOS1 upregulation in PH and potential therapeutic targets..... 255

ACKNOWLEDGEMENTS

First, I would like to acknowledge my mentor, Dr. Soban Umar for his kind, passionate and unwavering support and mentorship. Words can't express how grateful I am to you for giving me the opportunity to be a Ph.D. student in your lab. Thank you for always teaching and guiding me, listening to me, trusting me and valuing my opinions. You have been an unparalleled coach throughout this process.

I would like to thank all the talented past and present members of the Umar Lab for the support, expertise, patience, and helping hand. You've made the Umar Lab feel like my second home. In particular, I would like to thank Dr. Somanshu Banerjee for his invaluable time, guidance, and knowledge that he shared with me.

Thank you to my fantastic committee members Drs. Olujimi Ajijola, Mansoureh Eghbali and Michela Ottolia for your guidance and encouragement. You've been incredible role models for me, and I've learned so much from each of you. Thank you for your invaluable time and suggestions during oral qualifying exam and midstream evaluation.

Thank you to Dr. Mark Frye and Yesenia Rayos for their continuous and tireless work to ensure the Molecular, Cellular & Integrative Physiology program at UCLA runs smoothly and is supportive to all the students. I would like to acknowledge the entire department of Anesthesiology, the current chair, Dr. Maxime Cannesson, and vice chair, Dr. Thomas Vondriska for providing the most supportive environment to conduct research.

I would also like to extend my gratitude to our close collaborators Drs. Jason Hong, Catherine Cahill, Shino Magaki and Greg Fishbein. Dr. Jason Hong has been extremely helpful throughout my Ph.D. journey with RNASeq analysis. Thank you for providing me

with all the transcriptomic analysis and guiding me through the data. Thank you to Dr. Catherine Cahill for performing the elegant rat surgeries for the RTX experiment. Thank you to Drs. Shino Magaki and Greg Fishbein for providing us with the most precious human autopsy samples.

Thank you to the MCIP Cohort Class of 2019; You guys are the best group of caring scientists and friends I could have ever asked for. I'm very proud of the journey each of you have taken and the incredible science you've produced.

I would also like to extend my gratitude to the friends and family who have supported, loved, and cheered me throughout this arduous journey. I'm so grateful for our moments of laughter, fun, and all the encouragements.

I would also like to acknowledge and thank my funding sources, who provided fiscal support and career development throughout my training including: Ruth L. Kirschstein National Research Service Award (T32HL069766).

Finally, I would like to thank my parents for their boundless love, prayers and support. Dad, thank you for always encouraging me to pursue my dream. You've led by example, taught me that through dedication and hard work any goal is achievable. Mom, "Thank you" is never enough for everything that you have done for me being the most all-encompassing, never-ending source of truly unconditional love and support. To my wife, the love of my life, I couldn't have done it without your unconditional love, care, support and dedication. You allowed me to complete this Ph.D. journey, while taking care of both of our kids; I'm so very grateful to your benevolence. And to my dearest son Farhan and daughter Tahera, the fuel of my engine: You guys get me going everyday. I cannot imagine going through this journey without your motivation—This dissertation is dedicated to you!

ASIF RAZEE

EDUCATION

University of California, Los Angeles Expected: Dec. 2023
Ph.D. Candidate: Molecular, Cellular & Integrative Physiology

University of California, Los Angeles December 2019
Master of Science: Physiological Science

University of California, Los Angeles December 2008
Bachelor of Science: Ecology and Evolutionary Biology

TEACHING EXPERIENCE

Teaching Associate (TA) University of California Los Angeles 2009-2021
Department of Life Science 39 Quarters
Department of Ecology and Evolutionary Biology 26 Quarters
Department of Psychology 1 Quarter
Department of Physiological Science 37 Quarters

RESEARCH EXPERIENCE

Ph.D. Research Fall'19- Fall'23
Primary Investigator: Soban Umar, MD, PhD. Anesthesiology, UCLA
Thesis: Pharmacologic Neuromodulation Targeting Neuroinflammation as a Novel Therapeutic Strategy for Experimental Pulmonary Hypertension.

Masters Research Fall'17- Sp'19
Primary Investigator: David Glanzman, PhD. Integrative Biology & Physiology, UCLA
Thesis: Induction of short-term sensitization with an aversive sensory stimulation in zebrafish larvae.

HONORS AND AWARDS:

- Best of abstract scholarship award, 2021,22,23
  American Thoracic Society Conference
- NIH/HL69766 T32 Predoctoral Training Grant (**2 Years**) 2021-23
- Best of Basic Science Abstract, 2020,21
  American Society of Anesthesiology Conference
- Best of Basic Science Abstract: 2021
  3CPR Council of American Heart Association
- Travel Grant Award 2021
  American Heart Association Conference
- Certificate of Distinction in Teaching 2009-13
  Life Sciences Division, UCLA (**5 Times**)

LEADERSHIP

President 2012-2022
Norwalk Manor Homeowner's Association

PUBLICATIONS

1. **Razee A**, Banerjee S, Hong J, Magaki S, Fishbein G, Ajijola OA, Umar S. Thoracic Spinal Cord Neuroinflammation as a Novel Therapeutic Target in Pulmonary Hypertension. Hypertension. 2023 Jun;80(6):1297-1310. doi: 10.1161/HYPERTENSIONAHA.122.20782. Epub 2023 Apr 24. PMID: 37092338.

2. **Razee A**, Umar S. Pulmonary Artery Denervation for Pulmonary Hypertension: Recent Updates and Future Perspectives. Trends in Cardiovascular Medicine. 2020 May 17;S1050-1738(20)30065-7.
3. Park JF, Clark VR, Banerjee S, Hong J, **Razee A**, Williams T, Fishbein G, Saddic L, Umar S. Transcriptomic Analysis of Right Ventricular Remodeling in Two Rat Models of Pulmonary Hypertension: Identification and Validation of Epithelial-to-Mesenchymal Transition in Human Right Ventricular Failure. Circ Heart Fail. 2021 Feb;14(2):e007058. doi: 10.1161/CIRCHEARTFAILURE.120.007058. Epub 2021 Feb 5. PMID: 33541093; PMCID: PMC7887079.
4. Roberts AC, Alzagatiti JB, Ly DT, Chornak JM, Ma Y, **Razee A**, Zavradyan G, Khan U, et al. Induction of Short-Term Sensitization by an Aversive Chemical Stimulus in Zebrafish Larvae. eNeuro. 2020 Dec 4;7(6):ENEURO.0336-19.2020. doi: 10.1523/ENEURO.0336-19.2020. PMID: 33004417; PMCID: PMC7729299.

SELECTED ABSTRACTS

- **Razee, A.**, Banerjee, S., Hong, J., Saggar, R., Magaki, S., Gregory, F., Umar, S.(2023). Cell Type Specific Targeting of Microglial Activation in the Thoracic Spinal Cord as a Novel Therapeutic Strategy for Pulmonary Hypertension and Right Ventricular Failure. American Thoracic Society, Washington D.C.
- Banerjee, S., Clark, V., Martineau, S., Hong, J., **Razee, A.**, Bonnet, S., Umar, S.(2023). Rescue of Pulmonary Hypertension-Induced Right Ventricular Failure by Silencing Snai1 Induces Alterations in Methylation Status of Critical Genes Regulating Endothelial-to-Mesenchymal-Transition and Fibrosis. AHA, Philadelphia.
- **Razee, A.**, Banerjee, S., Hong, J., Saggar, R., Magaki, S., Gregory, F., Umar, S.(2022, May 13-18). Pharmacologic Neuromodulation Targeting Neuroinflammation as a Novel Right Ventricular Specific Therapeutic Strategy for Pulmonary Hypertension-induced Right Ventricular Failure. [Conference Session]. American Thoracic Society Annual Conference, San Francisco, CA.
- **Razee, A.**, Banerjee, S., Hong, J., Haggar, C., Umar, S.(2021, May 14-18). Intrathecal Neuronal Nitric Oxide Synthase Inhibition Attenuates Pulmonary Hypertension and Rescues Right Ventricular Failure in Rats. [Conference Session]. American Thoracic Society Annual Conference, Virtual Meeting.
- **Razee, A.**, Banerjee, S., Hong, J., Umar, S.(2021, Nov 13-15). Targeted Intrathecal NOS1 Inhibition Rescues Pulmonary Hypertension and Right Ventricular Failure in Rats by Reducing Neuroinflammation, Apoptosis and Sympathoexcitation. [Conference Session]. American Heart Association Annual Conference, Virtual Meeting.
- **Razee, A.**, Hong, J., Said, E., Umar, S.(2020, October 2-5). Transcriptomic Analysis of Thoracic Spinal Cords in Experimental Pulmonary Hypertension Reveals Novel Therapeutic Targets [Conference Session]. Anesthesiology Annual Meetings, Virtual Meeting. https://epostersonline.com/asa2020/
- **Razee, A.**, Hong, J., Clark, V., Park, J., Said, E., Zargari, M., Umar, S.(2020, May 14-18). Transcriptomic Analysis of Thoracic Spinal Cords in Experimental Pulmonary Hypertension Reveals Novel Therapeutic Targets [Conference Session]. IARS-AUA-SOCCA Annual Meetings, San Francisco, CA. USA. https://meetings.iars.org/ (Conference cancelled).

CHAPTER 1: Introduction

Abstract

Pulmonary hypertension (PH) is a progressive and debilitating disease characterized by elevated pressure in the lung vasculature, resulting in right ventricular failure (RVF) and premature death. The pathogenesis of PH is complex and multifactorial, involving a dysregulated autonomic nervous system and neuroinflammation in the brain and spinal cord. Inflammatory mechanisms have been linked to the development and progression of PH; however, these are usually restricted to systemic and/or local lung tissue. Neuroinflammation, on the other hand, involves activation of the microglia and astrocytes, the innate immune cells that are found specifically in the brain and spinal cord. The activation of these resident glial cells results in the release of several proinflammatory cytokines, chemokines, reactive oxygen species and reactive nitrogen species that trigger neuroinflammation, and has been implicated in the pathogenesis of several disease conditions such as Alzheimer's, Parkinson's, hypertension, atherosclerosis, pain and metabolic disorders. Microglial activation mediated neuroinflammation in the brain has been implicated in sympathetic nervous system (SNS) hyperactivity in experimental PH. We recently reported astrocytic activation in the thoracic spinal cord (TSC) in PH rats. However, the role and precise mechanism of the intricate interplay between TSC neuroinflammation and SNS activation in PH is still unknown. In this section we focus on cardiovascular autonomic neural circuits in the CNS that regulate sympathetic activity and introduce the concept of neuroinflammation regulating SNS activity in the context of PH.

1. Overview

Pulmonary hypertension (PH) is a progressive and debilitating disease characterized by elevated pulmonary arterial pressure (>20mmHg at rest) due to excessive pulmonary vascular remodeling, vascular wall stiffening, vasoconstriction and loss of distal pulmonary

arteries[1](Figure 1). Vascular remodeling in PH is characterized by endothelial dysfunction, smooth muscle cell proliferation, arteriolar muscularization, fibrosis, extracellular matrix deposition, thrombosis and inflammatory cell recruitment[1]. These factors result in persistent increase in pulmonary vascular resistance (PVR), pressure overload, right ventricular hypertrophy (RVH) and right ventricular failure (RVF) leading to premature death[1](Figure 1). Although endothelial dysfunction and excessive pulmonary artery smooth muscle proliferation resulting from upregulation of endothelin pathway and downregulation of nitric oxide and prostacyclin pathways have been identified as the main causes of PH, the pathophysiology is still incompletely understood. PH affects approximately 1% of the global population, up to 10% of individuals >65 years, and at least 50% of patients with heart failure[2]. The median survival is only 46 months, whereas the prognosis is even worse in the elderly (37 months >65 years) and very elderly (28 months >75 years) patients[3]. Based on similar histopathology, clinical presentation, hemodynamic characteristics, and therapeutic management, the World Health Organization described and classified the known causes of PH by group: (1) Pulmonary arterial hypertension (PAH); including idiopathic (IPAH), heritable, drug/toxin induced or associated with other systemic diseases, such as HIV, lupus and schistosomiasis; (2) PH due to left heart disease; (3) PH due to chronic lung disease and/or hypoxemia; (4) PH due to thromboembolic disease; (5) PH due to unclear multifactorial mechanisms[4].

PAH features precapillary PH, defined as mean pulmonary arterial pressure (mPAP) of 20 mm Hg or greater, pulmonary artery wedge pressure (PAWP) of 15 mm Hg or less and PVR of 3 Wood units (WU) or greater[5]. At present, 12 drugs have been approved by the US Food and Drug Administration to treat PAH, all of which target 1 of 3 pathways primarily involved in vasoconstriction. Although some may have beneficial off-target effects

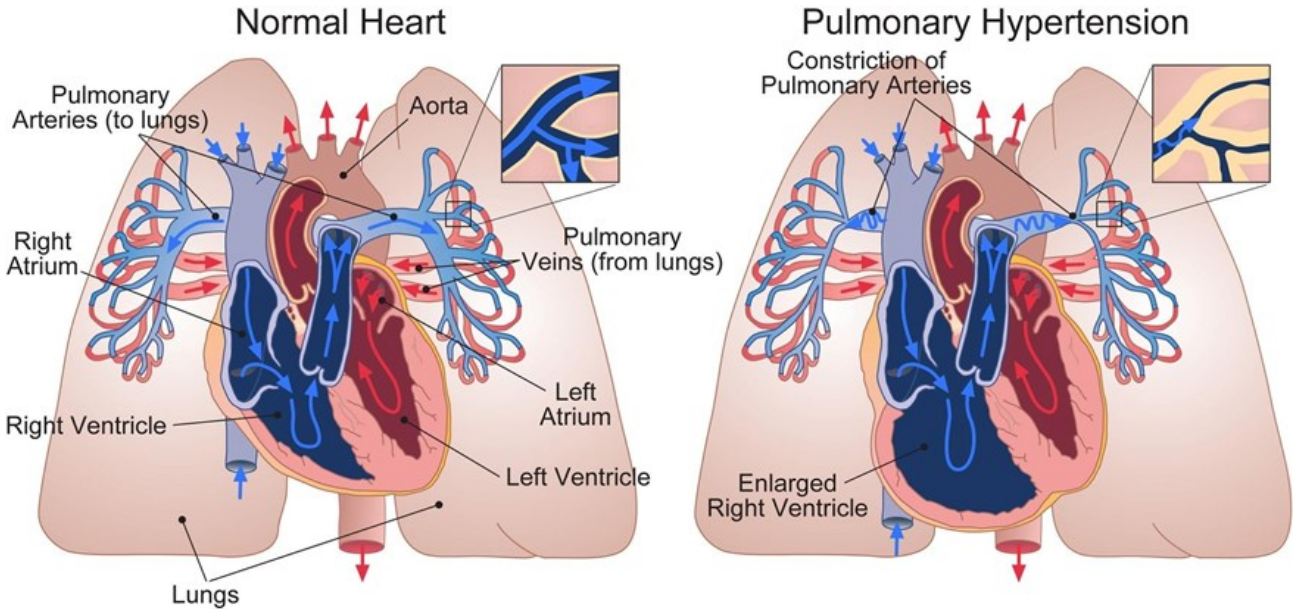

Figure 1. Overview of normal pulmonary circulation compared to pulmonary hypertension. Pulmonary hypertension is characterized by aberrant vasoconstriction of the pulmonary arterioles and increased pressure, hypertrophy, and failure of the right ventricle (RV). *Adapted from Columbus Ohio Adult Congenital Heart Disease Program at Nationwide Children's Hospital Heart Center, Columbus, Ohio.*

on the right ventricle (RV), none of the currently approved PAH therapies directly target RVF, which is the primary cause of death among patients with PAH[6,7]. This deficit is particularly unfortunate because RV failure often develops independently of pulmonary hemodynamics in experimental PH and patients with PAH, demonstrating the necessity of developing RV-specific therapies[8]. Numerous studies have indicated that continuous sympathoexcitation is one of the main contributors of pathological cardiac remodeling including hypertrophy, ventricular dysfunction and arrhythmia in several cardiovascular diseases, hence, strategies to reduce sympathetic vasomotor overactivity in cardiovascular diseases can be beneficial[9-13]. Growing body of evidence demonstrates the contribution of autonomic imbalance in the pathophysiology of PAH, strengthening the

hypothesis for the role of SNS activation in PAH progession[11,14-17]. The elevated PVR and RV afterload activate SNS and renin-angiotensin-aldosterone-system (RAAS) to compensate for low cardiac output in PAH, though, chronic SNS hyperactivity leads to arrhythmias, RVF and sudden death[11,16]. Alternatively, several reports have demonstrated that sympathoinhibition via pulmonary artery denervation[18], renal denervation[19], sympathetic ganglion blockade[20], vagal nerve stimulation[21] and beta-blocker therapy[22] might be potential target to improve PH outcome. However, the cellular and molecular mechanisms involved in sympathetic activation in PAH are still unknown, although a complex interplay of mechanical, neurohumoral, and inflammatory stresses was suggested[21].

The pathogenesis of PAH is very complex and multifactorial, including inflammation and dysregulation of the autonomic nervous response. The nervous and immune systems are intricately connected and their reciprocal communication may contribute to the etiology of SNS activation. Recently, neuroinflammation has been suggested to be involved in sympathetic activation in experimental PH[23,24]. According to Sharma et al[23], inflammation in the paraventricular nucleus, which contains nerves projecting directly to the RV, may lead to RV hypertrophy and failure. Therefore, it may be appealing to directly target neuroinflammation response in the brain to protect against PH. However, in clinical setting, pharmacological treatments to the specific brain regions can be challenging due to physical and biochemical obstacles created by the blood-brain barrier. Targeting spinal cord neuroinflammation for pharmacological interventions may be a better option, since intrathecal drug administration is already widely used in clinical practice.

Our focus in this chapter is to discuss the new concept of integration between neuroinflammation and sympathoexcitation in the development/progression of PH. We aim

to assess cardiovascular autonomic neural circuits in the CNS that regulate sympathetic activity, recent progress in neuroinflammation in PH, and introduce the hypothesis of a neuroinflammatory mediated sympathoexcitation role in PH and RVF. The economic, medical, and social impact of PH in terms of illness and mortality is substantial. Potential new and less invasive therapies that target autonomic imbalance and neuroinflammation should significantly improve therapeutic outcomes for patients with PH.

2. Cardiovascular autonomic neural circuits

In this section, we will review the cardiovascular neural circuitry within the brain and spinal cord that control beat-to-beat cardiac function via sympathetic outflow.

2.1. CNS control of sympathetic activity

Complex networks within the brain and spinal circuits regulate sympathetic vasomotor activity. Previous studies have demonstrated that alterations in the hypothalamic and medullary nuclei involved in sympathoexcitation regulation contributes to hypertension and heart failure[9,25,26]. The cardiac sympathetic neuraxis is distributed throughout the brain and spinal cord, including the anterior insula[27,28], anterior cingulate cortex (ACC)[29], subfornical organ (SFO)[30], amygdala[31], hypothalamus[32-34], periaqueductal gray matter[35], parabrachial nucleus[36], several regions of the medulla[37] and intermediolateral (IML) cell column[38-42] and controls beat-to-beat cardiac function[43]. These areas are critically involved in cardiac stress responses, and homeostatic reflexes and exert their influence on heart rate, cardiac contractility and cardiac output via the sympathetic and parasympathetic nervous systems[43].

2.2. Sensory Input

Cardiopulmonary afferent inputs are conveyed to the dorsal horn and intermediate gray

matter of the thoracic spinal cord by unmyelinated spinal neurons with their cell bodies in the dorsal root ganglia (DRG) following the trajectory spinal nerves[34]. Spinal afferents relay on second-order spinothalamic neurons of lamina I, which project to the parabrachial nucleus, periaqueductal gray (PAG), amygdala, various medullary and hypothalamic targets and thalamus[43,44]. Cardiac vagal afferents containing myelinated and unmyelinated neurons with cell bodies in the nodose ganglion, together with carotid baroreceptor afferents, provide inputs to the nucleus of the solitary tract (NTS). This nucleus initiates a variety of cardiovascular reflexes and also conveys cardiovascular receptor information to the thalamus and parabrachial nucleus. The parabrachial nucleus integrates spinal and brainstem afferents and conveys this information to the thalamus, amygdala, and hypothalamus. The thalamic relay nuclei receiving cardiac stress information from cardiovascular receptors project to the posterior insular cortex (IC) and dorsal ACC. The catecholaminergic neurons of the A1/C1 group of the ventrolateral medulla send a parallel viscerosensory pathway to the hypothalamus, PAG, and locus ceruleus (LC)[43-46](Figure 2).

2.3. Sympathetic output

The reciprocally interconnected forebrain areas including IC, ACC, central nucleus of the amygdala (CeA), and several hypothalamic nuclei form a network that initiates integrated autonomic response to stressful cardiac stimuli. These forebrain regions project to medullary and spinal nuclei directly or via a relay in the PAG to control cardiac function. The entire sympathetic outflow is regulated by paraventricular hypothalamic nucleus (PVN), A5 noradrenergic cell group, caudal raphe region, rostral ventrolateral medulla (RVLM), and ventromedial medulla. These cell groups send excitatory glutamatergic inputs to sympathetic preganglionic neurons (SPGN) of the IML cell columns in the thoracic spinal cord. The sympathetic innervation of the heart originates from these preganglionic

IML neurons that synapse with postganglionic noradrenergic neurons of the superior, middle cervical and cervicothoracic (stellate) ganglia. These ganglia innervate the heart via the superior, middle, and inferior cardiac nerves[43,44,47](Figure 2).

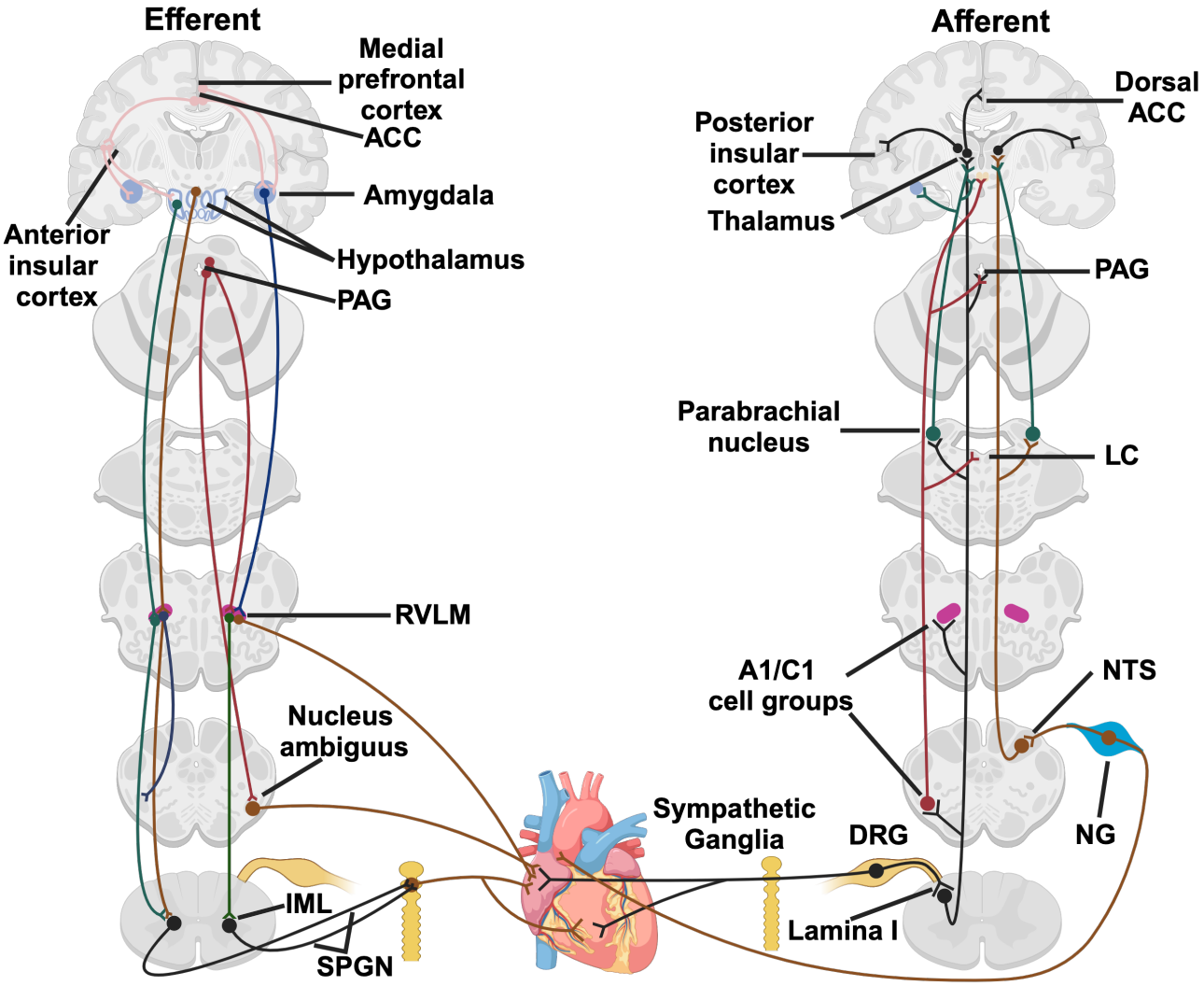

Figure 2: Afferent and efferent control of the cardiac function. Afferent: Sensory inputs from cardiac receptors are conveyed by spinal afferents that have their cell bodies in the DRG, or by vagal afferents with cell bodies in the nodose ganglion (NG). Spinal afferents relay on second-order neurons of lamina I, which project to the thalamus, parabrachial nucleus, PAG, and A1/C1 group of the ventrolateral medulla. The A1/C1 cell group send a parallel viscerosensory pathway to the hypothalamus, PAG, and locus

ceruleus (LC). Cardiac vagal afferents provide inputs to the NTS, which initiates a variety of cardiovascular reflexes and also conveys cardiovascular afferent input to the thalamus and parabrachial nucleus. The parabrachial nucleus integrates afferent input from spinal and brainstem afferents and conveys this information to the thalamus, amygdala, and hypothalamus. The thalamic relay nuclei sends afferent input to the posterior insular cortex and dorsal ACC. **Efferent:** Several forebrain areas, including the insular cortex, ACC, central nucleus of the amygdala, and several hypothalamic nuclei send efferent projections to medullary and spinal IML cell columns to control cardiac function. These efferent projections are either direct or via a relay in the PAG. Sympathetic activation is triggered by neurons of the RVLM, which send excitatory projections to the sympathetic preganglionic neurons (SPGN) of the IML cell columns in the spinal cord. These neurons activate nonadrenergic neurons of the sympathetic ganglia, for example, stellate, which send axons that contribute to the cardiac plexuses innervating the heart. On the other hand, parasympathetic output is mediated by vagal neurons in the nucleus ambiguus and dorsal motor nucleus of the vagus. These neurons send long preganglionic axons that synapse on cholinergic and noncholinergic neurons located in the cardiac ganglia. *Modified from Neural control of the heart: Recent concepts and clinical correlations. Neurology.*

2.4. Cardiovascular reflexes

Cardiopulmonary sensory afferents trigger a variety of cardiovascular reflexes[45] via spinal neurons and vagal afferents. Cardiac sympathetic afferent reflex (CSAR) involves chemical (endogenous humoral factors, such as bradykinin, adenosine and hydrogen peroxide produced in the ventricular wall) or mechanical (distension of the ventricles) stimulation of sympathetic afferent endings innervating the heart, which increases

sympathetic outflow, blood pressure and heart rate[48]. CSAR modulation and integration involves NTS, PVN, RVLM, sympathetic afferent fibers with cell bodies in the thoracic DRG, specially T2-T6 and sympathetic pre-ganglionic neurons in IML[49]. Right atrial and ventricular hypertrophy due to increased blood volume activates myelinated vagal afferents, which trigger sympathetic reflex activation resulting in HR increase. Unmyelinated spinal and vagal afferents innervating the ventricles are activated by mechanical and chemical stimuli, including products of ischemia or inflammations such as adenosine triphosphate (ATP), serotonin, and prostanoids. Cardiopulmonary spinal afferents send sensory information to higher brain centers via spinothalamic tract from lamina I of dorsal horn neurons. Cardiac afferents also trigger excitatory cardiac reflexes via local interneurons projecting to the IML. Pulmonary arterial baroreceptors are also shown to elicit reflex vasoconstriction, respiratory stimulation and control cardiovascular function during hypoxic conditions[45].

2.5. Hypothalamus

The hypothalamus controls sympathetic output to the cardiovascular system via inputs from the PVN, dorsomedial nucleus of hypothalamus (DMH), and lateral hypothalamic area that project to the PAG, parabrachial nucleus, RVLM, nucleus ambiguous (NAmb), dorsal motor nucleus of the vagus, NTS, and IML cell column of the spinal cord[50-53]. During cardiac stress sympathoexcitatory responses are mediated by projections from the PVN, DMH, or lateral hypothalamus to the RVLM or IML[50-53]. Saper et al. discovered direct synaptic projection of neurons from PVN with sympathetic preganglionic nuclei in the spinal cord, NTS and RVLM[33,54](Figure 2). These PVN presympathetic neurons act as command neurons for sympathetic outflow to the cardiovascular system[32,34,55,56]. Strack et al demonstrated that besides PVN, A5 noradrenergic cell group, caudal raphe region,

RVLM and rostral ventromedial medulla (RVMM) also provide direct innervation of the entire sympathetic outflow to spinal interneurons in laminae VII and X[57]. PVN presympathetic neurons receive sensory information from cardiac receptors relayed by the NTS, A1 and A2 noradrenergic cell groups, median preoptic nucleus, SFO, arcuate nucleus and organum vasculosum lamina terminalis[58-64].

2.6. Rostral ventrolateral medulla

The RVLM contains premotor glutamatergic sympathoexcitatory neurons that tonically activate the cardiac SPGN in the IML (Figure 2). RVLM serves as a common effector of descending and reflex sympathoexcitatory pathways controlling blood pressure and cardiac function. RVLM neurons are activated directly by cardiac stress, pain, hypoxia, hypovolemia, and hypoglycemia and via descending inputs from the forebrain[37].

2.7. Nucleus of the Solitary Tract

The NTS is the first central relay station of cardiopulmonary afferent information for all medullary reflexes, including the baroreflex and cardiac reflexes controlling BP and HR[65](Figure 2). The caudal NTS receives afferent input from baroreceptors, cardiac receptors, chemoreceptors, and pulmonary receptors, primarily via vagal and glossopharyngeal nerves[66].

2.8. Insular Cortex

According to Craig et al, the posterior, middle, and anterior IC represent 3 consecutive steps of integration and processing[28]. The posterior IC receives thalamic inputs relaying converging pain, temperature, and visceral sensory information and provides primary interoceptive representation; the middle IC integrates this information with inputs from high-order polysensory cortex, ACC, and amygdala and then conveys this integrated input

to the anterior IC, which represents the neural substrate of awareness of the internal bodily state and is a key component of emotional experience[28].

2.9. Anterior cingulate cortex

The ACC integrates autonomic responses with behavioral arousal via its extensive connections with the IC, prefrontal cortex, amygdala, hypothalamus, and brainstem autonomic nuclei. Dorsal ACC activation during these tasks is associated with an increase in sympathetic drive, resulting in HR increase[29].

2.10. Central nucleus of the amygdala

The medial subdivision of the CeA projects to the hypothalamus and brainstem and triggers the autonomic, endocrine, and motor manifestations of the fear responses; sympathoexcitatory responses involve excitatory connections to the RVLM, and inhibition of barosensitive neurons of the NTS[31].

2.11. SPGN and their role in controlling cardiovascular function

The spinal circuitry is a complex network responsible for integrating signals from several brain regions and peripheral afferents related to the control of cardiovascular autonomic regulations. Although SPGN are arranged bilaterally and symmetrically, their activation regulate cardiovascular responses distinctly and preferentially. This was demonstrated by glutamate microinjection into the right IML (T2 level), which triggered a robust positive cardiac chronotropic effect, but little alteration in inotropism; whereas, glutamate microinjection into the left IML elicited less intense chronotropic effect was, but robust inotropism[39]. The spinal circuitry is sufficiently capable of generating rhythmic sympathetic vasomotor activity. Asphyxia elicited splanchnic nerve discharge pattern that varied between 2 and 3 Hz and renal nerve rhythmicity at a frequency of 10 Hz in spinalized

cats[40,41]. Moreover, spinalized animals exhibit Mayer waves in the sympathetic vasomotor outflow[42]. These findings consolidate the concept that the spinal cord is not merely a relay, but is instead a central site capable of regulating the periodicity of SPGN discharge to modulate control of the sympathetic vasomotor outflow either during rest or in situations that require rapid adjustment of cardiovascular parameters. Alterations in these mechanisms may trigger chronic changes in sympathetic vasomotor control in pathophysiological conditions.

2.12. Involvement of spinal neurons in the maintenance of sympathoexcitation

SPGN are key players to generate and maintain sympathetic vasomotor overactivation in various cardiovascular diseases, which is a major and important marker of disease severity. Using the Goldblatt two-kidney, one-clip (2K,1C) renovascular hypertension rat model, Milanez et al demonstrated that six weeks after renal artery clipping, 2K,1C animals had increased sympathetic overactivity, arterial hypertension, angiotensin II (ANG II) actions and ANG II type 1 (AT1) receptor mRNA expression in the thoracic spinal cord[67]. Since, AT1 receptors are expressed in the spinal IML neurons, intrathecal injection of losartan, a selective AT1 receptor antagonist, (spinal levels T10–T11) evoked a robust reduction in renal sympathetic nerve activity (RSNA) and BP in 2K,1C rats but not in normotensive animals. Interestingly, Leversha et al. also reported similar results in sheep with heart failure, as intrathecal administration of losartan (spinal levels T1–T2) caused a reduction in cardiac sympathetic nerve activity in sheep with heart failure[68]. Although ANG II-mediated increases in sympathetic nerve activity and BP are abolished by losartan antagonism of AT1 receptors in the IML, however, BP and sympathetic nerve activity were increased by selective antagonism of AT2 receptors in IML with PD123319[38]. Together, these findings suggest that, in addition to changes in various brain nuclei involved in

cardiovascular control, changes in ANG II actions on spinal cord neurons also contribute to the high activity of SPGN in hypertension.

Glutamate also plays a pivotal role in the regulation of SPGN overactivity in spinal cord, since intrathecal injection of kynurenic acid, a broad-spectrum ionotropic glutamate receptor antagonist, decreased in RSNA and BP in 2K,1C rats[67,310]. Similarly, intrathecal administration of 2-amino-5-phosphonovalerate (2APV), a selective antagonist of *N*-methyl-D-aspartate receptors (NMDAR), evoked a more robust hypotensive effect in spontaneously hypertensive rats than in normotensive rats[69].

3. Inflammation

3.1. Inflammation in PH

Inflammation is body's basic host defense response mechanism to injury, ischemia, toxins, or infectious agents that incorporates the innate and adaptive immune system, along with invasion of inflammatory cells (lymphocytes and macrophages) to the site of injury, and release of inflammatory mediators such as cytokines and chemokines[70]. Growing body of evidence suggests that inflammation plays a major contributory role in the development of pulmonary vascular remodeling in PH[71]. The pulmonary vascular cells produce and release inflammatory mediators, such as, high mobility group box 1 (HMGB1) in response to persistent tissue injury and inflammatory stimulation, which activates pattern recognition receptors or PRRs, including toll-like receptor 4 (TLR4). PRR activation is recognized as a starting point in activation of innate immunity, inducing the inflammation process, cell recruitment and tissue remodeling[72]. Infiltration of inflammatory cells in and around vascular lesions in PH include monocytes, macrophages, dendritic cells, T- and B-lymphocytes and mast cells[71,73]. Activation of these cells releases further inflammatory mediators, cytokines and chemokines, such as, nuclear factor of activated T cells, IL-1β,

IL-6, IL-8, IL-13, IL-18, monocyte chemotactic protein (MCP)-1, fractalkine (Cx3Cl1), CxCl12, CCL2, CCL5/RANTES and tumor necrosis factor (TNF)-α, which lead to vascular remodeling through vascular cell proliferation, collagen deposition, inflammatory cascades and apoptosis[71,73-75]. The progressive process generates plexiform lesions, medial hypertrophy, arterial muscularization, and even RV hypertrophy[76-79]. Serum and plasma levels of chemokines, cytokines, and autoantibodies are also increased in PAH patients and are correlated with disease severity and survival[74]. Interestingly, an increased prevalence of PH in patients with autoimmune disorders such as HIV, connective-tissue diseases, and thyroiditis has highlighted the importance of inflammation in PH[80,81].

3.2. Neuroinflammation: The CNS immune response

Neuroinflammation is the innate and adaptive immune responses of central nervous system (CNS) that are initiated toward a variety of harmful insults, such as, infection, ischemia, stress, and trauma through the release of inflammatory mediators, such as, cytokines, chemokines, and reactive oxygen species by various immune cells like microglia, astrocytes, peripherally derived immune cells, and endothelial cells[82]. Invading and local immune cells orchestrate a series of events that lead to either tissue repair or damage in response to neuroinflammation. During initial stages, neuroinflammation may play beneficial and protective role; however, chronic or excessive neuroinflammation can act as a critical pathological driver of several neurological and peripheral diseases, such as cerebrovascular diseases, traumatic brain and spinal cord injuries, neurodegenerative diseases, epilepsy, multiple sclerosis, psychological disorders, cardiovascular diseases and chronic pain[82-86]. Neuroinflammation is the common mechanism that connects ischemic, degenerative, traumatic, demyelinating, epileptic, and psychiatric pathologies[82-86]. Neuroinflammation typically involves four categories of stereotyped mechanisms: (i)

Functional activation and proliferation of microglia and astrocytes in pathology-specific CNS regions[87]. (ii) Increased tissue concentrations of inflammatory mediators, such as cytotoxic reactive oxygen species (ROS), nitric oxide (˙NO), reactive nitrogen species (RNS), prostaglandins, pro-inflammatory cytokines and chemokines, ATP and matrix metalloproteases (MMP2, MMP9)[88]. (iii) Peripheral immune cell infiltration from the systemic circulation including monocytes-macrophages, T- and B- lymphocytes[89]. (iv) Neuronal cell death, caused by the resulting neurotoxic context[90].

3.3. Microglia: Resident immune cells of the CNS

The CNS is comprised of neurons and three different kinds of glial cells: microglia, astrocytes and oligodendrocytes. Microglia account for 5 – 20 % of all adult human brain cells and are considered to be the key players in mediating immune responses in the CNS by secreting various inflammatory factors[91]. Microglia originates from bone marrow-derived progenitors that migrate throughout the healthy and injured areas into the CNS[92]. Chemokines, such as, MCP-1 or CC-chemokine ligand-2 (MCP/CCL-2), along with its receptor CCR2, play a major role in the recruitment of resident microglia as well as microglial progenitors to the lesion area[93]. Microglial cells phagocytose cellular debris and/or toxic substances to maintain homeostasis. They constitute the first line of defense against invading pathogens, infections and tissue injury. During physiological conditions, the “ramified” form of microglia possesses a small cell body and many fine processes that send multiple branches extending in all directions. This “resting” microglia is fairly motionless, but its branches constantly move to survey the surrounding areas for signs of brain lesions or nervous system dysfunction. Conversely, the ramified microglia undergoes structural changes to become amoeboid possessing larger cell body with thicker and shorter branches, which are characterized as “activated” microglia in response to insults in

the CNS[92]. The amoeboid form enables the entire microglial cell to migrate through the CNS, and translocate to the site of injury to perform immunological functions. Microglia motility is enhanced by ATP, serotonin, IL-4, IL-8, MCP-1 and VEGF[92,94,95]. Microglia can interact with neurons electrically, chemically and physically, modulating neuronal responses including sympathetic activation[92]. Thus, chronic stimulation of neurons might induce microglial activation. Further, this increased interaction between microglia and neurons might stimulate the increase in sympathetic activity observed in pre-clinical and clinical PH that augments PH prognosis and severity[151]. During physiological conditions, microglia reside within close proximity to preautonomic PVN neurons to regulate sympathetic outflow. Several studies demonstrated that during experimental hypertension PVN and NTS regions are infiltrated with additional microglia and the levels of proinflammatory cytokines, chemokines, and ROS within these regions rise influencing increased neuronal activity and sympathetic outflow[96-98]. It is noteworthy that while short-term microglial activation might be beneficial, chronic activation is detrimental, and has been implicated as a potential mechanism in neurodegeneration[99].

Studies have shown that microglial activation can also modulate respiratory responses by influencing neuronal activity. Microglial activation is induced in the NTS, the integration center for respiratory peripheral chemoreceptors during the first hour of exposure to chronic hypoxia. However, inhibition of microglial activation with minocycline resulted in lack of ventilatory acclimatization to hypoxia indicating that microglial cells modulate respiratory responses[100]. Interestingly, microglia exposure to LPS or hypoxia during gestation period induces an enhanced ventilatory response to re-exposure in vitro, suggesting that microglia has the ability to “remember” prior exposures[101].

Activated microglia release a swarm of immuno- and neuroregulatory factors and

neurotoxins that include pro-inflammatory cytokines, chemokines, ˙NO, ROS and RNS, all of which mediate neuroinflammation and contribute to neurodegeneration[99]. Cytokines released by activated microglia consist of interleukins (IL-1 and IL-6), IFN-γ, and TNF-α, while chemokines include MCP-1, macrophage inflammatory protein-1 (MIP-1), and RANTES[102]. IL-1, IL-6, and TNF-α are pro-inflammatory cytokines that actively participate in the initiation and coordination of inflammatory processes following microglial activation[103]. Excessive production of these cytokines leads to cytotoxicity and apoptosis on the surrounding neurons and oligodendrocytes[104]. Activated microglia can also increase the release of glutamate from adjacent astrocytes to cause potentially toxic and neuromodulatory effects[105](Figure 2). On the other hand, chemokines of microglial origin initiate leukocyte invasion via enhanced expression of endothelial adhesion molecules. The chemokine receptors expressed by microglia include IL-8R, CXCR2, CXCR3, CXCR4, CCR3, CCR5, and CX3CR1[106]. Microglia also express receptors for numerous cytokines, neurotransmitters (e.g., glutamate, GABA and norepinephrine) and neurohormones (e.g., angiotensin-II, glucocorticoids and mineralocorticoids) that aiding their ability to sense disturbances to homeostasis[92]. Microglia detects infection and tissue damage through toll-like receptors (TLRs), specifically TLR-4 is well known to recognize lipopolysaccharides (LPS), mediates microglial activation and production of inflammatory mediators[92]. A previous study reported that exogenous Ang II stimulates TLR4 via AT1R, leading to the activation of hypothalamic microglia ex vivo[307]. TLR4 inhibitor, TAK-242 administration has been shown to abolish microglial activation and preserve blood brain barrier (BBB) integrity in the PVN, RVLM, and NTS in spontaneously hypertensive rats (SHRs)[108]. Moreover, TLR4 blockade attenuated SNS activation and progression of MAP increases in SHRs[108]. Importantly, TLR4-deficient mice is less susceptible to develop hypoxia-induced

PH and showed decreased pulmonary vascular inflammatory response[305]. TLR-4 deficiency resulted in decreased microglia-mediated neuroinflammation and apoptosis, thus offers protection against PH pathophysiology[109].

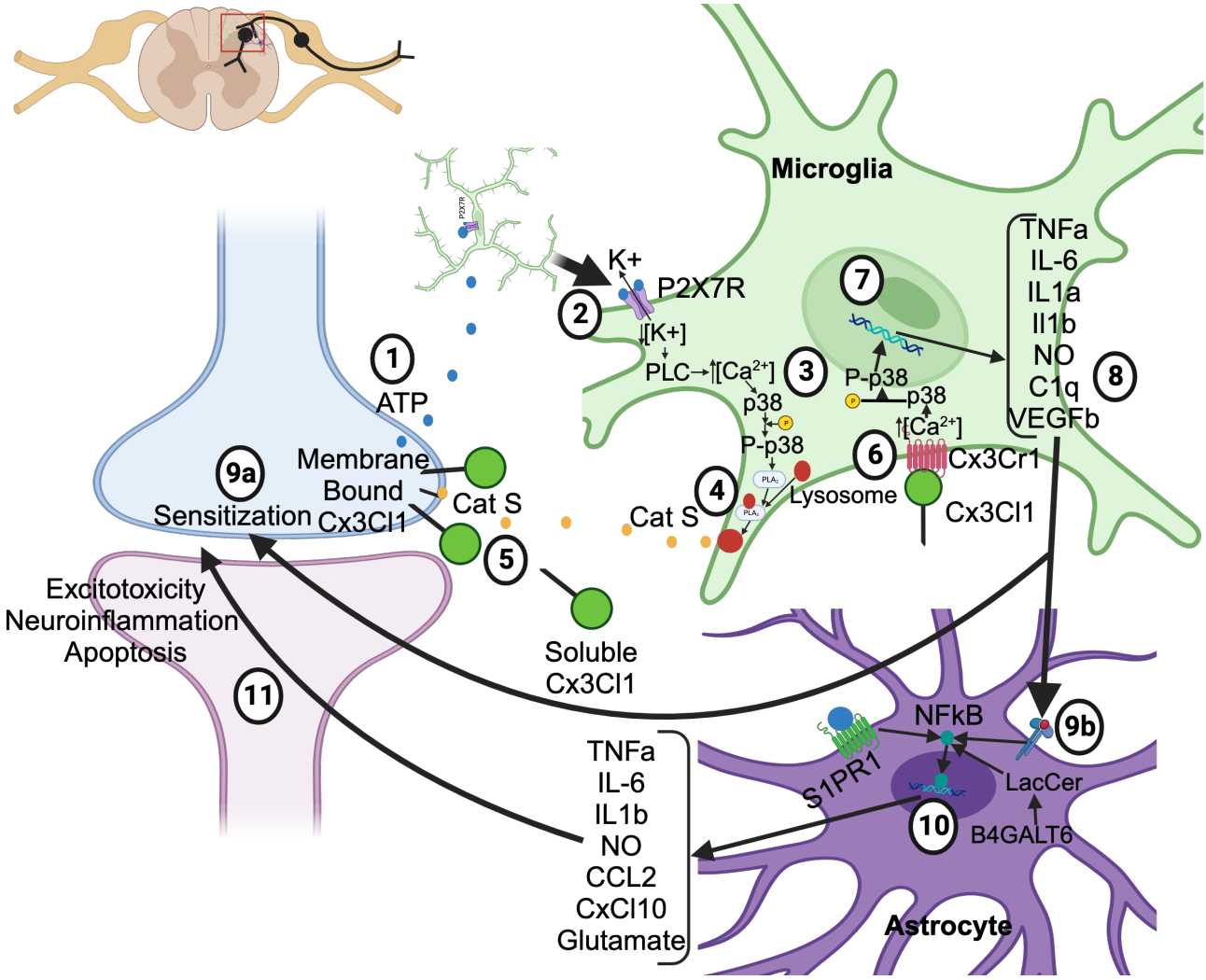

Figure 3: Schematic representation of the interactions between neurons, microglia and astrocytes mediated by CX3CL1/CX3CR1. 1. During pathological conditions ATP released from neurons binds to and activates the P2X7 receptor on resting microglia, resulting in activation of microglia. 2. Activated P2X7 receptor leads to potassium efflux and Ca2+influx resulting in decreased intracellular potassium, increased intracellular Ca2+

concentration and subsequent activation of phospholipase C (PLC), which ultimately leads to further increase in the intracellular calcium concentration. 3. Increased intracellular calcium activates p38 MAPK by phosphorylating to P-p38 that allows phospholipase A2 (PLA2) mediated translocation of lysosomes to microglial membrane. 4. Microglial lysosomes release cathepsin S (CatS), which translocate to the neurons. 5. CatS cleaves the soluble chemokine domain of CX3CL1 from its membrane tether on the surface of neurons. 6. Soluble CX3CL1 binds to, and activates, CX3CR1 on microglial surface, resulting in an increase in intracellular calcium mobilization and further activation of p38. 7. P-p38 alters gene transcription 8. This results in the synthesis and release of pro-inflammatory mediators from microglia. 9a. The pro-inflammatory mediators bind to and activates receptors on neurons resulting in their sensitization. 9b. The pro-inflammatory mediators from microglia bind to astrocytic receptor and activate nuclear transcription factor, NF-kB. NF-kB activation is also triggered by the sphingolipids S1P and LacCer. 10. NF-κB activation results in the synthesis and release of several pro-inflammatory mediators and glutamate from astrocyte. 11. The pro-inflammatory mediators and glutamate from astrocyte lead to excitotoxicity, neuroinflammation and neuronal apoptosis. *Modified from Chemokine mediated neuron-glia communication and aberrant signalling in neuropathic pain states. Curr Opin Pharmacol.*

3.4. Astrocytes: The non-immune glial cells

Astrocytes are the predominant neural type of glia in the CNS, that originate from the embryonic neurectoderm like neurons, oligodendrocytes and Schwan cells[110]. Astrocytes therefore cannot be designated as “immune cells” even though they participate in innate immune reactions within the CNS. Astrocytes and microglia are homogeneously intermingled throughout the tissue parenchyma of the CNS where they tightly cooperate

functionally both in homeostatic and pathological conditions[110]. Astrocytes are highly ramified cells that extend long and thin leaflets between neuronal processes and around synapses and perform their well-known roles in regulation of synaptogenesis, neuronal differentiation, survival, activity and in structural, metabolic and neuroprotective support to neurons, extracellular fluid homeostasis by clearing excess neurotransmitters, stabilizing and regulating the blood-brain barrier, promoting synapse formation and electrical isolation of excitable cells[111,112]. Astrocytes also actively contribute to the pathogenesis of multiple neurological disorders by responding to inflammatory signals and promoting inflammation, which makes them important players in neurologic diseases including multiple sclerosis (MS), Alzheimer disease (AD), Parkinson disease (PD), Huntington disease (HD) and amyotrophic lateral sclerosis (ALS)[113-117]. Astrocyte pathologies manifest in two main forms: astrocytopathy and astrogliosis. Astrocytopathy includes genetic, traumatic, toxic and other insult that can alter the astrocyte network's ability to carry out one or more of its essential functions leading to a variety of neurological diseases[118]. Astrogliosis is a complex neuroimmunological malfunctional process in which inflammatory signals from microglia, synapses, neurons, and sites of injury cause astrocytes to undergo rapid remodeling and become reactive. During astrogliosis, various ions, transcription factors, metabolic and pro-inflammatory molecules, such as, interleukin-6 (IL-6), transforming growth factor-alpha (TGF-α), leukemia inhibitory factor, and ciliary neurotrophic factor promote increased expression of markers of inflammatory astrocytes, such as glial fibrillary acidic protein (GFAP) and vimentin, hypertrophy of foot processes and expression of pro-inflammatory gene products[118]. Astrogliosis isolate damaged CNS tissues and protect the healthy tissue, creating glial scars, and repair damage to the blood-brain barrier while guiding post-traumatic neuroplasticity[118].

Inflammatory astrocytes express increased nuclear factor kappa-light-chain-enhancer of activated B cells (NF-κB) pathway, activation of master transcriptional regulator MAFG and mTOR signaling in response to pro-inflammatory stimuli, such as TNFα, IL-1β, IL-17, ROS, Toll-like receptor (TLR) engagement and sphingolipids, such as sphingosine 1-phosphate (S1P) and lactosylceramide (LacCer)[119-123]. During inflammation, nuclear translocation of the NF-κB plays the central role in astrocyte activation and contributes to the progression of various CNS pathologies[124](Figure 3). Selective blockade of astrocyte NF-κB signaling in CNS inflammatory and injury models including experimental autoimmune encephalomyelitis (EAE), spinal cord injury (SCI) and optic neuritis improved clinical outcomes and is associated with decreased levels of pro-inflammatory cytokines and oxidative stress, demonstrating a central role for NF-κB in astrocytes' response to inflammatory stimuli and other insults[125-127]. Moreover, astrocytes upregulate sphingolipid receptor S1PR1 expression upon activation, whereas supression of S1PR1 in astrocytes results in diminished EAE severity and increased neuronal survival by suppressing NF-κB mediated IL-6, TNF-α, granulocyte-macrophage colony-stimulating factor (GM-CSF), chemokine (C-C motif) ligand 2 (CCL2) and ˙NO production[128,129]. Interestingly, selective inactivation of LacCer catalyst, β−1,4-galactosyltransferase 6 (B4GALT6) in astrocytes suppressed NF-κB recruitment to the promoter regions of Ccl2, Csf2 and Nos2, which subsequently induced cytokine production, microglial activation, and infiltration of pro-inflammatory monocytes into the CNS[130]. These data collectively demonstrated that sphingolipid signaling plays a major regulatory role in astrocytic and microglial activation mediated inflammation in the CNS (Figure 3).

Inflammatory astrocytes can affect microglia and infiltrating immune cells by secreting immune factors such as cytokines (IL-1β, IL-6, TNFα) and chemokines (CCL2, CCL5,

CxCl10), neurotrophic factors, complement proteins, as well as extracellular matrix molecules such as hyaluronan (HA) and chondroitin sulfate proteoglycans, and cytotoxic factors, such as ·NO, ATP, and mitochondrial fragment[131-136]. B4GALT6/LacCer dependent signaling in reactive astrocytes has been shown to modulate transcriptional programs in microglia and infiltrating monocytes via the GM-CSF production[137]. Moreover, CRISPR/Cas9-based inactivation of sigma receptor 1 (SigmaR1), inositol-requiring enzyme-1α (IRE1α), or transcription factor X-box binding protein 1 (XBP1) in astrocytes decreased pro-inflammatory gene expression in microglia and monocytes, demonstrating that SigmaR1-IRE1α-XBP1 signaling modulates astrocyte-microglia crosstalk[138]. In turn astrocyte can also sense and respond to pro-inflammatory cytokines secreted by CNS-resident and CNS-recruited peripheral immune cells, and modulate the responses of neighboring cells throughout the CNS[131]. Specifically, astrocytes and microglia interact to regulate each other's function and the function of neurons[110]. Inflammatory astrocytes secrete factors that modulate the activity of microglia, while they are impacted by factors secreted by microglia[136,139]. Liddelow et al reported that activated microglia secrete IL-1α, TNF-α, and complement component 1q (C1q) that induces a neurotoxic phenotype in reactive astrocytes[140]. Moreover, aryl hydrocarbon receptor (AHR) signaling modulates microglial expression of vascular endothelial growth factor (VEGF)-B and TGF-α, which regulates the expression of pro-inflammatory genes (Ccl2, IL1b, Nos2) in astrocytes[141]. Bezzi et al reported that microglial TNF-α production regulates astrocytic stromal cell-derived factor (SDF)-1a signaling through C-X-C chemokine receptor type 4 (CXCR4), which promotes excessive glutamate release, resulting in excitotoxicity and neuronal loss[142]. Moreover, microglia-astrocyte crosstalk has been shown to regulate disease pathology, for example through the release of chemokines/cytokines and direct protein-

protein interaction through axon guidance molecules, such as Sema4D/PlexinB2 and EphrinB3/EphB3[131,143]. Astrocytes express various DAMP and PAMP receptors, among which several TLRs and purinergic receptors, such as P2X7, get activated by extracellular ATP and elicits neurodegeneration[131,144]. Astrocytes can also activate themselves in an autocrine manner by releasing cytokines, ATP, inflammatory HA, and LacCer[133,139,145]. Astrocytes release glutamate, ATP and other signaling molecules to regulate neuronal function[146]. They buffer potassium, remove excess cytotoxic glutamate and modulate blood flow in the CNS[147]. Astrocytes contribute to GABA tone in neural circuits that regulate sympathetic outflow and blood pressure by removing GABA through the GABA transporter 3[148]. Like microglia, astrocytes also reside in close proximity to preautonomic PVN neurons and are capable of sensing and responding to hypertensive and obesigenic stimuli[149]. Consequently, microglia and astrocyte form “triad” with neurons in the CNS and play critically important role governing neuroinflammation and apoptosis through Cx3Cl1 signaling during pathological processes[90,306].

Astrocytes also initiate neuronal death and can trigger demyelinating disease. In idiopathic PD, neurons in the substantia nigra die when alpha-synuclein deposits accumulate in reactive astrocytes to trigger the immune system to destroy surrounding neurons by releasing pro-inflammatory signals. The astrocytic variant of monoamine oxidase B converts 1-methyl-4-phenyl-1,2,3,6-tetra hydropyridine (MPTP) into its neurotoxic form, 1-methyl-4-phenylpyridium (MPP), which can trigger the neurodegenerative processes[150]. In MS, astrocytes trigger inflammatory responses in the CNS by attracting CD4+ T-lymphocytes and signaling them with interleukins to attack nearby myelin sheaths resulting in demyelination[150]. In inherited ALS, mutated SOD1 aggregates accumulate activating astrocytes, which begin to release pro-inflammatory cytokines (e.g., IL-6 and TGF-β)

that impair communication between neurons and astrocytes and initiates autoimmune targeting of neurons by reactive astrocytes and microglia via STAT3 signaling errors[150].

3.5. Evidence of neuroinflammation in experimental PH

Neuroinflammation in the brain and spinal cord has recently been implicated in the SNS activation found in several rodent models of severe PH-RVF[151-154]. In a recent well-studied monocrotaline (MCT) rat model of PH-RVF, researchers observed that cardiac and pulmonary pathophysiology associated with PH-RVF, demonstrated by increased right ventricular systolic pressure (RVSP, a surrogate marker) and RVH was associated with increase in microglial number, percent activation and expression of proinflammatory cytokines (IL-1β, IL-6 and TNF-α) in the PVN, suggesting for the first time that microglial activation-mediated neuroinflammation could be involved in the pathogenesis of PH-RVF. Furthermore, ICV infusion of minocycline, a specific microglial activation inhibitor, inhibited all of the above parameters and significantly attenuated PH-RVF[151]. In another study by Oliveira et al chronic exposure of hypoxia for 3 weeks significantly increased RVSP and RVH in WT mice. This was accompanied by increased number and percent activation of microglial cells in the PVN of hypoxia-treated WT mice. A positive correlation between the number of activated PVN microglia and RVSP was observed in these animals suggesting that increased activated PVN microglial cells is associated with an increase in the RVSP. In contrast, no significant changes in all of the above parameters were observed in $CX3CR1^{GFP/GFP}$ mice exposed to hypoxia[152]. The data from the above studies demonstrated that increase in PVN microglial activation-mediated neuroinflammation leads to development of PH-RVF.

We reported for the first time significantly increased GFAP, pro-inflammatory marker chemokine (C-C motif) ligand 3 (CCL3) and angiogenesis marker adhesion molecule

CD31 expression in the thoracic spinal cord (TSC) indicating severe neuroinflmmation in MCT-induced PH rats[153]. We believe peripheral sensitization of sensory afferent neurons in response to local tissue injury or inflammation lead the sensory neurons to release increased neurotransmitters such as substance P (SP) and calcitonin gene-related peptide (CGRP) in the dorsal horn causing sustained astrocyte activation and neuroinflammation in the TSC of PH rats in our study. However, the exact mechanism and impact of TSC neuroinflammation on cardiopulmonary function in PH remained elusive.

4. Mechanisms of CNS neuroinflammation and sympathoexcitation

4.1. Role of RAS in neuroinflammation and sympathoexcitation

4.1.1. Role of RAS in neuroinflammation

The RAS includes angiotensin converting enzyme (ACE), whose metabolic action leads to the formation of angiotensin II (Ang II), a vasoactive peptide. Ang II exerts its actions by stimulating two different G-protein-coupled angiotensin receptors, the AT1- and the AT2-receptor (AT1R and AT2R). However, since AT2R expression is very low in adult tissues, most of the classical actions of Ang II are mediated by AT1R. Additionally, a counter-regulatory system to the classical RAS is comprised of angiotensin converting enzyme2 (ACE2), its metabolic product, angiotensin-(1-7) [Ang-(1-7)], and the receptor Mas was recently discovered, which together forms the ACE2/Ang-(1-7)/Mas axis, and opposes the detrimental effects of ACE-AngII-AT1R axis[155,156]. All of the above-mentioned RAS components are expressed in the brain and spinal cord[157]. AT1R activation in the brain leads to regulation of immune cell infiltration, modulation of antigen-presenting cells, suppression of regulatory T cells, and induction of T helper cells (TH1 and TH17), all of which are involved in neuroinflammation[158].

There are two components to Ang-II induction of microglia in the cardiovascular autonomic

centers during hypertension. In vitro studies have confirmed the presence of AT1R on microglial cells, which may be directly stimulated by ANG-II, triggering the release of pro-inflammatory cytokines and $^{\cdot}NO$[92]. Moreover, Sherrod et al showed that AT1R are expressed on microglia and angiotensin receptor blockers reduce LPS-induced inflammation in vitro by inhibiting microglial activation and reducing the production of cytokines and NF-κB, the potent cytokine transcription factor[107]. It has been reported that microglia expresses AT2 receptors during rest and AT1 during activated period[92]. In addition, upregulation of MCP-1; or CCL-2 has been documented in neurons, microglia and astrocytes during various pathological conditions including nerve injury, neurodegenerative and cardiovascular diseases[81]. An indirect effect via neuronal AT1R leads to secretion of MCP-1/CCL2, which binds to its receptors, CCR2 on microglia stimulating their activation, proliferation and migration towards PVN pre-autonomic neurons[93]. Studies have demonstrated that Ang-II stimulation also induce release of inflammatory progenitor cells from the bone marrow, whereas CCL2/CCR2 mediates their migration to the cardiovascular autonomic centers of the brain and differentiation into activated microglia[4].

Astrocytes also participate in the neuroimmune regulation of SNS activation and blood pressure through RAS modulation in the brain. Astrocytes express angiotensinogen (AGT) and AT1R, therefore, astrocytic AT1R activation by Ang-II can induce neuroinflammation and regulate of cardiovascular function[107,159]. On the other hand, astrocytes also exert some neuroprotective effects through ACE2 expression, as this enzyme allows Ang-(1-7)'s cardiovascular regulatory actions in the RVLM[160].

4.1.2. Role of RAS in sympathoexcitation

Increased circulating Ang-II can activate densely populated AT1R in the SFO, which sends

direct projections to the PVN and other cardiovascular regulatory sites leading to increased sympathetic tone and elevated blood pressur[161]. Conversely, lesioning of the SFO or interfering with ACE-AngII-AT1R axis within the SFO attenuated elevated SNS activity and blood pressure in experimental hypertension[30]. In addition to influencing the PVN via activating SFO through excitatory afferents, Ang-II can also act locally within the PVN to enhance SNS activity through several mechanisms. AT1R are located post-synaptically on pre-autonomic glutamate neurons of the PVN and Ang-II can directly activate these neurons to increase SNS activity[162]. Moreover, presynaptic AT1R activation within the PVN reduces GABA release, which activates RVLM and spinally-projecting pre-autonomic neurons through presynaptic disinhibition[163].

Chronic Ang II infusion resulted in increased sympathoexcitation and hypertension in normal rats, which was associated with AT1R-mediated microglial activation and proinflammatory cytokine release (IL-1β, IL-6 and TNFα) as well as decreased expression of anti-inflammatory IL-10 in the PVN. Moreover, this neuroinflammation was accompanied by changes in the brain RAS components[97]. Further, intracerebroventricular administration of minocycline in the PVN decreased number of activated microglia and proinflammatory cytokines and attenuated Ang II-induced SNS activation, hypertension and associated cardiac pathology[97]. Interestingly, acute application of IL-1β into the left ventricle or the PVN in normal rats also resulted in a significant increase in mean arterial pressure (MAP). A direct neuronal connection between the PVN and the right-ventricle of the heart was also demonstrated using retrograde tracing with pseudo rabies virus (PRV) in this study. Furthermore, even a single dose of intra-peritoneal (I.P.) injection of Ang II induced increased microglial activation, circulating levels of $CD4^+/IL17^+$ T cells, expression of IL17, neuronal activity in several cardioregulatory autonomic brain regions including the SFO,

PVN and RVLM resulting in an increased MAP for over 24 hours[164]. Similarly activation of AT1R in the TSC leads to neuroinflammation and increased sympathetic drive. These studies indicate that microglial activation in response to Ang-II stimulation results in neuroinflammation, which increases cytokine, chemokine, ROS and RNS production that can modulate the activity of cardiovascular autonomic centers leading to SNS activation and hypertension.

4.1.3. Role of RAS in neuroinflammation mediated sympathoexcitation in PH

Overwhelming evidence from preclinical and clinical studies supports the chronic activation of RAS in the development and progression of PH[165,166]. All of the components of ACE-AngII-AT1R axis significantly increase during PH[165]. The activation of the ACE-AngII-AT1R axis increases inflammation, oxidative stress, and exerts pro-thrombotic, hypertrophic, and pro-fibrotic effects in different organs. In PH, ACE activity is increased by 50% in pulmonary vessels and about 4 fold higher in the right ventricle after 2-weeks of hypoxia exposure in rats, exacerbating pulmonary vascular remodeling and cardiac hypertrophy. Blocking ACE-AngII-AT1R axis with the AT1R antagonist, losartan or the ACE inhibitor, captopril improved cardiopulmonary hemodynamics in MCT- and hypoxia-induced PH models[165,167,168].

4.2. Role of TRPV1 in neuroinflammation and sympathoexcitation

4.2.1. Role of TRPV1 in neurological inflammation in the brain

Transient receptor potential vanilloid 1 (TRPV1) is a ligand-gated non-selective cation channel with high Ca^{2+} permeability that is widely expressed in the neuro-immune axis throughout the nervous system, where it regulates neuronal and glial activities including microglia and astrocyte, inflammatory signaling pathways, nociceptive sensory transmission due to heat, protons and several vanilloids, including capsaicin and

anandamide as well as cardiac sympathetic afferent reflex[169-175]. TRPV1 has been implicated in immune cell functioning, neurogenic inflammation, neuropathic pain, autoimmune disorders and cancer, where it promotes glial cell activation via membrane depolarization, morphological changes, proliferation, migration, phagocytic activity, secretion of inflammatory cytokines, and ROS[176-180]. TRPV1 regulates the development of various inflammatory neurological diseases and injury states by amplifying the effects of IL-1β and IL-6 and TNF-α[181-183,314] in the CNS via altering synaptic transmission and promoting excitotoxic neuronal damage[184,185]. Peripheral immune cells also infiltrate into the CNS through blood brain barrier dysfunction during various neurological diseases and communicate with glial cells to play a vital role in the neuroinflammation process[186]. TRPV1 was shown to regulate infiltrated T cell receptor-induced signaling, cytokine release, and pro-inflammatory properties of $CD4^+$ T cells[187]. Activation of TRPV1 signaling has been shown to exacerbate neuroinflammatory actions by activating pro-inflammatory STAT3 and NF-κB signaling[186,188](Figure 4). Interestingly, LPS-induced TLR4 activation has been shown to sensitize TRPV1 activity and upregulate its expression in sensory neurons and glial cells[189] by inducing the expression and production of pro-inflammatory chemokines and cytokines CXCL10, IL-1α, IL-1β and prostaglandin E2[190]. Moreover, TRPV1 antagonists suppressed morphine-induced increases in p38 mitogen-activated protein kinase (p38 MAPK) and NF-κB expression[191] in the dorsal striatum. Furthermore, central (i.c.v.) administration of TRPV1 antagonist, IRTX blocks FAAH substrate-mediated attenuation of TLR4-induced IL-6 expression[192]. These studies illustrated that TRPV1 activation increases pro-inflammatory cytokines and chemokines leading to neuroinflammation in the brain, while blocking TRPV1 activity shows anti-inflammatory effects[315].

4.2.2. Role of TRPV1 mediated SP and CGRP release in neuroinflammation

Several studies have indicated that TRPV1 activation induces neurogenic inflammation by promoting the release of proinflammatory neuropeptides SP and calcitonin gene-related peptide (CGRP), which regulate various overlapping signaling pathways leading in Ca^{2+} dependent activation of MAPK[193]. SP and CGRP are also known to exert their pro-inflammatory role by interacting with their receptors in microglia, T lymphocytes, macrophages and mast cells arousing immune responses[194]. LPS-induced activation of TRPV1 and TLR4 in trigeminal sensory neurons lead to CGRP release, which activated NF-κB nuclear translocation contributing to neuroinflammation[195]. In urban particle matter and formaldehyde (FA)-induced murine asthma model upregulated TRPV1 expression was associated with enhanced SP and CGRP release contributing to neurogenic inflammation, whereas CPZ treatment effectively reduced the level of these neuropeptides[196]. Taken together, these studies demonstrate the crosstalk between TRPV1 and neuropeptides leading to neuroinflammation.

4.2.3. Role of TRPV1 in sensory afferent transmission in the spinal dorsal horn

TRPV1 activation leads to Ca^{2+} influx and glutamate release from the sensory afferent nerve endings, which activates post-synaptic NMDARs to regulate neuronal nitric oxide synthase (NOS1) mediated ˙NO production as well as microglial and astrocytic activation in the spinal dorsal horn[197-199]. Consequently, TRPV1 ablation by capsaicin administration or spinal dorsal horn resection reduced proinflammatory cytokine expression[200]. Moreover, intraperitoneal and intrathecal administration of RTX, an ultrapotent and TRPV1 specific agonist has been shown to abolish TRPV1 expression in the dorsal horn leading to decreased pain sensation, inflammation and over-activated CSAR, thereby preventing myocardial hypertrophy, fibrosis, and apoptosis[201-203](Figure 4).

4.2.4. Role of TRPV1 in microglial activation

Overwhelming amount of studies indicate that TRPV1 modulates microglial activity in the CNS and TRPV1 activity is sensitized via coupling with second messenger cascades by a variety of pro-inflammatory agents. TRPV1 has been shown to modulate NADPH oxidase-mediated ROS production in microglia[204]. Activation of TRPV1 by capsaicin induced upregulation of kinin B1 receptor (B1R) via oxidative stress, superoxide anion production, pro-inflammatory cytokines and the NF-κB pathway in rat spinal dorsal horn microglial cells, which resulted in intraspinal release of ˙NO and activation of NK-1R and NMDA-R[205]. TRPV1 activation depolarized mitochondria by increasing intramitochondrial Ca^{2+} concentration, which resulted in ROS production, MAPK activation as well as enhancement of microglial chemotaxis and migratory activity[177]. However, TRPV1 inhibition abolished ROS production after lysophosphatidylcholine stimulation, which demonstrates that TRPV1 contributes to microglial damage via Ca^{2+} signaling and mitochondrial disruption[206]. Additionally, capsaicin treatment resulted in increased IL-1β and ROS generation and upregulated NF-κB pathway in spinal cord microglia, indicating that TRPV1 mediates microglia-induced neuroinflammation[198,205]. Alternatively, TRPV1 antagonist WIN-55,212-2 treatment decreased microglial activation, reduced pro-inflammatory cytokines production and increased the anti-inflammatory cytokine IL-1Rα, as well as increased hippocampal neurogenesis, demonstrating the role of TRPV1 in hippocampal inflammation[207]. Using $TRPV1^{-/-}$ mice or conditional overexpression of TRPV1 in microglia, Huang et al showed that TRPV1 promoted microglial activation and increased TNF-α, IL-1β, IL-6, and HMGB1 expression in repetitive febrile seizure mice[179].On the other hand, TRPV1 antagonist capsazepine has been reported to reduce the release of TNF-α and IFN-γ in innate immune response[208] and inhibit neurotoxicity[209].

Importantly, TRPV1 activation has been shown to induce proinflammatory NF-κB and STAT 3 signaling activation in microglia resulting in release of chemokines and cytokines[188]. Cerebral ischemia resulted in neurological deficiency and motor dysfunction in WT C57BL/6 mice[210]. This was accompanied by increased microglia/macrophages, astrocytes and neutrophils in those mice. Interestingly, intracerebroventricular injection of capsazepine improved neurological outcome and reduced infarct volume in WT mice, but not in TRPV1-KO mice demonstrating the role of ischemic stroke induced TRPV1 activation in neurological and motor deficits and infarction in the brain[210](Figure 4).

4.2.5. Role of TRPV1 in astrocytic activation

Besides microglia, TRPV1 increased astrocytic migration and chemotaxis during stress and injury by directly interacting with cytoskeletal elements[169,211]. Capsaicin treatment was shown to increase Iba1 and GFAP immunoreactivity in the spinal cord in mice with nociceptive, inflammatory, and neuropathic pain[198]. Also, capsaicin injections increased GFAP expression in acutely axotomized retina, however, this has been blocked by capsazepine[169,212]. TRPV1 activation has been shown to trigger the expression of the immediate early gene c-Fos in astrocytes in circumventricular organs[213]. Taken together, the aforementioned findings convincingly demonstrate that TRPV1 is expressed in microglia and astrocytes and plays important roles in these glial cell activation-mediated neuroinflammation leading to variety of neuro-immune diseases[314].

4.2.6. Role of TRPV1 in sympathoexcitation

Several electrophysiological studies demonstrated that TRPV1 activation mediates synaptic transmission via both presynaptic[35,214-217] and postsynaptic mechanisms[218,219]. TRPV1 stimulation by capsaicin or endogenous anandamide increased the frequency of spontaneous excitatory postsynaptic currents in the dopaminergic neurons of the

substantia nigra pars compacta[214], striatal neurons[216] and subpopulations of PAG neurons[35]. Moreover, ischemic stroke has been shown to increase various neurotransmitters and inflammatory substances, such as bradykinin[220] and prostaglandin[221], which induce TRPV1 activation via phosphorylation by protein kinase C (PKC)[222]. Additionally, bradykinin-induced PKC phosphorylation was shown to activate TRPV1 and potentiate glutamatergic synaptic transmission at the first sensory synapse[223]. TRPV1 activation in the presynaptic neurons allows Ca^{2+} influx, which triggers glutamate, SP and CGRP release tonically and independently of voltage-activated calcium channels in the central terminals of peripheral nerves[217,224]. Considering that glutamate is the primary excitatory neurotransmitter in the CNS that plays a critical role in triggering and sustaining sympathoexcitation via sympathetic premotor neurons in the PVN, RVLM and IML, and that the levels of the TRPV1 endogenous agonists in the CNS are elevated following various cardiovascular diseases, it is conceivable that excessive TRPV1 activation in the cardiovascular control centers during cardiovascular diseases leads to increased sympathetic vasomotor activation caused by glutamate-induced excitotoxicity[224-229]. Using histological and functional evidence Zahner et al demonstrated that the heart is innervated by TRPV1-expressing afferent nerves, which are essential for the cardiogenic sympathoexcitatory reflex during myocardial ischaemia[230]. In CHF and hypertension, over-activated CSAR has been shown to increase sympathetic tone and NE release elevating blood pressure and cardiac function, which is known as a positive feedback characteristic[231,232]. RTX was shown to reduce TRPV1 expression in the heart and DRG and weakened sympathoexcitatory responses to capsaicin stimulation[230]. Focal ablation of TRPV1-expressing CSAR afferents *via* epicardial application of RTX was shown to attenuate cardiac remodeling and autonomic dysfunction in HF[231]. Previous studies have

shown that TRPV1 channels in the neutral terminals play a complex role in modulating sympathetic efferent activities[230,233]. Shanks et al showed that inhibiting thoracic TRPV1-expressing afferent soma at the T1–T4 DRG by epidural application of RTX abolished cardiac and pulmonary sympathoexcitatory responses 10 weeks post-RTX administration[233]. Taken together, TRPV1 in neurons could be activated under ischemic conditions in response to various stimuli, and this could lead to an increase in neurotoxic glutamate release and adverse effects on neuronal survival. Our previous study demonstrated increased TRPV1 expression and activation, SP and Nf-kB expression, microglial and astrocytic activation mediated neuroinflammation and neuronal apoptosis in the TSC as well as increased sympathoexcitation in MCT- and SuHx-induced PH rats and human with PAH[154].

4.2.7. Role of TRPV1 in PH

TRPV1 is expressed in afferent fibers throughout the respiratory tract and intrapulmonary arteries and influences visceral tissue homeostasis, cytoskeletal architecture reorganization as well as proliferation and migration of pulmonary arterial smooth muscle cells (PASMC) through Ca^{2+} influx[234,235]. Several studies have demonstrated that depleting TRPV1+ afferent nerve endings improved PH and RVF in different PH models[236]. For example, TRPV1 ablation by capsaicin pretreatment attenuated PH severity by reducing pro-inflammatory cytokines and alleviating inflammation via p38MAPK pathway in the lung[237]. Moreover, depleting afferent nerve endings by capsacin treatment in the lung improved PH and RV hypertrophy in MCT, pulmonary banding and perinatal hypoxia PH models[238,239]. Several studies have shown that TRPV1 is involved in sensing blood pressure fluctuations and maintain the cardiovascular homoeostasis[240,241]. TRPV1 expressed in left ventricular tissues induces mitochondrial damage, autophagy and ROS

production[242]. Moreover, TRPV1 has been shown to play a major role in the progression of cardiac hypertrophy, fibrosis and apoptosis leading to heart failure[201]. Intraperitoneal and intrathecal administration of RTX has been shown to abolish TRPV1 expression in the dorsal horn leading to decreased pain sensation, inflammation and over-activated CSAR, thereby preventing myocardial hypertrophy, fibrosis, and apoptosis[201]. Horton et al reported that $TRPV_1$ antagonist BCTC (4-(3-Chloro-2-pyridinyl)-N-[4-(1,1-dimethylethyl)phenyl]1-piperazinecarboxamide) treatment in transverse aortic constriction mice significantly reduced markers of fibrosis, inflammation, tissue remodeling, apoptosis, brain natriuretic peptide, collagen, MMP-9, interleukin 6 and caspase 3 cleavage demonstrating that TRPV1 blockade protects against the progression of hypertrophic, fibrotic, tissue remodeling and apoptotic changes in congestive heart failure[243].

4.3. Role of Glutamate-induced excitotoxicity in neuroinflammation and sympathoexcitation

4.3.1. Role of Glutamate-induced excitotoxicity in neuroinflammation

Glutamate, the primary excitatory amino acid neurotransmitter in the CNS, is synthesized in neurons and stored in synaptic vesicles near the axon terminal until released into the synaptic cleft initiating a receptor-mediated signaling pathway[244]. Glutamate can act on both ionotropic (AMPA, NMDA and kainate) and metabotropic (mGluR 1-8) receptors on neurons and glia and activate different signaling pathways[244]. Both type of receptors mediate microglial response to glutamate-induced excitotoxicity and participate in neuroinflammation and neurodegeneration in the CNS[245,311,312]. Karim et al demonstrated that mGluR1 and mGluR5 in dorsal horn neurons activate ERK1 and ERK2 signaling leading to inflammatory pain in mice[146]. mGluR1 agonists have been shown to boost T cell

proliferation in the CNS and promote the activation of the MAPK signaling cascade leading to neuroinflammation[147]. The interaction of microglial mGluR5 and soluble amyloid-β peptide oligomers (sAβo) triggers microglial activation, which leads to the release of TNF-α, interferon (IFN)-γ, and IL-6[248]. Activation of microglial mGlu2 receptors triggers TNFα-induced neuroinflammation and toxicity associated with the Fas receptor ligand[249,311]. Both TNFα and Fas ligand are soluble molecules that stimulate caspase-mediated neuronal apoptosis via the TNF receptor, TNFR1. Thus, glutamate receptor activation in microglia may kill neighboring neurons in a TNFα/Fas ligand and caspase-dependent manner[249](Figure 4).

NMDA receptor subunits have been identified on microglia, and these receptors may enhance the release of TNFα, IL-1 and ˙NO[250,313]. NMDAR stimulation has been shown to activate microglia in the brain and spinal cord that leads to inducible nitric oxide synthase (NOS2)-mediated ˙NO and ROS generation as well as increase IL1a, IL1b, IL3, IL5, IL9, IL12 (p70), IL17, eotaxin, GMCSF, MCP1, and TNFa release[251,313]. Moreover, microglial NMDA receptors trigger neuroinflammation and neuronal death via the nuclear enzyme poly(ADP-ribose) polymerase-1 (PARP-1)/transient receptor potential cation channel subfamily M member 2 (TRMP2) signaling, which is facilitated by Ca2+ influx-dependent ERK1/2-mediated phosphorylation[252]. Activated microglia produce large amounts of glutamate, which is a major determinant of microglia neurotoxicity induced by NMDA receptors. This leads to increased Ca^{2+} influx activating the Ca^{2+}/calmodulin-dependent protein kinase (CaMK), cAMP-response element-binding protein (CREB) and ERK, which ultimately inhibits mitochondrial function leading to ATP depletion[244,253]. Thus NMDAR-mediated glutamate excitotoxicity leads to neuronal necrosis and apoptosis[308]. Moreover, AMPA and kainate receptor activation have been implicated in microglial reactivity and

motor neuron toxicity[244,309,310].

Extracellular glutamate levels increase when excess glutamate is released from presynaptic terminals during various pathological conditions, or glutamate reuptake is impaired in the CNS[254]. As discussed above, during pathological conditions, activated microglia and reactive astrocytes also release large amounts of glutamate. Elevated levels of extracellular glutamate lead to the overactivation of NMDARs in the postsynaptic neuron, resulting in Ca^{2+} influx[255-157]. Aberrant high levels of intracellular Ca2+ activate catalytic enzymes, produce toxic radicals, and impair production of cellular energy, which ultimately induces necrosis and apoptosis[258]. Various pain, neurodegenerative and cardiovascular disease studies have indicated that this process may activate a variety of enzymes, including kinases, phospholipases, neuronal nitric oxide synthases (NOS1), and proteases[255-257]. Subsequent increase of ˙NO production not only reinforces the glutamatergic signaling through retrograde transfer but also activates astrocytes and microglia to produce further ˙NO, cytokines and chemokines[255-257]. ˙NO in the CNS that has been well documented to play a complex dual role, protective and deleterious, depending on the pathophysiological conditions[36,259-261]. ˙NO activates soluble guanylate cyclase (sGC)-cGMP signal transduction pathway to modulate various physiological effects in the CNS and cardiovascular system including synaptic plasticity, retrograde signaling, neurodevelopment, vasodilation, inhibition of platelet aggregation and antiapoptotic effects[262]. On the other hand, during pathological conditions associated with increased oxidative stress and inflammation, excessive ˙NO combines with superoxide ($O_2^{\bullet -}$) to form peroxynitrite ($ONOO^-$), which induces neuroinflammation and neuronal excitotoxicity via protein oxidation and nitration, S-nitrosylation (S-NO), lipid peroxidation and activation of matrix metalloproteinases (MMPs) and cyclooxygenase (COX)[36,259-

[261,263,264]. Moreover, peroxynitrite breaks DNA, activating the nuclear enzyme poly(ADP-ribose) polymerase-1 (PARP-1) that causes cell death by rapid depletion of cell energy. Overactivated PARP also facilitates the expression of a variety of inflammatory genes leading to increased inflammation and associated oxidative stress, thus facilitating the progression of cardiovascular dysfunction and heart failure[36,259-261].

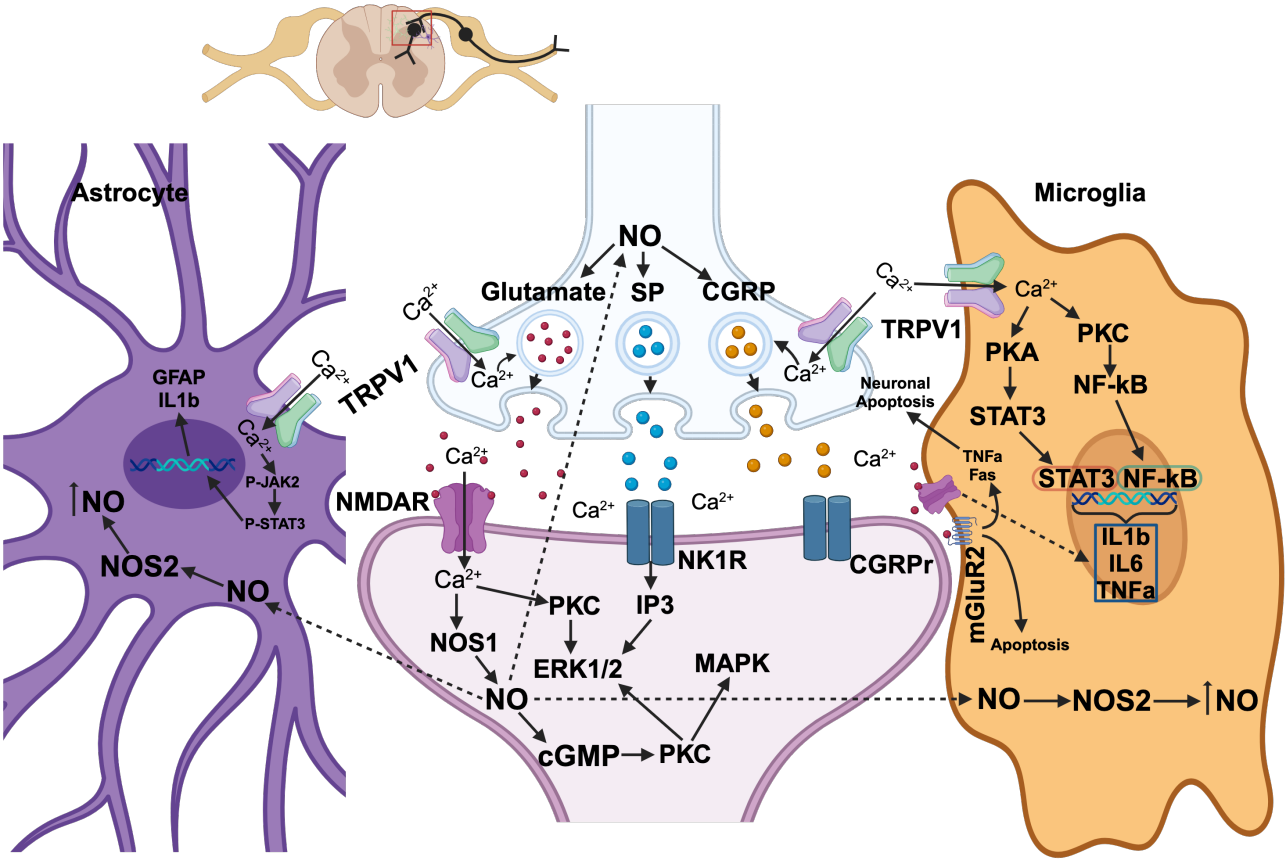

Figure 4: Schematic representation of TRPV1-mdiated NOS1 activation and regulation of neuroinflammation in the thoracic dorsal horn. Cardiopulmonary afferent signaling activates TRPV1 receptors in the thoracic dorsal horn, which allow Ca2+ influx mobilizing vesicles with neurotransmitter, such as, glutamate, SP and CGRP in the sensory nerve endings. The resulting release and binding of glutamate, SP and CGRP to their respective receptors lead to activation of various inflammatory mediators. Glutamate

binds to NMDA receptors in the spinothalamic neurons and allow Ca2+ influx activating NOS1, which leads to NO production. NO activates cGMP to further activate MAPK through PKC. PKC activation also activates ERK1/2. NO can induce further glutamate release from sensory nerve endings through retrograde transfer, diffuse into and activate microglia and astrocyte to produce further NO by NOS2 activation. SP binds to NK1 receptors in the spinothalamic neurons, which allow IP3 mediated activation of ERK1/2. The binding of glutamate to microglial NMDA receptors lead to production of IL-1b, IL-6 and TNFα. Alternatively, glutamate binding to mGluR2 leads to microglial apoptosis and Fas mediated TNFα production, which leads to neuronal apoptosis. Microglial TRPV1 activation leads to Ca2+ influx, which activates STAT3 and NF-kB to produce pro-inflammatory cytokines. Astrocytic TRPV1 activation leads to Ca2+ influx leading to STAT3 activation and production of IL-1b and GFAP.

4.3.2. Role of Glutamate-induced excitotoxicity in sympathoexcitation

Stimulation of spinal glutamate receptors of NMDA subtype tonically activate Nos1 and synthesize NO, which exerts both inhibitory and excitatory effects on the preganglionic sympathetic nerve activity related to cardiovascular control of the BP[4]. Microglial activation and release of pro-inflammatory cytokines induced neural excitotoxicity via increased glutamate release in the RVLM leading to increased plasma NE, blood pressure and sympathetic vasomotor activity in rats following stress-induced hypertension (SIH). Attenuation of microglial activation via intracisternal infusion of minocycline showed an antihypertensive effect by lowering NE, HR and sympathetic tone and attenuating

glutamate-induced neural excitotoxicity in the RVLM of SIH[265]. In several neuropathological and cardiovascular conditions, upregulation of NOS1 in the CNS induces oxidative and nitrosative stress, neuroinflammation, chemokine release, excitotoxicity, and neuronal apoptosis, indicating the involvement of ˙NO, whereas NOS1 inhibition induces neuroprotection[255,256,266]. NOS1 expression plays a complex dual role in sympathoexcitation regulation that depends on the pathophysiological conditions[36,260,261,267]. Several studies demonstrated that during physiological conditions, NOS1 has a sympathoinhibitory effect by acting on the PVN, NST, RVLM, and carotid body (CB) of the CNS[36,260,261]. On the other hand, a number of studies demonstrated that during various pathological conditions including hypertension, myocardial infarction, chronic heart failure and sepsis, NOS1 upregulation plays an essential role in the sympathoexcitatory action of ˙NO at the RVLM, NTS and TSC by increasing systemic arterial pressure, heart rate and sympathetic neurogenic vasomotor tone mediated by norepinephrine release from the sympathetic nerve terminals[259,261,268]. Ji et al demonstrated that i.c.v. administration of adrenomedullin activates ˙NO producing neurons in the PVN, NTS, supraoptic nucleus and nucleus paragigantocelluaris laterialis, causes hypertension and increases sympathetic outflow, indicating that central ˙NO may mediate sympathoexcitatory effects of adrenomedullin[269]. Microinjection of Nomega-nitro-l-arginine methyl ester (to block NO synthesis) or carboxy-2-phenyl-4,4,5, 5-tetramethylimidazoline-1-oxyl 3-oxide (Carboxy PTIO, NO trapper) into the NTS decreased arterial pressure, heart rate and RSNA. Alternatively, microinjection of Et2N[N(O)NO]Na (NO donor) caused increases in arterial pressure, HR and RSNA, which was inhibited by the pre-microinjection of Carboxy PTIO[270]. Moreover, microinjection of L-glutamate or NO donor, sodium nitroprusside or a cyclic GMP agonist, 8-bromocyclic GMP into the RVLM

increased arterial pressure, whereas injection of NOS1 inhibitor, Nomega-nitro-L-arginine methyl ester or a soluble guanylate cyclase inhibitor, methylene blue or preinjection of a glutamate receptor antagonist kynurenate decreased arterial pressure[271]. NOS inhibition with L-NAME resulted in a profound decline in RSNA and heart rate in conscious, unrestrained rats on normal (NS), high-(HS), and low-sodium (LS) diets[272]. Increased ˙NO produced by upregulated NOS1 in the TSC has been shown to facilitates bradykinin-induced increase in the cardiac sympathetic afferent reflex by activating glutamatergic neurons[36,260].

4.4. Role of Cx3Cl1/Cx3Cr1 in neuroinflammation and sympathoexcitation

4.4.1. Role of Cx3Cl1/Cx3Cr1 in neuroinflammation

One of the pathways through which neuron-microglia interaction regulates neuroinflammation and sympathoexcitation is CX3CR1-CX3CL1 axis. Cx3Cl1 is constitutively produced during physiological conditions by neurons in the brain, spinal cord and DRG through transcription, membrane insertion and proteolytic release[273]. Astrocytes also express *de novo* Cx3Cl1 in the spinal dorsal horn during various pathological conditions[123]. There are two forms of CX3CL1; membrane-bound, which is tethered to the cell membrane and as soluble protein following cleavage[274]. Cx3Cr1, the receptor for CX3CL1, is constitutively expressed predominantly in microglia in the brain and spinal cord[275]. Cx3Cr1 expression is increased significantly during pathological conditions leading to increased expression and/or proliferation and recruitment of microglia[276].

Under pathological conditions ATP released from neurons binds to and activates the P2X7 receptor on the surface membrane of microglia resulting in microglial activation in the spinal cord. Previous studies have indicated that P2X7R is involved in regulating cardiovascular activity in the central regions. Intraperitoneal injection of P2X7R

antagonists or P2X7 siRNA attenuated the increased levels of pro-inflammatory cytokines in the PVN and the augmented SNS activity after myocardial infarction, resulting in improved cardiac function[277]. Activated P2X7 receptor acts as a ligand-gated potassium channel, allowing potassium efflux to decrease its intracellular concentration, which leads to PLC activation and intracellular calcium concentration increase[276]. This phosphorylates p38 and activates p38 MAPK leading to PLA2 mediated translocation of lysosomes to the microglial membrane and exocytosis[278]. Cathepsin S (CatS), a microglial lysosomal protease, cleaves the soluble chemokine domain of CX3CL1 from its membrane tether on neuronal surface[279]. Soluble CX3CL1 then binds to, and activates CX3CR1 on microglial membrane, resulting in an increase in intracellular calcium concentration and further activation of p38[278]. Via altered gene transcription, this results in the synthesis and release of proinflammatory mediators, such as IL-1β, IL-6 and ˙NO from microglia[278]. These diffuse and bind to receptors on dorsal horn neurons, resulting in the hypersensitivity and spontaneous firing that is characteristic of central sensitization, and also provide a feedback mechanism by which further microglia are activated[280](Figure 3)

4.4.2. Role of Cx3Cl1/Cx3Cr1 in sympathoexcitation

Microglia in CX3CR1-deficient mice remain in “resting state” and fail to modify in response to environmental effectors, which leads to impairment of hippocampal cognitive function and synaptic plasticity[281]. Remarkably, CX3CR1-KO mice were associated with reduction of microglial cell number and activation in the PVN and altered microglia–neuron cross-talk that influenced synaptic activity, leading to blunted sympathetic activity and an attenuated response to hypoxia-induced PH[152]. Furthermore, the level of pro-inflammatory cytokines, including IL-1β, IL-6, TNF-α, Cx3Cl1, and CX3CR1 were all elevated in the NTS two weeks after fructose feeding in normal rats. These were accompanied by increased

systemic blood pressure and SNS activity. Intracerebroventricular (ICV) administration of CX3CR1 inhibitor, AZD8797 a attenuated fructose-induced hypertension and the expression of pro-inflammatory cytokines[282]. Zhang et al demonstrated that reduced microglial activation in the RVLM in stressed Cre-CX3CR1/RAGE fl/fl mice significantly decreased MAP and RSNA, which implied that microglial Cx3Cr1 and HMGB1/RAGE axis contributed to augmenting sympathetic activities[283]. These data demonstrate the important regulatory role of Cx3Cl1/Cx3Cr1 axis in the CNS in synaptic activity, microglial activation mediated neuroinlammation and SNS activation in various cardiovascular diseases.

4.4.3. Role of Cx3Cl1/Cx3Cr1 in PH

Amsellem et al reported that CX3CR1 deficiency in lung protects against hypoxia-induced PH by modulating monocyte recruitment, macrophage polarization, and PA-SMC proliferation[75]. Balabanian et al have found that CX3CL1/CX3CR1 levels are upregulated in patients with PAH compared to control subjects[284]. However, CX3CL1 is known to mediate transendothelial migration of CX3CR1+ cells, such as, monocytes/macrophages[285], lymphocytes[286], immature and mature DC[287] and neuroblastoma[288]. These observations support the notion that PH-related upregulation of CX3CL1 in the lung plays a critical role in promoting transendothelial migration of CX3CR1+ leukocytes and monocyte/macrophage accumulation in vascular remodeling[289]. Zhang et al demonstrated that hypoxia-stimulated upregulation of endothelial CX3CL1 induced SMC phenotypic switching from contractile to proliferative state in human lung microvascular endothelial cells, however CX3CR1 inhibition prevented CX3CL1 stimulation of SMC proliferation and monolayer expansion. Moreover, CX3CR1 deficiency attenuated spiral muscle expansion, distal vessel muscularization and pressure increase in response to hypoxia, indicating that capillary endothelium relies on the CX3CL1-CX3CR1

axis to sense alveolar hypoxia and promote peripheral vessel muscularization in PH[290].

4.5. Role of microglia mediated neuroinflammation in sympathoexcitation

Increased microglial activation mediated neuroinflammation and sympathetic hyperactivity contribute to the progression of hypertension[291]. Targeting neuroinflammation with an anti-inflammatory reagent or overexpression of interleukin-10 in the brain attenuates hypertension[97,292]. In a chronic systemic inflammation-induced hypertension model, sustained hypertension was induced after 2-weeks of LPS infusion. This was accompanied by the activation of microglia, increased IL-1β, IL-6 and TNF-α expression, and O_2^- production in the RVLM. However, inhibiting microglial activation blunted all of the above changes[293]. In another study, Ang II- and L-N^G-nitro-l-arginine methyl ester-induced hypertension was accompanied by microgliosis and proinflammatory cytokine upregulation in the PVN and motor cortex[294]. Targeted depletion of microglia significantly attenuated neuroinflammation and glutamate receptor expression in the PVN, as well as plasma vasopressin level, kidney norepinephrine concentration, and BP[294]. Wang et al demonstrated that TLR4 mediated microglial activation and NF-κB pathway regulation resulted in IL-1β, TNF-α and ROS production in the PVN leading to sympathetic hyperactivity Post-MI[295]. Moreover, microglial receptor, macrophage-inducible C-type lectin (Mincle) in the PVN was shown to contribute to sympathetic hyperactivity in acute MI rat by via downstream NOD-like receptor family pyrin domain-containing 3 (NLRP3) inflammasome/IL-1β axis[296]. Other studies using the specific microglial activation inhibitor minocycline reported the effective inhibition of sympathetic activity and the attenuation of hypertension in spontaneously hypertensive and chronic Ang II-infused rat models[297]. Sharma et al demonstrated that icv. administration of chemically modified tetracycline-3 (CMT-3) inhibited microglial activation and neuroinflammation in the PVN, decreased

sympathetic activity and attenuated MAP in Ang II rats[298]. These results provide direct evidence that microglia are central to neuroinflammation, neuronal regulation of SNS activation and hypertension. Several studies have shown that microglia play an important role in regulating SNS activities and cardiovascular function by releasing various substances, including cytokines, chemokines, ROS, RNS and growth factors[299].

Microglia activation and increased levels of pro-inflammatory cytokines in the PVN following myocardial infarction (MI) was shown to activate the hypothalamus-pituitary-adrenal axis, increase the activity of the sympathetic nervous system and contribute to the acute pro-inflammatory response in the myocardium[300,301]. In addition, activated microglia were also detected in other cardiovascular regulatory regions including the RVLM, NTS and PAG. In another rat MI model, prolonged microglial activation in the PVN was seen to sustain for over 12 weeks after myocardial infarction[302]. Furthermore, ICV infusion of minocycline, starting one week prior to infarction, significantly attenuated the increase in microglial activation by at least 50% in the PVN, RVLM, PAG and NTS, and neuronal activation was significantly reduced by 50% in the PVN and virtually abolished in the PAG, RVLM and NTS[303]. These data suggest that MI induces microglial activation in the cardiovascular regulatory centers within the CNS, and activated microglia contribute to increased SNS activity.

Microglial activation mediated cytokine release in the PVN resulted in increase of RAS components, sympathetic drive and plasma NE in MCT-induced PH rats, suggesting that microglial activation-mediated neuroinflammation and a dysregulated brain RAS is involved in the pathogenesis of PH-RVF. Furthermore, ICV infusion of minocycline attenuated microglial activation mediated sympathoexcitation in PH[151]. Oliveira et al demonstrated that chronic hypoxia-induced microglial activation in the PVN resulted in a

fivefold increase in the sympathetic/vagal balance (low frequency/high frequency ratio), suggesting an increase in sympathetic activity in PH mice. However, CX3CR1$^{GFP/GFP}$ mice were protected from hypoxia-induced microglial activation in the PVN and sympathoexcitation[152]. The data from the above studies demonstrated that increase in PVN microglial activation-mediated neuroinflammation leads to increased sympathetic activity and development of PH-RVF. Neuroinflammation, being the basis of a dysfunctional autonomic-cardiopulmonary communication in the development and progression of PH, may become a potential therapeutic target for PH therapy.

5. Conclusion

In conclusion, here we have summarized in detail the cardiovascular autonomic neural circuits within the brain and spinal cord that regulate sympathetic activity. We assessed the process of microglial and astrocytic activation mediated neuroinflammation and introduced the concept of neuroinflammation regulating SNS activity in the context of PH. We reviewed current literature illustrating some of the cellular and molecular mechanisms that may be involved in glial activation and sympathoexcitation. The work in this dissertation will focus on investigating the role and precise mechanism of TSC microglial and astrocytic activation mediated neuroinflammation and sympathetic activation in cardiopulmonary function in PH. Such a field of study is promising and may culminate in the formulation of new therapeutic approaches given that the intrathecal route is already widely used in clinical practice to treat several comorbidities[304]. We and others have demonstrated that targeting the dysregulated sympathetic nervous system could be a promising therapy to improve RV function and pulmonary vascular remodeling.

References

1. Simonneau G, Montani D, Celermajer DS, Denton CP, Gatzoulis MA, Krowka M, Williams PG, Souza R. Hemodynamic definitions and updated clinical classification of pulmonary hypertension. Eur Respir J2019; 53:doi: 10.1183/13993003.01913-2018.
2. Hoeper MM, Humbert M, Souza R, Idrees M, Kawut SM, Sliwa-Hahnle K, Jing ZC, Gibbs JS. A global view of pulmonary hypertension. Lancet Respir Med. 2016 Apr;4(4):306-22. doi: 10.1016/S2213-2600(15)00543-3. Epub 2016 Mar 12. PMID: 26975810.
3. Ginoux M, Turquier S, Chebib N, Glerant JC, Traclet J, Philit F, Sénéchal A, Mornex JF, and Cottin V. Impact of comorbidities and delay in diagnosis in elderly patients with pulmonary hypertension. ERJ Open Res 4: 2018.
4. Miyoshi M, Miyano K, Moriyama N, Taniguchi M, Watanabe T. Angiotensin type 1 receptor antagonist inhibits lipopolysaccharide-induced stimulation of rat microglial cells by suppressing nuclear factor kappaB and activator protein-1 activation. Eur J Neurosci. 2008;27:343–351.
5. Simonneau G, Montani D, Celermajer DS, Denton CP, Gatzoulis MA, Krowka M, Williams PG, Souza R. Haemodynamic definitions and updated clinical classification of pulmonary hypertension. Eur Respir J. 2019 Jan 24;53(1):1801913. doi: 10.1183/13993003.01913-2018. PMID: 30545968; PMCID: PMC6351336.
6. Voelkel NF, Quaife RA, Leinwand LA, Barst RJ, McGoon MD, Meldrum DR, et al. Right ventricular function and failure: report of a National Heart, Lung, and Blood Institute working group on cellular and molecular mechanisms of right heart

failure. Circulation. 2006;114(17):1883–1891.
doi: 10.1161/CIRCULATIONAHA.106.632208.

7. Hemnes AR, Brittain EL. Autonomic Nervous System in Pulmonary Arterial Hypertension: Time to Rest and Digest. Circulation. 2018 Feb 27;137(9):925-927. doi: 10.1161/CIRCULATIONAHA.117.032355. PMID: 29483171; PMCID: PMC5830155.
8. van de Veerdonk MC, Kind T, Marcus JT, Mauritz GJ, Heymans MW, Bogaard HJ, Boonstra A, Marques KM, Westerhof N, Vonk-Noordegraaf A. Progressive right ventricular dysfunction in patients with pulmonary arterial hypertension responding to therapy.J Am Coll Cardiol. 2011; 58:2511–2519.
9. Fonkoue IT, Le NA, Kankam ML, DaCosta D, Jones TN, Marvar PJ, Park J. Sympathoexcitation and impaired arterial baroreflex sensitivity are linked to vascular inflammation in individuals with elevated resting blood pressure. Physiol Rep. 2019 Apr;7(7):e14057. doi: 10.14814/phy2.14057. PMID: 30968587; PMCID: PMC6456445.
10. Veiga AC, Milanez MIO, Ferreira GR, Lopes NR, Santos CP, De Angelis K, Garcia ML, Oyama LM, Gomes GN, Nogueira FN, Carvalho PM, Campos RR, Bergamaschi CT, Nishi EE. Selective afferent renal denervation mitigates renal and splanchnic sympathetic nerve overactivity and renal function in chronic kidney disease-induced hypertension. J Hypertens 38: 765–773, 2020. doi:10.1097/HJH.0000000000002304.
11. Vaillancourt M, Chia P, Sarji S, Nguyen J, Hoftman N, Ruffenach G, Eghbali M, Mahajan A, Umar S. Autonomic nervous system involvement in pulmonary arterial

hypertension. Respir Res. 2017 Dec 4;18(1):201. doi: 10.1186/s12931-017-0679-6. PMID: 29202826; PMCID: PMC5715548.

12. Wang M, Li S, Zhou X, et al. Increased inflammation promotes ventricular arrhythmia through aggravating left stellate ganglion remodeling in a canine ischemia model. Int J Cardiol. 2017;248:286–293. doi: 10.1016/j.ijcard.2017.08.011
13. Wang Y, Jiang W, Chen H, et al. Sympathetic nervous system mediates cardiac remodeling after myocardial infarction in a circadian disruption model. Front Cardiovasc Med. 2021;8:668387. doi: 10.3389/fcvm.2021.668387.
14. Wensel R, Jilek C, Dörr M, Francis DP, Stadler H, Lange T, Blumberg F, Opitz C, Pfeifer M, and Ewert R. Impaired cardiac autonomic control relates to disease severity in pulmonary hypertension. Eur Respir J 34: 895–901, 2009.
15. Velez-Roa S, Ciarka A, Najem B, Vachiery JL, Naeije R, and van de Borne P. Increased sympathetic nerve activity in pulmonary artery hypertension. Circulation 110: 1308–1312, 2004.
16. Ciarka A, Doan V, Velez-Roa S, Naeije R, and van de Borne P. Prognostic significance of sympathetic nervous system activation in pulmonary arterial hypertension. Am J Respir Crit Care Med 181: 1269–1275, 2010.
17. Oliveira AC, Richards EM, Raizada MK. Pulmonary hypertension: Pathophysiology beyond the lung. Pharmacol Res. 2020 Jan;151:104518. doi: 10.1016/j.phrs.2019.104518. Epub 2019 Nov 13. PMID: 31730803; PMCID: PMC6981289.
18. Rothman A.M., Arnold N.D., Chang W. Pulmonary artery denervation reduces pulmonary artery pressure and induces histological changes in an acute porcine model of pulmonary hypertension. Circ Cardiovasc Interv. 2015;8(11):e002569.

19. da Silva Gonçalves Bos D., Happé C., Schalij I. Renal denervation reduces pulmonary vascular remodeling and right ventricular diastolic stiffness in experimental pulmonary hypertension. J Am Coll Cardiol Basic Trans Science. 2017;2:22–35.
20. Na S, Kim OS, Ryoo S, Kweon TD, Choi YS, Shim HS, Oh YJ. Cervical ganglion block attenuates the progression of pulmonary hypertension via nitric oxide and arginase pathways. Hypertension. 2014 Feb;63(2):309-15. doi: 10.1161/HYPERTENSIONAHA.113.01979. Epub 2013 Dec 9. PMID: 24324044.
21. Yoshida K, Saku K, Kamada K, Abe K, Tanaka-Ishikawa M, Tohyama T, Nishikawa T, Kishi T, Sunagawa K, Tsutsui H. Electrical Vagal Nerve Stimulation Ameliorates Pulmonary Vascular Remodeling and Improves Survival in Rats With Severe Pulmonary Arterial Hypertension. JACC Basic Transl Sci. 2018 Nov 12;3(5):657-671. doi: 10.1016/j.jacbts.2018.07.007. PMID: 30456337; PMCID: PMC6234524.
22. Bogaard H.J., Natarajan R., Mizuno S. Adrenergic receptor blockade reverses right heart remodeling and dysfunction in pulmonary hypertensive rats. Am J Respir Crit Care Med. 2010;182:652–660.
23. Sharma RK, Oliveira AC, Kim S, Rigatto K, Zubcevic J, Rathinasabapathy A, Kumar A, Lebowitz JJ, Khoshbouei H, Lobaton G, Aquino V, Richards EM, Katovich MJ, Shenoy V, and Raizada MK. Involvement of Neuroinflammation in the Pathogenesis of Monocrotaline-Induced Pulmonary Hypertension. Hypertension 71: 1156–1163, 2018.
24. Oliveira AC, Sharma RK, Aquino V, Lobaton G, Bryant AJ, Harrison JK, Richards EM, and Raizada MK. Involvement of Microglial Cells in Hypoxia-induced Pulmonary Hypertension. Am J Respir Cell Mol Biol 59: 271–273, 2018.

25. Korim WS, Elsaafien K, Basser JR, Setiadi A, May CN, Yao ST. In renovascular hypertension, TNF-α type-1 receptors in the area postrema mediate increases in cardiac and renal sympathetic nerve activity and blood pressure. Cardiovasc Res 115: 1092–1101, 2019. doi:10.1093/cvr/cvy268.
26. Biancardi VC, Campos RR, Stern JE. Altered balance of gamma-aminobutyric acidergic and glutamatergic afferent inputs in rostral ventrolateral medulla-projecting neurons in the paraventricular nucleus of the hypothalamus of renovascular hypertensive rats. J Comp Neurol 518: 567–585, 2010. doi:10.1002/cne.22256.
27. Oppenheimer SM, Gelb A, Girvin JP, Hachinski VC. Cardiovascular effects of human insular cortex stimulation. Neurology 1992;42:1727–1732.
28. Nagai M, Hoshide S, Kario K. The insular cortex and cardiovascular system: a new insight into the brain-heart axis. J Am Soc Hypertens 2010;4:174–182.
29. Critchley HD, Mathias CJ, Josephs O, et al. Human cingulate cortex and autonomic control: converging neuroimaging and clinical evidence. Brain 2003;126:2139–2152.
30. Young CN, Cao X, Guruju MR, Pierce JP, Morgan DA, Wang G, et al. ER stress in the brain subfornical organ mediates angiotensin-dependent hypertension. J Clin Invest. 2012;122:3960–3964.
31. Ulrich-Lai YM, Herman JP. Neural regulation of endocrine and autonomic stress responses. Nat Rev Neurosci 2009;10:397–409.
32. Jansen AS, Nguyen XV, Karpitskiy V, Mettenleiter TC, Loewy AD. Central command neurons of the sympathetic nervous system: basis of the fight-or-flight response. Science 270: 644–646, 1995. doi:10.1126/science.270.5236.644.

33. Pyner S, Coote JH. Identification of branching paraventricular neurons of the hypothalamus that project to the rostroventrolateral medulla and spinal cord. Neuroscience 100: 549–556, 2000. doi:10.1016/S0306-4522(00)00283-9.
34. Benarroch EE. Paraventricular nucleus, stress response, and cardiovascular disease. Clin Auton Res 15: 254–263, 2005. doi:10.1007/s10286-005-0290-7.
35. H. Kawahara, G.M. Drew, M.J. Christie, C.W. Vaughan, Inhibition of fatty acid amide hydrolase unmasks CB1 receptor and TRPV1 channel-mediated modulation of glutamatergic synaptic transmission in midbrain periaqueductal grey, Br. J. Pharmacol. 163 (2011) 1214e1222.
36. Guo ZL, Moazzami AR, Longhurst JC. Stimulation of cardiac sympathetic afferents activates glutamatergic neurons in the parabrachial nucleus: relation to neurons containing nNOS. Brain Res. 2005 Aug 16;1053(1-2):97-107. doi: 10.1016/j.brainres.2005.06.051. PMID: 16054113.
37. Guyenet PG. The sympathetic control of blood pressure. Nat Rev Neurosci 2006;7:335–346.
38. Chao J, Gao J, Parbhu K-JK, Gao L. Angiotensin type 2 receptors in the intermediolateral cell column of the spinal cord: negative regulation of sympathetic nerve activity and blood pressure. Int J Cardiol 168: 4046–4055, 2013. doi:10.1016/j.ijcard.2013.06.051.
39. Sundaram K, Murugaian J, Sapru H. Cardiac responses to the microinjections of excitatory amino acids into the intermediolateral cell column of the rat spinal cord. Brain Res 482: 12–22, 1989. doi:10.1016/0006-8993(89)90537-4.
40. Gootman PM, Cohen MI. Sympathetic rhythms in spinal cats. J Auton Nerv Syst 3: 379–387, 1981. doi:10.1016/0165-1838(81)90076-X.

41. McCall RB, Gebber GL. Brain stem and spinal synchronization of sympathetic nervous discharge. Brain Res. 1975 May 16;89(1):139-43. doi: 10.1016/0006-8993(75)90141-9. PMID: 1148837.
42. Ghali GZ, Zaki Ghali MG, Ghali EZ. Spinal genesis of Mayer waves. Neural Regen Res 15: 1821–1830, 2020. doi:10.4103/1673-5374.280306.
43. Palma JA, Benarroch EE. Neural control of the heart: recent concepts and clinical correlations. Neurology. 2014 Jul 15;83(3):261-71. doi: 10.1212/WNL.0000000000000605. Epub 2014 Jun 13. PMID: 24928126.
44. Dampney RA. Functional organization of central pathways regulating the cardiovascular system. Physiol Rev. 1994 Apr;74(2):323-64. doi: 10.1152/physrev.1994.74.2.323. PMID: 8171117.
45. Hainsworth R. Cardiovascular control from cardiac and pulmonary vascular receptors. Exp Physiol 2014;99:312–319.
46. Verberne AJ, Owens NC. Cortical modulation of the cardiovascular system. Prog Neurobiol 1998;54:149–168.
47. Kawashima T. The autonomic nervous system of the human heart with special reference to its origin, course, and peripheral distribution. Anat Embryol 2005;209:425–438.
48. Wang, W. & Ma, R. 2000. Cardiac sympathetic afferent reflexes in heart failure. Heart Fail Rev 5, 57–71.
49. Chen WW, Xiong XQ, Chen Q, Li YH, Kang YM, Zhu GQ. Cardiac sympathetic afferent reflex and its implications for sympathetic activation in chronic heart failure and hypertension. Acta Physiol (Oxf). 2015 Apr;213(4):778-94. doi: 10.1111/apha.12447. Epub 2015 Jan 17. PMID: 25598170.

50. Saper CB, Loewy AD, Swanson LW, Cowan WM. Direct hypothalamo-autonomic connections. Brain Res 1976;117:305–312.
51. Coote JH. A role for the paraventricular nucleus of the hypothalamus in the autonomic control of heart and kidney. Exp Physiol 2005;90:169–173.
52. Stocker SD, Simmons JR, Stornetta RL, Toney GM, Guyenet PG. Water deprivation activates a glutamatergic projection from the hypothalamic paraventricular nucleus to the rostral ventrolateral medulla. J Comp Neurol 2006;494:673–685.
53. Dampney RA. Functional organization of central pathways regulating the cardiovascular system. Physiol Rev 1994;74:323–364.
54. Saper CB, Loewy AD, Swanson LW, Cowan WM. Direct hypothalamo-autonomic connections. Brain Res 117: 305–312, 1976. doi:10.1016/0006-8993(76)90738-1.
55. Dampney RA, Coleman MJ, Fontes MA, Hirooka Y, Horiuchi J, Li YW, Polson JW, Potts PD, Tagawa T. Central mechanisms underlying short- and long-term regulation of the cardiovascular system. Clin Exp Pharmacol Physiol 29: 261–268, 2002. doi:10.1046/j.1440-1681.2002.03640.x.
56. Sladek CD, Michelini LC, Stachenfeld NS, Stern JE, Urban JH. Endocrine-Autonomic Linkages. Compr Physiol 5: 1281–1323, 2015. doi:10.1002/cphy.c140028.
57. Strack AM, Sawyer WB, Hughes JH, Platt KB, Loewy AD. A general pattern of CNS innervation of the sympathetic outflow demonstrated by transneuronal pseudorabies viral infections. Brain Res 491: 156–162, 1989. doi:10.1016/0006-8993(89)90098-X.
58. Coote JH. A role for the paraventricular nucleus of the hypothalamus in the autonomic control of heart and kidney. Exp Physiol 90: 169–173, 2005. doi:10.1113/expphysiol.2004.029041

59. McKinley MJ, Yao ST, Uschakov A, McAllen RM, Rundgren M, Martelli D. The median preoptic nucleus: front and centre for the regulation of body fluid, sodium, temperature, sleep and cardiovascular homeostasis. Acta Physiol (Oxf) 214: 8–32, 2015. doi:10.1111/apha.12487.
60. Shi P, Martinez MA, Calderon AS, Chen Q, Cunningham JT, Toney GM. Intra-carotid hyperosmotic stimulation increases Fos staining in forebrain organum vasculosum laminae terminalis neurones that project to the hypothalamic paraventricular nucleus. J Physiol 586: 5231–5245, 2008. doi:10.1113/jphysiol.2008.159665.
61. Sladek CD, Michelini LC, Stachenfeld NS, Stern JE, Urban JH. Endocrine-Autonomic Linkages. Compr Physiol 5: 1281–1323, 2015. doi:10.1002/cphy.c140028.
62. Stocker SD, Hunwick KJ, Toney GM. Hypothalamic paraventricular nucleus differentially supports lumbar and renal sympathetic outflow in water-deprived rats. J Physiol 563: 249–263, 2005. doi:10.1113/jphysiol.2004.076661.
63. Cassaglia PA, Hermes SM, Aicher SA, Brooks VL. Insulin acts in the arcuate nucleus to increase lumbar sympathetic nerve activity and baroreflex function in rats. J Physiol 589: 1643–1662, 2011. doi:10.1113/jphysiol.2011.205575.
64. Rahmouni K, Morgan DA. Hypothalamic arcuate nucleus mediates the sympathetic and arterial pressure responses to leptin. Hypertension 49: 647–652, 2007. doi:10.1161/01.HYP.0000254827.59792.b2.
65. Dampney RA, Horiuchi J. Functional organisation of central cardiovascular pathways: studies using c-fos gene expression. Prog Neurobiol 2003;71:359–384.

66. Jean A. The nucleus tractus solitarius: neuroanatomic, neurochemical and functional aspects [in French]. Arch Int Physiol Biochim Biophys 1991;99:A3–A52. 25.
67. Milanez MIO, Nishi ÉE, Sato AYS, Futuro Neto HA, Bergamaschi CT, Campos RR. Control of renal sympathetic nerve activity by neurotransmitters in the spinal cord in Goldblatt hypertension. Brain Res 1698: 43–53, 2018. doi:10.1016/j.brainres.2018.06.025.
68. Leversha S, Allen AM, May CN, Ramchandra R. Intrathecal administration of losartan reduces directly recorded cardiac sympathetic nerve activity in ovine heart failure. Hypertension 74: 896–902, 2019. doi:10.1161/HYPERTENSIONAHA.119.12937.
69. Mills E, Minson J, Drolet G, Chalmers J. Effect of intrathecal amino acid receptor antagonists on basal blood pressure and pressor responses to brainstem stimulation in normotensive and hypertensive rats. J Cardiovasc Pharmacol 15: 877–883, 1990. doi:10.1097/00005344-199006000-00004.
70. Harrison DG, Guzik TJ, Lob HE, Madhur MS, Marvar PJ, Thabet SR, et al. Inflammation, immunity, and hypertension. Hypertension. 2011;57(2):132–140. doi: 10.1161/HYPERTENSIONAHA.110.163576.
71. Dorfmüller P, Perros F, Balabanian K, and Humbert M. Inflammation in pulmonary arterial hypertension. Eur Respir J 22: 358–363, 2003.
72. Liang, S., Desai, A.A., Black, S.M., Tang, H. (2021). Cytokines, Chemokines, and Inflammation in Pulmonary Arterial Hypertension. In: Wang, YX. (eds) Lung Inflammation in Health and Disease, Volume I. Advances in Experimental Medicine

and Biology, vol 1303. Springer, Cham. https://doi.org/10.1007/978-3-030-63046-1_15.

73. Rabinovitch M, Guignabert C, Humbert M, and Nicolls MR. Inflammation and immunity in the pathogenesis of pulmonary arterial hypertension. Circ Res 115: 165–175, 2014.

74. Soon E, Holmes AM, Treacy CM, Doughty NJ, Southgate L, Machado RD, et al. Elevated levels of inflammatory cytokines predict survival in idiopathic and familial pulmonary arterial hypertension. Circulation. 2010;122(9):920–927. doi: 10.1161/CIRCULATIONAHA.109.933762.

75. Amsellem V, Abid S, Poupel L, Parpaleix A, Rodero M, Gary-Bobo G, Latiri M, Dubois-Rande JL, Lipskaia L, Combadiere C, and Adnot S. Roles for the CX3CL1/CX3CR1 and CCL2/CCR2 Chemokine Systems in Hypoxic Pulmonary Hypertension. Am J Respir Cell Mol Biol 56: 597–608, 2017.

76. Humbert M, Monti G, Brenot F, Sitbon O, Portier A, Grangeot-Keros L, Duroux P, Galanaud P, Simonneau G, and Emilie D. Increased interleukin-1 and interleukin-6 serum concentrations in severe primary pulmonary hypertension. Am J Respir Crit Care Med 151: 1628–1631, 1995.

77. Molossi S, Clausell N, and Rabinovitch M. Reciprocal induction of tumor necrosis factor-alpha and interleukin-1 beta activity mediates fibronectin synthesis in coronary artery smooth muscle cells. J Cell Physiol 163: 19–29, 1995.

78. Savale L, Tu L, Rideau D, Izziki M, Maitre B, Adnot S, and Eddahibi S. Impact of interleukin-6 on hypoxia-induced pulmonary hypertension and lung inflammation in mice. Respir Res 10: 6, 2009.

79. Stacher E, Graham BB, Hunt JM, Gandjeva A, Groshong SD, McLaughlin VV, Jessup M, Grizzle WE, Aldred MA, Cool CD, and Tuder RM. Modern age pathology of pulmonary arterial hypertension. Am J Respir Crit Care Med 186: 261–272, 2012.
80. Chu JW, Kao PN, Faul JL, Doyle RL. High prevalence of autoimmune thyroid disease in pulmonary arterial hypertension. Chest. 2002;122(5):1668–1673. doi: 10.1378/chest.122.5.1668.
81. Nicolls MR, Taraseviciene-Stewart L, Rai PR, Badesch DB, Voelkel NF. Autoimmunity and pulmonary hypertension: a perspective. Eur Respir J. 2005;26(6):1110–1118. doi: 10.1183/09031936.05.00045705.
82. Ní Chasaide C., Lynch M.A. The role of the immune system in driving neuroinflammation. Brain Neurosci. Adv. 2020;4 doi: 10.1177/2398212819901082.
83. Aguzzi A, Barres BA, Bennett ML. Microglia: scapegoat, saboteur, or something else? Science. 2013;339(6116):156–161. doi: 10.1126/science.1227901.
84. Hirsch EC, Hunot S. Neuroinflammation in Parkinson's disease: a target for neuroprotection? Lancet Neurol. 2009;8(4):382–397. doi: 10.1016/S1474-4422(09)70062-6.
85. Gilhus N.E., Deuschl G. Neuroinflammation—A common thread in neurological disorders. Nat. Rev. Neurol. 2019;15:429–430. doi: 10.1038/s41582-019-0227-8.
86. Ferrucci, L., and Fabbri, E. (2018). Inflammageing: chronic inflammation in ageing, cardiovascular disease, and frailty. Nat. Rev. Cardiol. 15, 505–522. doi: 10.1038/s41569-018-0064-2
87. Radenovic, L., Nenadic, M., Ulamek-Koziol, M., Januszewski, S., Czuczwar, S. J., Andjus, P. R., et al. (2020). Heterogeneity in brain distribution of activated microglia

and astrocytes in a rat ischemic model of Alzheimer's disease after 2 years of survival. Aging 12, 12251–12267. doi: 10.18632/aging.103411.

88. Chitnis, T., and Weiner, H. L. (2017). CNS inflammation and neurodegeneration. J. Clin. Invest. 127, 3577–3587. doi: 10.1172/jci90609.

89. Dansokho, C., Ait Ahmed, D., Aid, S., Toly-Ndour, C., Chaigneau, T., Calle, V., et al. (2016). Regulatory T cells delay disease progression in Alzheimer-like pathology. Brain 139, 1237–1251. doi: 10.1093/brain/awv408.

90. Skaper, S. D., Facci, L., Zusso, M., and Giusti, P. (2018). An inflammation-centric view of neurological disease: beyond the neuron. Front. Cell. Neurosci. 12:72. doi: 10.3389/fncel.2018.00072.

91. Ginhoux F, Lim S, Hoeffel G, Low D, Huber T. Origin and differentiation of microglia. Front Cell Neurosci. 2013;7:45. doi: 10.3389/fncel.2013.00045.

92. Kettenmann H, Hanisch UK, Noda M, Verkhratsky A. Physiology of microglia. Physiol Rev. 2011;91(2):461–553. doi: 10.1152/physrev.00011.2010.

93. Old EA, Malcangio M. Chemokine mediated neuron-glia communication and aberrant signalling in neuropathic pain states. Curr Opin Pharmacol. 2012;12(1):67–73. doi: 10.1016/j.coph.2011.10.015.

94. Davalos D, Grutzendler J, Yang G, Kim JV, Zuo Y, Jung S, Littman DR, Dustin ML, and Gan WB. ATP mediates rapid microglial response to local brain injury in vivo. Nat Neurosci 8: 752–758, 2005.

95. Krabbe G, Matyash V, Pannasch U, Mamer L, Boddeke HW, and Kettenmann H. Activation of serotonin receptors promotes microglial injury-induced motility but attenuates phagocytic activity. Brain Behav Immun 26: 419–428, 2012.

96. Waki H, Gouraud SS, Maeda M, Paton JF. Specific inflammatory condition in nucleus tractus solitarii of the SHR: novel insight for neurogenic hypertension? Auton Neurosci. 2008b;142:25–31.
97. Shi P, Diez-Freire C, Jun JY, Qi Y, Katovich MJ, Li Q, et al. Brain microglial cytokines in neurogenic hypertension. Hypertension. 2010;56:297–303.
98. Zubcevic J, Waki H, Raizada MK, Paton JF. Autonomic-immune-vascular interaction: an emerging concept for neurogenic hypertension. Hypertension. 2011;57:1026–1033.
99. Qian L, Hong JS, Flood PM. Role of microglia in inflammation-mediated degeneration of dopaminergic neurons: neuroprotective effect of interleukin 10. J Neural Transm Suppl. 2006;70:367–371. doi: 10.1007/978-3-211-45295-0_56.
100. Stokes JA, Arbogast TE, Moya EA, Fu Z, and Powell FL. Minocycline blocks glial cell activation and ventilatory acclimatization to hypoxia. J Neurophysiol 117: 1625–1635, 2017.
101. Johnson SM, Randhawa KS, Epstein JJ, Gustafson E, Hocker AD, Huxtable AG, Baker TL, and Watters JJ. Gestational intermittent hypoxia increases susceptibility to neuroinflammation and alters respiratory motor control in neonatal rats. Respir Physiol Neurobiol 256: 128–142, 2018.
102. Smith JA, Das A, Ray SK, Banik NL. Role of pro-inflammatory cytokines released from microglia in neurodegenerative diseases. Brain Res Bull. 2012;87(1):10–20. doi: 10.1016/j.brainresbull.2011.10.004.
103. Nakamura Y, Si QS, Kataoka K. Lipopolysaccharide-induced microglial activation in culture: temporal profiles of morphological change and release of cytokines and

nitric oxide. Neurosci Res. 1999;35(2):95–100. doi: 10.1016/S0168-0102(99)00071-1.

104. Graeber MB, Li W, Rodriguez ML. Role of microglia in CNS inflammation. FEBS Lett. 2011;585(23):3798–3805. doi: 10.1016/j.febslet.2011.08.033.

105. Kettenmann H, Kirchhoff F, Verkhratsky A. Microglia: new roles for the synaptic stripper. Neuron. 2013;77(1):10–18. doi: 10.1016/j.neuron.2012.12.023.

106. Ramesh G, MacLean AG, Philipp MT. Cytokines and chemokines at the crossroads of neuroinflammation, neurodegeneration, and neuropathic pain. Mediators Inflamm. 2013;2013:480739.

107. Sherrod M, Davis DR, Zhou X, Cassell MD, Sigmund CD. Glial-specific ablation of angiotensinogen lowers arterial pressure in renin and angiotensinogen transgenic mice. Am J Physiol Regul Integr Comp Physiol. 2005;289:R1763–1769.

108. Mowry FE, Peaden SC, Stern JE, et al. TLR4 and AT1R mediate blood-brain barrier disruption, neuroinflammation, and autonomic dysfunction in spontaneously hypertensive rats. Pharmacol Res. 2021;174:105877. doi: 10.1016/j.phrs.2021.105877

109. Huang Z, Zhou T, Sun X, Zheng Y, Cheng B, Li M, Liu X, He C. Necroptosis in microglia contributes to neuroinflammation and retinal degeneration through TLR4 activation. Cell Death Differ. 2018 Jan;25(1):180-189. doi: 10.1038/cdd.2017.141. Epub 2017 Sep 8. PMID: 28885615; PMCID: PMC5729519.

110. Moyse E, Krantic S, Djellouli N, Roger S, Angoulvant D, Debacq C, Leroy V, Fougere B, Aidoud A. Neuroinflammation: A Possible Link Between Chronic Vascular Disorders and Neurodegenerative Diseases. Front Aging Neurosci. 2022

May 19;14:827263. doi: 10.3389/fnagi.2022.827263. PMID: 35663580; PMCID: PMC9161208.

111. Wei DC, Morrison EH. Histology, Astrocytes. [Updated 2023 May 1]. In: StatPearls [Internet]. Treasure Island (FL): StatPearls Publishing; 2023 Jan-. Available from: https://www.ncbi.nlm.nih.gov/books/NBK545142/.

112. Reid JK, Kuipers HF. She Doesn't Even Go Here: The Role of Inflammatory Astrocytes in CNS Disorders. Front Cell Neurosci. 2021 Sep 3;15:704884. doi: 10.3389/fncel.2021.704884. PMID: 34539348; PMCID: PMC8446364.

113. Diaz-Castro B, Gangwani MR, Yu X, Coppola G, and Khakh BS (2019). Astrocyte molecular signatures in Huntington's disease. Sci Transl Med 11.

114. Gu X-L, Long C-X, Sun L, Xie C, Lin X, and Cai H (2010). Astrocytic expression of Parkinson's disease-related A53T alpha-synuclein causes neurodegeneration in mice. Mol Brain 3, 12.

115. Habib N, McCabe C, Medina S, Varshavsky M, Kitsberg D, Dvir-Szternfeld R, Green G, Dionne D, Nguyen L, and Marshall JL (2020). Disease-associated astrocytes in Alzheimer's disease and aging. Nature Neuroscience, 1–6.

116. Wheeler MA, and Quintana FJ (2019). Regulation of Astrocyte Functions in Multiple Sclerosis. Cold Spring Harbor perspectives in medicine 9.

117. Wheeler MA, Clark IC, Tjon EC, Li Z, Zandee SEJ, Couturier CP, Watson BR, Scalisi G, Alkwai S, Rothhammer V, et al. (2020a). MAFG-driven astrocytes promote CNS inflammation. Nature 578, 593–599.

118. Pekny M, Pekna M, Messing A, Steinhäuser C, Lee JM, Parpura V, Hol EM, Sofroniew MV, Verkhratsky A. Astrocytes: a central element in neurological diseases. Acta Neuropathol. 2016 Mar;131(3):323-45.

119. Lian, H., Yang, L., Cole, A., Sun, L., Chiang, A. C., Fowler, S. W., et al. (2015). NF-kB-activated astroglial release of complement C3 compromises neuronal morphology and function associated with Alzheimer's disease. Neuron 85, 101–115. doi: 10.1016/j.neuron.2014.11.018

120. Wheeler, M. A., Jaronen, M., Covacu, R., Zandee, S. E. J., Rothhammer, V., Tjon, E. C., et al. (2020b). Environmental control of astrocyte pathogenic activities in CNS inflammation. Cell 176, 581.e18–596.e18. doi: 10.1016/j.cell.2018.12.012.

121. Chandel NS, Trzyna WC, McClintock DS, and Schumacker PT (2000). Role of Oxidants in NF-κB Activation and TNF-α Gene Transcription Induced by Hypoxia and Endotoxin. The Journal of Immunology 165, 1013–1021.

122. Kawai T, and Akira S (2007). Signaling to NF-κB by Toll-like receptors. Trends in Molecular Medicine 13, 460–469.

123. Rothhammer V, Kenison JE, Tjon E, Takenaka MC, Lima K.A.d., Borucki DM, Chao C-C, Wilz A, Blain M, Healy L, et al. (2017). Sphingosine 1-phosphate receptor modulation suppresses pathogenic astrocyte activation and chronic progressive CNS inflammation. Proceedings of the National Academy of Sciences 114, 2012–2017.

124. Linnerbauer M, Wheeler MA, Quintana FJ. Astrocyte Crosstalk in CNS Inflammation. Neuron. 2020 Nov 25;108(4):608-622. doi: 10.1016/j.neuron.2020.08.012. Epub 2020 Sep 7. PMID: 32898475; PMCID: PMC7704785.

125. Brambilla R, Morton PD, Ashbaugh JJ, Karmally S, Lambertsen KL, and Bethea JR (2014). Astrocytes play a key role in EAE pathophysiology by orchestrating in the

CNS the inflammatory response of resident and peripheral immune cells and by suppressing remyelination. Glia 62, 452–467.

126. Brambilla R, Bracchi-Ricard V, Hu W-H, Frydel B, Bramwell A, Karmally S, Green EJ, and Bethea JR (2005). Inhibition of astroglial nuclear factor κB reduces inflammation and improves functional recovery after spinal cord injury. The Journal of Experimental Medicine 202, 145–156.

127. Brambilla R, Dvoriantchikova G, Barakat D, Ivanov D, Bethea JR, and Shestopalov VI (2012). Transgenic inhibition of astroglial NF-κB protects from optic nerve damage and retinal ganglion cell loss in experimental optic neuritis. Journal of Neuroinflammation 9, 213.

128. Choi JW, Gardell SE, Herr DR, Rivera R, Lee C-W, Noguchi K, Teo ST, Yung YC, Lu M, Kennedy G, and Chun J (2011). FTY720 (fingolimod) efficacy in an animal model of multiple sclerosis requires astrocyte sphingosine 1-phosphate receptor 1 (S1P1) modulation. Proceedings of the National Academy of Sciences 108, 751–756.

129. Rothhammer V, Kenison JE, Tjon E, Takenaka MC, Lima K.A.d., Borucki DM, Chao C-C, Wilz A, Blain M, Healy L, et al. (2017). Sphingosine 1-phosphate receptor modulation suppresses pathogenic astrocyte activation and chronic progressive CNS inflammation. Proceedings of the National Academy of Sciences 114, 2012–2017.

130. Mayo L, Trauger SA, Blain M, Nadeau M, Patel B, Alvarez JI, Mascanfroni ID, Yeste A, Kivisäkk P, Kallas K, et al. (2014). Regulation of astrocyte activation by glycolipids drives chronic CNS inflammation. Nature Medicine 20, 1147–1156.

131. Clark, D. P. Q., Perreau, V. M., Shultz, S. R., Brady, R. D., Lei, E., Dixit, S., et al. (2019). Inflammation in traumatic brain injury: roles for toxic A1 astrocytes and microglial-astrocytic crosstalk. Neurochem. Res. 44, 1410–1424. doi: 10.1007/s11064-019-02721-8.

132. Liddelow, S. A., and Barres, B. A. (2017). Reactive astrocytes: production, function and therapeutic potential. Immunity 46, 957–967. doi: 10.1016/j.immuni.2017.06.006

133. Nagy, N., Kuipers, H. F., Marshall, P. L., Wang, E., Kaber, G., and Bollyky, P. L. (2019). Hyaluronan in immune dysregulation and autoimmune diseases. Matrix Biol. 78–79, 292–313. doi: 10.1016/j.matbio.2018.03.022.

134. Stephenson, E. L., Mishra, M. K., Moussienko, D., Laflamme, N., Rivest, S., Ling, C. C., et al. (2018). Chondroitin sulfate proteoglycans as novel drivers of leucocyte infiltration in multiple sclerosis. Brain 141, 1094–1110. doi: 10.1093/brain/awy033.

135. Orellana, J. A., Froger, N., Ezan, P., Jiang, J. X., Bennett, M. V. L., Naus, C. C., et al. (2011). ATP and glutamate released via astroglial connexin43 hemichannels mediate neuronal death through activation of pannexin 1 hemichannels. J. Neurochem. 118, 826–840. doi: 10.1111/j.1471-4159.2011.07210.x.

136. Joshi, A. U., Minhas, P. S., Liddelow, S. A., Haileselassie, B., Andreasson, K. I., Dorn, G. W., et al. (2019). Fragmented mitochondria released from microglia trigger A1 astrocytic response and propagate inflammatory neurodegeneration. Nat. Neurosci. 22, 1635–1648. doi: 10.1038/s41593-019-0486-0.

137. Mayo L, Trauger SA, Blain M, Nadeau M, Patel B, Alvarez JI, Mascanfroni ID, Yeste A, Kivisäkk P, Kallas K, et al. (2014). Regulation of astrocyte activation by glycolipids drives chronic CNS inflammation. Nature Medicine 20, 1147–1156.

138. Wheeler MA, Jaronen M, Covacu R, Zandee SEJ, Scalisi G, Rothhammer V, Tjon EC, Chao C-C, Kenison JE, Blain M, et al. (2019). Environmental Control of Astrocyte Pathogenic Activities in CNS Inflammation. Cell 176, 581–596.e518.

139. Zamanian, J. L., Xu, L., Foo, L. C., Nouri, N., Zhou, L., Giffard, R. G., et al. (2012). Genomic analysis of reactive astrogliosis. J. Neurosci. 32, 6391–6410. doi: 10.1523/JNEUROSCI.6221-11.2012.

140. Liddelow SA, Guttenplan KA, Clarke LE, Bennett FC, Bohlen CJ, Schirmer L, Bennett ML, Münch AE, Chung W-S, Peterson TC, et al. (2017). Neurotoxic reactive astrocytes are induced by activated microglia. Nature 541, 481–487.

141. Rothhammer V, Borucki DM, Tjon EC, Takenaka MC, Chao C-C, Ardura-Fabregat A, Lima K.A.d., Gutiérrez-Vázquez C, Hewson P, Staszewski O, et al. (2018). Microglial control of astrocytes in response to microbial metabolites. Nature 557, 724–728.

142. Bezzi P, Domercq M, Brambilla L, Galli R, Schols D, Clercq ED, Vescovi A, Bagetta G, Kollias G, Meldolesi J, and Volterra A (2001). CXCR4-activated astrocyte glutamate release via TNFα: amplification by microglia triggers neurotoxicity. Nature Neuroscience 4, 702–710.

143. Clark, I. C., Gutiérrez-Vázquez, C., Wheeler, M. A., Li, Z., Rothhammer, V., Linnerbauer, M., et al. (2021). Barcoded viral tracing of single-cell interactions in central nervous system inflammation. Science 372:eabf1230. doi: 10.1126/science.abf1230.

144. Sidoryk-Wegrzynowicz, M., and Struzinska, L. (2021). Astroglial and microglial purinergic P2X7 receptor as a major contributor to neuroinflammation during the course of multiple sclerosis. Int. J. Mol. Sci. 22:8404. doi: 10.3390/ijms22168404.

145. Mayo, L., Trauger, S. A., Blain, M., Nadeau, M., Patel, B., Alvarez, J. I., et al. (2014). Regulation of astrocyte activation by glycolipids drives chronic CNS inflammation. Nat. Med. 20, 1147–1156. doi: 10.1038/nm.3681.

146. Orellana, J. A., Froger, N., Ezan, P., Jiang, J. X., Bennett, M. V. L., Naus, C. C., et al. (2011). ATP and glutamate released via astroglial connexin43 hemichannels mediate neuronal death through activation of pannexin 1 hemichannels. J. Neurochem. 118, 826–840. doi: 10.1111/j.1471-4159.2011.07210.x.

147. Ransohoff RM, Brown MA. Innate immunity in the central nervous system. J Clin Invest. 2012;122:1164–1171.

148. Park JB, Jo JY, Zheng H, Patel KP, Stern JE. Regulation of tonic GABA inhibitory function, presympathetic neuronal activity and sympathetic outflow from the paraventricular nucleus by astroglial GABA transporters. J Physiol. 2009;587:4645–4660.

149. Buckman LB, Thompson MM, Moreno HN, Ellacott KLJ. Regional astrogliosis in the mouse hypothalamus in response to obesity. J Comp Neurol. 2012

150. Li K, Li J, Zheng J, Qin S. Reactive Astrocytes in Neurodegenerative Diseases. Aging Dis. 2019 Jun;10(3):664-675.

151. Sharma RK, Oliveira AC, Kim S, Rigatto K, Zubcevic J, Rathinasabapathy A, Kumar A, Lebowitz JJ, Khoshbouei H, Lobaton G, Aquino V, Richards EM, Katovich MJ, Shenoy V, and Raizada MK. Involvement of Neuroinflammation in the Pathogenesis of Monocrotaline-Induced Pulmonary Hypertension. Hypertension 71: 1156–1163, 2018.

152. Oliveira AC, Sharma RK, Aquino V, Lobaton G, Bryant AJ, Harrison JK, Richards EM, and Raizada MK. Involvement of Microglial Cells in Hypoxia-induced Pulmonary Hypertension. Am J Respir Cell Mol Biol 59: 271–273, 2018.

153. Vaillancourt M, Chia P, Medzikovic L, Cao N, Ruffenach G, Younessi D, Umar S. Experimental Pulmonary Hypertension Is Associated With Neuroinflammation in the Spinal Cord. Front Physiol. 2019 Sep 20;10:1186. doi: 10.3389/fphys.2019.01186. PMID: 31616310; PMCID: PMC6764190.

154. Razee A, Banerjee S, Hong J, Magaki S, Fishbein G, Ajijola OA, Umar S. Thoracic Spinal Cord Neuroinflammation as a Novel Therapeutic Target in Pulmonary Hypertension. Hypertension. 2023 Jun;80(6):1297-1310. doi: 10.1161/HYPERTENSIONAHA.122.20782. Epub 2023 Apr 24. PMID: 37092338; PMCID: PMC10192067.

155. Ferreira AJ, Santos RA, Bradford CN, Mecca AP, Sumners C, Katovich MJ, et al. Therapeutic implications of the vasoprotective axis of the renin-angiotensin system in cardiovascular diseases. Hypertension. 2010;55(2):207–213. doi: 10.1161/HYPERTENSIONAHA.109.140145.

156. Santos RA, Ferreira AJ, Verano-Braga T, Bader M. Angiotensin-converting enzyme 2, angiotensin-(1-7) and Mas: new players of the renin-angiotensin system. J Endocrinol. 2013;216(2):R1–R17. doi: 10.1530/JOE-12-0341.

157. Grobe JL, Xu D, Sigmund CD. An intracellular renin-angiotensin system in neurons: fact, hypothesis, or fantasy. Physiology (Bethesda) 2008;23:187–193. doi: 10.1152/physiol.00002.2008.

158. Platten M, Youssef S, Hur EM, Ho PP, Han MH, Lanz TV, et al. Blocking angiotensin-converting enzyme induces potent regulatory T cells and modulates

TH1- and TH17-mediated autoimmunity. Proc Natl Acad Sci U S A. 2009;106(35):14948–14953. doi: 10.1073/pnas.0903958106.

159. Fuchtbauer L, Groth-Rasmussen M, Holm TH, Lobner M, Toft-Hansen H, Khorooshi R, et al. Angiotensin II Type 1 receptor (AT1) signaling in astrocytes regulates synaptic degeneration-induced leukocyte entry to the central nervous system. Brain Behav Immun. 2011;25:897–904.

160. Guo F, Liu B, Tang F, Lane S, Souslova EA, Chudakov DM, et al. Astroglia are a possible cellular substrate of angiotensin(1-7) effects in the rostral ventrolateral medulla. Cardiovasc Res. 2010;87:578–584.

161. Hilzendeger AM, Morgan DA, Brooks L, Dellsperger D, Liu X, Grobe JL, et al. A brain leptin-renin angiotensin system interaction in the regulation of sympathetic nerve activity. Am J Physiol Heart Circ Physiol. 2012;303:H197–206.

162. Kleiber AC, Zheng H, Sharma NM, Patel KP. Chronic AT1 receptor blockade normalizes NMDA-mediated changes in renal sympathetic nerve activity and NR1 expression within the PVN in rats with heart failure. American Journal of Physiology - Heart and Circulatory Physiology. 2010;298:H1546–H1555.

163. G.M. Verge, E.D. Milligan, S.F. Maier, L.R. Watkins, G.S. Naeve, A.C. Foster Fractalkine (CX3CL1) and fractalkine receptor (CX3CR1) distribution in spinal cord and dorsal root ganglia under basal and neuropathic pain conditions

Eur J Neurosci, 20 (2004), pp. 1150-1160.

164. Zubcevic J, Santisteban MM, Perez PD, Arocha R, Hiller H, Malphurs WL, Colon-Perez LM, Sharma RK, de Kloet A, Krause EG, Febo M, and Raizada MK. A Single Angiotensin II Hypertensive Stimulus Is Associated with Prolonged Neuronal and Immune System Activation in Wistar-Kyoto Rats. Front Physiol 8: 592, 2017.

165. de Man FS, Tu L, Handoko ML, Rain S, Ruiter G, Francois C, et al. Dysregulated renin-angiotensin-aldosterone system contributes to pulmonary arterial hypertension. Am J Respir Crit Care Med. 2012;186(8):780–789. doi: 10.1164/rccm.201203-0411OC.

166. Chung WK, Deng L, Carroll JS, Mallory N, Diamond B, Rosenzweig EB, et al. Polymorphism in the angiotensin II type 1 receptor (AGTR1) is associated with age at diagnosis in pulmonary arterial hypertension. J Heart Lung Transplant. 2009;28(4):373–379. doi: 10.1016/j.healun.2009.01.016.

167. Morrell NW, Atochina EN, Morris KG, Danilov SM, and Stenmark KR. Angiotensin converting enzyme expression is increased in small pulmonary arteries of rats with hypoxia-induced pulmonary hypertension. J Clin Invest 96: 1823–1833, 1995.

168. Morrell NW, Morris KG, and Stenmark KR. Role of angiotensin-converting enzyme and angiotensin II in development of hypoxic pulmonary hypertension. Am J Physiol 269: H1186–1194, 1995.

169. K.W. Ho, N.J. Ward, D.J. Calkins TRPV1: a stress response protein in the central nervous system. Am. J. Neurodegenerative Dis., 1 (2012), pp. 1-14

170. D. Martins, I. Tavares, C. Morgado. “Hotheaded”: the role of TRPV1 in brain functions. Neuropharmacology, 85 (2014), pp. 151-157

171. B.M. Assas, J.A. Miyan, J.L. Pennock Cross-talk between neural and immune receptors provides a potential mechanism of homeostatic regulation in the gut mucosa. Mucosal Immunol., 7 (2014), pp. 1283-1289

172. W.W. Chen, X.Q. Xiong, Q. Chen, Y.H. Li, Y.M. Kang, G.Q. Zhu, Cardiac sympathetic afferent reflex and its implications for sympathetic activation in chronic heart failure and hypertension, Acta Physiol. 213 (2015) 778–794.

173. M.R. Zahner, D.P. Li, S.R. Chen, H.L. Pan, Cardiac vanilloid receptor 1-expressing afferent nerves and their role in the cardiogenic sympathetic reflex in rats, J. Physiol. 551 (2003) 515–523.

174. Jia Y, Lee LY. Role of TRPV receptors in respiratory diseases. Biochim Biophys Acta. 2007 Aug;1772(8):915-27. doi: 10.1016/j.bbadis.2007.01.013. Epub 2007 Feb 1. Erratum in: Biochim Biophys Acta. 2007 Oct;1772(10):1182. PMID: 17346945.

175. Yoshie K, Rajendran PS, Massoud L, Kwon O, Tadimeti V, Salavatian S, Ardell JL, Shivkumar K, Ajijola OA. Cardiac vanilloid receptor-1 afferent depletion enhances stellate ganglion neuronal activity and efferent sympathetic response to cardiac stress. Am J Physiol Heart Circ Physiol. 2018 May 1;314(5):H954-H966. doi: 10.1152/ajpheart.00593.2017. Epub 2018 Jan 16. PMID: 29351450; PMCID: PMC6008140.

176. Bujak JK, Kosmala D, Szopa IM, Majchrzak K, Bednarczyk P. Inflammation, Cancer and Immunity-Implication of TRPV1 Channel. Front Oncol. 2019 Oct 16;9:1087. doi: 10.3389/fonc.2019.01087. PMID: 31681615; PMCID: PMC6805766.

177. T. Miyake, H. Shirakawa, T. Nakagawa, S. Kaneko Activation of mitochondrial transient receptor potential vanilloid 1 channel contributes to microglial migration. Glia, 63 (2015), pp. 1870-1882.

178. S. Hassan, K. Eldeeb, P.J. Millns, A.J. Bennett, S.P. Alexander, D.A. Kendall Cannabidiol enhances microglial phagocytosis via transient receptor potential (TRP) channel activation. Br. J. Pharmacol., 171 (2014), pp. 2426-2439.

179. W.X. Huang, F. Yu, R.M. Sanchez, Y.Q. Liu, J.W. Min, J.J. Hu, N.B. Bsoul, S. Han, J. Yin, W.H. Liu, X.H. He, B.W. Peng TRPV1 promotes repetitive febrile seizures by

pro-inflammatory cytokines in immature brain Brain Behav. Immun., 48 (2015), pp. 68-77.

180. T. Schilling, C. Eder Importance of the non-selective cation channel TRPV1 for microglial reactive oxygen species generation. J. Neuroimmunol., 216 (2009), pp. 118-121.

181. C.A. Reilly, J.L. Taylor, D.L. Lanza, B.A. Carr, D.J. Crouch, G.S. Yost Capsaicinoids cause inflammation and epithelial cell death through activation of vanilloid receptors. Toxicol. Sci., 73 (2003), pp. 170-181.

182. K.M. Walker, L. Urban, S.J. Medhurst, S. Patel, M. Panesar, A.J. Fox, P. McIntyre The VR1 antagonist capsazepine reverses mechanical hyperalgesia in models of inflammatory and neuropathic pain. J. Pharmacol. Exp. Ther., 304 (2003), pp. 56-62.

183. W.X. Huang, F. Yu, R.M. Sanchez, Y.Q. Liu, J.W. Min, J.J. Hu, N.B. Bsoul, S. Han, J. Yin, W.H. Liu, X.H. He, B.W. Peng TRPV1 promotes repetitive febrile seizures by pro-inflammatory cytokines in immature brain. Brain Behav. Immun., 48 (2015), pp. 68-77.

184. D. Centonze, L. Muzio, S. Rossi, F. Cavasinni, V. De.Chiara, A. Bergami, A. Musell a, M. D'Amelio, V. Cavallucci, A. Martorana, A. Bergamaschi, M.T. Cencioni, A. Dia mantini, E. Butti, G. Comi, G. Bernardi, F. Ceccon, L. Battistini, R. Furlan, G. Martino Inflammation triggers synaptic alteration and degeneration in experimental autoimmune encephalomyelitis. J. Neurosci., 29 (2009), pp. 3442-3452

185. Saffarzadeh, M.J. Eslamizade, T. Ghadiri, S.M. Modarres.Mousavi, M. Hadjighasse m, A. Gorji Effects of TRPV1 on the hippocampal synaptic plasticity in the epileptic rat brain. Synapse, 69 (2015), pp. 375-383.

186. Kong WL, Peng YY, Peng BW. Modulation of neuroinflammation: Role and therapeutic potential of TRPV1 in the neuro-immune axis. Brain Behav Immun. 2017 Aug;64:354-366. doi: 10.1016/j.bbi.2017.03.007. Epub 2017 Mar 22. PMID: 28342781.

187. S. Bertin, E. Raz Transient Receptor Potential (TRP) channels in T cells. Semin. immunopathol., 38 (2016), pp. 309-319.

188. Yoshida A, Furube E, Mannari T, Takayama Y, Kittaka H, Tominaga M, Miyata S. TRPV1 is crucial for proinflammatory STAT3 signaling and thermoregulation-associated pathways in the brain during inflammation. Sci Rep. 2016;6:26088.

189. H. Min, H. Lee, H. Lim, Y.H. Jang, S.J. Chung, C.J. Lee, S.J. Lee. TLR4 enhances histamine-mediated pruritus by potentiating TRPV1 activity. Mol. Brain, 7 (2014), pp. 59-68.

190. A. Diogenes, C.C. Ferraz, A.N. Akopian, M.A. Henry, K.M. Hargreaves LPS sensitizes TRPV1 via activation of TLR4 in trigeminal sensory neurons. J. Dent. Res., 90 (2011), pp. 759-764.

191. T.L. Nguyen, S.H. Kwon, S.I. Hong, S.X. Ma, Y.H. Jung, J.Y. Hwang, H.C. Kim, S.Y . Lee, C.G. Jang Transient receptor potential vanilloid type 1 channel may modulate opioid reward. Neuropsychopharmacology: official publication of the American College of. Neuropsychopharmacology, 39 (2014), pp. 2414-2422.

192. Henry RJ, Kerr DM, Flannery LE, Killilea M, Hughes EM, Corcoran L, Finn DP, Roche M. Pharmacological inhibition of FAAH modulates TLR-induced neuroinflammation, but not sickness behaviour: An effect partially mediated by central TRPV1. Brain Behav Immun. 2017 May;62:318-331. doi: 10.1016/j.bbi.2017.02.016. Epub 2017 Feb 22. PMID: 28237711.

193. Pan XQ, Gonzalez JA, Chang S, et al. Experimental colitis triggers the release of substance P and calcitonin gene-related peptide in the urinary bladder via TRPV1 signaling pathways. Exp Neurol. 2010;225:262–273.

194. Xu P, Shao RR, He Y. Bibliometric analysis of recent research on the association between TRPV1 and inflammation. Channels (Austin). 2023 Dec;17(1):2189038. doi: 10.1080/19336950.2023.2189038. PMID: 36919561; PMCID: PMC10026872.

195. Kaewpitak A, Bauer CS, Seward EP, et al. Porphyromonas gingivalis lipopolysaccharide rapidly activates trigeminal sensory neurons and may contribute to pulpal pain. Int Endod J. 2020;53:846–858.

196. Song J, Kang J, Lin B, Li J, Zhu Y, Du J, et al.. Mediating role of TRPV1 ion channels in the co-exposure to PM2.5 and formaldehyde of Balb/c mice asthma model. Sci Rep. (2017) 7:11926. 10.1038/s41598-017-11833-6.

197. Carletti F, Gambino G, Rizzo V, Ferraro G, Sardo P. Neuronal nitric oxide synthase is involved in CB/TRPV1 signalling: Focus on control of hippocampal hyperexcitability. Epilepsy Res. 2017 Dec;138:18-25. doi: 10.1016/j.eplepsyres.2017.09.018. Epub 2017 Oct 3. PMID: 29035821.

198. Chen Y, Willcockson HH, Valtschanoff JG. Influence of the vanilloid receptor TRPV1 on the activation of spinal cord glia in mouse models of pain. Exp Neurol. 2009 Dec;220(2):383-90. doi: 10.1016/j.expneurol.2009.09.030. Epub 2009 Oct 6. PMID: 19815011; PMCID: PMC2784271.

199. Hwang SJ, Burette A, Rustioni A, Valtschanoff JG. Vanilloid receptor VR1-positive primary afferents are glutamatergic and contact spinal neurons that co-express neurokinin receptor NK1 and glutamate receptors. J Neurocytol. 2004 May;33(3):321-9. doi: 10.1023/B:NEUR.0000044193.31523.a1. PMID: 15475687.

200. K. Fujiu, M. Shibata, Y. Nakayama, F. Ogata, S. Matsumoto, K. Noshita, et al., A heart-brain-kidney network controls adaptation to cardiac stress through tissue macrophage activation, Nat. Med. 23 (2017) 611–622.

201. Wang D., Wu Y., Chen Y., Wang A., Lv K., Kong X., et al. (2019). Focal Selective Chemo-Ablation of Spinal Cardiac Afferent Nerve by Resiniferatoxin Protects the Heart from Pressure Overload-Induced Hypertrophy. Biomed. Pharmacother. 109, 377–385. 10.1016/j.biopha.2018.10.156.

202. M. Bishnoi, C.A. Bosgraaf, L.S. Premkumar, Preservation of acute pain and efferent functions following intrathecal resiniferatoxin-induced analgesia in rats, J. Pain 12 (2011) 991–1003.

203. M. Leo, M. Schulte, L.I. Schmitt, M. Schafers, C. Kleinschnitz, T. Hagenacker, Intrathecal resiniferatoxin modulates TRPV1 in DRG neurons and reduces TNF-induced pain-related behavior, Mediat. Inflamm. 2017 (2017) 2786427.

204. T. Schilling, C. Eder Stimulus-dependent requirement of ion channels for microglial NADPH oxidase-mediated production of reactive oxygen species. J. Neuroimmunol., 225 (2010), pp. 190-194.

205. Talbot S, Dias JP, Lahjouji K, Bogo MR, Campos MM, Gaudreau P, Couture R. Activation of TRPV1 by capsaicin induces functional kinin B(1) receptor in rat spinal cord microglia. J Neuroinflammation. 2012 Jan 20;9:16. doi: 10.1186/1742-2094-9-16. PMID: 22264228; PMCID: PMC3282640.

206. M. Naziroglu Molecular role of catalase on oxidative stress-induced Ca(2+) signaling and TRP cation channel activation in nervous system. J. Recept. Signal Transduction Res., 32 (2012), pp. 134-141.

207. Y. Marchalant, H.M. Brothers, G.J. Norman, K. Karelina, A.C. DeVries, G.L. Wenk Cannabinoids attenuate the effects of aging upon neuroinflammation and neurogenesis. Neurobiol. Dis., 34 (2009), pp. 300-307.

208. E.S. Fernandes, C.X. Brito, S.A. Teixeira, R. Barboza, A.S. dos Reis, A.P. Azevedo-Santos, M. Muscara, S.K. Costa, C.R. Marinho, S.D. Brain, M.A. Grisotto TRPV1 antagonism by capsazepine modulates innate immune response in mice infected with Plasmodium berghei ANKA. Mediators Inflamm., 2014 (2014), pp. 506450-506461.

209. Z. Feng, L.V. Pearce, Y. Zhang, C. Xing, B.K. Herold, S. Ma, Z. Hu, N.A. Turcios, P. Yang, Q. Tong, A.K. McCall, P.M. Blumberg, X.Q. Xie Multi-Functional Diarylurea Small Molecule Inhibitors of TRPV1 with Therapeutic Potential for Neuroinflammation. AAPS J, 18 (2016), pp. 898-913.

210. Miyanohara J, Shirakawa H, Sanpei K, Nakagawa T, Kaneko S. A pathophysiological role of TRPV1 in ischemic injury after transient focal cerebral ischemia in mice. Biochem Biophys Res Commun. 2015 Nov 20;467(3):478-83. doi: 10.1016/j.bbrc.2015.10.027. Epub 2015 Oct 8. PMID: 26456642.

211. K.W. Ho, W.S. Lambert, D.J. Calkins Activation of the TRPV1 cation channel contributes to stress-induced astrocyte migration. Glia, 62 (2014), pp. 1435-1451.

212. M. Leonelli, D.O. Martins, L.R. Britto TRPV1 receptors are involved in protein nitration and Muller cell reaction in the acutely axotomized rat retina. Exp. Eye Res., 91 (2010), pp. 755-768.

213. T. Mannari, S. Morita, E. Furube, M. Tominaga, S. Miyata Astrocytic TRPV1 ion channels detect blood-borne signals in the sensory circumventricular organs of adult mouse brains. Glia, 61 (2013), pp. 957-971.

214. S. Marinelli, V. Di Marzo, N. Berretta, I. Matias, M. Maccarrone, G. Bernardi, N.B. Mercuri, Presynaptic facilitation of glutamatergic synapses to dopaminergic neurons of the rat substantia nigra by endogenous stimulation of vanilloid receptors, J. Neurosci. 23 (2003) 3136e3144.

215. H.E. Gibson, J.G. Edwards, R.S. Page, M.J. Van Hook, J.A. Kauer, TRPV1 channels mediate long-term depression at synapses on hippocampal interneurons, Neuron 57 (2008) 746e759.

216. A. Musella, V. De Chiara, S. Rossi, C. Prosperetti, G. Bernardi, M. Maccarrone, D. Centonze, TRPV1 channels facilitate glutamate transmission in the striatum, Mol. Cell Neurosci. 40 (2009) 89e97.

217. K. Shoudai, J.H. Peters, S.J. McDougall, J.A. Fawley, M.C. Andresen, Thermally active TRPV1 tonically drives central spontaneous glutamate release, J. Neurosci. 30 (2010) 14470e14475.

218. A.E. Chavez, C.Q. Chiu, P.E. Castillo, TRPV1 activation by endogenous anandamide triggers postsynaptic long-term depression in dentate gyrus, Nat. Neurosci. 13 (2010) 1511e1518.

219. B.A. Grueter, G. Brasnjo, R.C. Malenka, Postsynaptic TRPV1 triggers cell type specific long-term depression in the nucleus accumbens, Nat. Neurosci. 13 (2010) 1519e1525.

220. M. Groger, D. Lebesgue, D. Pruneau, J. Relton, S.W. Kim, J. Nussberger, € N. Plesnila, Release of bradykinin and expression of kinin B2 receptors in the brain:

role for cell death and brain edema formation after focal cerebral ischemia in mice, J. Cereb. Blood Flow. Metab. 25 (2005) 978e989.

221. T. Kawano, J. Anrather, P. Zhou, L. Park, G. Wang, K.A. Frys, A. Kunz, S. Cho, M. Orio, C. Iadecola, Prostaglandin E2 EP1 receptors: downstream effectors of COX-2 neurotoxicity, Nat. Med. 12 (2006) 225e229.

222. M. Tominaga, T. Tominaga Structure and function of TRPV1. Pflugers Arch., 451 (2005), pp. 143-150.

223. P. Sikand, L.S. Premkumar, Potentiation of glutamatergic synaptic transmission by protein kinase C-mediated sensitization of TRPV1 at the first sensory synapse, J. Physiol. 581 (2007) 631e647.

224. Peng J, Li YJ. The vanilloid receptor TRPV1: role in cardiovascular and gastrointestinal protection. Eur J Pharmacol. 2010 Feb 10;627(1-3):1-7. doi: 10.1016/j.ejphar.2009.10.053. Epub 2009 Oct 30. PMID: 19879868.

225. Mourão AA, Shimoura CG, Andrade MA, Truong TT, Pedrino GR, Toney GM. Local ionotropic glutamate receptors are required to trigger and sustain ramping of sympathetic nerve activity by hypothalamic paraventricular nucleus TNFα. Am J Physiol Heart Circ Physiol. 2021 Sep 1;321(3):H580-H591. doi: 10.1152/ajpheart.00322.2021. Epub 2021 Aug 6. PMID: 34355986; PMCID: PMC8461846.

226. Sved AF. Tonic glutamatergic drive of RVLM vasomotor neurons? Am J Physiol Regul Integr Comp Physiol. 2004 Dec;287(6):R1301-3. doi: 10.1152/ajpregu.00616.2004. PMID: 15528400.

227. T.W. Lai, S. Zhang, Y.T. Wang, Excitotoxicity and stroke: identifying novel targets for neuroprotection, Prog. Neurobiol. 115 (2014) 157e188.

228. A. Franklin, S. Parmentier-Batteur, L. Walter, D.A. Greenberg, N. Stella, palmitoylethanolamide increases after focal cerebral ischemia and potentiates microglial cell motility, J. Neurosci. 23 (2003) 7767e7775.

229. S. Muthian, D.J. Rademacher, C.T. Roelke, G.J. Gross, C.J. Hillard, Anandamide content is increased and CB1 cannabinoid receptor blockade is protective during transient, focal cerebral ischemia, Neuroscience 129 (2004) 743e750.

230. M.R. Zahner, D.P. Li, S.R. Chen, H.L. Pan, Cardiac vanilloid receptor 1-expressing afferent nerves and their role in the cardiogenic sympathetic reflex in rats, J. Physiol. 551 (2003) 515–523.

231. H.J. Wang, W. Wang, K.G. Cornish, G.J. Rozanski, I.H. Zucker, Cardiac sympathetic afferent denervation attenuates cardiac remodeling and improves cardiovascular dysfunction in rats with heart failure, Hypertension 64 (2014) 745–755.

232. G.Q. Zhu, Y. Xu, L.M. Zhou, Y.H. Li, L.M. Fan, W. Wang, et al., Enhanced cardiac sympathetic afferent reflex involved in sympathetic overactivity in renovascular hypertensive rats, Exp. Physiol. 94 (2009) 785–794.

233. J. Shanks, Z. Xia, S.J. Lisco, G.J. Rozanski, H.D. Schultz, I.H. Zucker, et al., Sympatho-excitatory response to pulmonary chemosensitive spinal afferent activation in anesthetized, vagotomized rats, Physiol. Rep. 6 (2018) e13742.

234. Martin E, Dahan D, Cardouat G, Gillibert-Duplantier J, Marthan R, Savineau JP, Ducret T. Involvement of TRPV1 and TRPV4 channels in migration of rat pulmonary arterial smooth muscle cells. Pflugers Arch. 2012 Sep;464(3):261-72. doi: 10.1007/s00424-012-1136-5. Epub 2012 Jul 22. PMID: 22820913.

235. Parpaite T, Cardouat G, Mauroux M, Gillibert-Duplantier J, Robillard P, Quignard JF, Marthan R, Savineau JP, Ducret T. Effect of hypoxia on TRPV1 and TRPV4 channels in rat pulmonary arterial smooth muscle cells. Pflugers Arch. 2016 Jan;468(1):111-130. doi: 10.1007/s00424-015-1704-6. Epub 2015 Mar 24. PMID: 25799977.

236. Lo CCW, Moosavi SM, Bubb KJ. The Regulation of Pulmonary Vascular Tone by Neuropeptides and the Implications for Pulmonary Hypertension. Front Physiol. 2018 Aug 23;9:1167. doi: 10.3389/fphys.2018.01167. PMID: 30190678; PMCID: PMC6116211.

237. Xu Y, Gu Q, Qu C. Capsaicin pretreatment reversed pulmonary arterial hypertension by alleviating inflammation via p38MAPK pathway. Exp Lung Res. 2017 Feb;43(1):8-18. doi: 10.1080/01902148.2016.1271481. Epub 2017 Mar 10. PMID: 28281854.

238. Zhou, K. R., and Lai, Y. L. (1993). Capsaicin pretreatment attenuates monocrotaline-induced ventilatory dysfunction and pulmonary hypertension. J. Appl. Physiol. 75, 2781–2788. doi: 10.1152/jappl.1993.75.6.2781.

239. Katzman, N. J., and Lai, Y. L. (2000). Capsaicin pre- and post-treatment on rat monocrotaline pneumotoxicity. Chin. J. Physiol. 43, 171–178.

240. Du Q, Liao Q, Chen C, Yang X, Xie R, Xu J. The Role of Transient Receptor Potential Vanilloid 1 in Common Diseases of the Digestive Tract and the Cardiovascular and Respiratory System. Front Physiol. 2019 Aug 21;10:1064. doi: 10.3389/fphys.2019.01064. PMID: 31496955; PMCID: PMC6712094.

241. Randhawa PK, Jaggi AS. $TRPV_1$ channels in cardiovascular system: A double edged sword? Int J Cardiol. 2017 Feb 1;228:103-113. doi: 10.1016/j.ijcard.2016.11.205. Epub 2016 Nov 9. PMID: 27863349.

242. Lu S., Xu D. (2013). Cold Stress Accentuates Pressure Overload-Induced Cardiac Hypertrophy and Contractile Dysfunction: Role of TRPV1/AMPK-Mediated Autophagy. Biochem. Biophysical Res. Commun. 442, 8–15. 10.1016/j.bbrc.2013.10.128.

243. J.S. Horton, C.L. Buckley, A.J. Stokes Successful TRPV1 antagonist treatment for cardiac hypertrophy and heart failure in mice Channels (Austin), 7 (1) (Jan 1 2013), pp. 17-22.

244. Zhang X, Wang D, Zhang B, Zhu J, Zhou Z, Cui L. Regulation of microglia by glutamate and its signal pathway in neurodegenerative diseases. Drug Discov Today. 2020 Jun;25(6):1074-1085. doi: 10.1016/j.drudis.2020.04.001. Epub 2020 Apr 19. PMID: 32320851.

245. Liu, H.; Leak, R.K.; Hu, X. Neurotransmitter receptors on microglia. Stroke Vasc. Neurol. 2016, 1, 52–58.

246. Karim F, Wang CC, Gereau RW 4th. Metabotropic glutamate receptor subtypes 1 and 5 are activators of extracellular signal-regulated kinase signaling required for inflammatory pain in mice. J Neurosci. 2001 Jun 1;21(11):3771-9. doi: 10.1523/JNEUROSCI.21-11-03771.2001. PMID: 11356865; PMCID: PMC6762705.

247. Pacheco, R.; Ciruela, F.; Casadó, V.; Mallol, J.; Gallart, T.; Lluis, C.; Franco, R. Group I metabotropic glutamate receptors mediate a dual role of glutamate in T cell activation. J. Biol. Chem. 2004, 279, 33352–33358.

248. A. Kumar, et al. Therapeutic potential of mGluR5 targeting in Alzheimer's disease Front. Neurosci., 9 (2015), p. 215.

249. Fazio F, Ulivieri M, Volpi C, Gargaro M, Fallarino F. Targeting metabotropic glutamate receptors for the treatment of neuroinflammation. Curr Opin Pharmacol. 2018 Feb;38:16-23. doi: 10.1016/j.coph.2018.01.010. Epub 2018 Feb 19. PMID: 29471184.

250. H. Takeuchi, et al. Tumor necrosis factor-α induces neurotoxicity via glutamate release from hemichannels of activated microglia in an autocrine manner. J. Biol. Chem., 281 (2006), pp. 21362-21368.

251. Kaindl, A.M.; Degos, V.; Peineau, S.; Gouadon, E.; Chhor, V.; Loron, G.; Le Charpentier, T.; Josserand, J.; Ali, C.; Vivien, D.; et al. Activation of microglial N-methyl-D-aspartate receptors triggers inflammation and neuronal cell death in the developing and mature brain. Ann. Neurol. 2012, 72, 536–549.

252. Raghunatha, P.; Vosoughi, A.; Kauppinen, T.M.; Jackson, M.F. Microglial NMDA receptors drive pro-inflammatory responses via PARP-1/TRMP2 signaling. Glia 2020, 68, 1421–1434.

253. A. Ivanov, et al. Opposing role of synaptic and extrasynaptic NMDA receptors in regulation of the extracellular signal-regulated kinases (ERK) activity in cultured rat hippocampal neurons. J. Physiol., 572 (2006), pp. 789-798.

254. Lin, C. L., Kong, Q., Cuny, G. D., and Glicksman, M. A. (2012). Glutamate transporter EAAT2: a new target for the treatment of neurodegenerative diseases. Future Med. Chem. 4, 1689–1700. doi: 10.4155/fmc.12.122.

255. Ahlawat A, Rana A, Goyal N, Sharma S. Potential role of nitric oxide synthase isoforms in pathophysiology of neuropathic pain. Inflammopharmacology. 2014

Oct;22(5):269-78. doi: 10.1007/s10787-014-0213-0. Epub 2014 Aug 6. PMID: 25095760.

256. Rameau GA, Chiu LY, Ziff EB. NMDA receptor regulation of nNOS phosphorylation and induction of neuron death. Neurobiol Aging. 2003 Dec;24(8):1123-33. doi: 10.1016/j.neurobiolaging.2003.07.002. PMID: 14643384.

257. Freire MA, Guimarães JS, Leal WG, Pereira A. Pain modulation by nitric oxide in the spinal cord. Front Neurosci. 2009 Sep 15;3(2):175-81. doi: 10.3389/neuro.01.024.2009. PMID: 20011139; PMCID: PMC2751623.

258. Dutta, R., and Trapp, B. D. (2011). Mechanisms of neuronal dysfunction and degeneration in multiple sclerosis. Prog. Neurobiol. 93, 1–12. doi: 10.1016/j.pneurobio.2010.09.005.

259. Chan SH, Wang LL, Wang SH, Chan JY. Differential cardiovascular responses to blockade of nNOS or iNOS in rostral ventrolateral medulla of the rat. Br J Pharmacol. 2001 Jun;133(4):606-14. doi: 10.1038/sj.bjp.0704105. PMID: 11399678; PMCID: PMC1572812.

260. Wang Y, Golledge J. Neuronal nitric oxide synthase and sympathetic nerve activity in neurovascular and metabolic systems. Curr Neurovasc Res. 2013 Feb;10(1):81-9. doi: 10.2174/156720213804805963. PMID: 23151079.

261. Vayssettes-Courchay C, Bouysset F, Verbeuren TJ. Involvement of COX and NOS induction in the sympatho-activation during sepsis. Auton Neurosci. 2002 Jun 28;98(1-2):33-6. doi: 10.1016/s1566-0702(02)00027-9. PMID: 12144036.

262. Cury Y, Picolo G, Gutierrez VP, Ferreira SH. Pain and analgesia: The dual effect of nitric oxide in the nociceptive system. Nitric Oxide. 2011 Oct 30;25(3):243-54. doi: 10.1016/j.niox.2011.06.004. Epub 2011 Jun 24. PMID: 21723953.

263. Janes K, Neumann WL, Salvemini D. Anti-superoxide and anti-peroxynitrite strategies in pain suppression. Biochim Biophys Acta. 2012 May;1822(5):815-21. doi: 10.1016/j.bbadis.2011.12.008. Epub 2011 Dec 19. PMID: 22200449; PMCID: PMC3478755.

264. Pacher P, Beckman JS, Liaudet L. Nitric oxide and peroxynitrite in health and disease. Physiol Rev. 2007 Jan;87(1):315-424. doi: 10.1152/physrev.00029.2006. PMID: 17237348; PMCID: PMC2248324.

265. Du D, Hu L, Wu J, Wu Q, Cheng W, Guo Y, Guan R, Wang Y, Chen X, Yan X, Zhu D, Wang J, Zhang S, Guo Y, Xia C. Neuroinflammation contributes to autophagy flux blockage in the neurons of rostral ventrolateral medulla in stress-induced hypertension rats. J Neuroinflammation. 2017 Aug 23;14(1):169. doi: 10.1186/s12974-017-0942-2. PMID: 28835252; PMCID: PMC5569471.

266. Pacher P, Beckman JS, Liaudet L. Nitric oxide and peroxynitrite in health and disease. Physiol Rev. 2007 Jan;87(1):315-424. doi: 10.1152/physrev.00029.2006. PMID: 17237348; PMCID: PMC2248324.

267. Calabrese V, Mancuso C, Calvani M, Rizzarelli E, Butterfield DA, Stella AM. Nitric oxide in the central nervous system: neuroprotection versus neurotoxicity. Nat Rev Neurosci. 2007 Oct;8(10):766-75. doi: 10.1038/nrn2214. PMID: 17882254.

268. Poon YY, Tsai CY, Cheng CD, Chang AY, Chan SH. Endogenous nitric oxide derived from NOS I or II in thoracic spinal cord exerts opposing tonic modulation on sympathetic vasomotor tone via disparate mechanisms in anesthetized rats. Am J Physiol Heart Circ Physiol. 2016 Sep 1;311(3):H555-62. doi: 10.1152/ajpheart.00246.2016. Epub 2016 Jul 1. PMID: 27371683.

269. Ji SM, Wang ZM, Li XP, He RR. Intracerebroventricular administration of adrenomedullin increases the expression of c-fos and activates nitric oxide-producing neurons in rat cardiovascular related brain nuclei. Sheng Li Xue Bao. 2004 Jun 25;56(3):328-34. PMID: 15224145.

270. Matsumura K, Tsuchihashi T, Kagiyama S, Abe I, Fujishima M. Role of nitric oxide in the nucleus of the solitary tract of rats. Brain Res. 1998 Jul 6;798(1-2):232-8. doi: 10.1016/s0006-8993(98)00420-x. PMID: 9666137.

271. Morimoto S, Sasaki S, Miki S, Kawa T, Nakamura K, Itoh H, Nakata T, Takeda K, Nakagawa M, Fushiki S. Nitric oxide is an excitatory modulator in the rostral ventrolateral medulla in rats. Am J Hypertens. 2000 Oct;13(10):1125-34. doi: 10.1016/s0895-7061(00)01182-1. PMID: 11041168.

272. McKeogh DF, O'Donaughy TL, Brooks VL. NO and endogenous angiotensin II interact in the generation of renal sympathetic nerve activity in conscious rats. Am J Physiol Heart Circ Physiol. 2004 Apr;286(4):H1258-65. doi: 10.1152/ajpheart.00791.2003. Epub 2003 Dec 4. PMID: 14656704.

273. P.M. Hughes, M.S. Botham, S. Frentzel, A. Mir, V.H. Perry Expression of fractalkine (CX3CL1) and its receptor, CX3CR1, during acute and chronic inflammation in the rodent CNS Glia, 37 (2002), pp. 314-327.

274. J.F. Bazan, K.B. Bacon, G. Hardiman, W. Wang, K. Soo, D. Rossi, D.R. Greaves, A . Zlotnik, T.J. Schall A new class of membrane-bound chemokine with a CX3C motif Nature, 385 (1997), pp. 640-644.

275. A. Nishiyori, M. Minami, Y. Ohtani, S. Takami, J. Yamamoto, N. Kawaguchi, T. Kum e, A. Akaike, M. Satoh Localization of fractalkine and CX3CR1 mRNAs in rat brain:

does fractalkine play a role in signaling from neuron to microglia? FEBS Lett, 429 (1998), pp. 167-172.

276. J.K. Harrison, Y. Jiang, S. Chen, Y. Xia, D. Maciejewski, R.K. McNamara, W.J. Strei t, M.N. Salafranca, S. Adhikari, D.A. Thompson, et al. Role for neuronally derived fractalkine in mediating interactions between neurons and CX3CR1-expressing microglia Proc Natl Acad Sci USA, 95 (1998), pp. 10896-10901.

277. Du D, Jiang M, Liu M, et al. Microglial P2X(7) receptor in the hypothalamic paraventricular nuclei contributes to sympathoexcitatory responses in acute myocardial infarction rat. Neurosci Lett. 2015;587:22–28. doi: 10.1016/j.neulet.2014.12.026.

278. Z.Y. Zhuang, Y. Kawasaki, P.H. Tan, Y.R. Wen, J. Huang, R.R. Ji Role of the CX3CR1/p38 MAPK pathway in spinal microglia for the development of neuropathic pain following nerve injury-induced cleavage of fractalkine Brain Behav Immun, 21 (2007), pp. 642-651.

279. A.K. Clark, P.K. Yip, J. Grist, C. Gentry, A.A. Staniland, F. Marchand, M. Dehvari, G . Wotherspoon, J. Winter, J. Ullah, et al. Inhibition of spinal microglial cathepsin S for the reversal of neuropathic pain Proc Natl Acad Sci USA, 104 (2007), pp. 10655-10660.

280. Old EA, Malcangio M. Chemokine mediated neuron-glia communication and aberrant signalling in neuropathic pain states. Curr Opin Pharmacol. 2012 Feb;12(1):67-73. doi: 10.1016/j.coph.2011.10.015. Epub 2011 Nov 3. PMID: 22056024.

281. Rogers, J.T. et al. CX3CR1 deficiency leads to impairment of hippocampal cognitive function and synaptic plasticity. J. Neurosci. 31, 16241–16250 (2011).

282. Ho CY, Lin YT, Chen HH, Ho WY, Sun GC, Hsiao M, Lu PJ, Cheng PW, Tseng CJ. CX3CR1-microglia mediates neuroinflammation and blood pressure regulation in the nucleus tractus solitarii of fructose-induced hypertensive rats. J Neuroinflammation. 2020 Jun 12;17(1):185. doi: 10.1186/s12974-020-01857-7. PMID: 32532282; PMCID: PMC7291459.

283. Zhang S, Hu L, Jiang J, Li H, Wu Q, Ooi K, Wang J, Feng Y, Zhu D, Xia C. HMGB1/RAGE axis mediates stress-induced RVLM neuroinflammation in mice via impairing mitophagy flux in microglia. J Neuroinflammation. 2020 Jan 10;17(1):15. doi: 10.1186/s12974-019-1673-3. PMID: 31924219; PMCID: PMC6953162.

284. Balabanian K, Foussat A, Dorfmuller P, Durand-Gasselin I, Capel F, Bouchet-Delbos L, Portier A, Marfaing-Koka A, Krzysiek R, Rimaniol AC, Simonneau G, Emilie D, Humbert M. CX(3)C chemokine fractalkine in pulmonary arterial hypertension. Am J Respir Crit Care Med. 2002;165:1419–1425.

285. Popovic M, Laumonnier Y, Burysek L, Syrovets T, Simmet T. Thrombin-induced expression of endothelial CX3CL1 potentiates monocyte CCL2 production and transendothelial migration. J Leukoc Biol. 2008;84:215–223.

286. McComb JG, Ranganathan M, Liu XH, Pilewski JM, Ray P, Watkins SC, Choi AM, Lee JS. CX3CL1 up-regulation is associated with recruitment of CX3CR1+ mononuclear phagocytes and T lymphocytes in the lungs during cigarette smoke-induced emphysema. Am J Pathol. 2008;173:949–961.

287. Dichmann S, Herouy Y, Purlis D, Rheinen H, Gebicke-Harter P, Norgauer J. Fractalkine induces chemotaxis and actin polymerization in human dendritic cells. Inflamm Res. 2001;50:529–533.

288. Nevo I, Sagi-Assif O, Meshel T, Ben-Baruch A, Johrer K, Greil R, Trejo LE, Kharenko O, Feinmesser M, Yron I, Witz IP. The involvement of the fractalkine receptor in the transmigration of neuroblastoma cells through bone-marrow endothelial cells. Cancer Lett. 2009;273:127–139.

289. Zhang J, Patel JM. Role of the CX3CL1-CX3CR1 axis in chronic inflammatory lung diseases. Int J Clin Exp Med. 2010 Aug 10;3(3):233-44. PMID: 20827321; PMCID: PMC2929949.

290. Zhang J, Hu H, Palma NL, Harrison JK, Mubarak KK, Carrie RD, Alnuaimat H, Shen X, Luo D, Patel JM. Hypoxia-induced endothelial CX3CL1 triggers lung smooth muscle cell phenotypic switching and proliferative expansion. Am J Physiol Lung Cell Mol Physiol. 2012 Nov 15;303(10):L912-22. doi: 10.1152/ajplung.00014.2012. Epub 2012 Sep 21. PMID: 23002075; PMCID: PMC3517676.

291. Wang M, Pan W, Xu Y, Zhang J, Wan J, Jiang H. Microglia-Mediated Neuroinflammation: A Potential Target for the Treatment of Cardiovascular Diseases. J Inflamm Res. 2022 May 25;15:3083-3094. doi: 10.2147/JIR.S350109. PMID: 35642214; PMCID: PMC9148574.

292. Segiet A, Smykiewicz P, Kwiatkowski P, et al. Tumour necrosis factor and interleukin 10 in blood pressure regulation in spontaneously hypertensive and normotensive rats. Cytokine. 2019;113:185–194. doi: 10.1016/j.cyto.2018.07.003.

293. Wu KLH, Chan SHH, Chan JYH. Neuroinflammation and oxidative stress in rostral ventrolateral medulla contribute to neurogenic hypertension induced by systemic inflammation. J Neuroinflammation. 2012;9(1):212. doi: 10.1186/1742-2094-9-212.

294. Shen XZ, Li Y, Li L, et al. Microglia participate in neurogenic regulation of hypertension. Hypertension. 2015;66(2):309–316. doi: 10.1161/HYPERTENSIONAHA.115.05333.

295. Wang Y, Hu H, Yin J, Shi Y, Tan J, Zheng L, Wang C, Li X, Xue M, Liu J, Wang Y, Li Y, Li X, Liu F, Liu Q, Yan S. TLR4 participates in sympathetic hyperactivity Post-MI in the PVN by regulating NF-κB pathway and ROS production. Redox Biol. 2019 Jun;24:101186. doi: 10.1016/j.redox.2019.101186. Epub 2019 Apr 2. PMID: 30978539; PMCID: PMC6460304.

296. Wang Y, Yin J, Wang C, Hu H, Li X, Xue M, Liu J, Cheng W, Wang Y, Li Y, Shi Y, Tan J, Li X, Liu F, Liu Q, Yan S. Microglial Mincle receptor in the PVN contributes to sympathetic hyperactivity in acute myocardial infarction rat. J Cell Mol Med. 2019 Jan;23(1):112-125. doi: 10.1111/jcmm.13890. Epub 2018 Oct 24.

297. Santisteban MM, Ahmari N, Carvajal JM, et al. Involvement of bone marrow cells and neuroinflammation in hypertension. Circ Res. 2015;117(2):178–191. doi: 10.1161/CIRCRESAHA.117.305853.

298. Sharma RK, Yang T, Oliveira AC, et al. Microglial cells impact gut microbiota and gut pathology in angiotensin II-induced hypertension. Circ Res. 2019;124(5):727–736. doi: 10.1161/CIRCRESAHA.118.313882.

299. Badoer E. Microglia: activation in acute and chronic inflammatory states and in response to cardiovascular dysfunction. Int J Biochem Cell Biol. 2010;42(10):1580–1585. doi: 10.1016/j.biocel.2010.07.005.

300. Rana I, Stebbing M, Kompa A, et al. Microglia activation in the hypothalamic PVN following myocardial infarction. Brain Res. 2010;1326:96–104. doi: 10.1016/j.brainres.2010.02.028 .

301. Francis J, Chu Y, Johnson AK, et al. Acute myocardial infarction induces hypothalamic cytokine synthesis. Am J Physiol Heart Circ Physiol. 2004;286(6):H2264–71. doi: 10.1152/ajpheart.01072.2003.

302. Dworak M, Stebbing M, Kompa AR, et al. Sustained activation of microglia in the hypothalamic PVN following myocardial infarction. Auton Neurosci. 2012;169(2):70–76. doi: 10.1016/j.autneu.2012.04.004.

303. Dworak M, Stebbing M, Kompa AR, et al. Attenuation of microglial and neuronal activation in the brain by ICV minocycline following myocardial infarction. Auton Neurosci. 2014;185:43–50. doi: 10.1016/j.autneu.2014.03.007.

304. Milanez MIO, Nishi EE, Bergamaschi CT, Campos RR. Role of spinal neurons in the maintenance of elevated sympathetic activity: a novel therapeutic target? Am J Physiol Regul Integr Comp Physiol. 2020 Sep 1;319(3):R282-R287. doi: 10.1152/ajpregu.00122.2020. Epub 2020 Jun 24. PMID: 32579387.

305. Young KC, Hussein SM, Dadiz R, de Mello D, Devia C, Hehre D, et al. Toll-like receptor 4-deficient mice are resistant to chronic hypoxia-induced pulmonary hypertension. Exp Lung Res. 2010;36(2):111–119. doi: 10.3109/01902140903171610.

306. Cerbai F, Lana D, Nosi D, Petkova-Kirova P, Zecchi S, Brothers HM, Wenk GL, Giovannini MG. The neuron-astrocyte-microglia triad in normal brain ageing and in a model of neuroinflammation in the rat hippocampus. PLoS One. 2012;7(9):e45250. doi: 10.1371/journal.pone.0045250. Epub 2012 Sep 18. PMID: 23028880; PMCID: PMC3445467.

307. Biancardi VC, Stranahan AM, Krause EG, et al. Cross talk between AT 1 receptors and Toll-like receptor 4 in microglia contributes to angiotensin II-derived ROS

production in the hypothalamic paraventricular nucleus. Am J Physiol Heart Circ Physiol. 2016;310(3):H404–H415. doi: 10.1152/ajpheart.00247.2015.

308. Zhao, W.; Xie, W.; Le, W.; Beers, D.R.; He, Y.; Henkel, J.S.; Simpson, E.P.; Yen, A.A.; Xiao, Q.; Appel, S.H. Activated microglia initiate motor neuron injury by a nitric oxide and glutamate-mediated mechanism. J. Neuropathol. Exp. Neurol. 2004, 63, 964–977.

309. Ceprian, M.; Fulton, D. Glial Cell AMPA Receptors in Nervous System Health, Injury and Disease. Int. J. Mol. Sci. 2019, 20, 2450.

310. Zhang, X.-M.; Zhu, J. Kainic Acid-induced neurotoxicity: Targeting glial responses and glia-derived cytokines. Curr. Neuropharmacol. 2011, 9, 388–398.

311. Fazio, F.; Ulivieri, M.; Volpi, C.; Gargaro, M.; Fallarino, F. Targeting metabotropic glutamate receptors for the treatment of neuroinflammation. Curr. Opin. Pharmacol. 2018, 38, 16–23.

312. Byrnes, K.R.; Loane, D.J.; Faden, A.I. Metabotropic glutamate receptors as targets for multipotential treatment of neurological disorders. Neurother. J. Am. Soc. Exp. Neurother. 2009, 6, 94–107.

313. Murugan M, Sivakumar V, Lu J, et al. Expression of N-methyl D-aspartate receptor subunits in amoeboid microglia mediates production of nitric oxide via NF-kappaB signaling pathway and oligodendrocyte cell death in hypoxic postnatal rats. Glia 2011;59:521–39.

314. Yang XL, Wang X, Shao L, Jiang GT, Min JW, Mei XY, He XH, Liu WH, Huang WX, Peng BW. TRPV1 mediates astrocyte activation and interleukin-1β release induced by hypoxic ischemia (HI). J Neuroinflammation. 2019 May 29;16(1):114. doi: 10.1186/s12974-019-1487-3. PMID: 31142341; PMCID: PMC6540554.

315. Giordano C, Cristino L, Luongo L, Siniscalco D, Petrosino S, Piscitelli F, Marabese I, Gatta L, Rossi F, Imperatore R, et al. TRPV1-dependent and -independent alterations in the limbic cortex of neuropathic mice: impact on glial caspases and pain perception. Cereb Cortex. 2012;22:2495–518.

Chapter 2: Thoracic Spinal Cord Neuroinflammation as a Novel Therapeutic Target in Pulmonary Hypertension

Version of Razee A, Banerjee S, Hong J, Magaki S, Fishbein G, Ajijola OA, Umar S (2023). Thoracic Spinal Cord Neuroinflammation as a Novel Therapeutic Target in Pulmonary Hypertension. Hypertension. 2023 Jun;80(6):1297-1310. doi: 10.1161/HYPERTENSIONAHA.122.20782. Epub 2023 Apr 24. PMID: 37092338; PMCID: PMC10192067.

Abstract

Background

Pulmonary hypertension (PH) is associated with aberrant sympathoexcitation leading to right ventricular failure (RVF), arrhythmias, and death. Microglial activation and neuroinflammation have been implicated in sympathoexcitation in experimental PH. We recently reported the first evidence of thoracic spinal cord (TSC) neuroinflammation in PH rats. Here, we hypothesize that PH is associated with increased cardiopulmonary afferent signaling leading to TSC-specific neuroinflammation and sympathoexcitation. Furthermore, inhibition of TSC neuroinflammation rescues experimental PH and RVF.

Methods

We performed transcriptomic analysis and its validation on the TSC of monocrotaline (n=8) and Sugen hypoxia (n=8) rat models of severe PH-RVF. A group of monocrotaline rats received either daily intrathecal microglial activation inhibitor minocycline (200 μg/kg per day, n=5) or PBS (n=5) from day 14 through 28. Echocardiography and right ventricle-catheterization were performed terminally. Real-time quantitative reverse transcription PCR, immunolocalization, microglia+astrocyte quantification, and terminal deoxynucleotidyl transferase dUTP nick end labeling were assessed. Plasma catecholamines were measured by ELISA. Human spinal cord autopsy samples (Control n=3; pulmonary arterial hypertension n=3) were assessed to validate preclinical findings.

Results

Increased cardiopulmonary afferent signaling was demonstrated in preclinical and clinical PH. Our findings delineated common dysregulated genes and pathways highlighting neuroinflammation and apoptosis in the remodeled TSC and highlighted increased sympathoexcitation in both rat models. Moreover, we validated significantly increased

microglial and astrocytic activation and CX3CL1 expression in TSC of human pulmonary arterial hypertension. Finally, amelioration of TSC neuroinflammation by minocycline in monocrotaline rats inhibited microglial activation, decreased proinflammatory cytokines, sympathetic nervous system activation and significantly attenuated PH and RVF.

Conclusions

Targeting neuroinflammation and associated molecular pathways and genes in the TSC may yield novel therapeutic strategies for PH and RVF.

Nonstandard Abbreviations and Acronyms

PH	Pulmonary hypertension
RV	Right ventricle
RVF	Right ventricular failure
TSC	Thoracic spinal cord
PVR	Pulmonary vascular resistance
CTRL	Control
MCT	Monocrotaline
SuHx	Sugen hypoxia
RVSP	Right ventricular systolic pressure
PBS	Phosphate buffered saline
FDR	False discovery rate
PAT	Pulmonary artery acceleration time
PET	Pulmonary ejection time
RVIDd	RV internal diameter at end-diastole
ELISA	Enzyme-linked immunosorbent assay
RAAS	Renin-angiotensin-aldosterone-system

SNS	Sympathetic nervous system
DEG	Differentially expressed gene
TUNEL	Terminal deoxynucleotidyl transferase dUTP nick end labeling
SP	Substance P
TRPV1	Transient receptor potential vanilloid 1

Graphical Abstract

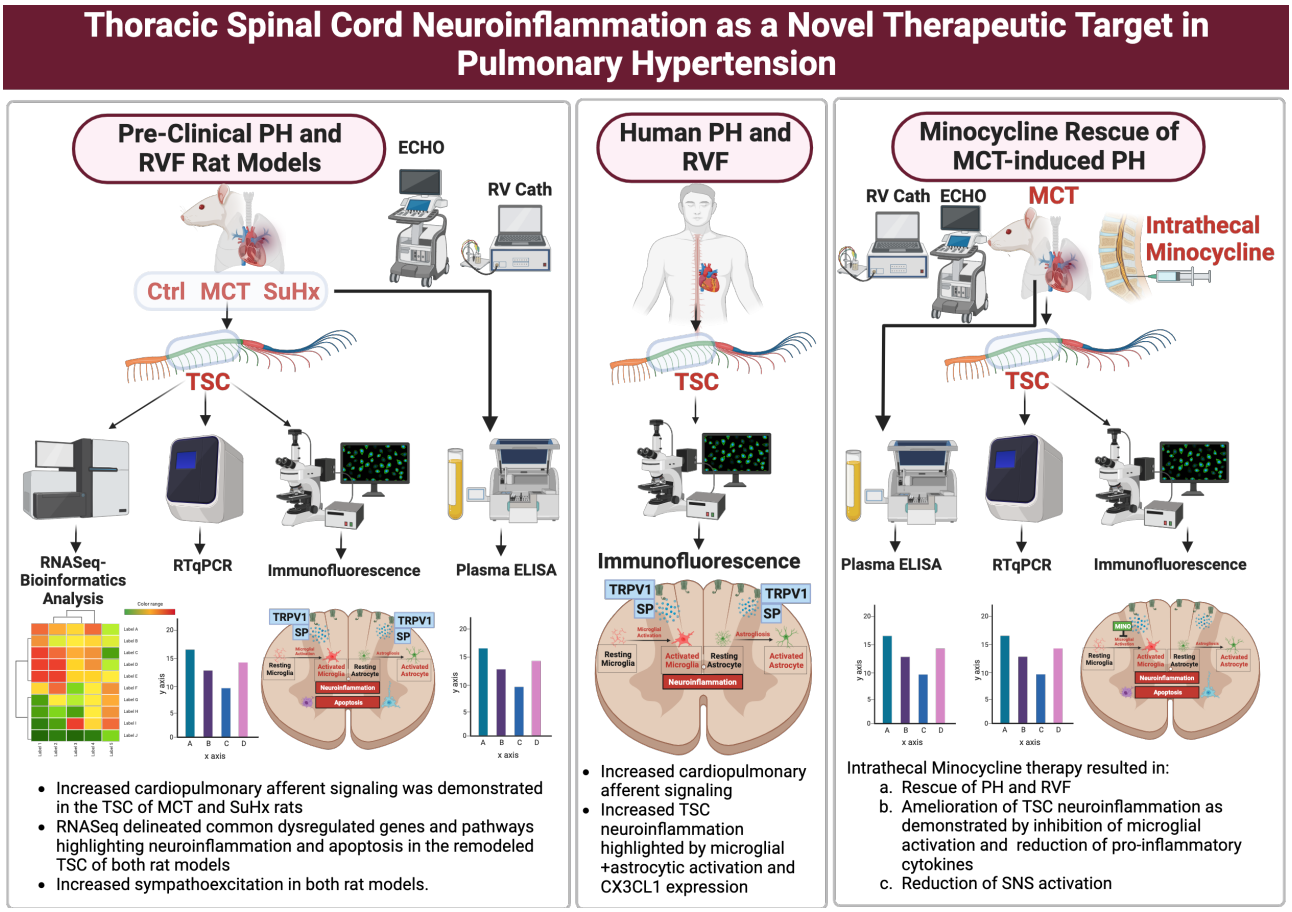

Introduction

Pulmonary hypertension (PH) is a progressive, fatal disease characterized by pulmonary vascular remodeling, resulting in increased pulmonary vascular resistance, right ventricular hypertrophy, right ventricular failure (RVF), arrhythmias, and ultimately death.[1,2] With about 200 000 Americans hospitalized each year with PH, the estimated prevalence for PH is between 15 and 50 cases per million individuals. If left untreated, the life span of an individual with PH is about 2.8 years and the 5-year survival rate is only around 62%.[3]

PH is a complex disorder associated with dysregulation of the autonomic nervous system.[4] Although autonomic dysregulation is not the main cause of PH, as the disease progresses, the elevated pulmonary vascular resistance and increased right ventricle (RV) afterload activate sympathetic nervous system (SNS) and increase renin-angiotensin-aldosterone-system activity. Increased SNS and renin-angiotensin-aldosterone-system activation may initially contribute to maintain hemodynamic homeostasis; however, aberrant sympathoexcitation leads to arrhythmias, RVF, and sudden death.[4–6] In fact, multiple studies have demonstrated that SNS activation portends poor prognosis in patients with PH including those with RVF.[5–8] However, there is a knowledge gap in understanding the relevant contributions of the central nervous system (brain and spinal cord) in SNS activation or sympathoexcitation in PH and RVF.

Several heart failure and myocardial ischemia studies have demonstrated that cardiac sympathetic afferents are responsible for cardiogenic transmission to the spinal dorsal horn during pathological conditions.[9–11] During cardiac stress, metabolites such as bradykinin stimulate these sensory afferent neurons by sensitizing the TRPV1 (transient receptor potential vanilloid 1) receptors at their central terminals and allowing Ca2+ influx to release substance P (SP) and glutamate.[11–13] This excitatory glutamatergic synaptic

transmission activates second-order neurons projecting into the spinothalamic tract that eventually leads to sympathoexcitation through the efferent pathway.[9,12] The activation of new gene expression profile contributing to the excitotoxicity and plasticity of signaling neurons during the development of sympathetic reflex have been documented throughout the peripheral and central nervous system including the stellate ganglion, dorsal root ganglia, cardiac intrinsic neurons, and thoracic spinal cord (TSC) after myocardial infarction.[14–17] Similarly, we postulated that in severe PH and RVF, afferent signaling from cardiopulmonary neurons via dorsal root ganglia to the dorsal horn of TSC is mediated by TRPV1 that leads to molecular and transcriptomic changes within the TSC. These changes contribute to the plasticity of signaling neurons, such as nerve sprouting, altering the distribution of ion channels and receptors and even neuroinflammation and cell death.[9,18] Consequently, this triggers sympathoexcitation via efferent pathways from the ventral horn.[9,18] A comprehensive description of the changes in gene expression that take place in the TSC due to PH and associated RVF is crucial in understanding the role of neuroinflammation, apoptosis, and sympathoexcitation in PH progression.

Microglial activation and neuroinflammation in the brain have been implicated in the SNS activation observed in experimental PH.[19–21] Moreover, intracerebroventricular infusion of minocycline has been shown to inhibit microglial activation, decrease SNS activation, and attenuate PH.[19] Recently, we discovered the first evidence of neuroinflammation in the TSC of monocrotaline (MCT)-induced PH rats.[22] However, the details of TSC remodeling in PH remain elusive. Here, we hypothesize that PH is associated with increased cardiopulmonary afferent signaling leading to TSC-specific neuroinflammation and sympathoexcitation. Furthermore, inhibition of TSC neuroinflammation may rescue experimental PH and RVF.

Materials and Methods

All animal studies were performed in accordance with the National Institutes of Health (NIH) Guide for the Care and Use of Laboratory Animals. Protocols received UCLA animal research committee approval. The details of materials and methods can be found in the online data supplement.

Animal Models of Pulmonary Hypertension

Adult male Sprague Dawley (SD) rats (200-250g) received either a single subcutaneous injection of pulmonary endothelial toxin Monocrotaline (MCT, 60mg/kg, n=8) and were followed for 30-days or VEGF-receptor antagonist Sugen (SU5416, 20mg/kg, SuHx group, n=8) and kept in hypoxia (10% oxygen) for 3-weeks followed by 2-weeks of normoxia. Phosphate buffered saline (PBS) treated rats served as controls (CTRL, n=8).

Time Course of Disease Development in MCT Rats

For time-course experiment, adult male SD rats (200-250g) received a single subcutaneous 60mg/kg MCT injection and were followed for either 7-days (n=6) or 14-days (n=6). PBS treated rats served as controls (Day-0, n=6).

Role of TRPV1 Receptors in Bradykinin-induced Cardiopulmonary Sympathetic Afferent Signaling in MCT Rats

To determine whether TRPV1 receptors mediate the bradykinin-induced cardiopulmonary sympathetic afferent transmission in PH, heart rate and blood pressure responses to RV-epicardial and pulmonary vascular application of bradykinin were measured in MCT and control rats (n=5 per group). After tracheostomy and thoracotomy, direct right heart catheterization (Millar SPR-671) was performed terminally to record baseline right ventricular systolic pressure (RVSP) and heart rate for 10 min. Bradykinin (60 μg/mL; Sigma, B3259)[23] was dissolved in 0.1M acetic acid+PBS and applied to the anterior

surface of the right ventricle as well as pulmonary vasculature with a pipette. Following bradykinin application, the RVSP and heart rate were recorded continuously for another 5 min.

Intrathecal Minocycline Injection

Intrathecal minocycline injections were performed daily on a group of MCT-treated rats from day 14-28 post MCT injection and were compared with MCT rats treated with daily intrathecal PBS (n=5 per group). Briefly, rats were anesthetized with isoflurane/O_2 mixture (3-4%), and body temperature was maintained at 37±1°C using heating pads. MCT-treated rats either received daily intrathecal Minocycline (200μg/kg, Sigma-Aldrich, St. Louis, MO in 30μl PBS)[19,24] or 30μl PBS from day 14-28. Intrathecal injections were administered with a 29-gage needle at L4-5 level to avoid spinal cord injury; successful injections were documented with prominent tail flicks.

Echocardiography and Cardiopulmonary Hemodynamic Measurements

Serial echocardiography (Vevo3100) was performed to monitor cardiopulmonary hemodynamics and the development of PH and RV dysfunction. Direct right heart catheterization (Millar SPR-671) was performed terminally to assess disease severity.

RNA Extraction and qRT-PCR

Real-time quantitative reverse transcription PCR (qRT-PCR) was performed with total RNA extracted from the thoracic and lumbar regions of spinal cord from control, MCT and SuHx rats using Trizol (Invitrogen).

RNA Sequencing Analysis

NextSeq400 (Illumina) was performed on rat TSC tissue and differential expression analysis was conducted. Differentially expressed genes (DEGs) with false discovery rate (FDR) <0.05 were considered statistically significant. Gene set enrichment analysis was

performed and Hallmark[25] gene sets were obtained from molecular signature database (MSigDB).[26] Enriched pathways considered statistically significant were defined by adjusted p-value <0.05. The RV and lung transcriptomic analyses were also performed on previously published data from MCT and SuHx rats.[27,28]

Gross Histologic Analysis, Tissue Preparation, and Imaging

RV hypertrophy index was calculated as weight ratio of RV/(LV+IVS). Hearts, lungs and spinal cords were fixed and 4–6µm sections were obtained. Heart and lung tissue sections were stained with Masson's trichrome staining. Images were acquired using a confocal microscope (Nikon).

Human Thoracic Spinal Cord Tissue Sections

To validate some of the key findings from rat TSC in human PAH spinal cords we collected autopsy samples from PAH patients (n=3) and controls (n=3) through our collaborators at the UCLA Department of Pathology. Tissues were sectioned at 4–6µm for immunostainings.

Immunofluorescence Staining and Quantification

TSC sections were stained with the primary antibodies against TRPV1 (Anti-TRPV1), substance P (Anti-SP), Cx3Cl1 (Anti- Cx3Cl1), microglia (Anti-IBA1), astrocytes (Anti-GFAP), neurons (Anti-NeuN), neuropeptide Y (Anti-NPY) and cleaved Caspase-3 (Asp175). Quantifications were performed using ImageJ (1.45p, NIH, Bethesda, MD).

Terminal Deoxynucleotidyl Transferase dUTP Nick End Labeling Staining

Thoracic spinal cord sections were stained with the terminal deoxynucleotidyl transferase dUTP nick end labeling (TUNEL) Assay Kit-BrdU-Red (Abcam, ab66110) and the $TUNEL^+$ cells were calculated as integrated optical density using ImageJ (1.45p, NIH, Bethesda, MD).

Plasma Norepinephrine Assays

Plasma norepinephrine levels were quantified using an enzyme-linked immunosorbent assay (ELISA) kit (Abnova, KA1877) following the manufacturer's protocols.

Statistical Analysis

Unpaired t test and 1-way ANOVA tests were used to com- pare between groups using GraphPad Prism. When significant differences were detected, individual mean values were com- pared by post hoc tests that allowed for multiple comparisons. $P<0.05$ was considered statistically significant. Values are expressed as mean±SD. For RNA sequencing (RNA- seq), differential expression analysis was conducted using the R-program DeSeq2 correcting for multiple hypothesis testing using the Benjamini Hochberg method. Power analysis calculations were performed for primary end points (hemodynamic parameters such as RVSP, Fulton Index, RVFAC) as well as secondary analysis for all experiments. Sample sizes were determined by detecting effect sizes between groups (2 sample t test, 2-tailed, alpha=0.05) that provided adequate power (80%).

Results

Development of Severe PH and RVF in MCT and SuHx Rats

Severe PH and RVF were confirmed using serial transthoracic echocardiography and terminal right heart catheterization in rats treated with MCT or SuHx compared with PBS-treated control rats (Figure S1). Both MCT and SuHx rats developed significant PH and RVF. However, no significant differences were observed between SuHx-treated and MCT-treated groups. Interestingly, as additional controls groups, 3-weeks of hypoxia alone resulted in only mild PH without RV dysfunction whereas Sugen alone did not induce PH or RV dysfunction (Figure S10).

Transient Receptor Potential Vanilloid 1 and Substance P Mediate Cardio-pulmonary Afferent Signaling in the Dorsal Horn of Thoracic Spinal Cords in MCT- and SuHx-induced PH

TRPV1 and SP in the spinal dorsal horn have been shown to play a critical role in cardiogenic afferent sympathetic transmission.[11,13,29-31] The expression of TRPV1 and SP were assessed in the dorsal horn of TSC from MCT- and SuHx-induced PH rats to determine their role in cardiopulmonary afferent signaling in PH. Significantly increased TRPV1 immunoreactivity was observed in the TSC dorsal gray matter of MCT and SuHx rats (Figure 1A, B). Interestingly, significantly increased SP and it's colocalization with TRPV1 were also observed in the TSC dorsal gray matter of MCT and SuHx rats (Figure 1A, B). Additionally, RV-epicardial and pulmonary vascular application of bradykinin (60μg/mL) produced a significant increase in heart rate and RVSP in MCT-treated rats compared to control (Figure 1D). These data provide important histological and functional evidence that TRPV1 expressing afferent nerve endings in the thoracic spinal dorsal horn release increased SP in PH-RVF to mediate cardiopulmonary sympathoexcitatory reflex.

Increased Cardiopulmonary Afferent Signaling in the Dorsal Horn of Thoracic Spinal Cords of PAH Patients

Increased TRPV1 and SP immunoreactivity and their colocalization were observed in the thoracic dorsal gray matter of PAH patients indicating increased cardiopulmonary afferent signaling compared to controls (Figure 1C).

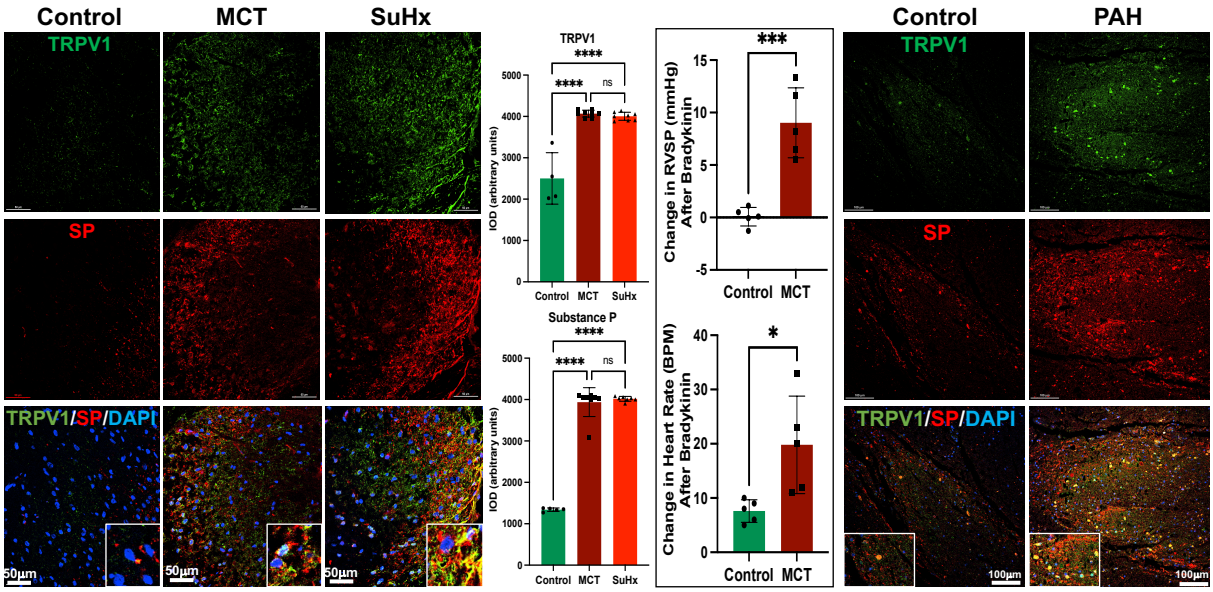

Figure 1. Increased cardiopulmonary afferent signaling in the thoracic spinal dorsal horn of MCT and SuHx rats and PAH patients. (**A**) Representative images of immunofluorescence staining with anti-TRPV1 (Green), anti-SP (Red), and DAPI (DNA; blue) from thoracic dorsal gray matter of Control, MCT and SuHx rats. Lower panel shows enlarged view of TRPV1 and SP colocalization (Yellow). N=3 per group. (**B**) Quantification of TRPV1 and SP immunolocalization (IOD: integrated optical density) in MCT and SuHx rats compared to controls. N=3 per group. ****p<0.0001. (**C**) Representative images of immunofluorescence staining with anti-TRPV1 (Green), anti-SP (Red), and DAPI (DNA; blue) from thoracic dorsal gray matter of Control and PAH patients. Lower panel shows enlarged view of TRPV1 and SP colocalization (Yellow). N=3 per group. (**D**) RVSP and heart rate responses to RV-epicardial and pulmonary vascular application of bradykinin

(60 μg/mL) in Control and MCT rats. N=5 per group. *p<0.05, ***p<0.001. RVSP and heart rate responses evoked by bradykinin were measured as the absolute change from baseline prior to bradykinin application.

Similar Transcriptomic Signature of Thoracic Spinal Cords in MCT- and SuHx-induced PH

RNASeq was performed to investigate the transcriptomic remodeling of the TSC of MCT- and SuHx-induced rats (Figures 2, S2-5, Tables S1-4). Hierarchical clustering of top DEGs (FDR<0.05) from RNASeq showed similar gene signatures between MCT and SuHx rats compared to controls (Figure 2A, S2, S3). MCT and SuHx rats revealed 1,655 and 3,653 differentially expressed genes (DEG), respectively, compared to control rats based on FDR<0.05 (Figure 2D). Both MCT- and SuHx-treated groups shared 1,414 DEGs that were either up- or down-regulated in a similar fashion (Figure 2D). The top common significantly up-regulated DEGs demonstrated association with excitatory glutamatergic signaling, neuroinflammation and apoptosis (Figure 2C).

Multiple Pathways are Commonly Altered in Thoracic Spinal Cords of MCT- and SuHx-induced PH

A ranked-based directional enrichment analysis of TSC transcriptome from control, MCT and SuHx-treated rats was performed. Gene Set Enrichment Analysis revealed 23 and 22 hallmark pathways significantly enriched (FDR<0.05) in MCT and SuHx rats, respectively, among which 20 pathways were overlapping (Figure 2E-F, S4, S5). Pro-inflammatory and pro-apoptotic pathways, such as, IL-6 JAK-STAT3 signaling and TNFα signaling via NF-κB as well as pathways associated with neuroinflammation and apoptosis, such as, hypoxia and KRAS signaling were significantly enriched in both MCT and SuHx.

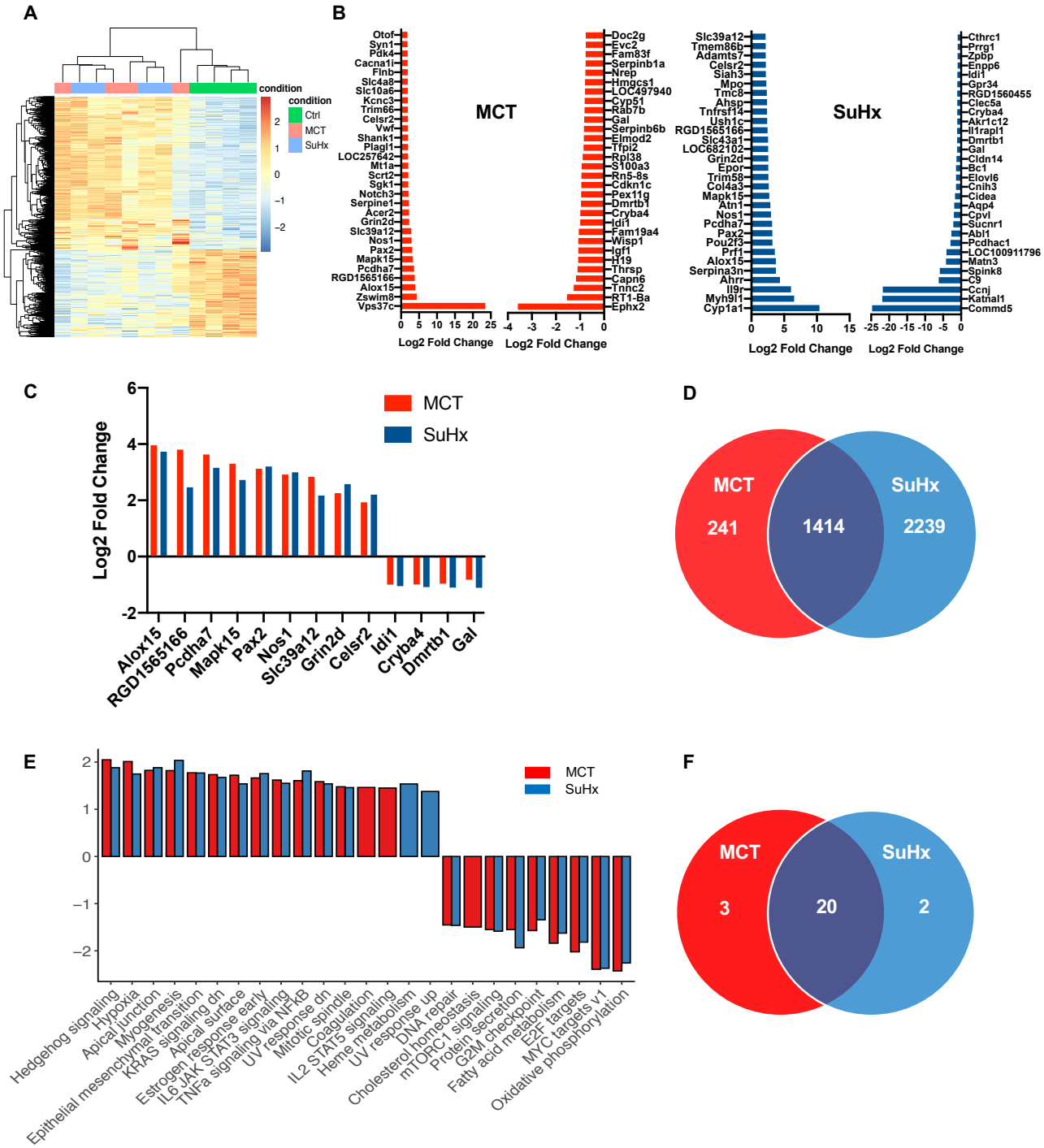

Figure 2. RNA-Seq based analysis of DEG's and pathway enrichment from thoracic spinal cords of MCT and SuHx rats. (**A**) RNA-Seq based heat map showing DEGs from thoracic spinal cord tissue in CTRL (green), MCT (red) and SuHx (blue) groups. (**B**) Top

30 up-regulated and down-regulated significant DEGs between MCT vs. CTRL and SuHx vs. CTRL. (**C**) Top common significantly upregulated genes from top 30 DEGs between MCT vs. SuHx (9) and Top common significantly downregulated genes (4) from top 30 DEGs between MCT vs. SuHx (**D**) Venn diagram showing significant DEGs (based on FDR<0.05) and their overlap in MCT (red) and SuHx (blue) groups. (**E**) Bar plot showing normalized enrichment scores (NES) for Hallmark pathways derived from Gene Set Enrichment Analysis (GSEA). For GSEA, differentially expressed genes between SuHx or MCT vs. control were ranked by the Wald statistic derived from DESeq2. Bars in red and blue represent statistically significant (FDR<0.05) pathways in MCT and SuHx, respectively, that are either up- or downregulated. (**F**) Venn diagram showing significant pathways (based on FDR<0.05) and their overlap in MCT (red) and SuHx (blue) groups compared to control. N=4 per group.

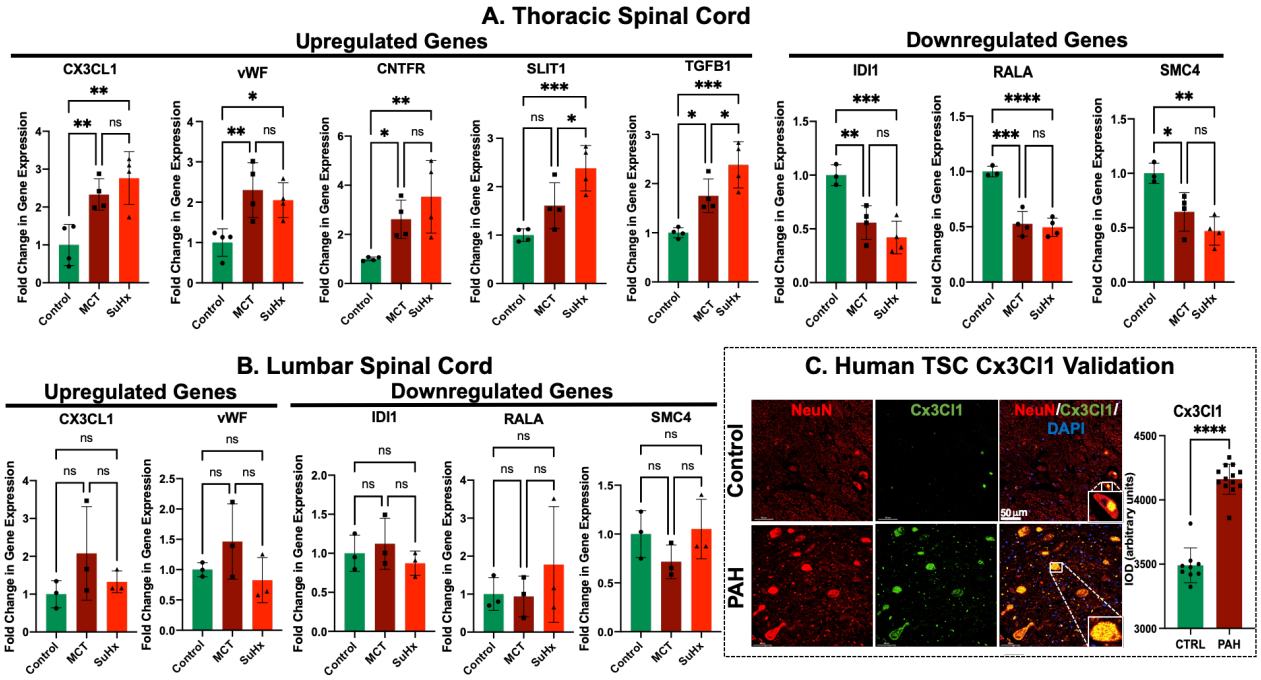

Figure 3. Validation of RNA-Seq based DEGs in thoracic and lumbar spinal cord of MCT and SuHx rats and in TSC of PAH patients. RT-qPCR data demonstrating differential gene expression of upregulated and downregulated genes from (**A**) thoracic and (**B**) lumbar spinal cord tissue of MCT and SuHx compared to control rats. N=3-4 per group. *p<0.05, **p<0.01, ***p<0.001, ****p<0.0001. (**C**) Representative immunofluorescence images of NeuN (Red), Cx3Cl1 (Green), and DAPI (DNA; blue) in controls and PAH patients. N=3 per group; ****p<0.0001.

qRT-PCR Validation of Selected Common Top Genes from RNA-Seq of Thoracic Spinal Cords of MCT- and SuHx-induced PH

RNA sequencing results and gene expression changes were validated with qRT-PCR by selecting several key common top DEGs from significantly enriched pathways from both MCT- and SuHx-treated rats that were identified by Hallmark pathway analysis. The qRT-PCR results of DEGs from hedgehog signaling (CNTFR, SLIT1), apical junction (CX3CL1, vWF), myogenesis (TGFβ1), epithelial mesenchymal transition (TGFβ1), KRAS signaling down (CNTFR), apical surface (CX3CL1), IL6 JAK STAT3 signaling (vWF, CNTFR), DNA repair (RALA), fatty acid metabolism (IDI1), mTORC1 signaling (IDI1), E2F target (SMC4) and G2M checkpoint (SMC4) pathways were consistent with the TSC RNA sequencing results (Figure 3A, B).

DEGs from Thoracic Spinal Cords are Unchanged in Lumbar Spinal Cords in MCT- and SuHx-induced PH

qRT-PCR was used to determine whether the upregulated and downregulated DEGs from TSC had similar expression profile in lumbar spinal cord as well. Interestingly, the dysregulated genes from TSC did not show any significant changes in the lumbar spinal

cord of either MCT- or SuHx-treated rats compared to controls (Figure 3B). This demonstrates that the transcriptomic remodeling is specific to the thoracic region of spinal cords from MCT- and SuHx-treated rats.

Increased Microglial Activation and Astrogliosis in Thoracic Spinal Cords of MCT- and SuHx-induced PH

Interactions between microglia and astrocytes critically influence neuroinflammatory responses in the central nervous system (CNS).[32] Both MCT and SuHx-treated rats had a significant increase in total number of ionized calcium binding adaptor molecule 1 (Iba1) positive cells in the TSC compared to controls (Figure 4A). Iba1 is a marker of mature microglia in the CNS. Only cells with a well-defined cell body were included in the analysis. When microglial cells display small cell body with thin and highly ramified branches extending in all directions, they are characterized as “resting” microglia. Conversely, these ramified microglia become amoeboid possessing larger cell body with thicker and shorter branches, which are characterized as “activated” microglia (Figure 4A) [19-21]. Significant increases in the number of activated microglial cells were observed in the TSC of both MCT and SuHx-treated rats compared to controls (Figure 4A). Both MCT and SuHx-treated rats also had a significant increase in total number of glial fibrillary acidic protein (GFAP) positive astrocytic cells in the TSC compared to controls (Figure 4B). Interestingly, additional control groups of hypoxia alone and Sugen alone did not show any signature of neuroinflammation demonstrated by unchanged mRNA levels of Cx3Cl1 and NOS1 in the TSC (Figure S10).

Increased Signature of Neuroinflammation in Thoracic Spinal Cords of PAH Patients

To validate the findings from our preclinical rat models and investigate the translational relevance of TSC neuroinflammation in humans, Cx3Cl1 expression, microglial activation

and astrogliosis were assessed in TSC autopsy samples from PAH patients (Figure 3C, 4C). Interestingly, significantly increased Cx3Cl1 expression, microglial count and activation were found in TSC of PAH patients. Furthermore, increased astrocytic activation was also demonstrated in the TSC of PAH patients compared to controls, indicating increased neuroinflammation (Figure 3C, 4C).

Multiple Pathways are Commonly Up-regulated in Thoracic Spinal Cords, RV and Lungs of MCT- and SuHx-induced PH

To assess potential overlap in gene expression profiles among lungs, RV and TSC in pre-clinical PH, a ranked-based directional enrichment analysis of TSC, lung[27] and RV[28] transcriptome from MCT- and SuHx-treated rats was performed. Gene Set Enrichment Analysis revealed 9 and 5 significantly up-regulated overlapping hallmark pathways from these organs (FDR<0.05) in MCT and SuHx rats, respectively (Figure S8A). The common up-regulated enriched pathways in both MCT and SuHx rats from TSC, RV and lung were TNFα via NF-kB, epithelial mesenchymal transition, hypoxia, KRAS signaling and IL6 JAK STAT3 signaling, which signifies multi-organ inflammatory and apoptotic signature of these severe PH rat models (Figure S8B).

Increased Apoptosis in Thoracic Spinal Cords of MCT- and SuHx-induced PH

Neuroinflammation and associated neuronal apoptosis in the CNS have been implicated in sympathetic hyperactivation in various cardiovascular diseases.[32,33] Increased apoptosis in the TSC of MCT and SuHx rats was validated by terminal deoxynucleotidyl transferase dUTP nick end labeling staining. Both MCT and SuHx rats displayed a significantly increased number of apoptotic cells compared with the control group (Figure 4D). Furthermore, increased cleaved Caspase-3 immunoreactivity and it's colocalization with NeuN in the TSC of MCT and SuHx rats confirmed neuronal apoptosis (Figure S9).

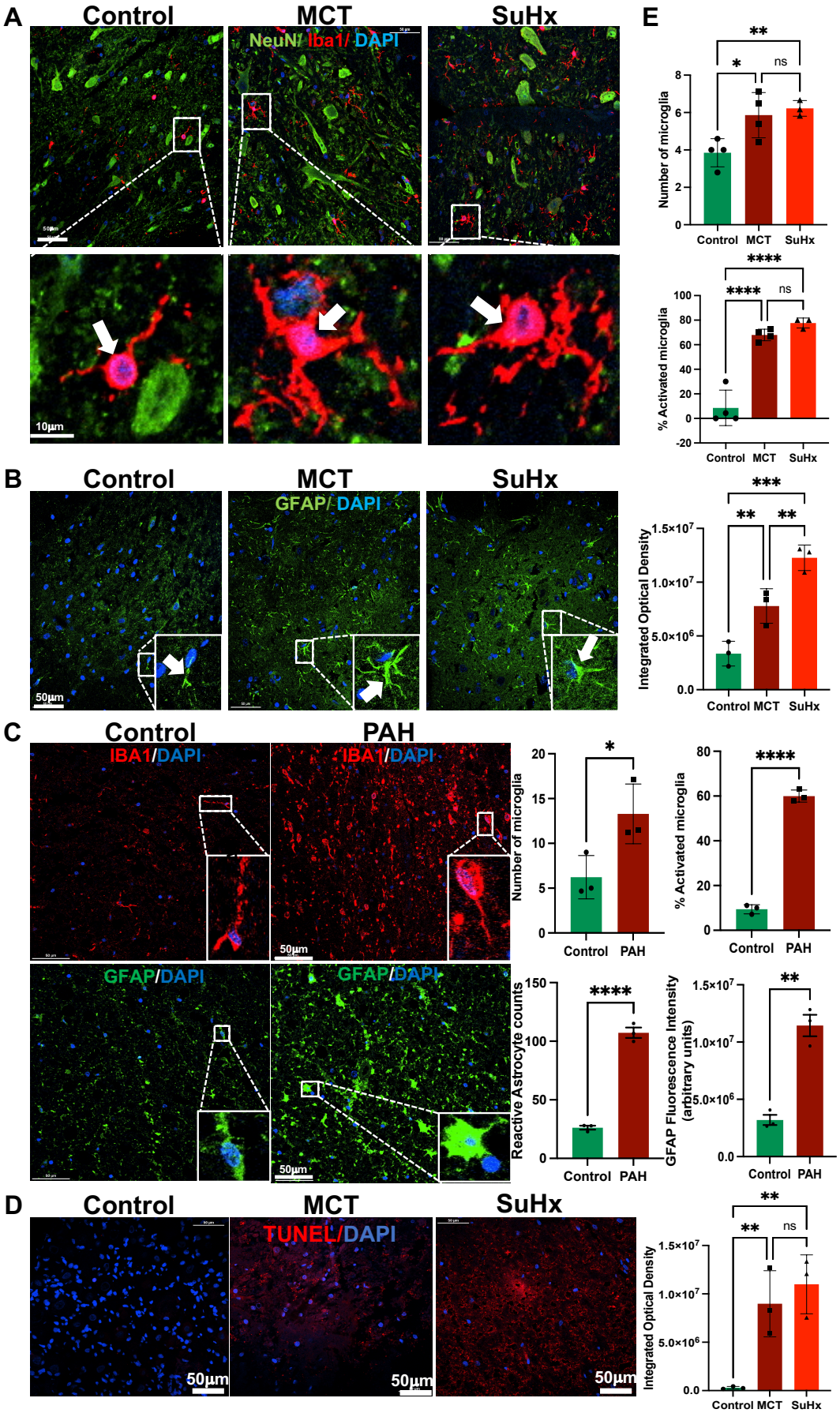
A
Control
MCT
SuHx
NeuN/ Iba1/ DAPI
10µm
E
Number of microglia
Control MCT SuHx
% Activated microglia
B
GFAP/ DAPI
50µm
Integrated Optical Density
C
PAH
IBA1/DAPI
GFAP/DAPI
Reactive Astrocyte counts
GFAP Fluorescence Intensity (arbitrary units)
D
TUNEL/DAPI
ns

Figure 4. Increased microglial activation and astrogliosis in the TSC of MCT, SuHx rats and human PAH. Increased apoptosis in the TSC of MCT and SuHx rats. (**A**) **Left Panel:** Representative images of immunofluorescence staining with anti-Iba1 (red), anti-NeuN (green), and DAPI (blue) in the TSC of Control, MCT and SuHx rats. Lower panel shows enlarged view of resting microglia in control compared with activated microglia in the MCT and SuHx (white arrows). **Right Panel:** Quantifications of number of microglia per high power field (HPF), and % microglial activation/HPF in the TSC of MCT and SuHx rats compared to controls. (**B**) **Left Panel:** Increased astrocytic (Green) immunolocalization in the TSC of MCT and SuHx rats compared to controls. **Right Panel:** Quantification of astrocytic activation (integrated optical density). (**C**) **Left Panel:** Immunofluorescence images of Iba1 (Red), GFAP (Green) and DAPI (blue) in controls and PAH patients. **Right Panel:** Quantifications of number of microglia per high power field (HPF), % microglial activation/HPF and astrocytic activation (integrated optical density) in the TSC of MCT and SuHx rats compared to controls as well as PAH patients compared to controls. (**D**) **Left Panel:** TUNEL staining showing DAPI (Blue) and BRDU (Red) validating increased apoptosis in the TSC of MCT and SuHx compared to control. **Right Panel:** Quantification of TUNEL positive cells (integrated optical density).
N=3-4 per group. *p<0.05, **p<0.01, ***p<0.001 ****p<0.0001.

Increased NPY in the Ventral Horn of Thoracic Spinal Cord and Circulating Catecholamines as Markers of Sympathoexcitation in MCT- and SuHx-induced PH

Previous studies demonstrated that neuropeptide Y (NPY) influences preganglionic sympathetic interneurons in the spinal cord, whereas it is co-released with norepinephrine from postganglionic sympathetic neurons at peripheral sites of action during sympathetic

activation.[34] Hence, NPY expression in the TSC ventral horn and plasma norepinephrine were assessed to validate increased sympathoexcitation in MCT and SuHx rats. Increased NPY immunoreactivity and its colocalization with NeuN were observed in the ventral horn gray matter of both models (Figure S7A). Moreover, plasma norepinephrine levels were significantly increased in both MCT and SuHx rats compared with controls (Figure S7B).

Time Dependent Development of TSC Neuroinflammation, Apoptosis and Sympathoexcitation in PH

To investigate the expression of key genes, microglial activation and astrogliosis in the TSC as well as sympathoexcitation as a function of PH and RVF development, a time-course experiment was performed in MCT rats. Hemodynamic parameters, TSC neuroinflammation and apoptosis and sympathoexcitation were assessed at day-0 (Control), day-7 and day-14 after MCT injection (Figure S6A). There was no significant increase in RVSP and Fulton Index at day-7 after MCT. However, RVSP and Fulton index were mildly but significantly increased at day-14 after MCT (Figure S6B, C). Interestingly, there were no significant neuroinflammatory responses in the TSC at day-7, as CX3CL1 transcription, immunoreactivity, microglial count and activation as well as astrogliosis were all unchanged compared to control (Figure S6E,F,H-J). Also, there was no increase in apoptosis in the TSC at day-7, as TGFβ1 expression was unchanged compared to control (Figure S6G). However, at day-14 we observed the initial signs of neuroinflammatory changes in the TSC through significantly increased CX3CL1 transcription, immunoreactivity, microglial activation and astrogliosis (Figure S5E, F, H-J). Interestingly, this coincided with a significant increase in RVSP and Fulton Index at day-14 (Figure S6B, C). Remarkably, apoptotic marker TGFβ1 was not significantly increased even at day-14 compared to control and day-7 (Figure S6G). Consequently, there were no significant

changes in sympathoexcitation at day-7 and day-14 after MCT (Figure S6K). These data provide important hemodynamic, molecular, and histological evidence that initial signs of PH coincide with early phase of TSC neuroinflammation without significant apoptosis and sympathoexcitation.

Microglial Activation Inhibitor Minocycline Rescues PH and RVF

To investigate the role of microglial activation in TSC neuroinflammation in PH, daily intrathecal microglial activation inhibitor minocycline was administered to MCT rats from day 14-28 (Figure 5A). Minocycline significantly attenuated PH severity, rescued RVF and RV hypertrophy but did not affect LV pressure and left ventricular ejection fraction (Figure 5B and 5C). Importantly, minocycline significantly reduced plasma norepinephrine (Figure 5C). Interestingly, minocycline significantly reduced lung vascular (arteriolar) wall thickness (Figure 5B and 5C). Furthermore, minocycline resulted in a significant decrease in total microglial count, microglial activation and expression of fractalkine CX3CL1 (Figure 5C through 5E) and pro- inflammatory cytokine TNF-α (Figure 5C) in TSC. Minocycline also attenuated proapoptotic TGF-β1 in the TSC (Figure 5C). These data suggest an important contributory role for microglial activation in TSC neuroinflammation in PH and potential therapeutic role of minocycline.

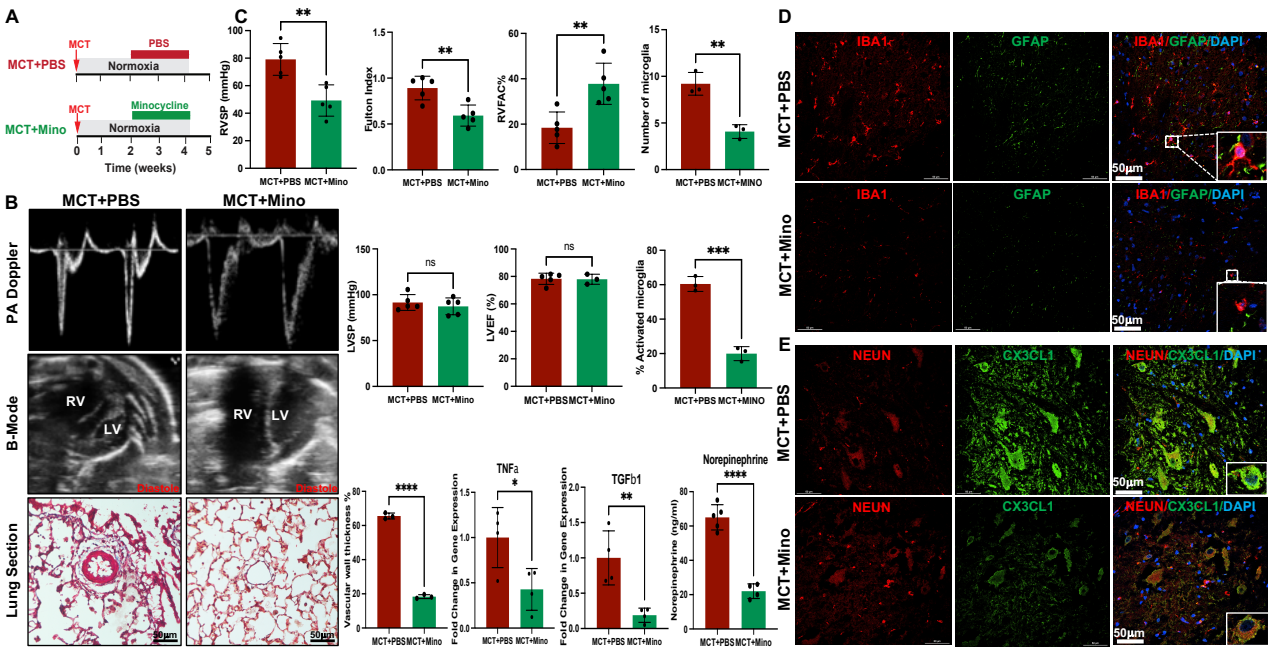

Figure 5. Minocycline attenuates MCT induced PH and RVF by attenuating TSC neuroinflammation and associated sympathoexcitation. (**A**) Experimental Protocol. (**B**) PA Doppler, B-Mode echo and cross section from lung in PBS and Minocycline treated MCT rats. (**C**) RVSP, Fulton index, RVFAC, LVSP, LVEF, quantification of pulmonary vascular (arteriolar) wall thickness, normalized qRT-PCR data of pro-inflammatory and apoptotic gene expression, quantification of number of microglia/HPF and percent activated microglia/HPF in the TSC of PBS and Minocycline treated MCT rats. N=3-5 per group. *p<0.05, **p<0.01, ***p<0.001 ****p<0.0001. Plasma norepinephrine level measured by ELISA in PBS and Minocycline treated MCT rats. N=4-5 per group. ****p<0.0001. (**D**) Representative images of immunofluorescence staining with microglial marker anti-Iba1 (Red), astrocytic marker anti-GFAP (Green) and DNA marker DAPI (Blue) in the TSC of PBS and Minocycline treated MCT rats. N=3 per group. (**E**) Representative images of immunofluorescence staining with neuronal marker NeuN (Red), Cx3Cl1 (Green) and DAPI (Blue) in the TSC of PBS and Minocycline treated MCT rats. N=3 per group.

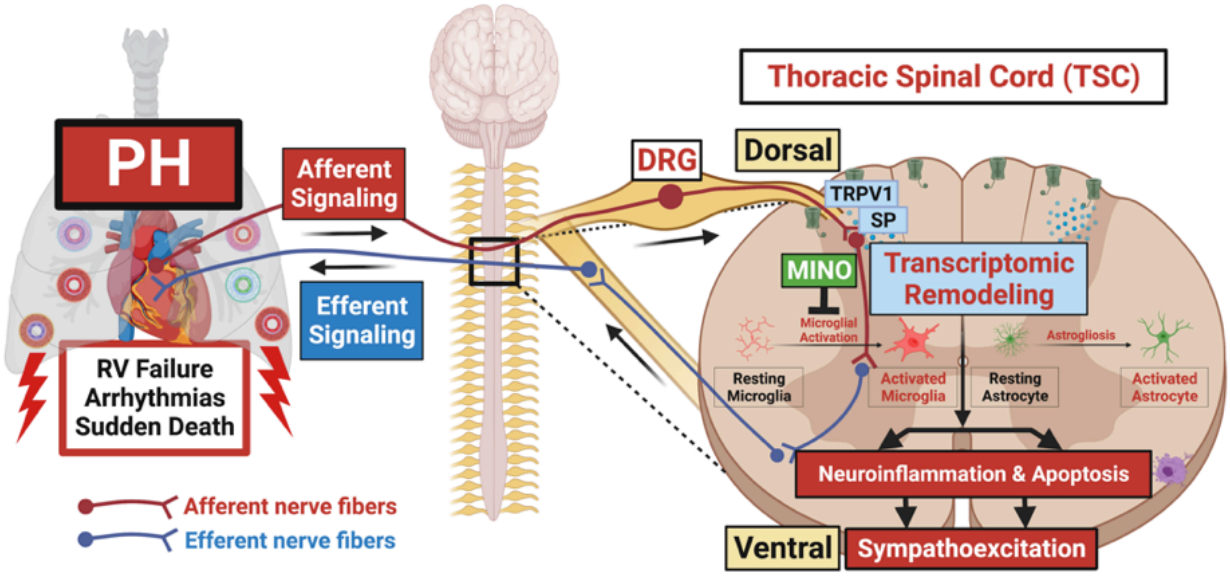

Figure 6. Hypothetical scheme showing transcriptomic remodeling of thoracic spinal cord characterized by neuroinflammation and apoptosis leading to sympathoexcitation in PH. Afferent signaling from cardiopulmonary neurons through DRG to the dorsal horn of thoracic spinal cord mediated *via* TRPV1 and SP results in transcriptomic remodeling characterized by neuroinflammation (microglial activation+astrogliosis) and apoptosis. We postulate that neuroinflammation and apoptosis lead to increased sympathoexcitation *via* efferent pathways resulting in worsening PH, RVF, arrhythmias and death. Inhibition of microglial activation by minocycline attenuates neuroinflammation and associated sympathoexcitation resulting in rescue of PH and RVF.

Discussion

Here we provide histological and functional evidence that TRPV1 expressing cardiopulmonary afferent neurons in the thoracic spinal dorsal horn mediate sympathoexcitatory signaling in PH. We performed the first-ever transcriptomic analysis on TSC of 2 clinically relevant animal models (MCT and SuHx) of severe PH and RVF that revealed distinct transcriptomic signatures with significant overlap of DEGs and pathways between the 2 models. PCR validation confirmed that MCT and SuHx rats shared similar gene expression profiles that were specific to the thoracic but not to lumbar spinal cord. Hallmark pathway analysis showed upregulation of multiple proinflammatory and proapoptotic pathways in TSC, which were also upregulated in RV[23] and lung[24] of MCT-induced and SuHx-induced PH rats. We observed microglial and astrocytic cell activation and increased fractalkine Cx3Cl1 expression in the TSC of both rat models and in human PAH. Terminal deoxynucleotidyl transferase dUTP nick end labeling and cleaved Caspase-3 immunostaining demonstrated increased neuronal apoptosis in the TSC of both rat models. Significantly elevated TSC NPY expression and plasma norepinephrine in both rat models confirmed increased sympathoexcitation. Interestingly, time-course experiments demonstrated that initial signs of PH coincided with early phase of TSC neuroinflammation without significant apoptosis and sympathoexcitation in the MCT rats. Finally, intrathecal minocycline decreased TSC microglial count, activation, and expression of proinflammatory cytokines, and reduced sympathoexcitation resulting in rescue of PH-RVF (Figure 6).

Neuroinflammation in the brain has recently been implicated in the SNS activation found in MCT-induced PH rats.[19-21] Subsequently, our lab reported the first evidence for TSC neuroinflammation in MCT-induced PH rats.[22] However, the precise molecular

mechanisms and impact of TSC neuroinflammation and associated SNS activation on cardiopulmonary function in PH and RVF are still unknown. In line with the previous reports on left ventricular ischemia,[9-13] we postulated that in severe PH and RVF, afferent signaling from cardiopulmonary neurons via DRG to the dorsal horn of TSC is mediated by TRPV1 that leads to molecular and transcriptomic changes within the TSC. These changes contribute to TSC specific neuroinflammation and apoptosis[18] resulting in efferent signaling via sympathetic preganglionic fibers from the TSC to postganglionic fibers that innervate and modulate activities of the heart and lung.[10,12,14] Our histological data demonstrated increased TRPV1 expression and it's colocalization with SP in the thoracic spinal dorsal horn of MCT and SuHx rats as well as human PAH (Figure 1) indicating increased excitatory synaptic transmission at the level of first synapse in the cardiopulmonary afferent pathway.[35] Moreover, bradykinin has been shown to activate TRPV1 receptors in the cardiac sympathetic afferent nerve endings eliciting autonomic reflex characterized by increased blood pressure, heart rate and sympathetic nerve activity during pathophysiological conditions.[11-13,14,29] RV-epicardial and pulmonary vascular application of bradykinin elicited significant increase in RVSP and heart rate in our MCT-treated rats, which demonstrated that TRPV1 expressing afferent nerve endings in the thoracic spinal dorsal horn may be responsible for sympathoexcitatory signal transmission in PH.

We further postulated that as PH and RVF progress, there is an analogous sequence of gene expression changes contributing to the excitotoxicity and plasticity of signaling neurons in the TSC, the processing center for incoming afferent fibers from the heart and lungs to the CNS.[9,14–18] Therefore, we performed transcriptomic analysis on TSC of MCT and SuHx rat models to determine the impact of PH and RVF on TSC gene expression.

Major proinflammatory path- ways such as IL-6 JAK-STAT3 signaling and TNF-α signaling via NF-κB as well as pathways associated with neuroinflammation such as hypoxia, KRAS signaling, and epithelial mesenchymal transition were some of the top upregulated pathways in both the models (Figure 2E). Many pro-inflammatory genes such as ALOX15, CX3CL1, EDN1, SERPINE1, RELA, mTOR, NOTCH3, NF-κB-1, STAT3, ICAM-1, NOS1, CLEC4E, SLPI, VEGFA, and PTGS2 were significantly enriched in these pathways (Tables S1-4). In fact, CX3CL1 has been implicated in classical microglial activation-mediated sympathoexcitation in the brain of MCT-treated rats and hypoxic mice.[19,21,36,37] Previous studies demonstrated that TRPV1 activation in sensory nerve endings releases neuropeptides, including calcitonin gene-related peptide (CGRP), glutamate, and SP, which modulate microglial activation via NF-κB.[38] NF-κB-mediated microglial activation is also regulated by notch signaling[39] and the mTOR (mammalian target of rapamycin).[40] Activated microglia express several proinflammatory factors, such as TNF-α, IL-6, MCP-1 (Monocyte chemoattractant protein-1), ICAM-1 (Inter- cellular Adhesion Molecule 1), and VCAM-1 (Vascular Cell Adhesion Molecule 1), which mediate neuroinflammation and excitotoxic neuronal damage.[11–13] Furthermore, several studies suggested that TRPV1-mediated activation of neuronal nitric oxide synthase (nNOS or NOS1) involves Ca2+ influx through activated NMDARs (N-methyl-D-aspartate receptors) in the spinal cord.[41] NOS1 activation is known to induce neuroinflammation, chemokine release, excitotoxicity, and apoptosis.[42,43] Our TSC RNA-seq demonstrated increased glutamatergic excitatory signaling and NOS1 upregulation that may lead to neuroinflammation, cell death, and associated sympathoexcitation in both the rat models. Interestingly, no significant changes in inflammation-related gene expression were seen in lumbar spinal cords of MCT- treated and SuHx-treated rats (Figure 3B) suggesting TSC-specific neuroinflammation likely due

to cardiopulmonary neural connections.

Both MCT-treated and SuHx-treated rats had a significant increase in total number of mature and activated microglia in the TSC, indicating neuroinflammation in this region (Figure 4A). Moreover, both the rat models showed significant increases in astrocytic cell activation in TSC (Figure 4B), further validating neuroinflammatory changes in this region as we recently demonstrated in MCT rats.[22] Interestingly, our data also demonstrated 5 common significantly upregulated proinflammatory and proapoptotic pathways from TSC, lung,[23] and RV[24] highlighting multiorgan inflammatory and apoptotic signature in MCT-treated and SuHx-induced PH rats (Figure S8). Importantly, we validated significantly increased Cx3Cl1 expression, microglial cell count, microglial activation, and astrocytic activation in patients with PAH indicating translational relevance of TSC neuroinflammation in human PAH (Figures 3C and 4C).

Previous research has demonstrated that neuron-microglia-astrocyte triad is fundamental for the functional organization of the SNS and plays a critical role in apoptosis during pathological processes.[32] Persistent excitatory glutamatergic signaling and microglial activa- tion-mediated release of neurotoxic substances, such as pyridinedicarboxylic acid and amines have been implicated in neuronal excitotoxicity and cell death.[44] Our TSC RNASeq revealed several pro-apoptotic genes such as TP53, PRF1, FOXO3, TGFβ1, TGFβR3, RET, NOS1, CELSR2 and NCOR2 that were enriched in pathways linked to apoptosis such as hypoxia, KRAS signaling down, estrogen response early, IL6 JAK STAT3 signaling and TNFα signaling via NF-kB (Figure 2E, Table S1, S3). Further, previous studies revealed that TREM2 deficiency exacerbates inflammatory cytokine release from activated M1 microglia and neuronal apoptosis.[45] Interestingly, our RNA-seq demonstrated significant decrease in TREM2 in the TSC of both rat models, which may

have contributed to the activated M1 microglia-mediated neuroinflammation and neuronal apoptosis (Figure 4D; Figure S9).

SNS activation has been well documented in experimental patients with PH and PAH.[5–7] Hypothalamic paraventricular nucleus, one of the major cardio regulatory nuclei that govern sympathetic outflow within CNS, enhances sympathetic activity via projections to the inter- mediolateral spinal column of TSC.[46] Classical microglial activation-mediated proinflammatory cytokines in the paraventricular nucleus have been shown to modulate sympathetic activity and cardiac sympathetic afferent reflex in rats.[45,47] Consistent with previous studies, our data demonstrated increased neuropeptide Y expression in TSC ventral horn and plasma norepinephrine levels in both MCT and SuHx rats terminally validating that both rat models of severe PH exhibit significantly increased sympathoexcitation, which may exacerbate RVF and result in increased mortality (Figure S7).[34] Our time-course experiments demonstrated that initial signs of PH coincided with early phase of TSC neuroinflammation without significant changes in apoptosis and sympathoexcitation (Figure S6). As PH progressed, TSC neuroinflammation and apoptosis increased, leading to aberrant sympathoexcitation and worsening RVF.

We provide evidence that daily intrathecal minocycline decreased microglial activation, astrogliosis, and expression of several proinflammatory cytokines in the TSC leading to decreased norepinephrine levels and improved cardiopulmonary structural and functional parameters resulting in attenuation of PH-RVF in MCT rats (Figure 5). In line with previous findings,[19–21,32,33] microglial activation in TSC could alter microglia–neuron crosstalk that influences synaptic activity leading to sympathoexcitation. As an anti-inflammatory antibiotic, minocycline inhibits microglial activation through several mechanisms that include inhibition of M1 polarization of microglia, attenuation of NMDA toxicity through p38

mitogen-activated protein kinase inhibition, and cytokine release by preventing 5-lipoxygenase translocation into the nucleus. Moreover, minocycline inhibits several enzymes, including matrix metalloproteinases, phospholipase A2, protein kinase C, cyclooxygenase-2 and nitric oxide synthase as well as pathways, such as inflammation, apoptosis, cell migration, and chemotaxis. Minocycline's anti-inflammatory protective actions may also include attenuation of astrogliosis as evidenced by decreased GFAP staining in the TSC of minocycline-treated MCT rats (Figure 5D).[19–21,26,48,49]

We acknowledge not including an untreated control group of rats (control+PBS) in the minocycline study as a potential limitation of our study. Also, our study did not investigate TSC gene expression in early versus late adaptation in PH. Future study should investigate specific role of TRPV1 mediated cardiopulmonary afferent signaling in TSC neuroinflammation, neuronal apoptosis and sympathoexcitation in PH-RVF.

Taken together, this study demonstrates common dysregulated genes and pathways highlighting neuroinflammation and apoptosis in the remodeled TSC and validates increased sympathoexcitation in the clinically relevant MCT and SuHx rat PH models. TSC remodeling is likely mediated by TRPV1 in the cardiac sympathetic afferent nerve endings leading to excitotoxicity. Finally, we demonstrated that amelioration of TSC neuroinflammation by minocycline in MCT rats inhibited microglial activation, decreased proinflammatory cytokines, SNS activation, and significantly attenuated PH-RVF. Targeting neuroinflammation and associated molecular pathways and genes in the TSC may yield novel therapeutic strategies for PH and RVF.

Perspectives

PH is a deadly disease without a definitive cure. As PH progresses, endothelial dysfunction coupled with vasoconstriction result in increased PVR and pulmonary arterial

pressure. Consequently, progressive increase in RV afterload and strain activates SNS as a compensatory mechanism, however chronic SNS hyperactivity is associated with arrhythmias and death. Recent reports have implicated neuroinflammation in the brain and thoracic spinal cord in pre-clinical PH, linking it to aberrant sympathoexcitation. However, the precise details of TSC remodeling and its contribution to neuroinflammation and sympathoexcitation in clinically relevant PH rat models are yet to be elucidated. We performed the first-ever transcriptomic analysis of TSC and its validation in two pre-clinical rat models of PH, which demonstrated several common key dysregulated genes in TSC that remained unchanged in lumbar spinal cord. Our study confirmed the activation of cardiopulmonary afferent signaling, pro-inflammatory and pro-apoptotic signature of thoracic spinal cord and increased circulating markers of sympathoexcitation common between MCT and SuHx rats. Moreover, we validated increased cardiopulmonary afferent signaling and neuroinflammation in TSC of human PAH. Finally, amelioration of TSC neuroinflammation by minocycline in MCT rats inhibited microglial activation, decreased pro-inflammatory cytokines, SNS activation and significantly attenuated PH and RVF. This novel study identifies new and promising therapeutic targets for PH and RV failure.

Acknowledgments:

1. Acknowledgements: We would like to thank Mylene Vaillancourt, M.Sc for her valuable technical expertise and UCLA Biostatistician Tristan Grogan for excellent statistical support.

2. Sources of funding: This work was funded by NIH NHLBI K08HL141995 and R01 HL161038 grants awarded to S.U. It was also supported by Ruth L. Kirschstein National Research Service Award T32HL069766 awarded to A.R.

3. Disclosures: Authors of this manuscript have no conflicts of interest.

Supplementary Materials and Methods

All animal studies were performed in accordance with the National Institutes of Health (NIH) Guide for the Care and Use of Laboratory Animals. Protocols received UCLA animal research committee approval.

Animal Models of Pulmonary Hypertension

Adult male Sprague Dawley rats (250-350g) received either a single subcutaneous injection of pulmonary endothelial toxin Monocrotaline (MCT, 60mg/kg, n=8) and were followed for 30 days or VEGF-receptor antagonist Sugen (SU5416, 20mg/kg, SuHx group, n=8) and kept in hypoxia (10% oxygen) for 3-weeks followed by 2-weeks of normoxia. PBS treated rats served as controls (CTRL, n=8). Serial transthoracic echocardiography was performed to monitor cardiopulmonary hemodynamics and development of PH and RV dysfunction. Direct RV and LV catheterization was performed terminally, and RV hypertrophy index was calculated as the weight ratio of RV/(LV+IVS). Thoracic and lumbar spinal cord tissue were collected.

RNA Sequencing Analysis

RNA-Seq was performed on rat TSC tissue. Libraries for RNA-Seq were prepared using SMARTer Stranded Total RNA-Seq Kit v2 - Pico Input Mammalian (Takara Bio). The resulting libraries were sequenced as single-end 50 base pair reads using NextSeq400 (Illumina). Reads were aligned to Rnor 6.0 genome using HISAT2 version 2.1.0 and transcripts were assembled and quantified using StringTie version v1.3.3b. Differential expression analysis was conducted using the R-program DeSeq2 version 1.25.16 correcting for multiple hypothesis testing using the Benjamini Hochberg method. Differentially expressed genes (DEGs) with FDR < 0.05 were considered statistically

significant. Gene set enrichment analysis was performed using the Bioconductor (release 3.1) fgsea[50] and R (version 3.6.1) software package. Hallmark[51] gene sets were obtained from molecular signature database (MSigDB)[52]. Enriched pathways considered statistically significant were defined by adjusted p-value <0.05.

Echocardiography and cardiopulmonary hemodynamic measurements

Transthoracic echocardiograms (VisualSonics Vevo3100, Toronto, Canada) were obtained using a rat specific probe (25 MHZ). Rats were anesthetized via inhaled isuflourane at 2-3%. Each rat was placed in supine position, and body temperature was maintained at 37°C. Echocardiograms including B-mode, M-mode and pulsed-wave Doppler images were obtained under isoflurane aesthesia. RV fractional area change (RVFAC) was measured from parasternal short-axis view at mid-papillary level. RV internal diameter at end-diastole (RVIDd) was measured using M-mode, parasternal short or long-axis views. LV ejection fraction (LVEF, %) was measured using M-mode echocardiographic images and pulmonary artery acceleration time (PAT) was assessed by pulmonary pulsed-wave doppler echocardiography of PA flow. The probe was placed in a parasternal long-axis position to visualize the PA outflow tract. Pulsed flow doppler imaging was then overlaid to observe the dynamics of blood flow through the PA valve. PAT was determined by calculating time taken from the start of flow to maximal velocity using echocardiogram software (Vevo 2100 version: 1.5.0).

The right ventricular systolic pressure (RVSP) and left ventricular systolic pressure (LVSP) were measured directly by inserting a catheter (1.4 F Millar SPR-671, ADInstruments) connected to a pressure transducer (Power Lab, ADInstruments) into the RV or LV just before sacrifice. Briefly, for cardiac catheterization, the rats were anesthetized with isoflurane. The animals were placed on a controlled warming pad to keep the body

temperature constant at 37 °C. After a tracheotomy was performed, a cannula was inserted, and the animals were mechanically ventilated. After a midsternal thoracotomy, rats were placed under a stereomicroscope (Zeiss, Hamburg, Germany) and a pressure-conductance catheter (model 1.4 F Millar SPR-671) was introduced via the apex into the RV or LV and positioned towards the pulmonary or aortic valve respectively. The catheter was connected to a signal processor (ADInstruments) and pressures were recorded digitally. After recording the pressures, heart, lung and spinal cord tissues were removed rapidly under deep anesthesia for preservation of protein and RNA integrity.

Gross histologic analysis, tissue preparation and imaging

The right ventricular (RV) wall, the left ventricular (LV) wall, and the interventricular septum (IVS) were dissected. RV, LV, IVS and lungs were weighed. The ratio of the RV to LV plus septal weight [RV/(LV + IVS)] was calculated as the Fulton index of RV hypertrophy. Lungs, hearts and spinal cords were fixed in 4% paraformaldehyde (PFA) in 0.1 M Na_2HPO_4 and 23 mM $NaHPO_4$ (pH 7.4) for 4h on ice. The tissue was then immersed in ice-cold 20% sucrose in 0.1 M Na_2HPO_4 and 23 mM $NaHPO_4$ (pH 7.4) overnight to cryoprotect the tissue, mounted using OCT, and transversal 4–6µm sections were obtained with a cryostat. Lung tissue sections were stained with Masson's trichrome staining. Images were acquired using a confocal microscope (Nikon).

RNA Extraction and qRT-PCR

Real-time quantitative reverse transcription PCR (qRT-PCR) was performed with total RNA that was extracted from the thoracic and lumbar regions of spinal cord from control, MCT and SuHx rats using Trizol (Invitrogen) according to the manufacturer's instructions. Two micrograms of total RNA were used for the cDNA synthesis using iScript™ cDNA Synthesis Kit (Bio-Rad). Target mRNAs were detected and quantified by a real-time PCR

instrument (CFX96 Touch, Bio-Rad) using iTaq Universal SYBR Green master mix (Bio-Rad). The results were analyzed using the comparative Ct method normalized against the housekeeping gene Gapdh. The primer sequences for real-time PCR are as follows:

Rat SLIT1 forward 5′ ATCTAGGTGCTACTCGAGCC 3′,

reverse 5′ TATCTCCAGGTGCTATCCCCA 3′

Rat VWF forward 5′ GCCTCTACCAGTGAGGTTTTGAAG 3′,

reverse 5′ ATCTCATCTCTTCTCTTCTGCTCCAGC 3′

Rat CX3CL1 forward 5′ GAATTCCTGGCGGGTCAGCACCTCGGCATA 3′,

reverse 5′ AAGCTTTTACAGGGCAGCGGTCTGGTGGT 3′

Rat TGFβ1 forward 5′ TCTCGACTCCACACAGT 3′,

reverse 5′ GCCGGGTCATTAGCTATATT 3′

Rat CNTFR forward 5′ TGGTGGTAACGAGATGGCTG 3′,

reverse 5′ GCCCAGACGCTCATACTGAA 3′

Rat RALA forward 5′ GATACAGCAGGGCAGGAAGA 3′,

reverse 5′ GTTCCCTGAAGTCCGCTGTA 3′

Rat IDI1 forward 5′ AGTCGCCAACACCATCTCTT 3′,

reverse 5′ TGCCAATCTAGCGTAGTCCT 3′

Rat SMC4 forward 5′ TGAATAGTATCCCTCCACCCC 3′,

reverse 5′ AGGTCCCAGAATTTTCTCTCCA 3′

Rat TNFα forward 5′ CCCAGACCCTCACACTCAGAT 3′,

reverse 5′ GTCCAAGAGAAGTTCCCTGTT 3′

Rat IL-6 forward 5′ GGGACTGATGTTGTTGACAG 3′,

reverse 5′ GGACCTCAAACACTTCTTGT 3′

Rat GAPDH forward 5′ ACAGCAACTCCCATTCTTCCA 3′,

reverse 5′ TCCAGGGTTTCTTACTCCTTGG 3′

Immunofluorescence staining

Thoracic spinal cord sections were fixed in 4% paraformaldehyde, then immersed in 20% sucrose, mounted with OCT compound, and sectioned at 4-6 μm. Sections were stained with the primary antibodies against substance P (Mouse Anti-SP, 1:1000, Abcam; ab14184), TRPV1 (Rabbit Anti-TRPV1, 1:200, Alomone; ACC-030), Cx3Cl1 (Rabbit Anti-Cx3Cl1, 1:250, ThermoFisher; 14-798681), microglia (Rabbit Anti-IBA1, 1:500, Fujifilm; 01919741), astrocyte (Goat Anti-GFAP, 1:100, Abcam; ab53554), neurons (Mouse Anti-NeuN, 1:500, SigmaAldrich; MAB377), Neuropeptide Y (Rabbit Anti-NPY, 1:200, Proteintech; 128331AP) and Cleaved Caspase-3 (Rabbit Anti-Asp175, 1:200, Cell Signaling; 9661). The sections were mounted using Fluoromount G with DAPI (Invitrogen # 00-4959-52). Images were acquired with a confocal microscope (Nikon).

Terminal deoxynucleotidyl transferase dUTP nick end labeling (TUNEL)

TUNEL staining was performed to assess for apoptosis in the thoracic spinal cords of MCT- and SuHx-induced PH rats. Spinal cord sections were subjected to staining with the TUNEL Assay Kit-BrdU-Red (Abcam ab66110) following the manufacturer's manual. The percentage of $TUNEL^+$ cells (integrated optical density) was calculated.

Plasma norepinephrine

Blood samples were collected from MCT- and SuHx-induced PH rats by cardiac puncture into a heparinized blood collection tube (BD Vacutainer, Franklin Lakes, NJ), and centrifuged immediately at 3000g for 10 min at 4°C. Sodium metabisulfite at a final concentration of 4 mmol/L, was added to the plasma to prevent catecholamine degradation. The enzyme immunoassay for the quantification of plasma norepinephrine levels were carried out in duplicate for each sample using a commercially available kit (Epinephrine/Norepinephrine ELISA Kit, abnova, KA1877) following the manufacturer's protocol.

Statistical Analysis

One-way ANOVA tests were used to compare between groups using GraphPad Prism. When significant differences were detected, individual mean values were compared by post-hoc tests that allowed for multiple comparisons. Analyses were run using GraphPad Prism. $P<0.05$ was considered statistically significant. Values are expressed as mean±SD. For RNAseq, differential expression analysis was conducted using the R-program DeSeq2 correcting for multiple hypothesis testing using the Benjamini Hochberg method.

Supplementary Results

Development of Severe PH and RVF in MCT and SuHx Rats

Severe PH and RVF were confirmed using serial transthoracic echocardiography and terminal right heart catheterization in rats treated with MCT or SuHx compared to PBS-treated control rats (Figure S1). Both MCT and SuHx rats developed significant PH as

evidenced by increased RV systolic pressure (RVSP) (MCT=94±14; SuHx=93±18, vs. control=37±2mmHg; p<0.0001 MCT vs. control, p<0.0001 SuHx vs. control) (Figure S1B). Additionally, decreased pulmonary artery acceleration time (PAT) (MCT=19±3; SuHx=18±3 vs. control=32±5ms; p<0.0001 MCT vs. control, p<0.0001 SuHx vs. control) and pulmonary artery acceleration time/pulmonary ejection time (PAT/PET) (MCT=0.24±0.04; SuHx=0.23±0.03 vs. control=0.41±0.04mmHg; p<0.0001 MCT vs. control, p<0.0001 SuHx vs. control) ratio also demonstrated severity of PH (Figure S1C, D,J). RV dysfunction was demonstrated by increased RV internal diameter at end-diastole ($RVID_d$) (MCT=3.5±1.04; SuHx=2.9±0.77 vs. control=1.9±0.66mm; p=0.002 MCT vs. control, p=0.032 SuHx vs. control) and decreased RV fractional area change (RVFAC) (MCT=13±5.35; SuHx=17±3.59 vs. control=40±14.1%; p=0.0007 MCT vs. control, p=0.003 SuHx vs. control) in MCT and SuHx rats (Figure S1E, F,J). MCT and SuHx rats also demonstrated an increase in Fulton index of RV hypertrophy (MCT=0.8±0.1; SuHx=0.6±0.1 vs. control=0.3±0.01; p<0.0001 MCT vs. control, p=0.001 SuHx vs. control) (Figure S1G). No significant differences were observed between SuHx- and MCT-treated groups in all the parameters. Left ventricular ejection fraction (LVEF) and left ventricular systolic pressure (LVSP) were preserved between control, MCT and SuHx groups (Figure S1H, I).

Supplementary Figures

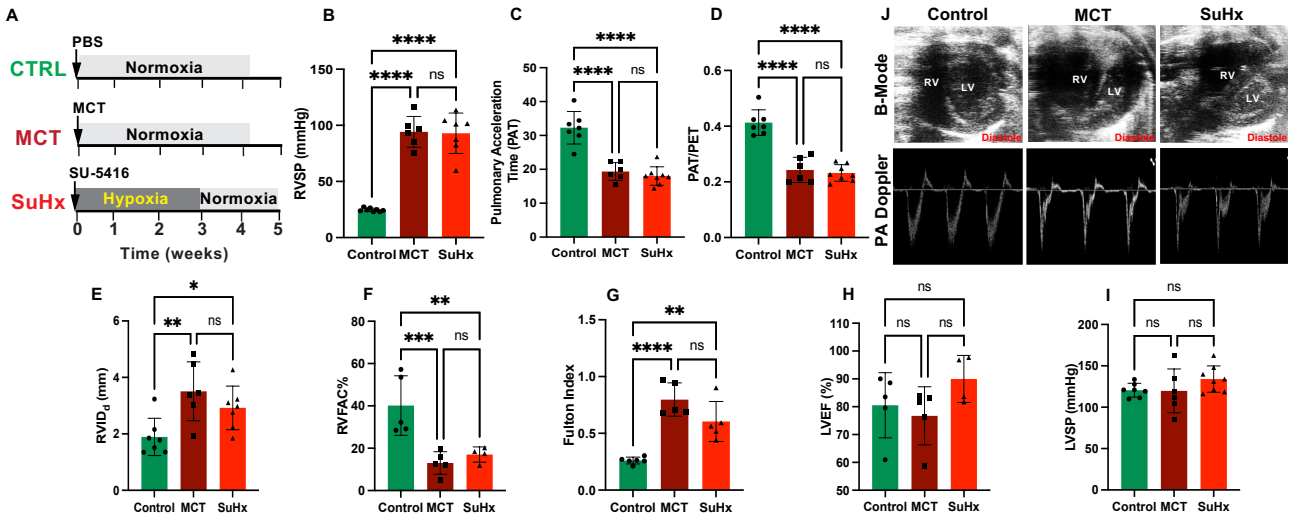

Figure S1. Experimental models of severe PH and RV failure in rats. (A) Experimental Protocol. (B) RV systolic pressure (RVSP, mmHg), (C) Pulmonary artery acceleration time (PAT, mS), (D) Pulmonary artery acceleration time/Pulmonary ejection time (PAT/PET) ratio, (E) RV internal diameter at end diastole ($RVID_d$, mm), (F) RV fractional area change (RVFAC, %), (G) Fulton index of RV hypertrophy [RV/(LV+IVS)], (H) Left ventricular ejection fraction (LVEF, %) and (I) LV systolic pressure (LVSP, mmHg) in control, MCT and SuHx groups. (J) From top to bottom: Images obtained from rat heart echocardiography in B-mode and pulsed-wave doppler mode from control, MCT and SuHx groups. N=4-8 per group. *p<0.05, **p<0.01, ***p<0.001, ****p<0.0001.

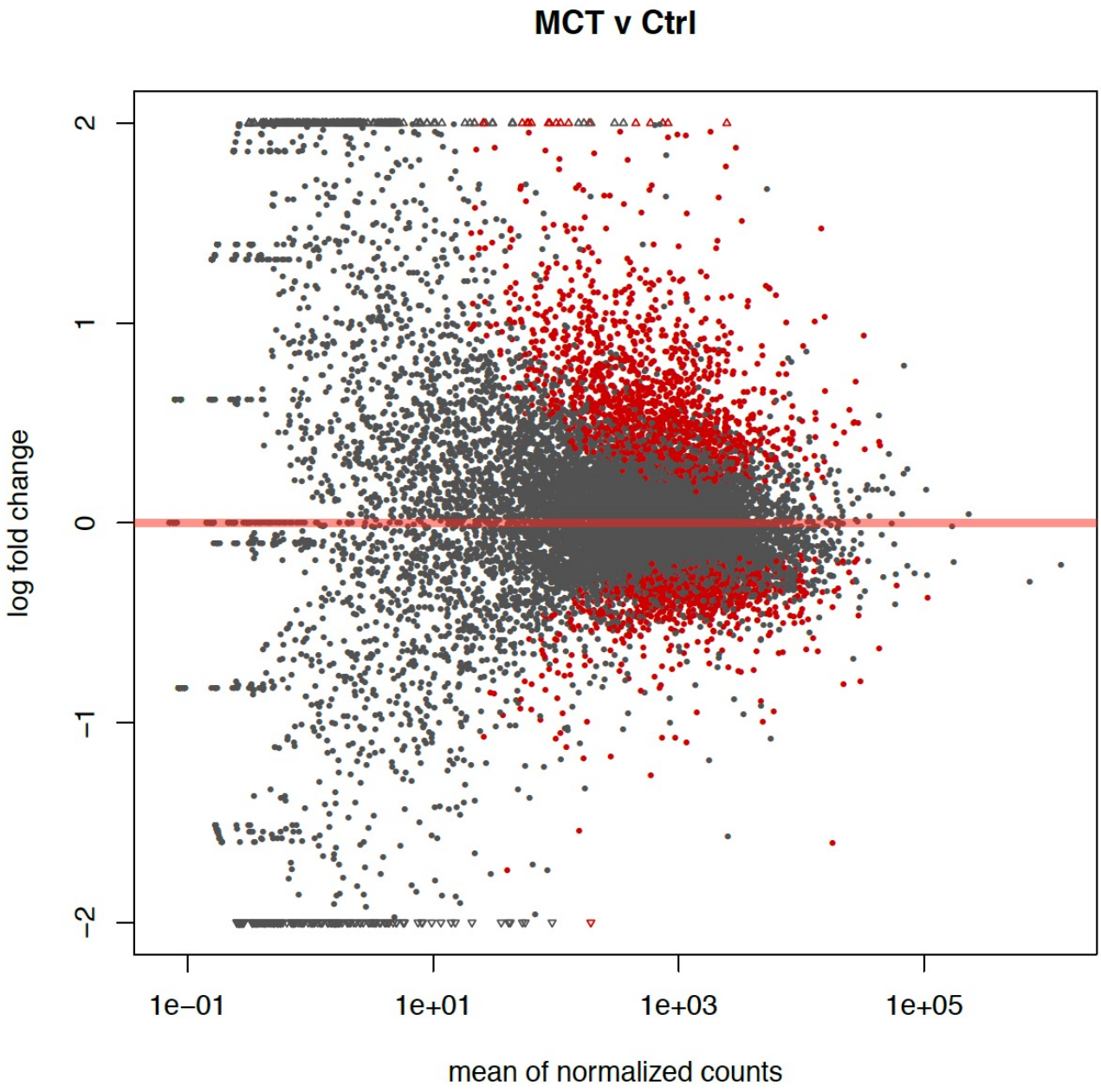

Figure S2. Volcano plot of log fold change vs. mean expression for all genes from thoracic spinal cords for comparing MCT vs. Control groups. Differentially expressed genes with FDR <0.05 are represented as red dots.

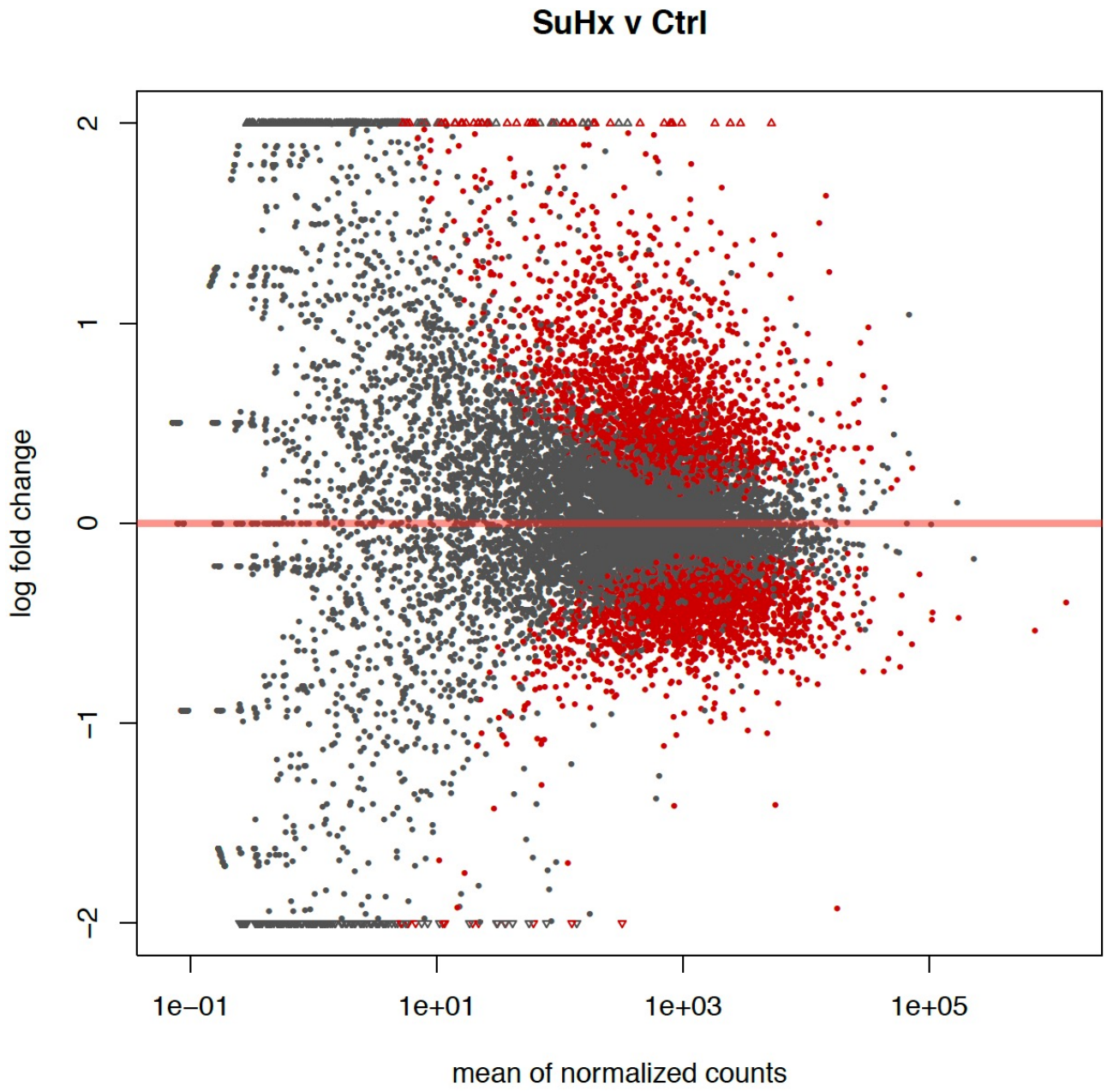

Figure S3. Volcano plot of log fold change vs. mean expression for all genes from thoracic spinal cords for comparing SuHx vs. Control groups. Differentially expressed genes with FDR <0.05 are represented as red dots.

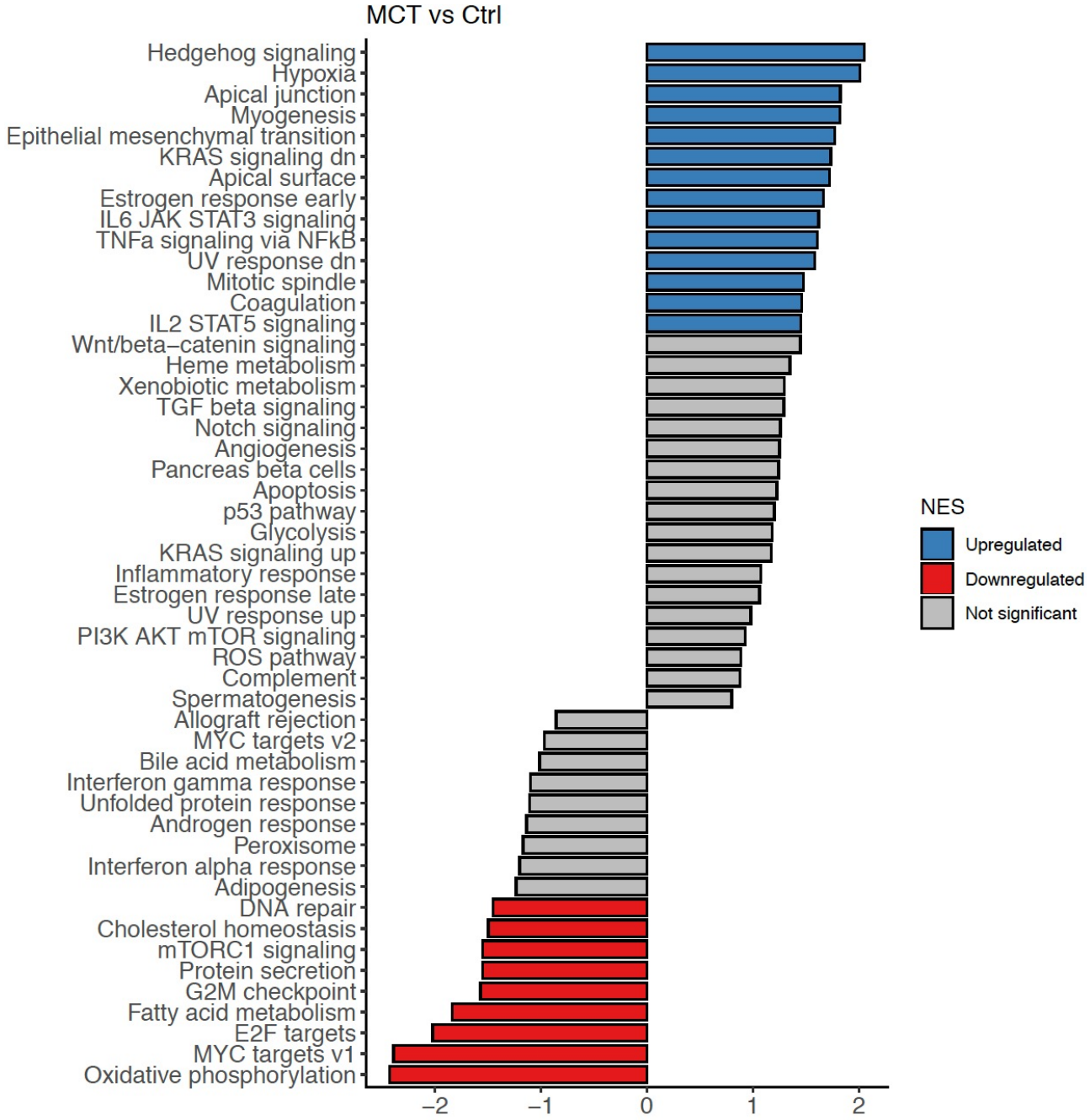

Figure S4. Bar plot showing normalized enrichment scores (NES) for Hallmark pathways derived from Gene Set Enrichment Analysis (GSEA). For GSEA, differentially expressed genes between MCT vs. Control were ranked by the Wald statistic derived from DESeq2. Bars in blue and red represent statistically significant (FDR<0.05) pathways up- and downregulated, respectively.

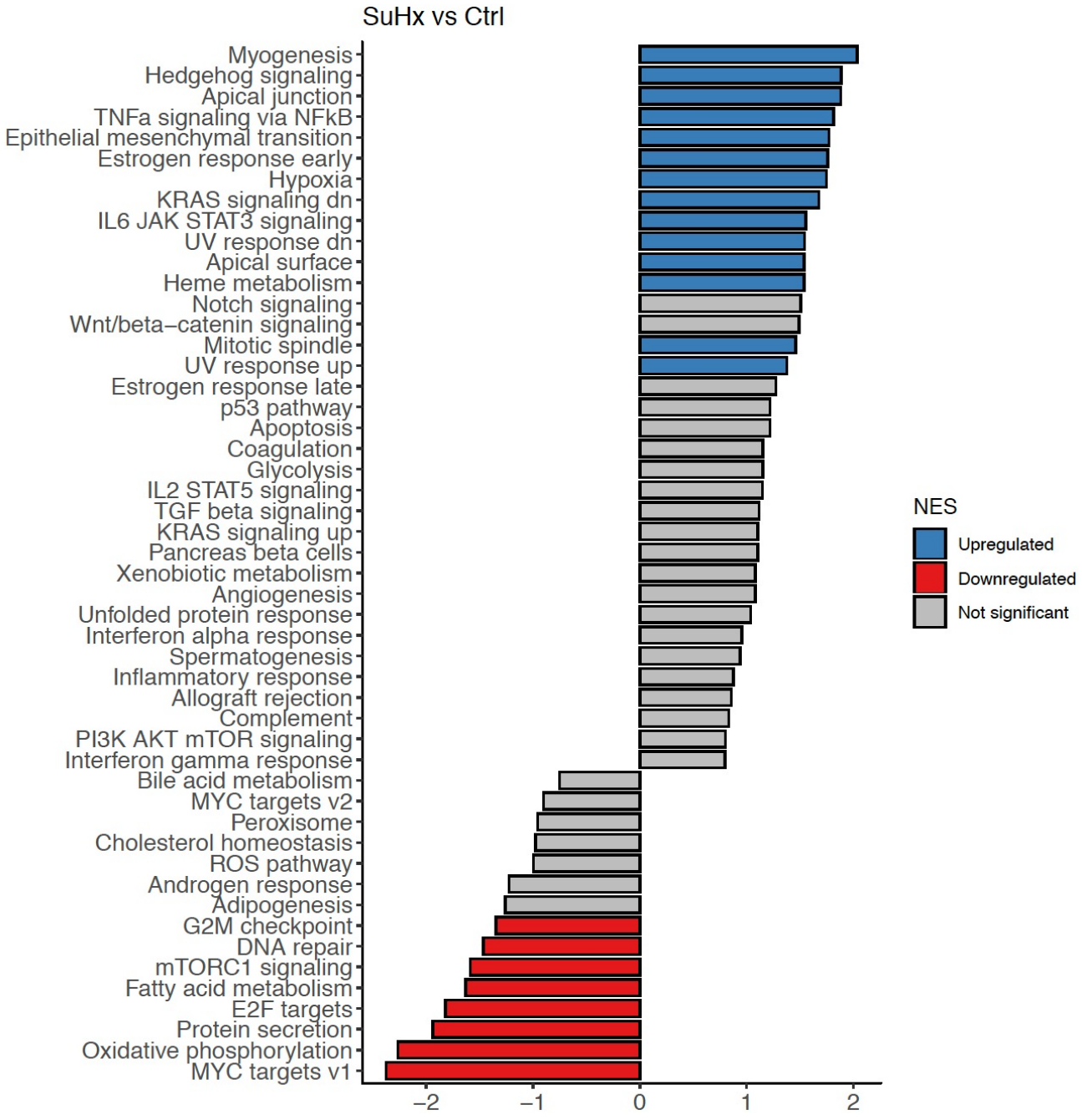

Figure S5. Bar plot showing normalized enrichment scores (NES) for Hallmark pathways derived from Gene Set Enrichment Analysis (GSEA). For GSEA, differentially expressed genes between SuHx vs. Control were ranked by the Wald statistic derived from DESeq2. Bars in blue and red represent statistically significant (FDR<0.05) pathways up- and downregulated, respectively.

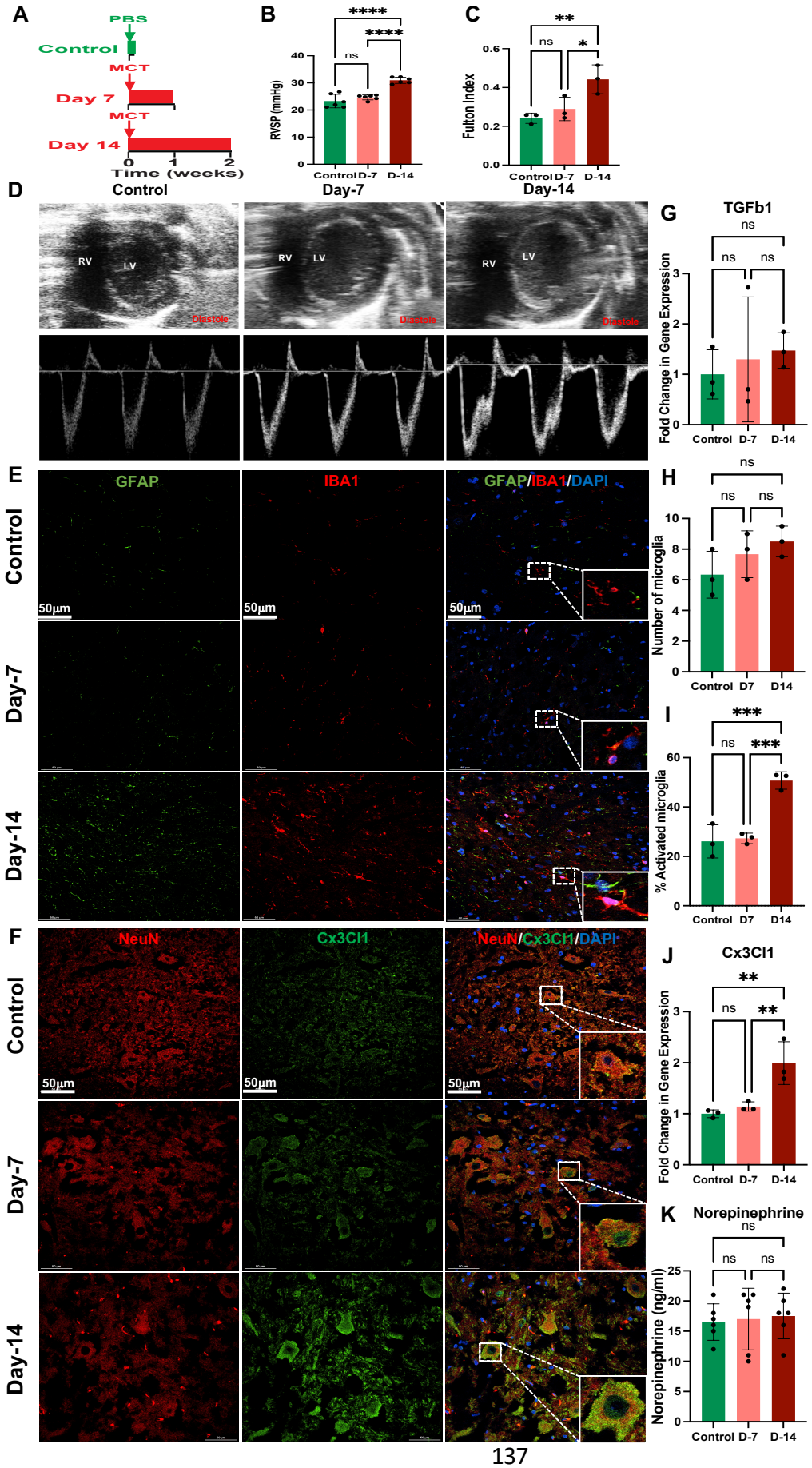
A
PBS
Control
MCT
Day 7
MCT
Day 14
0
1
2
Time (weeks)
B
****
****
ns
RVSP (mmHg)
40
30
20
10
0
Control D-7 D-14
C
**
ns
*
Fulton Index
0.6
0.4
0.2
0.0
Control D-7 D-14
D
Control
Day-7
Day-14
RV
LV
Diastole
E
GFAP
IBA1
GFAP/IBA1/DAPI
Control
Day-7
Day-14
50µm
F
NeuN
Cx3Cl1
NeuN/Cx3Cl1/DAPI
Control
Day-7
Day-14
50µm
G
TGFb1
ns
ns
ns
Fold Change in Gene Expression
3
2
1
0
Control D-7 D-14
H
ns
ns
ns
Number of microglia
10
8
6
4
2
0
Control D7 D14
I
***
ns
***
% Activated microglia
60
40
20
0
Control D7 D14
J
Cx3Cl1
**
ns
**
Fold Change in Gene Expression
3
2
1
0
Control D-7 D-14
K
Norepinephrine
ns
ns
ns
Norepinephrine (ng/ml)
25
20
15
10
5
0
Control D-7 D-14

Figure S6. Time dependent increase of PH, TSC neuroinflammation, apoptosis and associated sympathoexcitation in MCT-induced PH rats. (**A**) Experimental Protocol. (**B**) Right ventricular systolic pressure (RVSP) at day-0 (Control), -7 and -14 after MCT injection. N=6 per group, ****p<0.0001. (**C**) Fulton index at day-0 (Control), -7 and -14 after MCT injection. N=3 per group, *p<0.05, **p<0.01. (**D**) B-Mode echo and PA Doppler at day-0 (Control), -7 and -14 after MCT injection. (**E**) Representative images of immunofluorescence staining with microglial marker anti-Iba1 (Red), astrocytic marker anti-GFAP (Green) and DNA marker DAPI (Blue) in the TSC of rats at day-0 (Control), -7 and -14 after MCT injection. N=3 per group. (**F**) Representative images of immunofluorescence staining with neuronal marker NeuN (Red), Cx3Cl1 (Green) and DAPI (Blue) in the TSC of rats at day-0 (Control), -7 and -14 after MCT injection. N=3 per group. (**G**) Normalized qRT-PCR data of pro-apoptotic gene TGFβ1expression in the TSC from rats at day-0 (Control), -7 and -14 after MCT injection. N=3 per group. (**H**) Quantification of number of microglia/HPF in the TSC from rats at day-0 (Control), -7 and -14 after MCT injection. (**I**) Percent activated microglia/HPF in the TSC from rats at day-0 (Control), -7 and -14 after MCT injection. N=3 per group. ***p<0.001. (**J**) normalized qRT-PCR data of pro-inflammatory gene Cx3Cl1 expression in the TSC from rats at day-0 (Control), -7 and -14 after MCT injection. N=3 per group. **p<0.01. (**K**) Plasma norepinephrine level measured by ELISA from rats at day-0 (Control), -7 and -14 after MCT injection. N=6 per group.

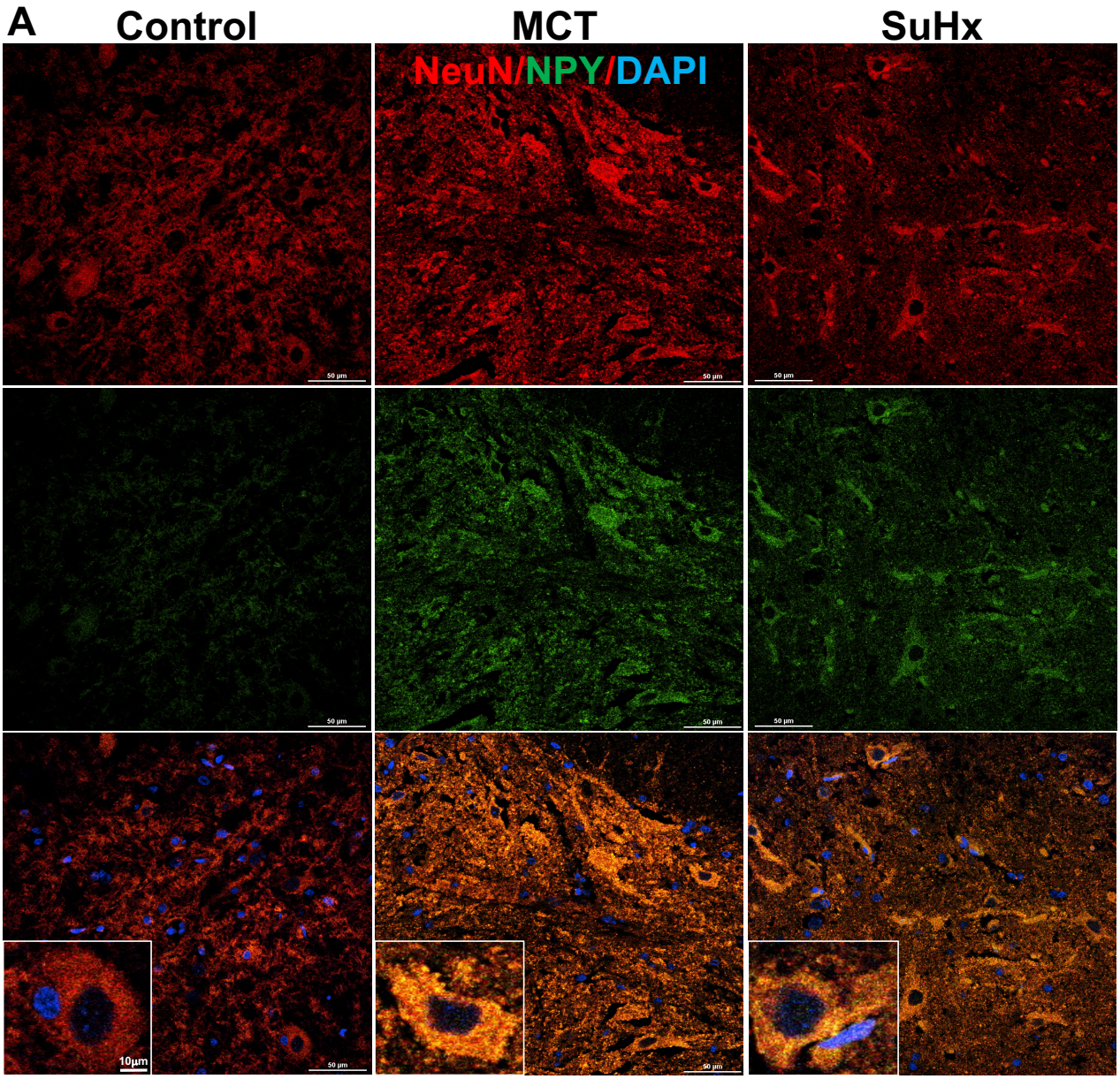
A
Control
MCT
SuHx
NeuN/NPY/DAPI
50 µm
10µm

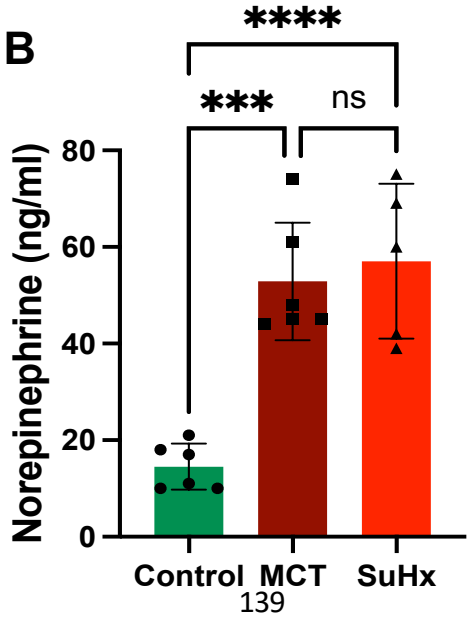
B
****
***
ns
Norepinephrine (ng/ml)
80
60
40
20
0
Control
MCT
SuHx

Figure S7. Increased NPY in the ventral horn of TSC and circulating catecholamines as markers of sympathoexcitation in MCT- and SuHx-induced PH. (**A**) Representative images of immunofluorescence staining with anti-NPY (Red), anti-NeuN (Green), and DAPI (DNA; blue) from ventral horn gray matter. Lower panel shows enlarged view of NPY and NeuN colocalization (Yellow) in control compared with MCT and SuHx. N=3 per group. (**B**) Plasma norepinephrine levels measured by ELISA are significantly increased in MCT and SuHx rats compared to controls. N=5-6 per group. ***p<0.001, ****p<0.0001.

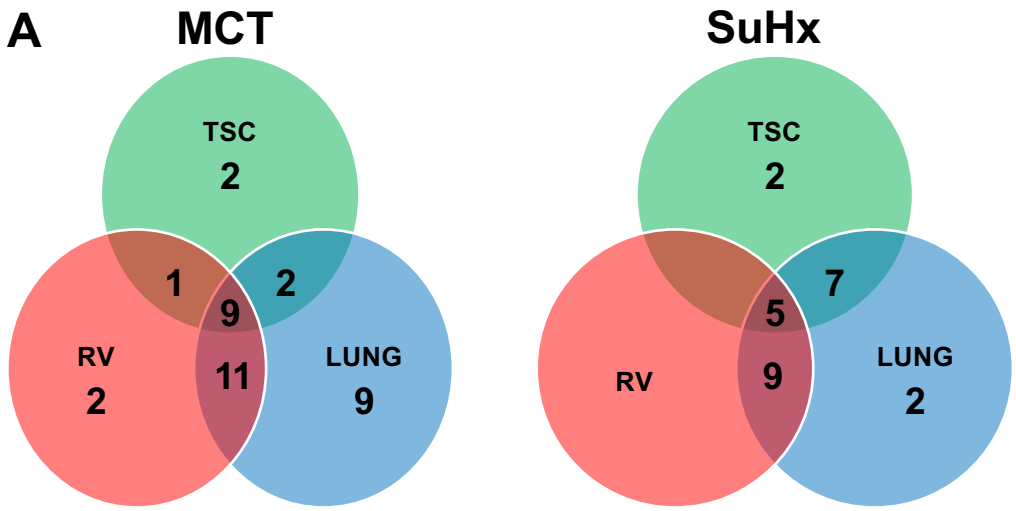

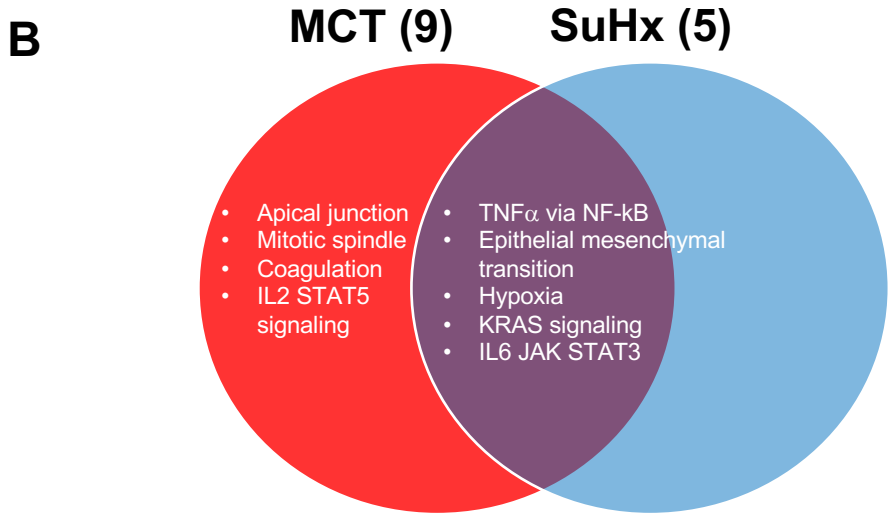

Figure S8. RNA-Seq based pathway enrichment analysis from TSC, right ventricles and lungs of MCT and SuHx rats. (A) Venn diagram showing significantly up-regulated pathways (based on FDR<0.05) and their overlap in thoracic spinal cords, right ventricles and lungs of MCT and SuHx groups respectively. (B) Venn diagram showing common significantly up-regulated pathways (based on FDR<0.05) in TSC, RV and lung highlighting proinflammatory signature in MCT- and SuHx-induced PH.

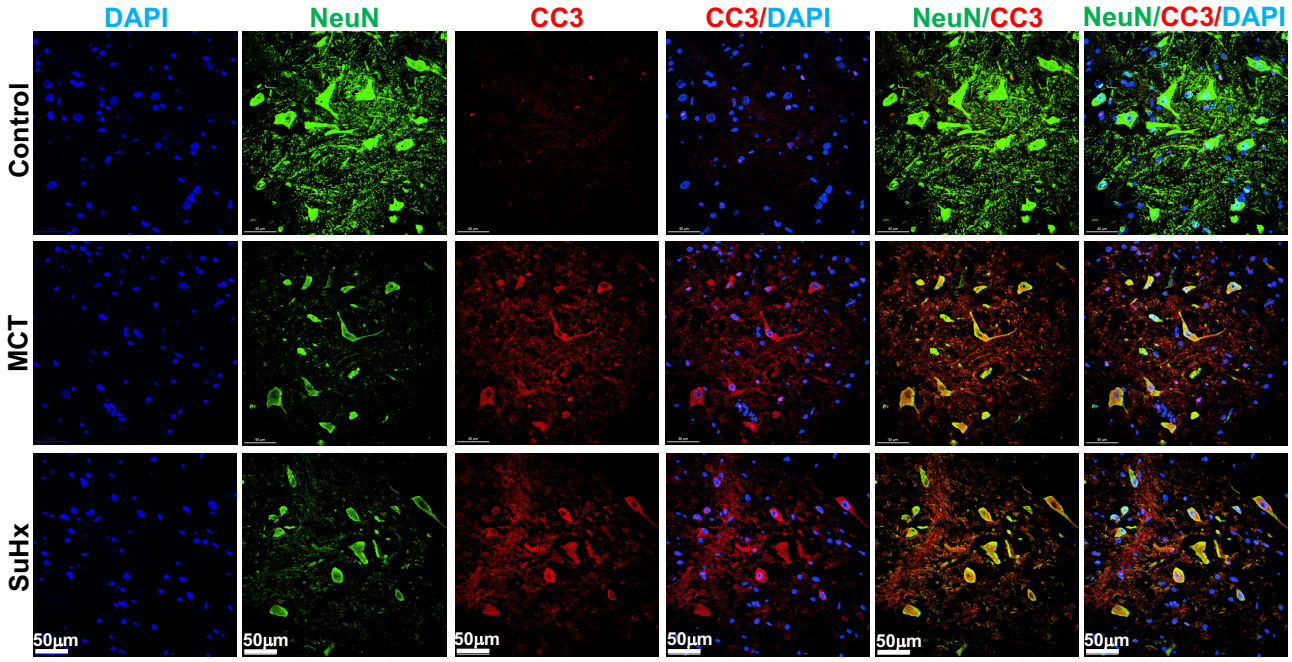

Figure S9. Increased neuronal apoptosis in the TSC of MCT and SuHx rats. (A) Representative images of immunofluorescence staining with DAPI (DNA; blue), anti-NeuN (Neuron; Green), anti-Cleaved Caspase-3 (CC3; Red), CC3 and DAPI colocalization, NeuN and CC3 colocalization (Yellow) and merged images from the TSC of control, MCT and SuHx rats. N=3 per group.

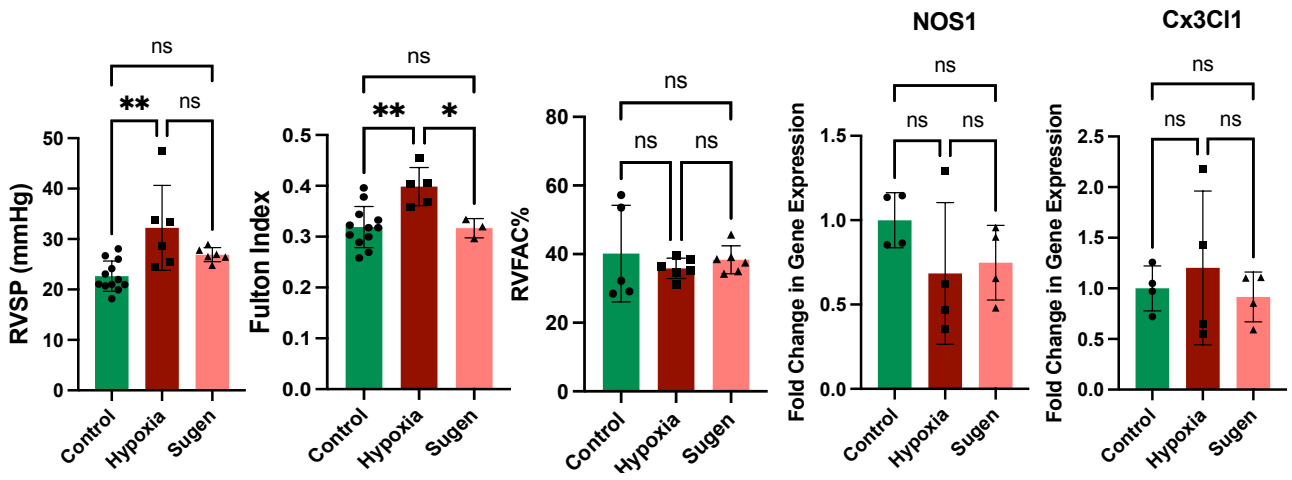

Figure S10. Hypoxia or Sugen alone do not induce TSC NOS1 and Neuroinflammation. RVSP, Fulton Index, RVFAC, expression of NOS1 and Cx3cl1 in Control, hypoxia, and Sugen alone. N=6-12. *p<0.05, **p<0.01.

Supplementary Tables

Table S1: Leading edge upregulated genes from MCT vs. Control

Hedgehog signaling	log2FC	padj	Hypoxia	log2FC	padj	Apical junction	log2FC	padj	Myogenesis	log2FC	padj	Epithelial mesenchymal transition	log2FC	padj	KRAS signaling dn	log2FC	padj
SLIT1	1.52923316	0.00132072	SERPINE1	2.15703066	0.00327275	VWF	1.93667602	3.81E-07	NOS1	2.91473019	0.0040949	SERPINE1	2.15703066	0.00327275	NOS1	2.91473019	0.0040949
L1CAM	1.2196331	0.00047839	MAFF	1.1804272	0.02459397	ATP1A3	1.47410359	3.37E-06	CACNA1H	1.30269704	0.00187157	COL4A1	1.21253977	0.00025107	SGK1	2.02187581	0.01781026
CNTFR	0.86338726	0.00040688	CTGF	1.12729245	0.00067825	ZYX	1.10264733	5.44E-08	CDKN1A	1.02703503	0.04111099	CTGF	1.12729245	0.00067825	CELSR2	1.92733061	0.00127072
ACHE	0.84116685	0.00012776	CDKN1A	1.02703503	0.04111099	NLGN2	1.01713745	0.00117823	TGFB1	0.95957948	0.01221739	ECM1	1.07790511	0.00758918	TCF7L1	1.29676197	0.00398718
NKX6-1	0.75475976	0.01954071	PFKL	1.00351614	1.55E-07	COL16A1	0.9830112	0.0150533	ACHE	0.84116685	0.00012776	FN1	1.00943264	3.00E-05	SLC5A5	1.2026906	0.00402044
VEGFA	0.64377283	0.02339733	NFIL3	0.84625767	0.0314438	JUP	0.8510631	0.01100947	MEF2D	0.82017115	0.0116954	COL16A1	0.9830112	0.0150533	SYNPO	1.15896479	0.00011156
TLE3	0.60021556	1.27E-06	IRS2	0.78999334	0.01191473	PKD1	0.83950447	0.00702429	GAA	0.74347084	0.00122352	SLIT3	0.97152188	0.00684493	EDN1	1.13918079	2.54E-06
CRMP1	0.49279734	0.03708276	ZFP36	0.77347349	0.00413902	NRXN2	0.82213913	0.00401279	GNAO1	0.70545644	0.00758918	TGFB1	0.95957948	0.01221739	ABCG4	0.93616392	0.00612042
RTN1	0.41531716	0.02179859	FOXO3	0.77076389	7.34E-05	FLNC	0.81853833	0.01739358	LPIN1	0.66252503	7.19E-06	LRP1	0.88346029	0.00301657	CLSTN3	0.90075433	0.00010213
LDB1	0.24365635	0.04444929	SLC2A1	0.74979411	2.65E-06	CX3CL1	0.80803224	0.00927777	SPTAN1	0.66097616	0.00711834	BGN	0.71395918	0.04776776	CNTFR	0.86338726	0.00040688

Table S2: Leading edge downregulated genes from MCT vs. Control

Oxidative phosphorylation	log2FC	padj	MYC targets v1	log2FC	padj	E2F targets	log2FC	padj	Fatty acid metabolism	log2FC	padj	G2M checkpoint	log2FC	padj	Protein secretion	log2FC	padj
ATP5I	-0.4602775	0.03014973	HSPE1	-0.4663213	0.0344881	HMMR	-0.5156615	0.00726704	IDI1	-0.9945439	2.85E-08	HMMR	-0.5156615	0.00726704	VAMP3	-0.4824885	0.00081044
HSD17B10	-0.4101781	0.02629044	SNRPB2	-0.4023445	0.0434563	PRIM2	-0.5146526	0.01640269	HMGCS1	-0.7918761	0.0395009	PRIM2	-0.5146526	0.01640269	RAB9A	-0.4238423	0.00604386
NDUFB5	-0.4096467	0.03641204	EIF1AX	-0.3749151	0.00840991	SMC4	-0.5053989	0.00069059	ALDH1A1	-0.525869	0.03224216	SMC4	-0.5053989	0.00069059	ARFIP1	-0.3679903	0.02110056
IDH1	-0.4018254	2.26E-05	ABCE1	-0.3419424	0.00023078	PLK4	-0.4664285	0.00996213	MCEE	-0.4607909	0.01928823	PLK4	-0.4664285	0.00996213	TMED2	-0.3091218	0.00594054
CYB5A	-0.3894884	0.01111554	EIF3J	-0.3413659	0.00404205	NASP	-0.3941683	0.00620641	HSD17B10	-0.4101781	0.02629044	KATNA1	-0.3945287	0.01961316	PPT1	-0.2441644	0.01115309
SDHC	-0.3624935	0.00643443	YWHAQ	-0.3406791	0.00277792	CBX5	-0.309343	0.04920589	IDH1	-0.4018254	2.26E-05	NASP	-0.3941683	0.00620641	GLA	-0.2226622	0.01178948
MRPL35	-0.3476328	0.03243418	EIF4A1	-0.337197	0.01133372	IPO7	-0.2848156	0.03661852	RDH11	-0.4004075	0.04287412	HIF1A	-0.2981458	0.0020636	RER1	-0.2076079	0.04832511
MRPS22	-0.3048557	0.0230967	HNRNPA1	-0.264461	0.02074197	EED	-0.2829055	0.02394236	HIBCH	-0.3830768	0.00297677	DTYMK	-0.2337329	0.04763575			
PRDX3	-0.2616599	0.01824858	CLNS1A	-0.2642205	0.02434174	AK2	-0.2786334	0.03587913	SDHC	-0.3624935	0.00643443	CTCF	-0.1979872	0.02459704			
HADHB	-0.2521579	0.0004723	PRDX3	-0.2616599	0.01824858	CSE1L	-0.2742685	0.00081044	ECI2	-0.3311596	0.03449003						

Table S3: Leading edge upregulated genes from SuHx vs. Control

Myogenesis	log2FC	padj	Apical junction	log2FC	padj	Hedgehog signaling	log2FC	padj	TNFa signaling via NFkB	log2FC	padj	Epithelial mesenchymal transition	log2FC	padj	Estrogen response early	log2FC	padj
NOS1	2.99711754	0.00011287	MYH9	2.23323215	0.05273871	SLIT1	1.89100726	1.99E-05	PER1	1.64049986	6.75E-05	TGFB1	1.27447756	0.00023292	CELSR2	2.20487632	7.69E-05
MYH9	2.23323215	0.05273871	ATP1A3	1.64037253	9.35E-08	L1CAM	1.4697053	6.94E-06	BCL3	1.577725	0.01898447	ECM1	1.24368912	0.0007332	NCOR2	1.79553703	2.00E-05
CACNA1H	1.56660571	5.31E-05	VWF	1.54761153	3.89E-05	ACHE	0.91605159	9.63E-06	KDM6B	1.44012204	0.00190701	SLIT3	1.12042022	0.00062203	CBFA2T3	1.38491412	0.00198345
TGFB1	1.27447756	0.00023292	NLGN2	1.20663041	3.53E-05	CNTFR	0.90803833	7.56E-05	NR4A1	1.34410983	0.00113308	COL4A1	1.1165481	0.00034093	WFS1	1.37086532	0.00053893
SOD3	1.24042158	0.00013149	CX3CL1	1.17070771	3.24E-05	NRP2	0.7289368	0.0379429	KLF2	1.18702462	1.84E-07	COL5A1	1.08843298	0.01862121	TJP3	1.30989669	0.02753758
NAV2	1.19070543	0.00736234	NRXN2	1.12139226	1.99E-05	NKX6-1	0.64121584	0.03201497	ZFP36	1.14086035	3.96E-06	CYR61	1.05610837	0.00128525	FLNB	1.21169322	0.00879893
MEF2D	0.97735456	0.00092609	ZYX	1.11408757	2.27E-08	TLE3	0.63564196	1.19E-07	CEBPB	1.06326416	0.0023259	COL16A1	1.02293558	0.00558921	NAV2	1.19070543	0.00736234
AGRN	0.95444814	0.00594105	COL16A1	1.02293558	0.00558921	RTN1	0.61294823	0.00015805	BTG2	1.06097519	0.00622523	LRP1	1.01943875	0.0002044	IGF1R	0.91300154	0.00293567
GAA	0.94641479	9.85E-06	JUP	1.00386351	0.00096895	CRMP1	0.58951571	0.00526393	EGR1	1.05773067	0.01987758	NOTCH2	0.94910812	0.00047049	FASN	0.85202853	0.02557508
MYOM2	0.93847503	0.01610441	PKD1	0.95409753	0.0008152	ETS2	0.39151693	0.02274943	CYR61	1.05610837	0.00128525	BGN	0.94102143	0.00317483	RET	0.81686885	1.73E-09

Table S4: Leading edge downregulated genes from SuHx vs. Control

MYC targets v1	log2FC	padj	Oxidative phosphorylation	log2FC	padj	Protein secretion	log2FC	padj	E2F targets	log2FC	padj	Fatty acid metabolism	log2FC	padj	mTORC1 signaling	log2FC	padj
MAD2L1	-0.6506953	0.01238654	CYCS	-0.6540507	0.01289529	STX7	-0.6860614	0.04223023	PAICS	-0.7376966	6.22E-06	CIDEA	-1.6971151	0.00011225	ELOVL6	-1.4139301	0.01643881
PSMC6	-0.6283155	0.00660682	ETFA	-0.6368364	0.00190588	YIPF6	-0.681641	0.00132626	SMC4	-0.691634	6.67E-07	IDI1	-1.0501473	1.73E-09	IDI1	-1.0501473	1.73E-09
SNRPB2	-0.6065325	0.00054773	TIMM8B	-0.6331286	0.03408694	CAV2	-0.6310332	0.00049914	MAD2L1	-0.6506953	0.01238654	OSTC	-0.5806135	0.00548695	PRDX1	-0.6667162	3.67E-05
EIF2S2	-0.6017194	0.00059868	COX6C	-0.5648643	0.03220819	VAMP7	-0.6033581	0.00014836	PLK4	-0.6486813	8.26E-05	HSD17B10	-0.5639058	0.00061283	TM7SF2	-0.6529173	0.01212614
PRDX4	-0.5738238	0.00119421	HSD17B10	-0.5639058	0.00061283	VAMP3	-0.5645947	2.78E-05	RPA3	-0.5991998	0.00501784	ALDH1A1	-0.5373104	0.01581011	PSMC6	-0.6283155	0.00660682
SNRPD1	-0.5626125	0.00843077	ATP5L	-0.5582338	0.04036535	SNAP23	-0.5637627	0.00222131	HMMR	-0.5895495	0.0007792	IDH1	-0.4898324	4.67E-08	TCEA1	-0.618892	0.00219411
RPL22	-0.5624908	0.01668785	COX7C	-0.5560833	0.04235892	BET1	-0.5588287	0.00333788	PRDX4	-0.5738238	0.00119421	HIBCH	-0.4882273	3.89E-05	PSMA3	-0.6038286	0.00175107
PPIA	-0.5316288	0.01970254	NDUFV2	-0.5516004	0.04313666	ARFIP1	-0.5546454	0.00011181	GINS4	-0.5442734	0.00738578	PTS	-0.4749547	0.00506911	EIF2S2	-0.6017194	0.00059868
NPM1	-0.5314841	0.02614638	CYB5A	-0.5515572	7.56E-05	RAB5A	-0.5544714	0.00085748	TIPIN	-0.5264054	0.02693264	DECR1	-0.4701517	0.00462211	CD9	-0.5453986	3.81E-05
HDDC2	-0.5256748	0.00680919	ATP6V1G1	-0.5435872	0.00582496	TPD52	-0.5037851	0.00090371	PRIM2	-0.5088931	0.00935769	DLD	-0.4439073	0.01595298	PPIA	-0.5316288	0.01970254

References

1. Rabinovitch M. Molecular pathogenesis of pulmonary arterial hypertension. J Clin Invest. 2012 Dec122(12):4306-13. doi: 10.1172/JCI60658.

2. Dandel M, Knosalla C, Kemper D, Stein J, Hetzer R. Assessment of right ventricular adaptability to loading conditions can improve the timing of listing to transplantation in patients with pulmonary arterial hypertension. J Heart Lung Transplant. 2015 Mar;34(3):319-28. doi: 10.1016/j.healun.2014.11.012.

3. Wijeratne DT, Lajkosz K, Brogly SB, Lougheed MD, Jiang L, Housin A, Barber D, Johnson A, Doliszny KM, Archer SL. Increasing Incidence and Prevalence of World Health Organization Groups 1 to 4 Pulmonary Hypertension: A Population-Based Cohort Study in Ontario, Canada. Circ Cardiovasc Qual Outcomes. 2018 Feb;11(2):e003973. doi: 10.1161/CIRCOUTCOMES.117.003973.

4. Vaillancourt M, Chia P, Sarji S, Nguyen J, Hoftman N, Ruffenach G, Eghbali M, Mahajan A, Umar S. Autonomic nervous system involvement in pulmonary arterial hypertension. Respir Res. 2017 Dec 4;18(1):201. doi: 10.1186/s12931-017-0679-6.

5. Ciarka A, Doan V, Velez-Roa S, Naeije R, van de Borne P. Prognostic significance of sympathetic nervous system activation in pulmonary arterial hypertension. Am J Respir Crit Care Med. 2010 Jun 1;181(11):1269-75. doi: 10.1164/rccm.200912-1856OC.

6. Mak S, Witte KK, Al-Hesayen A, Granton JJ, Parker JD. Cardiac sympathetic activation in patients with pulmonary arterial hypertension. Am J Physiol Regul Integr Comp Physiol. 2012 May 15;302(10):R1153-7. doi: 10.1152/ajpregu.00652.2011.

7. Velez-Roa S, Ciarka A, Najem B, Vachiery JL, Naeije R, van de Borne P. Increased sympathetic nerve activity in pulmonary artery hypertension. Circulation. 2004 Sep 7;110(10):1308-12. doi: 10.1161/01.CIR.0000140724.90898.D3.

8. Wensel R, Jilek C, Dörr M, Francis DP, Stadler H, Lange T, Blumberg F, Opitz C, Pfeifer M, Ewert R. Impaired cardiac autonomic control relates to disease severity in pulmonary hypertension. Eur Respir J. 2009 Oct;34(4):895-901. doi: 10.1183/09031936.00145708.

9. Saddic LA, Howard-Quijano K, Kipke J, Kubo Y, Dale EA, Hoover D, Shivkumar K, Eghbali M, Mahajan A. Progression of myocardial ischemia leads to unique changes in immediate-early gene expression in the spinal cord dorsal horn. Am J Physiol Heart Circ Physiol. 2018 Dec 1;315(6):H1592-H1601. doi: 10.1152/ajpheart.00337.2018.

10. Wang HJ, Rozanski GJ, Zucker IH. Cardiac sympathetic afferent reflex control of cardiac function in normal and chronic heart failure states. J Physiol. 2017 Apr 15;595(8):2519-2534. doi: 10.1113/JP273764. Epub 2017 Feb 27. PMID: 28116751; PMCID: PMC5390865.

11. Steagall RJ, Sipe AL, Williams CA, Joyner WL, Singh K. Substance P release in response to cardiac ischemia from rat thoracic spinal dorsal horn is mediated by TRPV1. Neuroscience. 2012 Jul 12;214:106-19. doi: 10.1016/j.neuroscience.2012.04.023. Epub 2012 Apr 21. PMID: 22525132.

12. Zahner MR, Li DP, Chen SR, Pan HL. Cardiac vanilloid receptor 1-expressing afferent nerves and their role in the cardiogenic sympathetic reflex in rats. J Physiol. 2003 Sep 1;551(Pt 2):515-23. doi: 10.1113/jphysiol.2003.048207. Epub 2003 Jun 26. PMID: 12829722; PMCID: PMC2343227.

13. Kong WL, Peng YY, Peng BW. Modulation of neuroinflammation: Role and therapeutic potential of TRPV1 in the neuro-immune axis. Brain Behav Immun. 2017 Aug;64:354-366. doi: 10.1016/j.bbi.2017.03.007. Epub 2017 Mar 22. PMID: 28342781.

14. Ajijola OA, Yagishita D, Patel KJ, Vaseghi M, Zhou W, Yamakawa K, So E, Lux RL, Mahajan A, Shivkumar K. Focal myocardial infarction induces global remodeling of cardiac

sympathetic innervation: neural remodeling in a spatial context. Am J Physiol Heart Circ Physiol. 2013 Oct 1;305(7):H1031-40. doi: 10.1152/ajpheart.00434.2013.

15. Ajijola OA, Yagishita D, Reddy NK, Yamakawa K, Vaseghi M, Downs AM, Hoover DB, Ardell JL, Shivkumar K. Remodeling of stellate ganglion neurons after spatially targeted myocardial infarction: Neuropeptide and morphologic changes. Heart Rhythm. 2015 May;12(5):1027-35. doi: 10.1016/j.hrthm.2015.01.045.

16. Nakamura K, Ajijola OA, Aliotta E, Armour JA, Ardell JL, Shivkumar K. Pathological effects of chronic myocardial infarction on peripheral neurons mediating cardiac neurotransmission. Auton Neurosci. 2016 May;197:34-40. doi: 10.1016/j.autneu.2016.05.001.

17. Armour JA, Linderoth B, Arora RC, DeJongste MJ, Ardell JL, Kingma JG Jr, Hill M, Foreman RD. Long-term modulation of the intrinsic cardiac nervous system by spinal cord neurons in normal and ischaemic hearts. Auton Neurosci. 2002 Jan 10;95(1-2):71-9. doi: 10.1016/s1566-0702(01)00377-0.

18. Gao C, Howard-Quijano K, Rau C, Takamiya T, Song Y, Shivkumar K, Wang Y, Mahajan A. Inflammatory and apoptotic remodeling in autonomic nervous system following myocardial infarction. PLoS One. 2017 May 18;12(5):e0177750. doi: 10.1371/journal.pone.0177750.

19. Sharma RK, Oliveira AC, Kim S, Rigatto K, Zubcevic J, Rathinasabapathy A, Kumar A, Lebowitz JJ, Khoshbouei H, Lobaton G *et al*. Involvement of Neuroinflammation in the Pathogenesis of Monocrotaline-Induced Pulmonary Hypertension. Hypertension. 2018 Jun;71(6):1156-1163. doi: 10.1161/HYPERTENSIONAHA.118.10934.

20. Hilzendeger AM, Shenoy V, Raizada MK, Katovich MJ. Neuroinflammation in pulmonary hypertension: concept, facts, and relevance. Curr Hypertens Rep. 2014

Sep;16(9):469. doi: 10.1007/s11906-014-0469-1.

21. Oliveira AC, Sharma RK, Aquino V, Lobaton G, Bryant AJ, Harrison JK, Richards EM, Raizada MK. Involvement of Microglial Cells in Hypoxia-induced Pulmonary Hypertension. Am J Respir Cell Mol Biol. 2018 Aug;59(2):271-273. doi: 10.1165/rcmb.2018-0042LE.

22. Vaillancourt M, Chia P, Medzikovic L, Cao N, Ruffenach G, Younessi D, Umar S. Experimental Pulmonary Hypertension Is Associated with Neuroinflammation in the Spinal Cord. Front Physiol. 2019 Sep 20;10:1186. doi: 10.3389/fphys.2019.01186.

23. Lin Y, Song B, Lin Q, Qian X, Chen H, Wang X, Lin S. [Neuroprotective mechanism of autophagy in bradykinin postconditioning after cardiac arrest in rats]. Zhonghua Wei Zhong Bing Ji Jiu Yi Xue. 2021 Sep;33(9):1099-1104. Chinese. doi: 10.3760/cma.j.cn121430-20210528-00791. PMID: 34839869.

24. Sun JS, Yang YJ, Zhang YZ, Huang W, Li ZS, Zhang Y. Minocycline attenuates pain by inhibiting spinal microglia activation in diabetic rats. Mol Med Rep. 2015 Aug;12(2):2677-82. doi: 10.3892/mmr.2015.3735. Epub 2015 May 6. PMID: 25955348.

25. Liberzon A, Birger C, Thorvaldsdóttir H, Ghandi M, Mesirov JP, Tamayo P. The Molecular Signatures Database (MSigDB) hallmark gene set collection. Cell Syst. 2015 Dec 23;1(6):417-425. doi: 10.1016/j.cels.2015.12.004.

26. Subramanian A, Tamayo P, Mootha VK, Mukherjee S, Ebert BL, Gillette MA, Paulovich A, Pomeroy SL, Golub TR, Lander ES *et al*. Gene set enrichment analysis: a knowledge-based approach for interpreting genome-wide expression profiles. Proc Natl Acad Sci U S A. 2005 Oct 25;102(43):15545-50. doi: 10.1073/pnas.0506580102.

27. Hong J, Arneson D, Umar S, Ruffenach G, Cunningham CM, Ahn IS, Diamante G, Bhetraratana M, Park JF, Said E *et al*. Single-Cell Study of Two Rat Models of Pulmonary Arterial Hypertension Reveals Connections to Human Pathobiology and Drug

Repositioning. Am J Respir Crit Care Med. 2021 Apr 15;203(8):1006-1022. doi: 10.1164/rccm.202006-2169OC. PMID: 33021809; PMCID: PMC8048757.

28. Park JF, Clark VR, Banerjee S, Hong J, Razee A, Williams T, Fishbein G, Saddic L, Umar S. Transcriptomic Analysis of Right Ventricular Remodeling in Two Rat Models of Pulmonary Hypertension: Identification and Validation of Epithelial-to-Mesenchymal Transition in Human Right Ventricular Failure. Circ Heart Fail. 2021 Feb;14(2):e007058. doi: 10.1161/CIRCHEARTFAILURE.120.007058. Epub 2021 Feb 5. PMID: 33541093; PMCID: PMC7887079.

29. Wang D, Wu Y, Chen Y, Wang A, Lv K, Kong X, He Y, Hu N. Focal selective chemo-ablation of spinal cardiac afferent nerve by resiniferatoxin protects the heart from pressure overload-induced hypertrophy. Biomed Pharmacother. 2019 Jan;109:377-385. doi: 10.1016/j.biopha.2018.10.156. Epub 2018 Nov 3. PMID: 30399572.

30. Ding X, Mountain DJ, Subramanian V, Singh K, Williams CA. The effect of high cervical spinal cord stimulation on the expression of SP, NK-1 and TRPV1 mRNAs during cardiac ischemia in rat. Neurosci Lett. 2007 Sep 7;424(2):139-44. doi: 10.1016/j.neulet.2007.07.040. Epub 2007 Aug 6. PMID: 17714867.

31. Heng YJ, Saunders CI, Kunde DA, Geraghty DP. TRPV1, NK1 receptor and substance P immunoreactivity and gene expression in the rat lumbosacral spinal cord and urinary bladder after systemic, low dose vanilloid administration. Regul Pept. 2011 Apr 11;167(2-3):250-8. doi: 10.1016/j.regpep.2011.02.004. Epub 2011 Feb 15. PMID: 21329730.

32. Cerbai F, Lana D, Nosi D, Petkova-Kirova P, Zecchi S, Brothers HM, Wenk GL, Giovannini MG. The neuron-astrocyte-microglia triad in normal brain ageing and in a model of neuroinflammation in the rat hippocampus. PLoS One. 2012;7(9):e45250. doi: 10.1371/journal.pone.0045250.

33. Shen XZ, Li Y, Li L, Shah KH, Bernstein KE, Lyden P, Shi P. Microglia participate in neurogenic regulation of hypertension. Hypertension. 2015 Aug;66(2):309-16. doi: 10.1161/HYPERTENSIONAHA.115.05333. Epub 2015 Jun 8. PMID: 26056339; PMCID: PMC4498964.

34. Lundberg JM, Franco-Cereceda A, Lacroix JS, Pernow J. Neuropeptide Y and sympathetic neurotransmission. Ann N Y Acad Sci. 1990;611:166-74. doi: 10.1111/j.1749-6632.1990.tb48930.x. PMID: 2174218.

35. De Biasi S, Rustioni A. Glutamate and substance P coexist in primary afferent terminals in the superficial laminae of spinal cord. Proc Natl Acad Sci U S A. 1988 Oct;85(20):7820-4. doi: 10.1073/pnas.85.20.7820. PMID: 2459717; PMCID: PMC282285.

36. Liu Y, Wu XM, Luo QQ, Huang S, Yang QW, Wang FX, Ke Y, Qian ZM. CX3CL1/CX3CR1-mediated microglia activation plays a detrimental role in ischemic mice brain via p38MAPK/PKC pathway. J Cereb Blood Flow Metab. 2015 Oct;35(10):1623-31. doi: 10.1038/jcbfm.2015.97. Epub 2015 May 13. PMID: 25966946; PMCID: PMC4640309.

37. Milior G, Lecours C, Samson L, Bisht K, Poggini S, Pagani F, Deflorio C, Lauro C, Alboni S, Limatola C *et al*. Fractalkine receptor deficiency impairs microglial and neuronal responsiveness to chronic stress. Brain Behav Immun. 2016 Jul;55:114-125. doi: 10.1016/j.bbi.2015.07.024.

38. Zhang X, Ye L, Huang Y, Ding X, Wang L. The potential role of TRPV1 in pulmonary hypertension: Angel or demon? Channels (Austin). 2019 Dec;13(1):235-246. doi: 10.1080/19336950.2019.1631106. PMID: 31189399; PMCID: PMC6602577.

39. Yao L, Kan EM, Kaur C, Dheen ST, Hao A, Lu J, Ling EA. Notch-1 signaling regulates microglia activation via NF-κB pathway after hypoxic exposure in vivo and in vitro. PLoS One. 2013 Nov 6;8(11):e78439. doi: 10.1371/journal.pone.0078439. PMID: 24223152;

PMCID: PMC3819391.

40. Xu T, Liu J, Li XR, Yu Y, Luo X, Zheng X, Cheng Y, Yu PQ, Liu Y. The mTOR/NF-κB Pathway Mediates Neuroinflammation and Synaptic Plasticity in Diabetic Encephalopathy. Mol Neurobiol. 2021 Aug;58(8):3848-3862. doi: 10.1007/s12035-021-02390-1. Epub 2021 Apr 15. PMID: 33860440.

41. Carletti F, Gambino G, Rizzo V, Ferraro G, Sardo P. Neuronal nitric oxide synthase is involved in CB/TRPV1 signalling: Focus on control of hippocampal hyperexcitability. Epilepsy Res. 2017 Dec;138:18-25. doi: 10.1016/j.eplepsyres.2017.09.018. Epub 2017 Oct 3. PMID: 29035821.

42. Ahlawat A, Rana A, Goyal N, Sharma S. Potential role of nitric oxide synthase isoforms in pathophysiology of neuropathic pain. Inflammopharmacology. 2014 Oct;22(5):269-78. doi: 10.1007/s10787-014-0213-0. Epub 2014 Aug 6. PMID: 25095760.

43. Rameau GA, Chiu LY, Ziff EB. NMDA receptor regulation of nNOS phosphorylation and induction of neuron death. Neurobiol Aging. 2003 Dec;24(8):1123-33. doi: 10.1016/j.neurobiolaging.2003.07.002. PMID: 14643384.

44. Parellada E, Gassó P. Glutamate and microglia activation as a driver of dendritic apoptosis: a core pathophysiological mechanism to understand schizophrenia. Transl Psychiatry. 2021 May 6;11(1):271. doi: 10.1038/s41398-021-01385-9. PMID: 33958577; PMCID: PMC8102516.

45. Wang M, Pan W, Xu Y, Zhang J, Wan J, Jiang H. Microglia-Mediated Neuroinflammation: A Potential Target for the Treatment of Cardiovascular Diseases. J Inflamm Res. 2022 May 25;15:3083-3094. doi: 10.2147/JIR.S350109. PMID: 35642214; PMCID: PMC9148574.

46. Dampney RA, Michelini LC, Li DP, Pan HL. Regulation of sympathetic vasomotor

activity by the hypothalamic paraventricular nucleus in normotensive and hypertensive states. Am J Physiol Heart Circ Physiol. 2018 Nov 1;315(5):H1200-H1214. doi: 10.1152/ajpheart.00216.2018. Epub 2018 Aug 10. PMID: 30095973; PMCID: PMC6297824.

47. Shi Z, Gan XB, Fan ZD, Zhang F, Zhou YB, Gao XY, De W, Zhu GQ. Inflammatory cytokines in paraventricular nucleus modulate sympathetic activity and cardiac sympathetic afferent reflex in rats. Acta Physiol (Oxf). 2011 Oct;203(2):289-97. doi: 10.1111/j.1748-1716.2011.02313.x. Epub 2011 May 27. PMID: 21624097.

48. Möller T, Bard F, Bhattacharya A, Biber K, Campbell B, Dale E, Eder C, Gan L, Garden GA, Hughes ZA *et al*. Critical data-based re-evaluation of minocycline as a putative specific microglia inhibitor. Glia. 2016 Oct;64(10):1788-94. doi: 10.1002/glia.23007. Epub 2016 Jun 1. PMID: 27246804.

49. Kobayashi K, Imagama S, Ohgomori T, Hirano K, Uchimura K, Sakamoto K, Hirakawa A, Takeuchi H, Suzumura A, Ishiguro N, et al. Minocycline selec- tively inhibits M1 polarization of microglia. Cell Death Dis. 2013;4:e525. doi: 10.1038/cddis.2013.54.

50. Korotkevich G, Sukhov V, Sergushichev A. Fast gene set enrichment analysis. bioRxiv 2019;060012.doi:10.1101/060012.

51. Liberzon A, Birger C, Thorvaldsdóttir H, Ghandi M, Mesirov JP, Tamayo P. The Molecular Signatures Database (MSigDB) hallmark gene set collection. Cell Syst 2015;1:417–425.

52. Subramanian A, Tamayo P, Mootha VK, Mukherjee S, Ebert BL, Gillette MA, Paulovich A, Pomeroy SL, Golub TR, Lander ES, Mesirov JP. Gene set enrichment analysis: a knowledge-based approach for interpreting genome-wide expression profiles. Proc Natl Acad Sci USA 2005;102:15545–15550.

Chapter 3: Chemo-ablation of Cardiopulmonary Afferents by Intrathecal RTX Prevents PH and RV Failure by Decreasing Thoracic Spinal Cord NOS1 and Neuroinflammation

Abstract

Introduction:

Pulmonary hypertension (PH) is associated with aberrant sympathoexcitation leading to RV failure (RVF), arrhythmias and death. We recently discovered that transient receptor potential vanilloid1+ (TRPV1+) cardiopulmonary afferent signaling mediated neuronal nitric oxide synthase (NOS1) activation leads to neuroinflammation and apoptosis in the thoracic spinal cord (TSC) that results in aberrant sympathoexcitation in preclinical and clinical PH-RVF. Resiniferatoxin (RTX) is a TRPV1 agonist that can selectively ablate TRPV1+ primary sensory afferents. We hypothesize that focal chemo-ablation of TRPV1+ afferents in the TSC may prevent PH-RVF by reducing NOS1-mediated TSC neuroinflammation.

Methods:

Male SD rats received s.c. MCT (60mg/kg, n=12, 4wk) or Sugen (SuHx, 20mg/kg, n=6, 3wk hypoxia+2wk normoxia). MCT rats received intrathecal RTX (2μg/30μl, L4/5, n=6) or PBS (30μl, L4/5, n=6) 5 days before MCT. Similarly, SuHx rats received intrathecal RTX (2μg/30μl, L4/5, n=3) or PBS (30μl, L4/5, n=3) 5 days before SuHx. Control rats received intrathecal RTX (2μg/30μl, L4/5, n=6). Echo, RV/LV catheterization were performed terminally. Lung+RV RNASeq as well as RT-qPCR, trichrome and immunofluorescence staining and quantifications were performed in rat TSC, lung and RV. Immunostaining of human TSC (Control=4; PAH=4) was also performed. Plasma catecholamines were measured by ELISA. Values are mean±SEM.

Results:

TRPV1+SP immunolocalization was significantly increased in the thoracic dorsal horns of MCT, SuHx and human PAH highlighting increased cardiopulmonary afferent signaling.

Intrathecal RTX abolished TRPV1 expression in thoracic dorsal horn of control, MCT and SuHx rats. RTX significantly decreased RVSP, heart rate, Fulton-index, RVIDd and plasma norepinephrine and increased RVFAC and body weight gain (all $p<0.05$) but did not affect LV pressure and LVEF in MCT and SuHx rats. However, RTX had no effects on any of the aforementioned parameters in control rats. Interestingly, RTX also significantly reduced total lung weight, pulmonary arteriolar wall thickness, perivascular and interstitial fibrosis in lung and RV of MCT and SuHx rats (all $p<0.05$). Further, RTX significantly decreased microglial count, percent activation, astrogliosis, NMDA-receptor GRIN2D and NOS1 expression as well as neuronal apoptosis in the TSC of MCT and SuHx rats (all $p<0.05$). RNASeq of lung and RV tissues from RTX-treated MCT rats demonstrated reversal of several pro-fibrotic (epithelial mesenchymal transition and TGFβ-signaling), inflammatory (mTORC1, IL2 STAT5, IL6 JAK STAT3 and TNFα-signaling via NFk-B) and apoptotic (p53 pathway) pathways and genes.

Conclusions:

Focal chemo-ablation of TRPV1+ afferents in the TSC attenuates PH severity and prevents RVF by decreasing NOS1-mediated TSC neuroinflammation in PH rats and may serve as a promising therapeutic target.

Key words: Pulmonary hypertension; transcriptome; thoracic spinal cord; neuroinflammation; sympathoexcitation.

Introduction

Pulmonary hypertension (PH) is characterized by persistent elevation of pulmonary arterial pressure caused by pulmonary vascular remodeling due to endothelial dysfunction, excessive smooth muscle cell proliferation and migration[1]. This leads to an increase in pulmonary vascular resistance (PVR), vasoconstriction, loss of distal pulmonary arteries, pressure overload, right ventricular hypertrophy, failure, arrhythmias and ultimately, death[2]. The pathogenesis of PH is associated with increased intracellular calcium leading to vasoconstriction, smooth muscle cell proliferation and migration as well as multi organ inflammation[1]. Particularly, microglial and astrocytic activation mediated neuroinflammation in the central nervous system (CNS) has been implicated in aberrant sympathoexcitation leading to arrhythmias and right ventricular failure (RVF) in PH[3-5]. Although RVF is the major cause of death among patients with PAH, none of the currently FDA approved therapies directly target right heart failure[6]. Sympathetic activity is always overactivated during the process of cardiac hypertrophy in PAH patients with relatively fixed stroke volume, hence, blocking aberrant sympathoexcitation would be a promising approach to prevent RVF[6].

The cardiac sympathetic afferent reflex (CSAR) regulates sympathetic tone through sympathetic afferent fibers, thoracic dorsal root ganglia (DRG) and spinal cord, hypothalamic and medullary brain regions and sympathetic efferent nerves[7]. Transient receptor potential vanilloid 1 (TRPV1) is expressed at the peripheral and central terminals of cardiopulmonary sensory afferents in the heart, lung and thoracic dorsal horn respectively and is responsible for sympathoexcitatory signal transmission[7-11]. Various inflammatory mediators modulate TRPV1 expression and activity in the CNS, while TRPV1 exerts reciprocal actions over neuroinflammatory processes[12]. TRPV1 in the thoracic

dorsal horn has been shown to mediate neuropathic pain, promote microglial phagocytosis and produce IL-1β and reactive oxygen species (ROS) as well as regulate NF-κB pathway mediated neuroinflammation[13-16]. Several lines of evidence suggest that TRPV1 activation allows Ca^{2+} influx to release glutamate from the sensory afferent nerve endings, which activates post-synaptic N-methyl-D-aspartate receptors (NMDARs) to regulate neuronal nitric oxide synthase (NOS1) mediated nitric oxide ($^{\cdot}NO$) production as well as microglial and astrocytic activation in the thoracic dorsal horn[17-20]. Consequently, TRPV1 ablation by epicardial capsaicin administration or spinal dorsal horn resection reduced proinflammatory cytokine expression[21]. TRPV1 is also expressed in afferent fibers throughout the respiratory tract and intrapulmonary arteries and influences visceral tissue homeostasis, cytoskeletal architecture reorganization as well as proliferation and migration of pulmonary arterial smooth muscle cells (PASMC) through Ca^{2+} influx[11,22,23]. Moreover, TRPV1 ablation by capsaicin pretreatment attenuated PH severity by reducing pro-inflammatory cytokines and alleviating inflammation via p38MAPK pathway in the lung[24,25]. Several studies have shown that TRPV1 is involved in sensing blood pressure fluctuations and maintain the cardiovascular homoeostasis[26,27]. TRPV1 expressed in left ventricular tissues induces mitochondrial damage, autophagy and ROS production[28]. Moreover, TRPV1 has been shown to play a major role in the progression of cardiac hypertrophy, fibrosis and apoptosis leading to heart failure[29,30,79]. We recently reported increased TRPV1 expression and activation in the inflamed thoracic spinal cord (TSC) in experimental PH-RVF and patients with PAH[3]. However, the role of TRPV1 activation in the TSC neuroinflammation, sympathoexcitation and cardiopulmonary function in PH are yet to be fully elucidated.

Resiniferatoxin (RTX) is an ultrapotent and selective TRPV1 agonist that can selectively

lesion TRPV1+ primary sensory afferents[30]. Intraperitoneal and intrathecal administration of RTX has been shown to abolish TRPV1 expression in the dorsal horn leading to decreased pain sensation, inflammation and over-activated CSAR, thereby preventing myocardial hypertrophy, fibrosis, and apoptosis[30-34]. Moreover, the application of RTX on the heart surface was shown to blunt CSAR that lasted for 10 weeks and attenuated cardiac remodeling as well as improved cardiovascular dysfunction in rats and swine with heart failure[35-37]. Recently, several phase1b studies targeting chemo-axotomy of the TRPV1+ afferents by intrathecal, epidural and intra-articular administration of RTX for cancer and osteoarthritis associated pain treatment have been successfully completed with no dose limiting toxicities[11,38]. Several studies have demonstrated that depleting TRPV1+ afferent nerve endings improved PH and RVF in different PH models[24]. Therefore, we administered RTX locally at the T1 to T2 and L4 to L5 spinal cord levels to ablate the TRPV1+ cardiopulmonary sensory nerve endings to determine the role of TRPV1 in TSC NOS1 expression, neuroinflammation, sympathoexcitation and cardiopulmonary function in two different rat models of severe PH-RVF. We hypothesize that focal chemo-ablation of TRPV1+ afferents in the TSC may prevent PH-RVF by reducing NOS1-mediated TSC neuroinflammation, apoptosis and sympathoexcitation. Investigating the effects of targeted TRPV1 inhibition will offer insights into a novel therapeutic strategy for PH and RVF.

Materials and Methods

All animal studies were performed in accordance with the National Institutes of Health (NIH) Guide for the Care and Use of Laboratory Animals. Protocols received UCLA animal

research committee approval. The details of materials and methods can be found in the online data supplement.

Animals and groups

RTX (Alomone Labs, Israel) was first dissolved in 100% ethanol to make the stock solution (concentration of 2 mg/ml) and then further diluted in 10 ml saline when used for.

Male Sprague Dawley rats (200–250 g, n = 35) were used for our experiments. Rats were randomly assigned to three groups. The RTX alone group (n = 6) received 2 μg/30μl[30] of single intrathecal (i.t.) RTX (L4/L5 intra spinal space), whereas the PBS+MCT group (n = 6) received 30μl of PBS (L4/L5) and RTX+MCT group (n = 6) received 2 μg/30μl[30] of single i.t. RTX (L4/L5) injection. 5-days after the PBS/RTX i.t. injections, the PBS+MCT and RTX+MCT rats received single subcutaneous (s.c.) injection of pulmonary endothelial toxin Monocrotaline (MCT, 60mg/kg) and were followed for 30-days (Fig. 1A). Similarly, PBS+SuHx group (n = 3) received single injection of 30μl PBS (L4/L5) and RTX+SuHx group (n = 3) received 2 μg/30μl[30] of single i.t. RTX (L4/L5) injection. 5-days after the PBS/RTX i.t. injections, these rats received single s.c. injection of VEGF-receptor antagonist Sugen (SU5416, 20mg/kg) and kept in hypoxia (10% oxygen) for 3-weeks followed by 2-weeks of normoxia (Fig. 2A). To investigate the efficacy of RTX delivery location, we performed another experiment where we delivered single i.t. RTX in the T2/T3 intra spinal space. Here, the RTX alone group (n = 3) received 2 μg/10μl[30] of single i.t. RTX (T2/T3), whereas the RTX+MCT group (n = 8) received 2 μg/10μl[30] of single i.t. RTX (T2/T3) injection. 5-days after the RTX i.t. injections, the RTX+MCT rats received single s.c. MCT injection (60mg/kg) and were followed for 30-days (Fig. 3A).

Intrathecal Injections

Briefly, rats were anesthetized with isoflurane/O_2 mixture (4%), and body temperature was maintained at 37±1°C using heating pads. Single intrathecal injections were administered with a 29-gage needle at L4/L5 level to avoid spinal cord injury; successful injections were documented with prominent tail flicks. For T2/T3 level drug delivery, a PE10 tube was inserted through cisterna magna to reach T2/T3. After delivering 2 μg/10μl of RTX through the PE10 tube, another 10μl of PBS was used to flush the tube.

Echocardiography and Cardiopulmonary Hemodynamic Measurements

Serial echocardiography (Vevo3100) was performed to monitor cardiopulmonary hemodynamics and the development of PH and RV dysfunction. Direct right heart catheterization (Millar SPR-671) was performed terminally to assess disease severity.

RNA Extraction and qRT-PCR

Real-time quantitative reverse transcription PCR (qRT-PCR) was performed with total RNA extracted from the TSC of RTX+PBS, PBS+MCT and RTX+MCT rats using Trizol (Invitrogen). Total RNA was also extracted from the RV and lung of PBS+MCT and RTX+MCT rats using Trizol (Invitrogen).

RNA Sequencing Analysis

NovaSeq S4 200 Cycles (Illumina) was performed on RV and lung tissues and differential expression analysis was conducted. Differentially expressed genes (DEGs) with false discovery rate (FDR) <0.05 were considered statistically significant. Gene set enrichment analysis was performed and Hallmark[3] gene sets were obtained from molecular signature database (MSigDB)[3]. Enriched pathways considered statistically significant were defined by adjusted p-value <0.05.

Gross Histologic Analysis, Tissue Preparation and Imaging

RV hypertrophy index was calculated as weight ratio of RV/(LV+IVS). Heart weight: body weight (HW:BW) and lung weight: body weight (LW:BW) ratio were calculated. Hearts, lungs and spinal cords were fixed and 4–6μm sections were obtained. Heart and lung tissue sections were stained with Masson's trichrome staining. Images were acquired using a confocal microscope (Nikon).

Immunofluorescence Staining and Quantification

Thoracic spinal cord sections were stained with the primary antibodies against transient receptor potential vanilloid 1 (Anti-TRPV1), NMDAR-2D (Anti-Grin2D), neuronal nitric oxide synthase-1 (Anti-NOS1), microtubule-associated protein 2 (Anti-MAP2), microglia (Anti-IBA1), astrocytes (Anti-GFAP), neurons (Anti-NeuN) and Cleaved Caspase-3 (Asp175). RV and lung sections were stained with the primary antibodies against alpha-smooth muscle actin (Anti-αSMA) and macrophage marker (Anti-F4/80). Quantifications were performed using ImageJ.

Plasma Norepinephrine Assays

Plasma norepinephrine levels were quantified using an enzyme-linked immunosorbent assay (ELISA) kit (Abnova, KA1877) following the manufacturer's protocols.

Statistical Analysis

Unpaired t-test and one-way ANOVA tests were used to compare between groups using GraphPad Prism. When significant differences were detected, individual mean values were compared by post-hoc tests that allowed for multiple comparisons. $P<0.05$ was considered statistically significant. Values are expressed as mean±SD. For RNA-seq, differential expression analysis was conducted using the R-program DeSeq2 correcting for multiple hypothesis testing using the Benjamini Hochberg method.

Results

Lumbar intrathecal RTX administration prevents PH and RVF in MCT rats

Previous studies have shown that TRPV1 is expressed in the superficial layers of the spinal dorsal horn, including laminae I and II and DRG[3,38,39], which can be selectively abolished by systemic or focal administration of RTX[30,31]. TRPV1 expression was increased in the thoracic dorsal horn and DRG of PBS+MCT rats. Lumbar intrathecal RTX administration abolished TRPV1 expression of the thoracic dorsal horn and DRG in RTX+PBS and RTX+MCT rats (Figure 1B,C, S2). Lumbar intrathecal RTX significantly attenuated PH severity as demonstrated by decreased RVSP and prevented RVF as shown by decreased Fulton index, heart weight/ body weight, as well as increased RVFAC% in RTX+MCT compared to PBS+MCT (Figure 1B). However, RTX did not affect LV pressure and LVEF (Figure 1B). Importantly, lumbar intrathecal RTX significantly reduced MCT-induced increases in lung weight/ body weight (Figure 1B). MCT significantly reduced body weight gain in PBS+MCT rats, however, lumbar intrathecal RTX significantly increased body weight gain in RTX+MCT rats (Figure 1B). MCT caused significant increase in plasma NE in PBS+MCT rats. Lumbar intrathecal RTX administration remarkably prevented the rise of plasma NE in RTX+MCT rats (Figure 1B). Interestingly, lumbar intrathecal RTX also decreased heart rate in RTX+MCT rats (Figure 1B). Echo data demonstrated that MCT caused significant decrease in RV contractility and increase in RV wall thickness and dilatation in PBS+MCT rats. Lumbar intrathecal RTX significantly increased RV contractility and decreased RV wall thickness and dilatation in RTX+MCT rats (Figure 1C). These data indicated that RTX injection via intrathecal route in L4/L5 segment can inhibit TRPV1 expression in the thoracic dorsal horn and improve

cardiopulmonary functions by decreasing sympathetic tone for a relatively long period in MCT-induced PH-RVF rats.

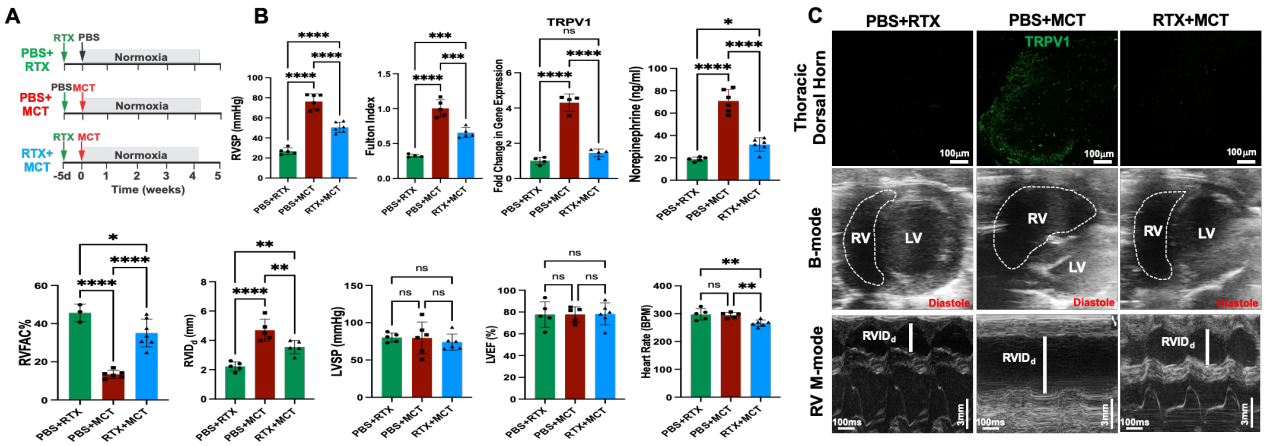

Figure 1. Lumbar intrathecal RTX administration prevents PH and RVF in MCT rats (**A**) Experimental protocol. (**B**) RVSP, Fulton index, normalized qRT-PCR data of TRPV1 gene expression, RVFAC%, $RVID_d$, LVSP, LVEF, heart rate and plasma norepinephrine levels of PBS+RTX, PBS+MCT and RTX+MCT rats. N=4-6 per group. *p<0.05, **p<0.01, ***p<0.001, ****p<0.0001. (**C**) Representative images of immunofluorescence staining with anti-TRPV1 (Green) from the thoracic dorsal horn of PBS+RTX, PBS+MCT and RTX+MCT rats. N=4 per group. B-Mode and RV view of M-Mode echo showing RV dilatation, wall thickness and contractility in PBS+RTX, PBS+MCT and RTX+MCT rats.

Lumbar intrathecal RTX administration prevents PH and RVF in SuHx rats

To investigate the effect of lumbar intrathecal RTX administration in SuHx-induced PH-RVF, we performed L4/L5 intrathecal RTX in the SuHx rats. TRPV1 expression was increased in the thoracic dorsal horn of PBS+SuHx rats. Lumbar intrathecal RTX administration abolished TRPV1 expression of the thoracic dorsal horn in RTX+SuHx rats (Figure 2C). Lumbar intrathecal RTX significantly attenuated PH severity as demonstrated by decreased RVSP and prevented RVF as shown by decreased Fulton index, heart

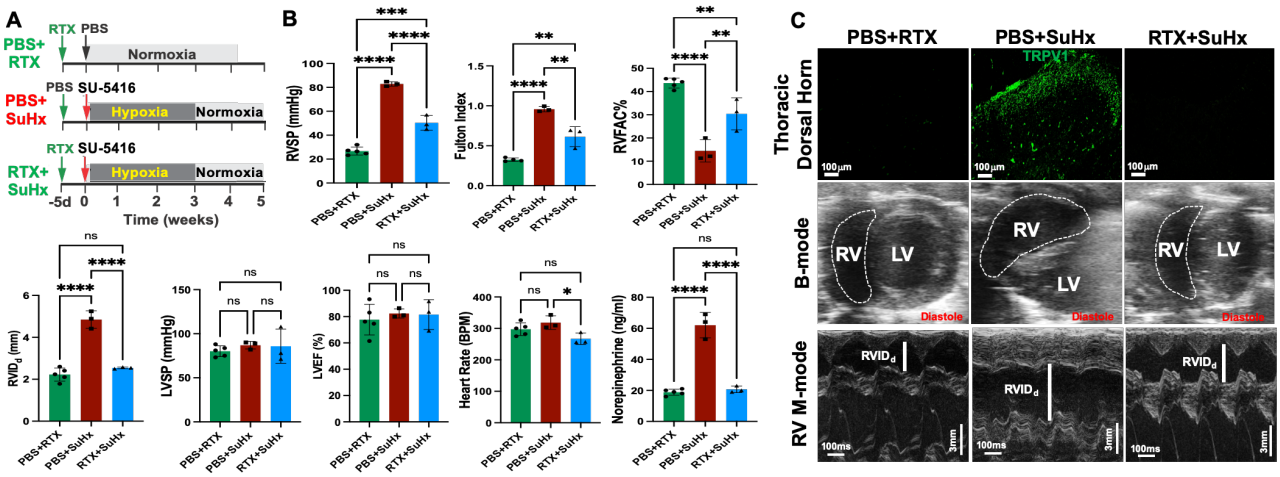

Figure 2. Lumbar intrathecal RTX administration prevents PH and RVF in SuHx rats

(**A**) Experimental protocol. (**B**) RVSP, Fulton index, RVFAC%, $RVID_d$, LVSP, LVEF, heart rate and plasma norepinephrine levels of PBS+RTX, PBS+SuHx and RTX+SuHx rats. N=3-5 per group. *p<0.05, **p<0.01, ***p<0.001, ****p<0.0001. (**C**) Representative images of immunofluorescence staining with anti-TRPV1 (Green) from the thoracic dorsal horn of PBS+RTX, PBS+SuHx and RTX+SuHx rats. N=3 per group. B-Mode and RV view of M-Mode echo showing RV dilatation, wall thickness and contractility in PBS+RTX, PBS+SuHx and RTX+SuHx rats.

weight/ body weight, as well as increased RVFAC% in RTX+SuHx compared to PBS+SuHx (Figure 2B). However, RTX did not affect LV pressure and LVEF (Figure 2B). Importantly, lumbar intrathecal RTX significantly reduced SuHx-induced increases in lung weight/ body weight (Figure 2B). SuHx significantly reduced body weight gain in PBS+SuHx rats, however, lumbar intrathecal RTX significantly increased body weight gain in RTX+SuHx rats (Figure 2B). SuHx caused significant increase in plasma NE in PBS+SuHx rats. Lumbar intrathecal RTX administration remarkably prevented the rise of

plasma NE in RTX+SuHx rats (Figure 2B). Interestingly, lumbar intrathecal RTX also decreased heart rate in RTX+SuHx rats (Figure 2B). Echo data demonstrated that SuHx caused significant decrease in RV contractility and increase in RV wall thickness and dilatation in PBS+MCT rats. Lumbar intrathecal RTX significantly increased RV contractility and decreased RV wall thickness and dilatation in RTX+SuHx rats (Figure 2C). These data indicated that RTX injection via intrathecal route in L4/L5 segment can inhibit TRPV1 expression in the thoracic dorsal horn and improve cardiopulmonary functions by decreasing sympathetic tone for a relatively long period in SuHx-induced PH-RVF rats.

Thoracic intrathecal RTX administration prevents PH and RVF in MCT rats

To investigate the efficacy of RTX delivery location in the spinal cord, we performed T2/T3 intrathecal RTX administration in the MCT rats. TRPV1 expression was increased in the thoracic dorsal horn of PBS+MCT rats. Thoracic intrathecal RTX administration abolished TRPV1 expression of the thoracic dorsal horn in RTX+PBS and RTX+MCT rats (Figure 3C). Thoracic intrathecal RTX significantly attenuated PH severity as demonstrated by decreased RVSP and prevented RVF as shown by decreased Fulton index, heart weight/ body weight, as well as increased RVFAC% in RTX+MCT compared to PBS+MCT (Figure 3B). However, RTX did not affect LV pressure and LVEF (Figure 3B). Importantly, thoracic intrathecal RTX significantly reduced MCT-induced increases in lung weight/ body weight (Figure 3B). MCT significantly reduced body weight gain in PBS+MCT rats, however, thoracic intrathecal RTX significantly increased body weight gain in RTX+MCT rats (Figure 3B). MCT caused significant increase in plasma NE in PBS+MCT rats. Thoracic intrathecal RTX administration remarkably prevented the rise of plasma NE in RTX+MCT rats (Figure 3B). Interestingly, thoracic intrathecal RTX also decreased heart rate in RTX+MCT rats (Figure 3B). Echo data demonstrated that MCT caused significant decrease in RV

contractility and increase in RV wall thickness and dilatation in PBS+MCT rats. Thoracic intrathecal RTX significantly increased RV contractility and decreased RV wall thickness and dilatation in RTX+MCT rats (Figure 3C). These data indicated that RTX injection via intrathecal route in T2/T3 segment can inhibit TRPV1 expression in the thoracic dorsal horn similar to L4/L5 RTX injection and improve cardiopulmonary functions by decreasing sympathetic tone for a relatively long period in MCT-induced PH-RVF rats.

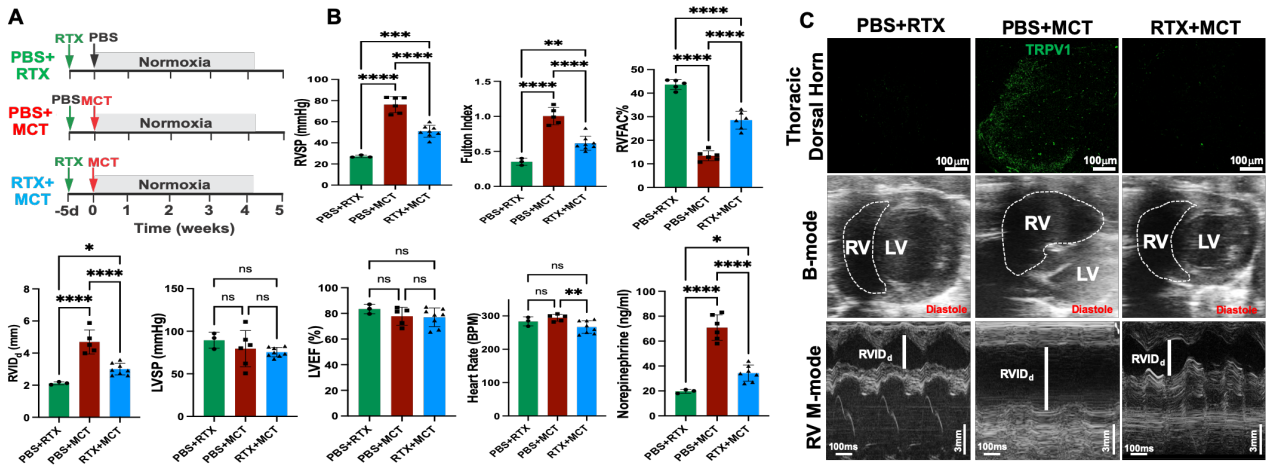

Figure 3. Thoracic intrathecal RTX administration prevents PH and RVF in MCT rats (**A**) Experimental protocol. (**B**) RVSP, Fulton index, RVFAC%, RVID$_d$, LVSP, LVEF, heart rate and plasma norepinephrine levels of PBS+RTX, PBS+MCT and RTX+MCT rats. N=3-8 per group. *p<0.05, **p<0.01, ***p<0.001, ****p<0.0001. (**C**) Representative images of immunofluorescence staining with anti-TRPV1 (Green) from the thoracic dorsal horn of PBS+RTX, PBS+MCT and RTX+MCT rats. N=4 per group. B-Mode and RV view of M-Mode echo showing RV dilatation, wall thickness and contractility in PBS+RTX, PBS+MCT and RTX+MCT rats.

TRPV1 ablation attenuates TSC NMDAR and NOS1 expression, neuroinflammation and apoptosis

TRPV1 activation has been implicated in the glutamatergic signaling mediated NOS1 activation in CNS[40], which leads to ˙NO production, oxidative and nitrosative stress, neuroinflammation, chemokine release, excitotoxicity, and neuronal apoptosis[41,42]. We investigated the role of TRPV1 ablation on TSC NMDAR and NOS1 expression, neuroinflammation as well as neuronal apoptosis. Lumbar intrathecal RTX administration significantly decreased MCT-induced increases in transcription and expression of NMDAR subunit, GRIN2D and NOS1 in the TSC of RTX+MCT rats (Figure 4A,B). Moreover, total microglial count, microglial percent activation, astrogliosis and expression of the fractalkine, CX3CL1 were significantly increased in the TSC of MCT-treated rats (Figure 5A,B). Lumbar intrathecal RTX administration significantly decreased TSC microglial count, percent activation, astrogliosis and CX3CL1 expression in the RTX+MCT rats (Figure 5A,B). Moreover, lumbar intrathecal RTX administration significantly decreased MCT-induced increases in neuronal apoptosis demonstrated by cleaved Caspase-3+NeuN co-immunoreactivity and TGFβ1 expression in the TSC of RTX+MCT rats (Figure 6). These data suggest an important regulatory role of TRPV1 in glutamatergic signaling mediated NOS1 expression, neuroinflammation and neuronal apoptosis in the TSC in PH-RVF.

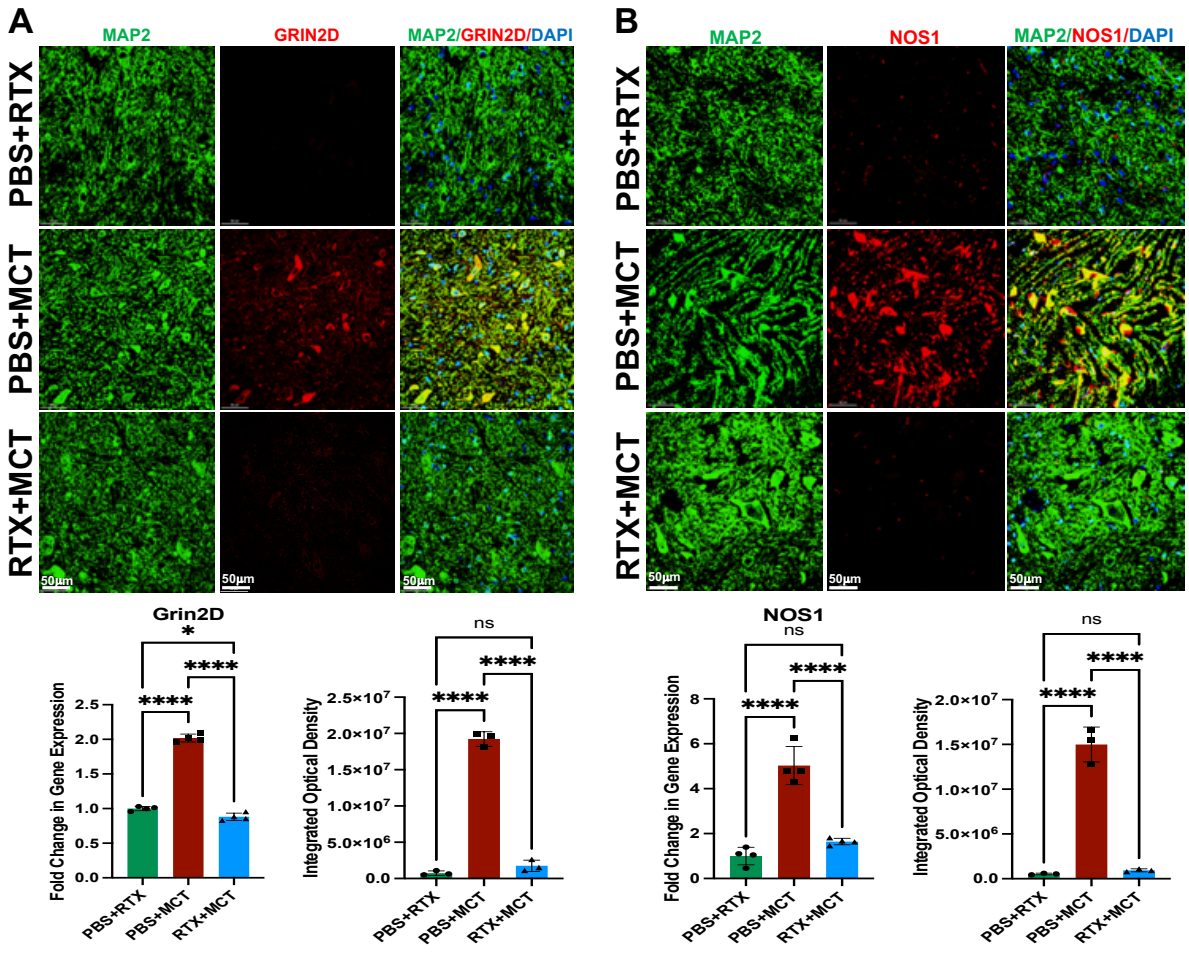

Figure 4. TRPV1 ablation attenuates TSC NMDAR and NOS1 expression (**A**) Representative images of immunofluorescence staining with neuronal marker anti-MAP2 (Green), NMDAR subunit GRIN2D marker anti-GRIN2D (Red) and DNA marker DAPI (Blue) in the TSC of PBS+RTX, PBS+MCT and RTX+MCT rats. N=4 per group. Quantification of GRIN2D IR (IOD: integrated optical density). qRT-PCR data of Grin2D gene expression in the TSC of PBS+RTX, PBS+MCT and RTX+MCT rats. N=4 per group. **p*<0.05, *****p*<0.0001. (**B**) Representative images of immunofluorescence staining with neuronal marker anti-MAP2 (Green), Neuronal Nitric Oxide Synthase 1 marker anti-NOS1 (Red) and DNA marker DAPI (Blue) in the TSC of PBS+RTX, PBS+MCT and RTX+MCT rats. N=4 per group. Quantification of NOS1 IR (IOD: integrated optical density). qRT-PCR

data of NOS1 gene expression in the TSC of PBS+RTX, PBS+MCT and RTX+MCT rats. N=4 per group. ****p<0.0001.

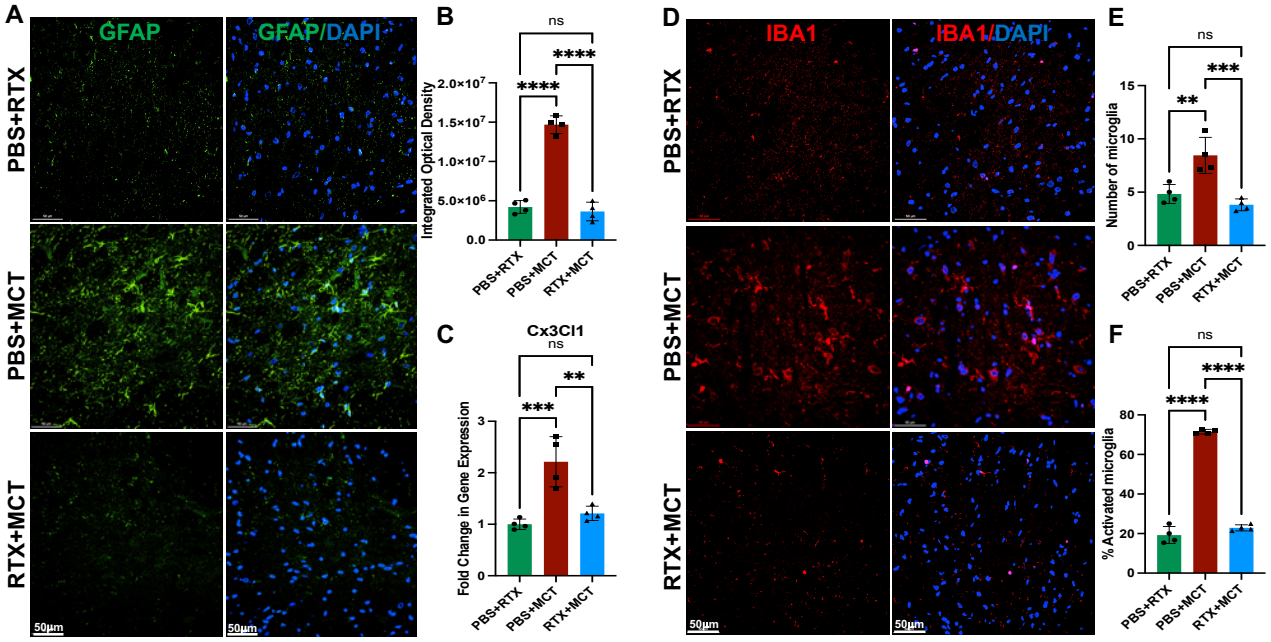

Figure 5. TRPV1 ablation attenuates TSC astrocytic and microglial activation (**A**) Representative images of immunofluorescence staining with astrocytic marker anti-GFAP (Green) and DNA marker DAPI (Blue) in the TSC of PBS+RTX, PBS+MCT and RTX+MCT rats. N=4 per group. Quantification of GFAP IR (IOD: integrated optical density). qRT-PCR data of fractalkine Cx3Cl1 gene expression in the TSC of PBS+RTX, PBS+MCT and RTX+MCT rats. N=4 per group. **p<0.01, ***p<0.001. (**B**) Representative images of immunofluorescence staining with microglial marker anti-IBA1 (Red) and DNA marker DAPI (Blue) in the TSC of PBS+RTX, PBS+MCT and RTX+MCT rats. N=4 per group. Quantifications of number of microglia per high power field (HPF), and % microglial activation/HPF in the TSC. N=4 per group.

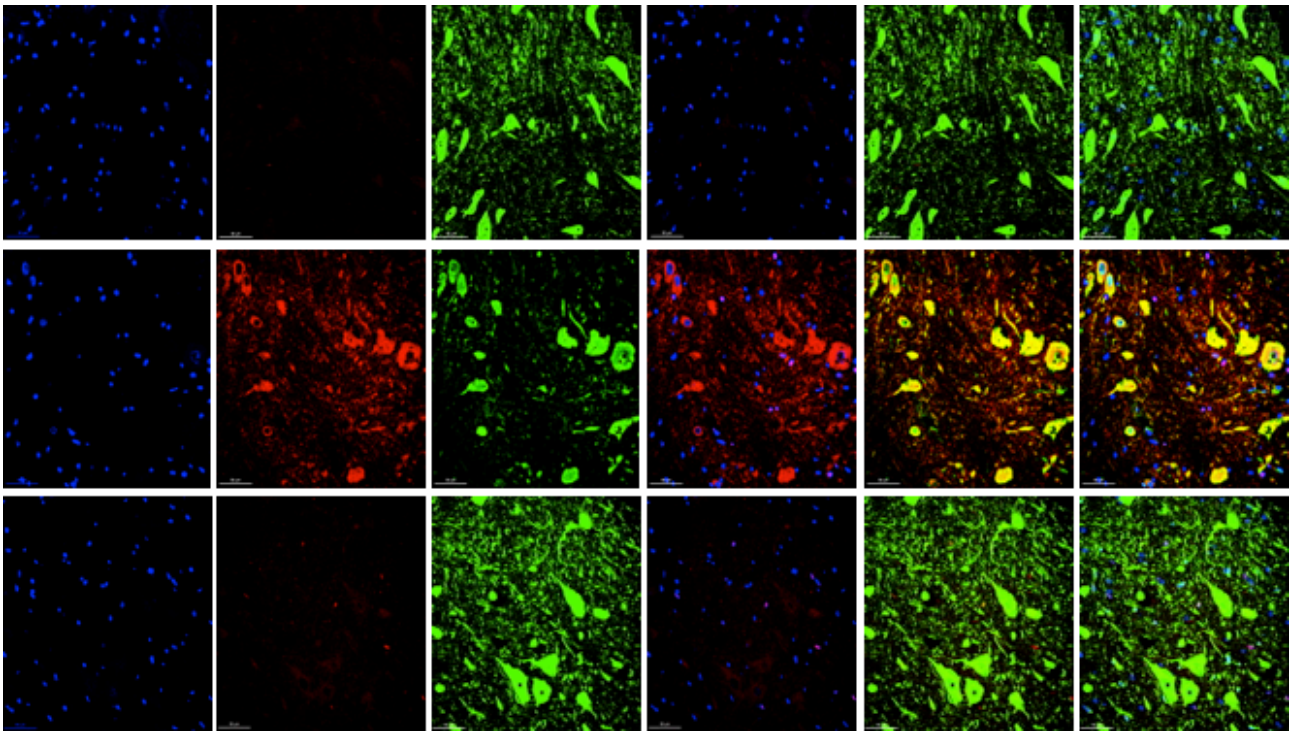

Figure 6. TRPV1 ablation attenuates neuronal apoptosis in the TSC. Representative images of immunofluorescence staining with DAPI (DNA; blue), anti-NeuN (Neuron; Green), anti-Cleaved Caspase-3 (CC3; Red), CC3 and DAPI colocalization, NeuN and CC3 colocalization (Yellow) and merged images from the TSC of PBS+RTX, PBS+MCT and RTX+MCT rats. N=4 per group.

TRPV1 ablation results in reversal of RV transcriptomic signature in MCT rats

To investigate the therapeutic effects of intrathecal TRPV1 ablation on MCT-induced RV remodeling, RNASeq of RV tissue was performed on PBS+MCT vs. RTX+MCT rats (Figures 7, Table 1). Hierarchical clustering of top DEGs (FDR<0.05) from RV RNASeq revealed 20 differentially expressed genes, among which 9 were up- and 11 down-regulated in the RTX-treated group compared to PBS-treated MCT rats (Figure 7A, Table

1). Gene Set Enrichment Analysis revealed 25 hallmark pathways significantly enriched (FDR<0.05) in RTX-treated group compared to PBS-treated MCT rats (Figure 7B). Hallmark analysis demonstrated significant down-regulation (FDR<0.05) of many pro-inflammatory pathways such as mTORC1 signaling, IL2 STAT5 signaling, TNFα signaling via NFk-B, IL6 JAK STAT3 signaling, PI3K AKT mTOR signaling and inflammatory response in RTX-treated MCT rats (Figure 7B). Many significantly downregulated pro-inflammatory genes, such as, MAP2K3, CxCr4, Tomm40 and NOTCH3 were enriched in these pathways (Table 1). Moreover, RV RNASeq revealed TGFβ-signaling and Wnt/beta-catenin signaling as some of the top down-regulated pro-fibrotic pathways along with downregulation of pro-fibrotic genes such as TGFβ1, Eng, FURIN, SMAD6 and ID1 in RTX-treated MCT rats (Figure 7B, Table 1). Similarly, several down-regulated pro-apoptotic genes such as PPP1R15A, TGFβ1, PERP, NDRG1 and IER5 were enriched in down-regulated p53 pathway in the RV of RTX-treated group (Figure 7B, Table 1). Interestingly, trichrome staining validated significantly decreased MCT-induced increases in perivascular and interstitial RV fibrosis in the RTX-treated rats (Figure 7C). Moreover, immunostaining with F4/80 confirmed MCT-induced increases in activated macrophages in the RV of PBS+MCT rats. Lumbar intrathecal RTX administration remarkably reduced activated macrophages in the RV in RTX+MCT rats (Figure 7D).

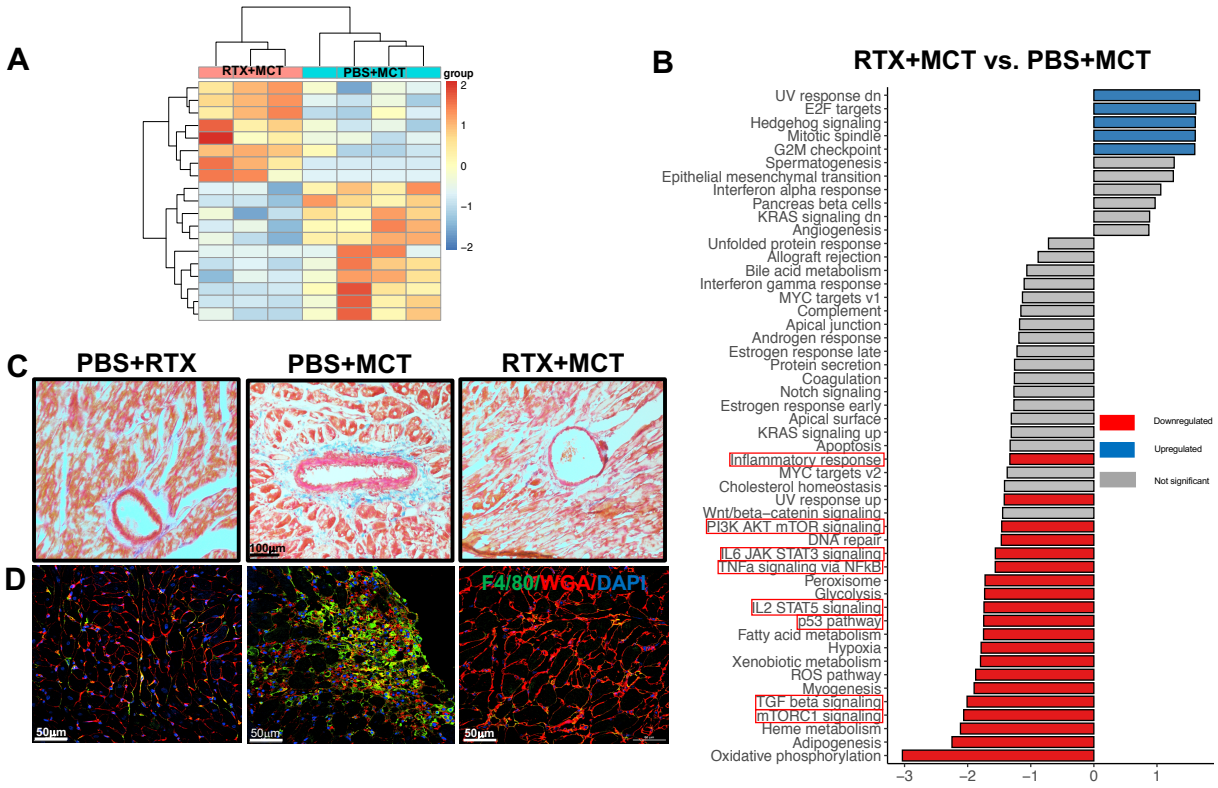

Figure 7. TRPV1 ablation results in reversal of RV transcriptomic signature in MCT rats. (**A**) RNA-Seq based heat map showing DEGs from the RV of PBS+MCT (Blue) and RTX+MCT (Red) groups. N=4 per group. (**B**) Bar plot showing normalized enrichment scores (NES) for Hallmark pathways derived from Gene Set Enrichment Analysis (GSEA). For GSEA, differentially expressed genes between PBS+MCT vs. RTX+MCT were ranked by the Wald statistic derived from DESeq2. Bars in blue and red represent statistically significant (FDR<0.05) pathways in PBS+MCT and RTX+MCT, respectively, that are either up- or downregulated. N=4 per group. Red boxes in the bar plot indicate downregulation of pro-fibrotic, pro-inflammatory and pro-apoptotic pathways. (**C**) Trichrome staining showing interstitial and perivascular fibrosis (Black arrow) in the RV of PBS+RTX, PBS+MCT and RTX+MCT rats. N=4 per group. (**D**) Representative images of immunofluorescence staining with activated macrophage marker F4-80, anti-F4-80

(Green), cell membrane marker WGA, anti-WGA (Red), and DAPI (blue) from the RV of PBS+RTX, PBS+MCT and RTX+MCT rats. N=4 per group.

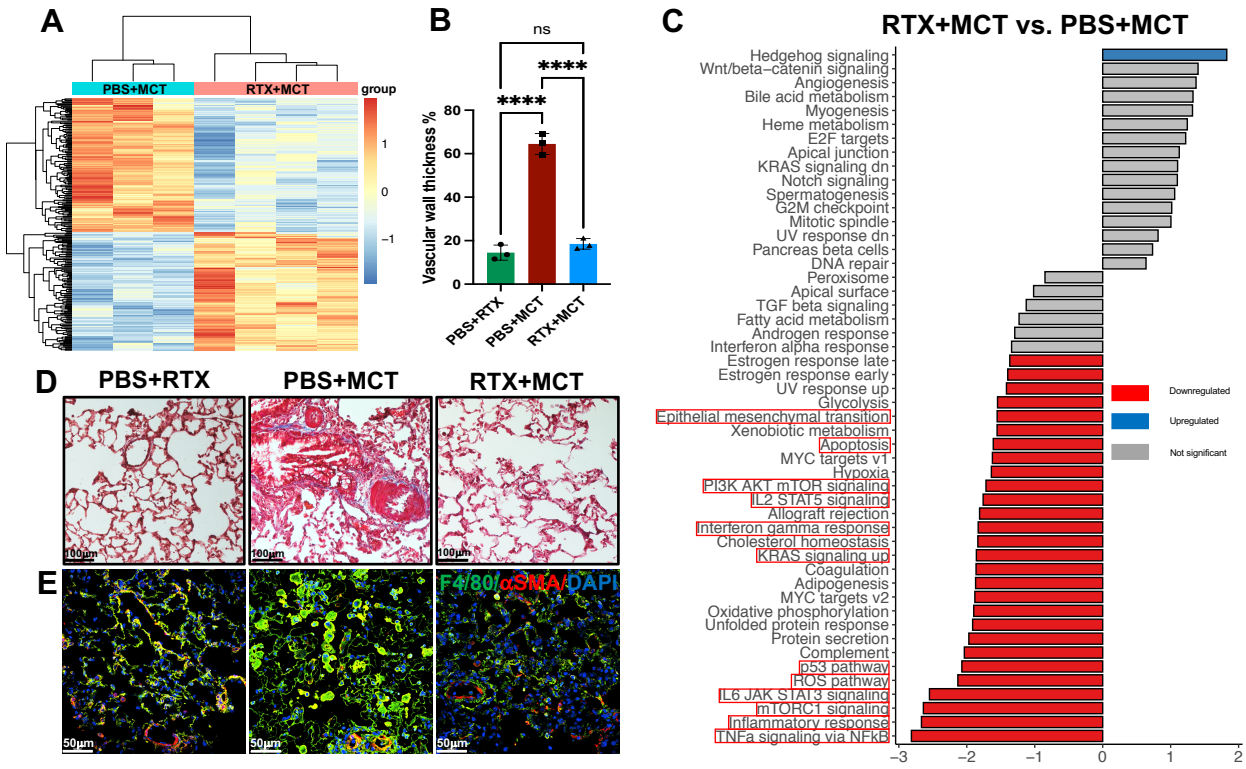

Figure 8. TRPV1 ablation results in reversal of lung transcriptomic signature in MCT rats. (**A**) RNA-Seq based heat map showing DEGs from the lung of PBS+MCT (Blue) and RTX+MCT (Red) groups. N=4 per group. (**B**) Bar plot showing normalized enrichment scores (NES) for Hallmark pathways derived from Gene Set Enrichment Analysis (GSEA). For GSEA, differentially expressed genes between PBS+MCT vs. RTX+MCT were ranked by the Wald statistic derived from DESeq2. Bars in blue and red represent statistically significant (FDR<0.05) pathways in PBS+MCT and RTX+MCT, respectively, that are either up- or downregulated. N=4 per group. Red boxes in the bar plot indicate downregulation of pro-fibrotic, pro-inflammatory and pro-apoptotic pathways. (**C**) Trichrome staining showing interstitial and perivascular fibrosis (Black arrow) and arteriolar wall thickness in the lung of PBS+RTX, PBS+MCT and RTX+MCT rats. N=4 per

group. (**D**) Representative images of immunofluorescence staining with activated macrophage marker F4-80, anti-F4-80 (Green), smooth muscle marker αSMA, anti-αSMA (Red), and DAPI (blue) from the lung of PBS+RTX, PBS+MCT and RTX+MCT rats. N=4 per group.

TRPV1 ablation results in reversal of lung transcriptomic signature in MCT rats

To investigate the therapeutic effects of intrathecal TRPV1 ablation on MCT-induced remodeling in the lung, RNASeq of lung tissue was performed on PBS+MCT vs. RTX+MCT rats (Figures 8, Table 1). Hierarchical clustering of top DEGs (FDR<0.05) from lung RNASeq revealed 260 differentially expressed genes that were either up- or down-regulated in the RTX-treated group compared to PBS-treated MCT rats (Figure 8A, Table 1). Gene Set Enrichment Analysis revealed 29 hallmark pathways significantly enriched (FDR<0.05) in RTX-treated group compared to PBS-treated MCT rats (Figure 8B). Hallmark analysis demonstrated significant down-regulation (FDR<0.05) of many pro-inflammatory pathways such as TNFα signaling via NFk-B, inflammatory response, mTORC1 signaling, IL6 JAK STAT3 signaling, KRAS signaling, Interferon gamma response, IL2 STAT5 signaling and PI3K AKT mTOR signaling in the lung of RTX-treated MCT rats (Figure 8B). Many significantly downregulated pro-inflammatory genes, such as, IL6, CD38, CxCl9, TNF and Cx3Cl1 were enriched in these pathways (Table 1). Moreover, lung RNASeq revealed TGFβ-signaling and epithelial mesenchymal transition as some of the top down-regulated pro-fibrotic pathways along with downregulation of pro-fibrotic genes such as Serpine2, Fabp4, Ctsk, Lgmn and CD44 in RTX-treated MCT rats (Figure

8B, Table 1). Similarly, several down-regulated pro-apoptotic genes such as MAPKAPK3, IER3, PLK3, BAK1 and Slc7a11 were enriched in down-regulated apoptosis and p53 pathway in the lung of RTX-treated group (Figure 8B, Table 1). Interestingly, trichrome staining validated significantly decreased MCT-induced increases in lung arteriolar wall thickness as well as perivascular and interstitial lung fibrosis in the RTX-treated rats (Figure 8C). Moreover, immunostaining with F4/80 confirmed MCT-induced increases in activated macrophages in the lung of PBS+MCT rats. Lumbar intrathecal RTX administration remarkably reduced activated macrophages in the lung in RTX+MCT rats (Figure 8D).

Discussion

In this study, we demonstrated that intrathecal RTX administration abolished TRPV1 expression of the thoracic dorsal horn, attenuated PH severity and prevented RVF by decreasing cardiac sympathetic tone in two pre-clinical rat models of severe PH-RVF induced by MCT and SuHx, respectively (Figure 1-3). Mechanistically, NMDAR-NOS1 mediated neuroinflammation and neuronal apoptosis in the TSC in PH is dependent on TRPV1 activation, as intrathecal RTX reduced NMDAR and NOS1 expression, microglial and astrocytic activation and apoptosis in the TSC of MCT rats (Figure 4-6). Importantly, intrathecal RTX administration prevented PH-induced RV remodeling, including RV hypertrophy, fibrosis, inflammation and apoptosis (Figure 1,7). Similarly, RTX prevented MCT-induced lung remodeling, including pulmonary arteriolar wall thickness, fibrosis, inflammation and apoptosis (Figure 8). To our knowledge, these findings are the first to reveal that selective chemo-ablation of TRPV1+ sensory afferents in the TSC might exert cardiopulmonary protective effects by ameliorating TSC neuroinflammation and associated sympatoexcitation in PH.

Our previous study demonstrated increased TRPV1 expression and activation, microglial and astrocytic activation mediated neuroinflammation and neuronal apoptosis in the TSC as well as increased sympathoexcitation in MCT- and SuHx-induced PH rats and human with PAH[3]. However, the role of TRPV1 activation in the TSC neuroinflammation, sympathoexcitation and cardiopulmonary function in PH are still unknown. The neuronal cell bodies of cardiac sympathetic afferent nerves are located in the thoracic DRG with one terminal projected to the epicardial surface, and the other mainly terminates in laminae I, V, VII, and X of spinal segments T2–T6[43]. TRPV1 is expressed in both of these terminals, which can be ablated for a long period through epicardial brushing of RTX at

the peripheral terminal or focal chemo-ablation at the spinal terminals[30-34,37]. The application of RTX on the heart surface by brushing was shown to successfully ablate cardiac TRPV1 expressing nociceptive afferents, blunt CSAR that lasted over 10 weeks and attenuate cardiac remodeling, autonomic dysfunction as well as improve cardiovascular dysfunction in rats and swine with heart failure[35-37,44]. However, brushing RTX on the surface of the heart or percutaneous epicardial RTX application in clinical background is challenging. Therefore, the spinal terminals of cardiac afferent nerves might be a potential target for focal chemo-ablation. In fact, intrathecal administration of RTX has been shown to abolish TRPV1 expression in the dorsal horn, which resulted in reduction of pain, inflammation, thermal hypersensitivity and over-activated CSAR, thereby preventing myocardial hypertrophy, fibrosis, and apoptosis[30-34,38]. Hence, we administered RTX intrathecally at the T2-T3 and L4-L5 spinal cord levels to ablate the TRPV1+ cardiopulmonary sensory nerve endings to determine the role of TRPV1 in TSC NOS1 expression, neuroinflammation, sympathoexcitation and cardiopulmonary function in two different rat models of severe PH-RVF. Consequently, we observed that intrathecal RTX administration selectively ablated the cardiopulmonary afferents by inhibiting TRPV1 expression in the thoracic dorsal horn in normal and PH rats.

TRPV1 activation in the thoracic dorsal horn has been shown to promote microglial activation mediated release of inflammatory cytokines and ROS as well as regulate NF-κB pathway mediated neuroinflammation[13-16]. TRPV1 activation has also been implicated in NMDAR mediated NOS1 activation and ˙NO production leading to oxidative and nitrosative stress, neuroinflammation, chemokine release, excitotoxicity, and neuronal apoptosis in the CNS[17-20]. A number of studies demonstrated that during various pathologic conditions including hypertension, myocardial infarction, and chronic heart

failure, NOS1 upregulation plays an essential role in the sympathoexcitatory and pressor action of ˙NO at the RVLM and TSC by increasing systemic arterial pressure, heart rate and sympathetic neurogenic vasomotor tone mediated by norepinephrine release from the sympathetic nerve terminals[10,19,25]. Therefore, the weakened effects of RTX administration on sympathetic tone demonstrated by decreased plasma NE and HR in the present study may be associated with decreased NMDAR-NOS1 mediated TSC neuroinflammation due to blunting spinal-cardiopulmonary nervous system interaction. In CHF and hypertension over-activated CSAR has been shown to increase sympathetic tone and NE release elevating blood pressure and cardiac function, which is known as a positive feedback characteristic[36,37,45,46]. RTX was shown to reduce TRPV1 expression in the heart and DRG and weakened sympathoexcitatory responses to capsaicin stimulation[8].

In the present study, intrathecal RTX administration significantly attenuated MCT- and SuHx-induced PH severity. Several studies have demonstrated that depleting afferent nerve endings by capsacin treatment in the lung improved PH and RV hypertrophy in MCT, pulmonary artery banding and perinatal hypoxia PH models[47,48]. Cardiac compliance is determined by the structural properties of the cardiac muscle and connective tissue[49,50]. Our study demonstrated that TRPV1+ cardiopulmonary afferent nerve ablation in the TSC by intrathecal RTX administration can protect the heart against PH-induced RV hypertrophy (Figure 1-3). In PH rats, cardiac fibrosis contributes to RV remodeling and systolic dysfunction[51]. Our histological data confirmed that intrathecal RTX administration significantly attenuated PH-induced interstitial and perivascular RV fibrosis and RV systolic dysfunction (Figures 1,7). Focal ablation of TRPV1-expressing CSAR afferents via epicardial application of RTX was shown to attenuate cardiac remodeling and autonomic dysfunction in HF[37]. Moreover, TRPV1 antagonist had also been reported to improve

cardiac hypertrophy, inflammation, fibrosis, and apoptosis[52]. RV inflammation contributes to impaired RV contractility, maladaptive remodeling and a vicious circle between RV and pulmonary vascular injury in PH[53]. The current study demonstrated significant reduction in PH-induced RV inflammation by intrathecal RTX administration in PH rats.

Previous studies have shown that TRPV1 channels in the neutral terminals play a complex role in modulating sympathetic efferent activities[8,54,55]. Shanks et al showed that inhibiting thoracic TRPV1-expressing afferent soma at the T1–T4 DRG by epidural application of RTX abolished cardiac and pulmonary sympathoexcitatory responses 10 weeks post-RTX administration[55]. These data and others demonstrate that TRPV1 is expressed in afferent fibers throughout the respiratory tract and intrapulmonary arteries and influences visceral tissue homeostasis, cytoskeletal architecture reorganization as well as proliferation and migration of pulmonary arterial smooth muscle cells (PASMC) through Ca^{2+} influx[11,22,23]. Moreover, TRPV1 ablation by capsaicin pretreatment attenuated PH severity by reducing pro-inflammatory cytokines and alleviating inflammation via p38MAPK pathway in the lung[24,25]. In the current study we demonstrated that intrathecal RTX administration significantly attenuated MCT-induced respiratory dysfunction and PH by decreasing pulmonary arteriolar wall thickness, interstitial and perivascular lung fibrosis and inflammation.

RNASeq of RV and lung tissues from intrathecal RTX-treated MCT rats demonstrated promising therapeutic potential of TRPV1+ cardiopulmonary sensory afferent inhibition through reversal of several pro-fibrotic, inflammatory and apoptotic pathways and genes in both organs (Figures 7,8; Tables 1,2). Fibrosis, inflammation and cell death are important contributors of cardiac and pulmonary remodeling under pressure overload in PH-RVF[49,56-

[58]. The anti-fibrotic, anti-inflammatory and anti-apoptotic effects of intrathecal RTX in our study might exert cardiopulmonary protective effects through reducing the rigidity of the heart and lung. NE has been shown to enhance cardiac fibrosis through TGFβ signaling[59-61]. Our data demonstrated a significant reduction of both plasma NE and TGFβ signaling in the RV of RTX-treated MCT rats leading to reduced fibrosis (Figures 1,7; Table 1). NE has been shown to induce oxidative stress, cardiomyocyte hypertrophy, fibrosis, activation of MAPK (Mainly p38 and ERK1/2) and AKT as well as NF-κB to release inflammatory cytokines in cultured cardiomyocytes[62,63]. Also, NE has been implicated in the activation of cardiac proinflammatory cytokines IL-6, IL-1β and TNF-α[64-67]. Moreover, NE is also known to induce apoptosis in cardiomyocytes[68,69]. Several studies have demonstrated that NE induces pulmonary injury with edema and inflammation by increased expression of several cytokines[70]. Elevated plasma norepinephrine leads to severe inflammatory reactions during transition into pulmonary fibrosis leading to the development of acute lung injury and acute respiratory distress syndrome[71]. Therefore, we believe that the reversal of fibrotic, inflammatory and apoptotic signatures in the lung and RV in our study were due to reduced NE release from the sympathetic nerve terminals in RTX-treated MCT rats.

Given that the TRPV1 channels are expressed in various organs and have diverse roles in pathophysiological conditions, systemic intervention of TRPV1 might be harmful[72]. Previous studies have shown that TRPV1 activation produced several beneficial effects on cardiovascular diseases, such as PH, atherosclerosis, hypertension, and ischemia-reperfusion injury, by modulating ˙NO and substance P production and Ca2+ influx[26,54,73,74]. TRPV1 activation by dietary capsaicin intake has been shown to reduce cardiac fibrosis, oxidative stress and hypertrophy, and prevent congestive HF development[75]. TRPV1 knock-out mice (TRPV1-/-) had excessive inflammation, cardiac

hypertrophy, and deteriorated cardiac function after transverse aortic constriction[76,79]. Therefore, in this study, we specifically ablated TRPV1 expression in the thoracic dorsal horn through intrathecal RTX administration in the T2-T3 and L4-L5 segments, which blunted the spinal terminal of the cardiac afferent nerve. The cardiopulmonary protective effects of RTX in the present study demonstrates the therapeutic potential of excitatory chemosensitive sympathetic afferents in PH.

The current study has few limitations. First, we didn't administer RTX systemically or through epicardial application. We could not confirm whether all cardiac afferents were abolished through lumbar or thoracic RTX administration; however, a previous study reported that injectants delivered through intrathecal route can gradually diffuse on the surface of the spinal cord[77]. Second, RTX injection was administered five days before MCT or Sugen injections in this study. Therefore, we could not confirm whether RTX has comparable therapeutic effects on neuroinflammation and cardiopulmonary protection if RTX was given several days or weeks after PH induction. Further studies are needed to decipher these issues. Moreover, future studies should investigate the role of NMDAR-NOS1 axis as downstream of TRPV1 gene in TSC neuroinflammation, sympathoexcitation and cardiopulmonary function in PH-RVF.

Supplementary Figures

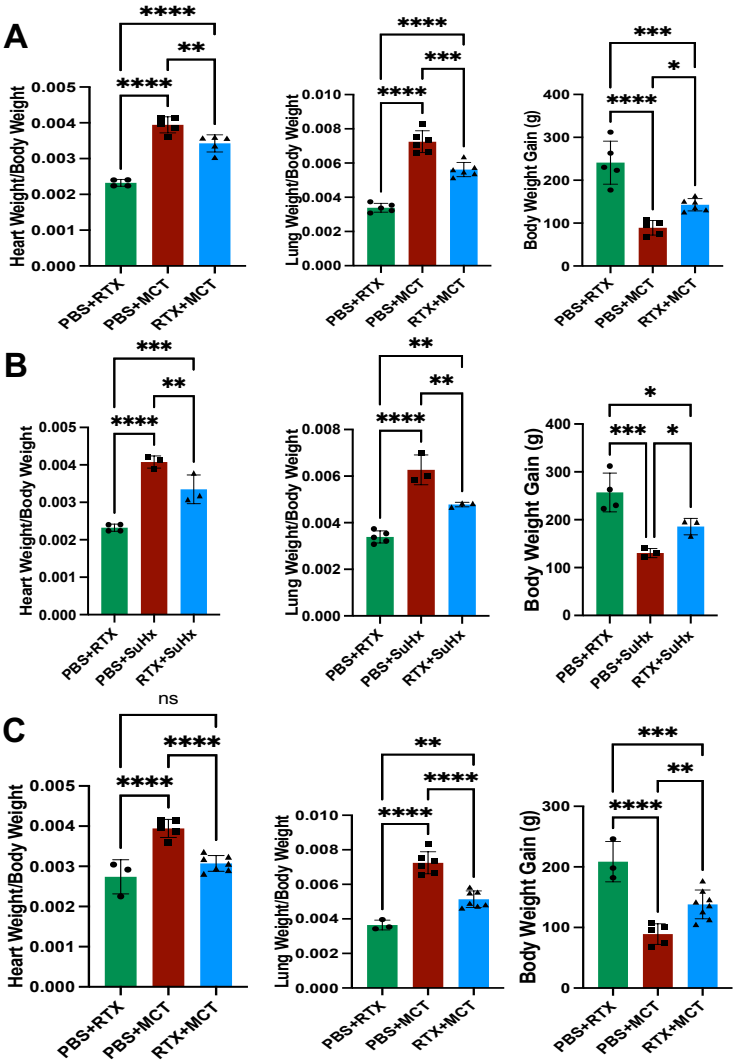

Figure S1. Intrathecal RTX administration prevents PH and RVF in MCT and SuHx rats (**A**) Heart weight/body weight, lung weight/body weight and body weight gain of PBS+RTX, PBS+MCT and RTX+MCT rats from lumbar intrathecal RTX administration. N=4-6 per group. *p<0.05, **p<0.01, ***p<0.001, ****p<0.0001. (**B**) Heart weight/body weight, lung weight/body weight and body weight gain of PBS+RTX, PBS+SuHx and RTX+SuHx rats from lumbar intrathecal RTX administration. N=4-6 per group. *p<0.05, **p<0.01, ***p<0.001, ****p<0.0001. (**C**) Heart weight/body weight, lung weight/body weight and body weight gain of PBS+RTX, PBS+MCT and RTX+MCT rats from thoracic

intrathecal RTX administration. N=4-6 per group. *p<0.05, **p<0.01, ***p<0.001, ****p<0.0001.

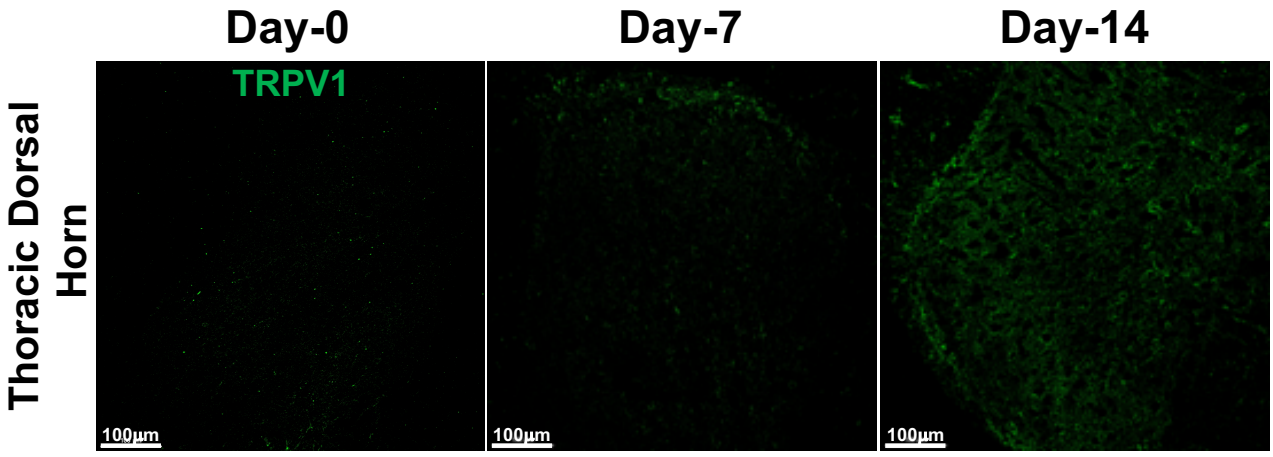

Figure S2. Timecourse of TRPV1 expression in the thoracic dorsal horn of MCT rats. Representative images of immunofluorescence staining with anti-TRPV1 (Green) from the thoracic dorsal horn of MCT-treated rats from Day-7 and Day-14 compared to control (Day-0). N=3 per group.

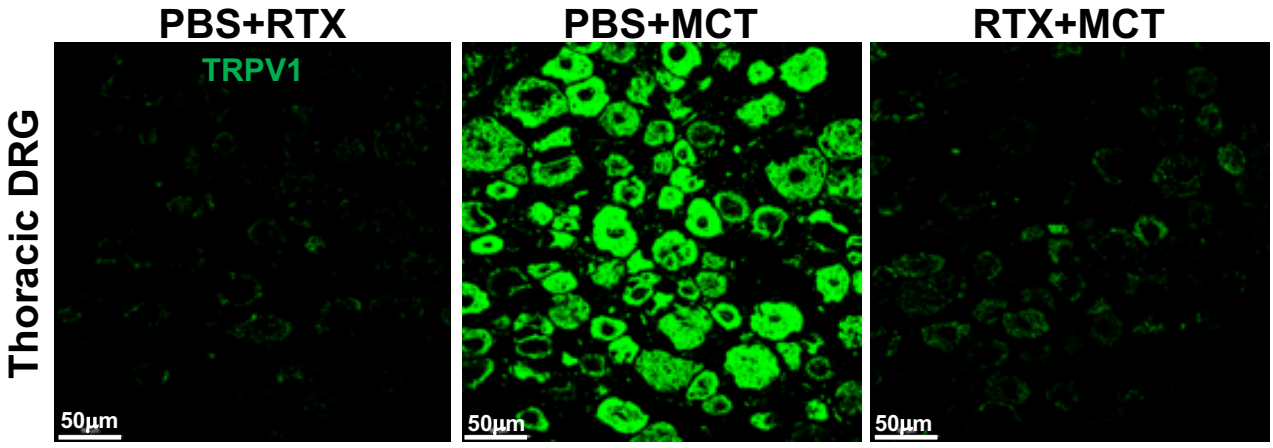

Figure S3. Lumbar intrathecal RTX administration reduces TRPV1 expression in the thoracic DRG in PBS and MCT rats. Representative images of immunofluorescence staining with anti-TRPV1 (Green) from the thoracic DRG of PBS+RTX, PBS+MCT and RTX+MCT rats. N=4 per group.

Supplementary Tables

Table S1: Leading edge down-regulated RV genes from RTX-treated MCT vs. PBS-treated MCT rats

Gene	Full Name	Expression	Log2Fold Change	Padj Value
Pro-Apoptotic Genes				
PPP1R15A RTX VS PBS	Protein Phosphatase 1 Regulatory Subunit 15A	Decreased	-0.584373892	0.001072462273
NDRG1 RTX VS PBS	N-Myc Downstream Regulated 1	Decreased	-0.792178613	0.001758628049
IER5 RTX VS PBS	Immediate Early Response 5	Decreased	-0.594494566	0.002687176717
RRAD RTX VS PBS	RRAD, Ras Related Glycolysis Inhibitor And Calcium Channel Regulator	Decreased	-0.777640479	0.009655909538
PERP RTX VS PBS	P53 Apoptosis Effector Related To PMP22	Decreased	-0.782562520	0.01036982568
TGFβ1 RTX VS PBS	Transforming Growth Factor Beta 1	Decreased	-0.506570152	0.02497108604
AK1 RTX VS PBS	Adenylate Kinase 1	Decreased	-0.621116930	0.03390791437

Gene	Full Name	Expression	Log2Fold Change	Padj Value
Pro-inflammatory Genes				
MAP2K3 RTX VS PBS	Mitogen-activated protein kinase kinase 3	Decreased	-1.154536817	0.001299501068
CxCr4 RTX VS PBS	C-X-C Motif Chemokine Receptor 4	Decreased	-0.562177884	0.009474014078
Tomm40 RTX VS PBS	Translocase Of Outer Mitochondrial Membrane 40	Decreased	-0.751712247	0.04683568158
SMAD6 RTX VS PBS	SMAD Family Member 6	Decreased	-1.374167942	2.35E-05
NDRG1 RTX VS PBS	N-Myc Downstream Regulated 1	Decreased	-0.792178613	0.001758628049
PPP1R15A RTX VS PBS	Protein Phosphatase 1 Regulatory Subunit 15A	Decreased	-0.584373892	0.001072462273
TGM2 RTX VS PBS	Transglutaminase 2	Decreased	-0.782464879	0.002822957236

Mapkapk2 RTX VS PBS	MAPK Activated Protein Kinase 2	Decreased	-0.647650570	0.02064542556
Ccr4 RTX VS PBS	C-C Motif Chemokine Receptor 3	Decreased	-3.590452604	0.02296810957
STAT3 RTX VS PBS	Signal Transducer And Activator Of Transcription 3	Decreased	-0.440311500	0.03257912905
Gene	**Full Name**	**Expression**	**Log2Fold Change**	**Padj Value**
Pro-fibrotic Genes				
TGFβ1 RTX VS PBS	Transforming Growth Factor Beta 1	Decreased	-0.506570152	0.02497108604
Eng RTX VS PBS	Endoglin	Decreased	-0.630935168	0.00098659581
FURIN RTX VS PBS	Furin	Decreased	-0.535934103	0.04186429496
SMAD6 RTX VS PBS	SMAD Family Member 6	Decreased	-1.374167942	2.35E-05
ID1 RTX VS PBS	Inhibitor Of DNA Binding 1	Decreased	-0.485496100	0.04359881798

Table S2: Leading edge down-regulated lung genes from RTX-treated MCT vs. PBS-treated MCT rats

Gene	**Full Name**	**Expression**	**Log2Fold Change**	**Padj Value**
Pro-Apoptotic Genes				
MAPKAPK3 RTX VS PBS	MAPK activated protein kinase 3	Decreased	-0.6990320819	0.0006962878
IER3 RTX VS PBS	Immediate Early Response 3	Decreased	-0.4907065252	0.0031226307
PLK3 RTX VS PBS	Polo Like Kinase 3	Decreased	-0.3262871934	0.0090156837
BAK1 RTX VS PBS	BCL2 Antagonist/Killer 1	Decreased	-0.2575605804	0.0242558071
Slc7a11 RTX VS PBS	Brain And Muscle ARNT-Like 1	Decreased	-1.822906869	1.86E-06
TXNIP RTX VS PBS	Thioredoxin Interacting Protein	Decreased	-0.6312734935	0.0053828510
ATF3 RTX VS PBS	Activating Transcription Factor 3	Decreased	-0.3889560628	0.0099213914
GM2A RTX VS PBS	Ganglioside GM2 activator	Decreased	-0.7558638396	0.0003259840
Gene	**Full Name**	**Expression**	**Log2Fold Change**	**Padj Value**
Pro-inflammatory Genes				

Socs3 RTX VS PBS	Suppressor of Cytokine Signaling-3	Decreased	-1.127566253	3.9E-07
Fabp4 RTX VS PBS	Fatty Acid Binding Protein 4	Decreased	-1.809232165	9.39E-05
Itgam RTX VS PBS	Integrin Subunit Alpha M	Decreased	-1.389226051	4.63E-08
Ctsk RTX VS PBS	Cathepsin K	Decreased	-1.854727808	2.34E-09
Lgmn RTX VS PBS	Legumain	Decreased	-0.896492831	0.00239978148
Cx3Cl1 RTX VS PBS	C-X3-C motif chemokine ligand 1	Decreased	-0.882417753	0.004424342001
TNF RTX VS PBS	Tumor Necrosis Factor	Decreased	-1.224910817	0.004519735874
SOD2 RTX VS PBS	Superoxide dismutase 2	Decreased	-1.167570759	9.62E-05
IL6 RTX VS PBS	Interleukin 6	Decreased	-1.961836844	0.0136557241
CxCl6 RTX VS PBS	C-X-C motif chemokine ligand 6	Decreased	-3.428559241	9.29E-07
CxCl1 RTX VS PBS	C-X-C motif chemokine ligand 1	Decreased	-1.849154413	1.62E-05
CxCl9 RTX VS PBS	C-X-C motif chemokine ligand 9	Decreased	-1.15168674	0.0015847566
CD38 RTX VS PBS	Brain And Muscle ARNT-Like 1	Decreased	-0.515125000	0.0079871566

Gene	Full Name	Expression	Log2Fold Change	Padj Value
Pro-fibrotic Genes				
Serpine2 RTX VS PBS	Microfibril Associated Protein 4	Decreased	-1.055447099	5.49E-05
Fabp4 RTX VS PBS	Fatty Acid Binding Protein 4	Decreased	-1.809232165	9.39E-05
Ctsk RTX VS PBS	Cathepsin K	Decreased	-1.854727808	2.34E-09
CD44 RTX VS PBS	CD44 molecule	Decreased	-0.350104654	0.0170278820
Lgmn RTX VS PBS	Legumain	Decreased	-0.896492831	0.0023997814
Slc7a11 RTX VS PBS	Brain And Muscle ARNT-Like 1	Decreased	-1.822906869	1.86E-06
Areg RTX VS PBS	Amphiregulin	Decreased	-1.758111764	9.51E-27
Areg RTX VS PBS	Urokinase Plasminogen Activator Surface Receptor	Decreased	-0.702078256	1.21E-08
Vim RTX VS PBS	Vimentin	Decreased	-0.253224478	0.1689562402

References

1. Rabinovitch M. Molecular pathogenesis of pulmonary arterial hypertension. J Clin Invest. 2012;122:4306–4313. doi: 10.1172/JCI60658.
2. Dandel M, et al. Assessment of right ventricular adaptability to loading conditions can improve the timing of listing to transplantation in patients with pulmonary arterial hypertension. J Heart Lung Transplant. 2015;3:319-28. doi: 10.1016/j.healun.2014.11.012.
3. Razee A, Banerjee S, Hong J, Magaki S, Fishbein G, Ajijola OA, Umar S (2023). Thoracic Spinal Cord Neuroinflammation as a Novel Therapeutic Target in Pulmonary Hypertension. Hypertension. 2023 Jun;80(6):1297-1310. doi: 10.1161/HYPERTENSIONAHA.122.20782. Epub 2023 Apr 24. PMID: 37092338; PMCID: PMC10192067.
4. Vaillancourt M, Chia P, Medzikovic L, et al. Experimental Pulmonary Hypertension Is Associated With Neuroinflammation in the Spinal Cord. Front Physiol. 2019;10:1186. Published 2019 Sep 20. doi:10.3389/fphys.2019.01186.
5. Sharma RK, Oliveira AC, Kim S, et al. Involvement of Neuroinflammation in the Pathogenesis of Monocrotaline-Induced Pulmonary Hypertension. Hypertension. 2018;71(6):1156-1163.
6. Rosenkranz S, Howard LS, Gomberg-Maitland M, Hoeper MM. Systemic Consequences of Pulmonary Hypertension and Right-Sided Heart Failure. Circulation. 2020 Feb 25;141(8):678-693. doi: 10.1161/CIRCULATIONAHA.116.022362. Epub 2020 Feb 24. PMID: 32091921.

7. W.W. Chen, X.Q. Xiong, Q. Chen, Y.H. Li, Y.M. Kang, G.Q. Zhu, Cardiac sympathetic afferent reflex and its implications for sympathetic activation in chronic heart failure and hypertension, Acta Physiol. 213 (2015) 778–794.
8. M.R. Zahner, D.P. Li, S.R. Chen, H.L. Pan, Cardiac vanilloid receptor 1-expressing afferent nerves and their role in the cardiogenic sympathetic reflex in rats, J. Physiol. 551 (2003) 515–523.
9. Jia Y, Lee LY. Role of TRPV receptors in respiratory diseases. Biochim Biophys Acta. 2007 Aug;1772(8):915-27. doi: 10.1016/j.bbadis.2007.01.013. Epub 2007 Feb 1. Erratum in: Biochim Biophys Acta. 2007 Oct;1772(10):1182. PMID: 17346945.
10. Yoshie K, Rajendran PS, Massoud L, Kwon O, Tadimeti V, Salavatian S, Ardell JL, Shivkumar K, Ajijola OA. Cardiac vanilloid receptor-1 afferent depletion enhances stellate ganglion neuronal activity and efferent sympathetic response to cardiac stress. Am J Physiol Heart Circ Physiol. 2018 May 1;314(5):H954-H966. doi: 10.1152/ajpheart.00593.2017. Epub 2018 Jan 16. PMID: 29351450; PMCID: PMC6008140.
11. Nahama A, Ramachandran R, Cisternas AF, Ji H. The role of afferent pulmonary innervation in ARDS associated with COVID-19 and potential use of resiniferatoxin to improve prognosis: A review. Med Drug Discov. 2020 Mar;5:100033. doi: 10.1016/j.medidd.2020.100033. Epub 2020 Apr 4. PMID: 32292906; PMCID: PMC7147194.
12. Kong WL, Peng YY, Peng BW. Modulation of neuroinflammation: Role and therapeutic potential of TRPV1 in the neuro-immune axis. Brain Behav Immun. 2017 Aug;64:354-366. doi: 10.1016/j.bbi.2017.03.007. Epub 2017 Mar 22. PMID: 28342781.

13. Talbot S, Dias JP, Lahjouji K, Bogo MR, Campos MM, Gaudreau P, Couture R. Activation of TRPV1 by capsaicin induces functional kinin B(1) receptor in rat spinal cord microglia. J Neuroinflammation. 2012 Jan 20;9:16. doi: 10.1186/1742-2094-9-16. PMID: 22264228; PMCID: PMC3282640.
14. Chen Y, Willcockson HH, Valtschanoff JG. Influence of the vanilloid receptor TRPV1 on the activation of spinal cord glia in mouse models of pain. Exp Neurol. 2009 Dec;220(2):383-90. doi: 10.1016/j.expneurol.2009.09.030. Epub 2009 Oct 6. PMID: 19815011; PMCID: PMC2784271.
15. Hassan S, Eldeeb K, Millns PJ, Bennett AJ, Alexander SP, Kendall DA. Cannabidiol enhances microglial phagocytosis via transient receptor potential (TRP) channel activation. Br J Pharmacol. 2014 May;171(9):2426-39. doi: 10.1111/bph.12615. PMID: 24641282; PMCID: PMC3997281.
16. Doly S, Fischer J, Salio C, Conrath M. The vanilloid receptor-1 is expressed in rat spinal dorsal horn astrocytes. Neurosci Lett. 2004 Mar 4;357(2):123-6. doi: 10.1016/j.neulet.2003.12.051. PMID: 15036590.
17. Carletti F, Gambino G, Rizzo V, Ferraro G, Sardo P. Neuronal nitric oxide synthase is involved in CB/TRPV1 signalling: Focus on control of hippocampal hyperexcitability. Epilepsy Res. 2017 Dec;138:18-25. doi: 10.1016/j.eplepsyres.2017.09.018. Epub 2017 Oct 3. PMID: 29035821.
18. Chen Y, Willcockson HH, Valtschanoff JG. Influence of the vanilloid receptor TRPV1 on the activation of spinal cord glia in mouse models of pain. Exp Neurol. 2009 Dec;220(2):383-90. doi: 10.1016/j.expneurol.2009.09.030. Epub 2009 Oct 6. PMID: 19815011; PMCID: PMC2784271.

19. Hwang SJ, Burette A, Rustioni A, Valtschanoff JG. Vanilloid receptor VR1-positive primary afferents are glutamatergic and contact spinal neurons that co-express neurokinin receptor NK1 and glutamate receptors. J Neurocytol. 2004 May;33(3):321-9. doi: 10.1023/B:NEUR.0000044193.31523.a1. PMID: 15475687.
20. Peters JH, McDougall SJ, Fawley JA, Smith SM, Andresen MC. Primary afferent activation of thermosensitive TRPV1 triggers asynchronous glutamate release at central neurons. Neuron. 2010 Mar 11;65(5):657-69. doi: 10.1016/j.neuron.2010.02.017. PMID: 20223201; PMCID: PMC2837850.
21. K. Fujiu, M. Shibata, Y. Nakayama, F. Ogata, S. Matsumoto, K. Noshita, et al., A heart-brain-kidney network controls adaptation to cardiac stress through tissue macrophage activation, Nat. Med. 23 (2017) 611–622.
22. Martin E, Dahan D, Cardouat G, Gillibert-Duplantier J, Marthan R, Savineau JP, Ducret T. Involvement of TRPV1 and TRPV4 channels in migration of rat pulmonary arterial smooth muscle cells. Pflugers Arch. 2012 Sep;464(3):261-72. doi: 10.1007/s00424-012-1136-5. Epub 2012 Jul 22. PMID: 22820913.
23. Parpaite T, Cardouat G, Mauroux M, Gillibert-Duplantier J, Robillard P, Quignard JF, Marthan R, Savineau JP, Ducret T. Effect of hypoxia on TRPV1 and TRPV4 channels in rat pulmonary arterial smooth muscle cells. Pflugers Arch. 2016 Jan;468(1):111-130. doi: 10.1007/s00424-015-1704-6. Epub 2015 Mar 24. PMID: 25799977.
24. Lo CCW, Moosavi SM, Bubb KJ. The Regulation of Pulmonary Vascular Tone by Neuropeptides and the Implications for Pulmonary Hypertension. Front Physiol. 2018 Aug 23;9:1167. doi: 10.3389/fphys.2018.01167. PMID: 30190678; PMCID: PMC6116211.

25. Xu Y, Gu Q, Qu C. Capsaicin pretreatment reversed pulmonary arterial hypertension by alleviating inflammation via p38MAPK pathway. Exp Lung Res. 2017 Feb;43(1):8-18. doi: 10.1080/01902148.2016.1271481. Epub 2017 Mar 10. PMID: 28281854.
26. Du Q, Liao Q, Chen C, Yang X, Xie R, Xu J. The Role of Transient Receptor Potential Vanilloid 1 in Common Diseases of the Digestive Tract and the Cardiovascular and Respiratory System. Front Physiol. 2019 Aug 21;10:1064. doi: 10.3389/fphys.2019.01064. PMID: 31496955; PMCID: PMC6712094.
27. Randhawa PK, Jaggi AS. $TRPV_1$ channels in cardiovascular system: A double edged sword? Int J Cardiol. 2017 Feb 1;228:103-113. doi: 10.1016/j.ijcard.2016.11.205. Epub 2016 Nov 9. PMID: 27863349.
28. Lu S., Xu D. (2013). Cold Stress Accentuates Pressure Overload-Induced Cardiac Hypertrophy and Contractile Dysfunction: Role of TRPV1/AMPK-Mediated Autophagy. *Biochem. Biophysical Res. Commun.* 442, 8–15. 10.1016/j.bbrc.2013.10.128
29. C.L. Buckley, A.J. Stokes, Mice lacking functional TRPV1 are protected from pressure overload cardiac hypertrophy, Channels 5 (2011) 367–374.
30. Wang D., Wu Y., Chen Y., Wang A., Lv K., Kong X., et al. (2019). Focal Selective Chemo-Ablation of Spinal Cardiac Afferent Nerve by Resiniferatoxin Protects the Heart from Pressure Overload-Induced Hypertrophy. *Biomed. Pharmacother.* 109, 377–385. 10.1016/j.biopha.2018.10.156
31. M. Bishnoi, C.A. Bosgraaf, L.S. Premkumar, Preservation of acute pain and efferent functions following intrathecal resiniferatoxin-induced analgesia in rats, J. Pain 12 (2011) 991–1003.

32. M. Leo, M. Schulte, L.I. Schmitt, M. Schafers, C. Kleinschnitz, T. Hagenacker, Intrathecal resiniferatoxin modulates TRPV1 in DRG neurons and reduces TNF-induced pain-related behavior, Mediat. Inflamm. 2017 (2017) 2786427.
33. L. Karai, D.C. Brown, A.J. Mannes, S.T. Connelly, J. Brown, M. Gandal, et al., Deletion of vanilloid receptor 1-expressing primary afferent neurons for pain control, J. Clin. Invest. 113 (2004) 1344–1352.
34. Horton J. S., Shiraishi T., Alfulaij N., Small-Howard A. L., Turner H. C., Kurokawa T., et al. (2019). TRPV1 Is a Component of the Atrial Natriuretic Signaling Complex, and Using Orally Delivered Antagonists, Presents a Valid Therapeutic Target in the Longitudinal Reversal and Treatment of Cardiac Hypertrophy and Heart Failure. *Channels* 13, 1–16. 10.1080/19336950.2018.1547611
35. T. Irie, K. Yamakawa, D. Hamon, K. Nakamura, K. Shivkumar, M. Vaseghi, Cardiac sympathetic innervation via middle cervical and stellate ganglia and antiarrhythmic mechanism of bilateral stellectomy, Am. J. Physiol. Heart Circ. Physiol. 312 (2017) H392–H405.
36. H.J. Wang, G.J. Rozanski, I.H. Zucker, Cardiac sympathetic afferent reflex control of cardiac function in normal and chronic heart failure states, J. Physiol. 595 (2017) 2519–2534.
37. H.J. Wang, W. Wang, K.G. Cornish, G.J. Rozanski, I.H. Zucker, Cardiac sympathetic afferent denervation attenuates cardiac remodeling and improves cardiovascular dysfunction in rats with heart failure, Hypertension 64 (2014) 745–755.

38. M.R. Sapio, J.K. Neubert, D.M. LaPaglia, D. Maric, J.M. Keller, S.J. Raithel, et al., Pain control through selective chemo-axotomy of centrally projecting TRPV1+ sensory neurons, J. Clin. Invest. 128 (April (4)) (2018) 1657–1670.
39. J.A. Jeffry, S.Q. Yu, P. Sikand, A. Parihar, M.S. Evans, L.S. Premkumar, Selective targeting of TRPV1 expressing sensory nerve terminals in the spinal cord for long lasting analgesia, PLoS One 4 (2009) e7021.
40. Gambino G, Rizzo V, Giglia G, Ferraro G, Sardo P. Cannabinoids, TRPV and nitric oxide: the three ring circus of neuronal excitability. Brain Struct Funct. 2020 Jan;225(1):1-15. doi: 10.1007/s00429-019-01992-9. Epub 2019 Dec 2. Erratum in: Brain Struct Funct. 2019 Dec 11;: PMID: 31792694.
41. Ahlawat A, Rana A, Goyal N, Sharma S. Potential role of nitric oxide synthase isoforms in pathophysiology of neuropathic pain. Inflammopharmacology. 2014 Oct;22(5):269-78. doi: 10.1007/s10787-014-0213-0. Epub 2014 Aug 6. PMID: 25095760.
42. Rameau GA, Chiu LY, Ziff EB. NMDA receptor regulation of nNOS phosphorylation and induction of neuron death. Neurobiol Aging. 2003 Dec;24(8):1123-33. doi: 10.1016/j.neurobiolaging.2003.07.002. PMID: 14643384.
43. D.C. Kuo, J.J. Oravitz, W.C. DeGroat, Tracing of afferent and efferent pathways in the left inferior cardiac nerve of the cat using retrograde and transganglionic transport of horseradish peroxidase, Brain Res. 321 (1984) 111–118.
44. K. Yoshie, P.S. Rajendran, L. Massoud, O. Kwon, V. Tadimeti, S. Salavatian, et al., Cardiac vanilloid receptor-1 afferent depletion enhances stellate ganglion neuronal activity and efferent sympathetic response to cardiac stress, Am. J. Physiol. Heart Circ. Physiol. 314 (May (5)) (2018) H954–H966.

45. W. Wang, H.D. Schultz, R. Ma, Cardiac sympathetic afferent sensitivity is enhanced in heart failure, Am. J. Physiol. 277 (1999) H812–7.
46. G.Q. Zhu, Y. Xu, L.M. Zhou, Y.H. Li, L.M. Fan, W. Wang, et al., Enhanced cardiac sympathetic afferent reflex involved in sympathetic overactivity in renovascular hypertensive rats, Exp. Physiol. 94 (2009) 785–794.
47. Zhou, K. R., and Lai, Y. L. (1993). Capsaicin pretreatment attenuates monocrotaline-induced ventilatory dysfunction and pulmonary hypertension. J. Appl. Physiol. 75, 2781–2788. doi: 10.1152/jappl.1993.75.6.2781
48. Katzman, N. J., and Lai, Y. L. (2000). Capsaicin pre- and post-treatment on rat monocrotaline pneumotoxicity. Chin. J. Physiol. 43, 171–178.
49. B. Swynghedauw, Molecular mechanisms of myocardial remodeling, Physiol. Rev. 79 (1999) 215–262.syndrome-associated PTPN11 mutation, J. Clin. Invest. 121 (2011) 1026–1043.
50. F.G. Spinale, Myocardial matrix remodeling and the matrix metalloproteinases: influence on cardiac form and function, Physiol. Rev. 87 (2007) 1285–1342.
51. Dai Z, Zhu MM, Peng Y, Machireddy N, Evans CE, Machado R, Zhang X, Zhao YY. Therapeutic Targeting of Vascular Remodeling and Right Heart Failure in Pulmonary Arterial Hypertension with a HIF-2α Inhibitor. Am J Respir Crit Care Med. 2018 Dec 1;198(11):1423-1434. doi: 10.1164/rccm.201710-2079OC. PMID: 29924941; PMCID: PMC6290950.
52. J.S. Horton, C.L. Buckley, A.J. Stokes, Successful TRPV1 antagonist treatment for cardiac hypertrophy and heart failure in mice, Channels 7 (2013) 17–22.

53. Sun XQ, Abbate A, Bogaard HJ. Role of cardiac inflammation in right ventricular failure. Cardiovasc Res. 2017 Oct 1;113(12):1441-1452. doi: 10.1093/cvr/cvx159. PMID: 28957536.

54. H. Sun, D.P. Li, S.R. Chen, W.N. Hittelman, H.L. Pan, Sensing of blood pressure increase by transient receptor potential vanilloid 1 receptors on baroreceptors, J. Pharmacol. Exp. Ther. 331 (2009) 851–859.

55. J. Shanks, Z. Xia, S.J. Lisco, G.J. Rozanski, H.D. Schultz, I.H. Zucker, et al., Sympatho-excitatory response to pulmonary chemosensitive spinal afferent activation in anesthetized, vagotomized rats, Physiol. Rep. 6 (2018) e13742.

56. L. Zhao, G. Cheng, R. Jin, M.R. Afzal, A. Samanta, Y.T. Xuan, et al., Deletion of interleukin-6 attenuates pressure overload-induced left ventricular hypertrophy and dysfunction, Circ. Res. 118 (2016) 1918–1929.

57. Park JF, Clark VR, Banerjee S, Hong J, Razee A, Williams T, Fishbein G, Saddic L, Umar S. Transcriptomic Analysis of Right Ventricular Remodeling in Two Rat Models of Pulmonary Hypertension: Identification and Validation of EMT in Human Right Ventricular Failure. Circ Heart Fail. 2021 Feb 5:CIRCHEARTFAILURE120007058. doi: 10.1161/CIRCHEARTFAILURE.120.007058. Online ahead of print. PMID: 33541093.

58. Hong J, Arneson D, Umar S, Ruffenach G, Cunningham CM, Ahn IS, Diamante G, Bhetraratana M, Park JF, Said E, Huynh C, Le T, Medzikovic L, Humbert M, Soubrier F, Montani D, Girerd B, Trégouët DA, Channick R, Saggar R, Eghbali M, Yang X. Single-cell Study of Two Rat Models of Pulmonary Arterial Hypertension Reveals Connections to Human Pathobiology and Drug Repositioning. Am J Respir

Crit Care Med. 2020 Oct 6. doi: 10.1164/rccm.202006-2169OC. Epub ahead of print. PMID: 33021809.

59. Akiyama-Uchida Y, Ashizawa N, Ohtsuru A, Seto S, Tsukazaki T, Kikuchi H, Yamashita S, Yano K. Norepinephrine enhances fibrosis mediated by TGF-beta in cardiac fibroblasts. Hypertension. 2002 Aug;40(2):148-54. doi: 10.1161/01.hyp.0000025443.61926.12. PMID: 12154105.
60. Tian CJ, Pang X. Ca2+-calcineurin signaling is involved in norepinephrine-induced cardiac fibroblasts activation. Int J Clin Exp Pathol. 2015 May 1;8(5):5210-6. PMID: 26191219; PMCID: PMC4503091.
61. Dincer HE, Gangopadhyay N, Wang R, Uhal BD. Norepinephrine induces alveolar epithelial apoptosis mediated by alpha-, beta-, and angiotensin receptor activation. Am J Physiol Lung Cell Mol Physiol. 2001 Sep;281(3):L624-30. doi: 10.1152/ajplung.2001.281.3.L624. PMID: 11504689.
62. Tang K, Zhong B, Luo Q, Liu Q, Chen X, Cao D, Li X, Yang S. Phillyrin attenuates norepinephrine-induced cardiac hypertrophy and inflammatory response by suppressing p38/ERK1/2 MAPK and AKT/NF-kappaB pathways. Eur J Pharmacol. 2022 Jul 15;927:175022. doi: 10.1016/j.ejphar.2022.175022. Epub 2022 May 13. PMID: 35569549.
63. Briest W, Hölzl A, Rassler B, Deten A, Leicht M, Baba HA, Zimmer HG. Cardiac remodeling after long term norepinephrine treatment in rats. Cardiovasc Res. 2001 Nov;52(2):265-73. doi: 10.1016/s0008-6363(01)00398-4. PMID: 11684074.
64. Briest W, Elsner C, Hemker J, Müller-Strahl G, Zimmer HG. Norepinephrine-induced expression of cytokines in isolated biventricular working rat hearts. Mol Cell

Biochem. 2003 Mar;245(1-2):69-76. doi: 10.1023/a:1022861609896. PMID: 12708746.

65. Barth W, Deten A, Bauer M, Reinohs M, Leicht M, Zimmer HG. Differential remodeling of the left and right heart after norepinephrine treatment in rats: studies on cytokines and collagen. J Mol Cell Cardiol. 2000 Feb;32(2):273-84. doi: 10.1006/jmcc.1999.1075. PMID: 10722803.
66. Leicht M, Briest W, Zimmer HG. Regulation of norepinephrine-induced proliferation in cardiac fibroblasts by interleukin-6 and p42/p44 mitogen activated protein kinase. Mol Cell Biochem. 2003 Jan;243(1-2):65-72. doi: 10.1023/a:1021655023870. PMID: 12619890.
67. Briest W, Rassler B, Deten A, Leicht M, Morwinski R, Neichel D, Wallukat G, Ziegelhöffer T, Zimmer HG. Norepinephrine-induced interleukin-6 increase in rat hearts: differential signal transduction in myocytes and non-myocytes. Pflugers Arch. 2003 Jul;446(4):437-46. doi: 10.1007/s00424-003-1043-x. Epub 2003 May 6. PMID: 12733076.
68. Fu YC, Chi CS, Yin SC, Hwang B, Chiu YT, Hsu SL. Norepinephrine induces apoptosis in neonatal rat endothelial cells via down-regulation of Bcl-2 and activation of beta-adrenergic and caspase-2 pathways. Cardiovasc Res. 2004 Jan 1;61(1):143-51. doi: 10.1016/j.car
69. Fu YC, Chi CS, Yin SC, Hwang B, Chiu YT, Hsu SL. Norepinephrine induces apoptosis in neonatal rat cardiomyocytes through a reactive oxygen species-TNF alpha-caspase signaling pathway. Cardiovasc Res. 2004 Jun 1;62(3):558-67. doi: 10.1016/j.cardiores.2004.01.039. PMID: 15158148.

70. Rassler B, Rohling MA, Reissig C, Briest W, Tannapfel A, Zimmer HG. Involvement of cytokines and inflammation in catecholamine-induced pulmonary injury in rats. Vascular Disease Prevention. 2005 Jan 1;2(1):1-9.
71. Rassler B, Marx G, Schierle K, Zimmer HG. Catecholamines can induce pulmonary remodeling in rats. Cell Physiol Biochem. 2012;30(5):1134-47. doi: 10.1159/000343304. Epub 2012 Oct 5. PMID: 23171784.
72. P.K. Randhawa, A.S. Jaggi, TRPV1 channels in cardiovascular system: a double edged sword? Int. J. Cardiol. 228 (2017) 103–113.
73. S. Xiong, P. Wang, L. Ma, P. Gao, L. Gong, L. Li, et al., Ameliorating endothelial mitochondrial dysfunction restores coronary function via transient receptor potential vanilloid 1-mediated protein kinase A/uncoupling protein 2 pathway, Hypertension 67 (2016) 451–460.
74. L. Wang, D.H. Wang, TRPV1 gene knockout impairs postischemic recovery in isolated perfused heart in mice, Circulation 112 (2005) 3617–3623.
75. Q. Wang, S. Ma, D. Li, Y. Zhang, B. Tang, C. Qiu, et al., Dietary capsaicin ameliorates pressure overload-induced cardiac hypertrophy and fibrosis through the transient receptor potential vanilloid type 1, Am. J. Hypertens. 27 (2014) 1521–1529.
76. B. Zhong, J. Rubinstein, S. Ma, D.H. Wang, Genetic ablation of TRPV1 exacerbates pressure overload-induced cardiac hypertrophy, Biomed. Pharmacother. 99 (2018) 261–270.
77. C. Njoo, C. Heinl, R. Kuner, In vivo SiRNA transfection and gene knockdown in spinal cord via rapid noninvasive lumbar intrathecal injections in mice, J. Visualized Exp. 22 (Mar. (85)) (2014).

78. Zahner MR, Li DP, Chen SR, Pan HL. Cardiac vanilloid receptor 1-expressing afferent nerves and their role in the cardiogenic sympathetic reflex in rats. J Physiol. 2003 Sep 1;551(Pt 2):515-23. doi: 10.1113/jphysiol.2003.048207. Epub 2003 Jun 26. PMID: 12829722; PMCID: PMC2343227.

79. Buckley CL, Stokes AJ. Mice lacking functional TRPV1 are protected from pressure overload cardiac hypertrophy. Channels (Austin). 2011 Jul-Aug;5(4):367-74. doi: 10.4161/chan.5.4.17083. Epub 2011 Jul 1. PMID: 21814047; PMCID: PMC3225734.

Chapter 4: Pharmacologic Neuromodulation Targeting NMDAR-NOS1 Axis Mediated Neuroinflammation and Apoptosis in the Thoracic Spinal Cord as a Novel Therapeutic Strategy for Pulmonary Hypertension and Right Ventricular Failure

Abstract

Rationale

Pulmonary hypertension (PH) is associated with aberrant sympathoexcitation leading to right ventricular failure (RVF), arrhythmias and death. Neuroinflammation is implicated in sympathoexcitation in experimental PH. We recently reported the first evidence of TRPV1+ cardiopulmonary afferent signaling mediated NMDAR-NOS1 axis activation, microgliosis, astrogliosis and apoptosis in thoracic spinal cord (TSC) and associated sympathoexcitation in PH. Here we hypothesize: 1) Cardiopulmonary afferent signaling in PH activates NMDAR-NOS1-axis leading to neuroinflammation and apoptosis in TSC; 2) Pharmacologic neuromodulation targeting TSC NMDAR-NOS1-axis may rescue PH and RVF.

Objectives

To investigate the role of NMDAR-NOS1-axis mediated neuroinflammation and apoptosis in TSC of experimental PH.

Methods

Monocrotaline (MCT) and Sugen-hypoxia (SuHx) rat models of PH were used. MCT-rats received intrathecal NOS1-inhibitor S-Methyl-L-thiocitrulline (SMTC; 0.5mg/kg/day, n=11), NMDAR antagonist AP-5 (30μg/rat/day, n=5) from day 14-28. Echocardiography and catheterization were performed. TSC, RV and lung RNASeq, RT-qPCR, NOS-activity+immunolocalization, microgliosis+astrogliosis, TUNEL and plasma norepinephrine were assessed. Human TSC from controls and PH were assessed by immunofluorescence.

Measurements and Main Results

TSC-transcriptomics highlighted neuroinflammation, nitrosative stress and apoptosis and

identified NOS1 as well as several NMDAR-subunit genes as some of the top-most upregulated genes in TSC but not lumbar. Increased TSC NOS1 was validated by PCR, immunostaining and activity assay in PH rats and patients with PAH. Mechanistically, TSC NOS1-activation was NMDAR-dependent as AP-5 decreased NOS1, neuroinflammation, apoptosis and attenuated PH-RVF in rats. SMTC rescued PH, reduced RV-hypertrophy and improved RV-function by decreasing TSC NOS-activity, microgliosis+astrogliosis and apoptosis resulting in reduced plasma norepinephrine. RV and lung-RNASeq from SMTC-group demonstrated reversal of pro-fibrotic, pro-proliferative, SNS/RAAS-related and pro-inflammatory signatures.

Conclusions

In PH, cardiopulmonary afferent signaling triggers NMDAR-mediated NOS1 activation leading to TSC neuroinflammation, apoptosis and excitotoxicity. Intrathecal NOS1-inhibition rescues PH and RVF.

Key words: Pulmonary hypertension; transcriptome; thoracic spinal cord; neuroinflammation; sympathoexcitation.

Introduction

Pulmonary hypertension (PH) is associated with aberrant sympathoexcitation leading to right ventricular failure (RVF), arrhythmias and death[1-3]. Neuroinflammation in the central nervous system (CNS) has been implicated in sympathetic nervous system (SNS) hyperactivity through microglial and astrocytic activation and release of several pro-inflammatory cytokines and chemokines in experimental PH[1-6]. The thoracic spinal cord (TSC) is responsible for integrating signals from cardiopulmonary sensory nerve endings and several brain regions related to the autonomic functions, which leads the sympathetic preganglionic neurons to regulate sympathetic vasomotor tone by releasing norepinephrine from their terminals[4,7]. We recently reported microglial and astrocytic activation mediated neuroinflammation in the TSC in pre-clinical and clinical PH-RVF[8]. However, the precise molecular mechanisms and impact of TSC neuroinflammation on cardiopulmonary function in PH are yet to be fully elucidated.

To this end, our recent study demonstrated transcriptomic remodeling in the TSC highlighting increased glutamatergic excitatory signaling and neuronal nitric oxide synthase (NOS1) upregulation in two pre-clinical rat models of severe PH-RVF[8]. N-methyl-D-aspartate receptor (NMDAR) mediated NOS1 upregulation in the CNS is known to induce oxidative and nitrosative stress, neuroinflammation, chemokine release, excitotoxicity, and neuronal apoptosis[9,10]. Various pain, neurodegenerative and cardiovascular disease studies have indicated that during pathologic conditions primary sensory nerve endings lead to increased glutamate release in the spinal dorsal horn, which in turn activates NMDARs in the second order spinothalamic neurons resulting in Ca^{2+} influx and activation of NOS1[9-17]. Subsequent increase of nitric oxide ($^{\cdot}NO$) production not only reinforces the glutamatergic signaling through retrograde transfer but

also activates astrocytes and microglia to produce further ˙NO, cytokines and chemokines [9-17]. Excessive ˙NO combines with superoxide ($O_2^{\bullet -}$) to form peroxynitrite ($ONOO^-$), which leads to neuroinflammation[18,19]. Peroxynitrite is a potent nitrating and oxidizing reactive nitrogen species (RNS), which is known to induce neuronal excitotoxicity and apoptosis through multiple mechanisms, including lipid peroxidation, mitochondrial damage, protein nitration, nitrosylation and oxidation, depletion of antioxidant reserves, and DNA damage followed by the activation of the nuclear enzyme poly(ADP-ribose) polymerase (PARP)[15,20].

In this study, we investigated whether NOS1 activation in the TSC is NMDAR-dependent and the role of NOS1-mediated TSC neuroinflammation, apoptosis and associated sympathoexcitation in PH-RVF. We hypothesize that in PH, cardiopulmonary afferent signaling activates NMDAR-NOS1 axis resulting in TSC neuroinflammation, apoptosis, and associated sympathoexcitation, which leads to further worsening of PH and RVF. Furthermore, targeted intrathecal NOS1 inhibition rescues PH and RVF by attenuating TSC neuroinflammation, apoptosis and associated sympathoexcitation. Elucidating the cellular and molecular mechanisms associated with TSC neuroinflammation underpinning the PH-RVF progression is crucial for developing new therapies. Investigating the effect of targeted TSC NOS1 inhibition will offer insights into a novel therapeutic strategy for PH and RVF.

Materials and Methods

All animal studies were performed in accordance with the National Institutes of Health (NIH) Guide for the Care and Use of Laboratory Animals. Protocols received UCLA animal research committee approval. The details of materials and methods can be found in the online data supplement.

Animal Models of Pulmonary Hypertension

Monocrotaline (MCT, n=8) and Sugen-hypoxia (SuHx, n=8) rat models of PH were used. Phosphate buffered saline (PBS) treated rats served as controls (CTRL, n=8) (Figure 1A). For time-course experiment, MCT-treated rats at day-7 (n=6) and day-14 (n=6) were used (Figure 1G).

Intrathecal Injections

Intrathecal NMDAR antagonist AP-5 (30μg/rat/day, Tocris, Cat. 0105, in 30μl PBS, n=4)[21,22] injections were performed daily on a group of MCT-treated rats from day 14-28 post MCT injection and were compared with MCT rats treated with daily intrathecal PBS (30μl, n=5). Similarly, intrathecal NOS1-inhibitor S-Methyl-L-thiocitrulline (SMTC; 0.5mg/kg/day, Millipore Sigma, Cat. M5171, in 30μl PBS n=11)[17] injections were performed daily on another group of MCT-treated rats from day 14-28 post MCT injection and were compared with MCT rats treated with daily intrathecal PBS (30μl, n=11). Briefly, rats were anesthetized with isoflurane/O_2 mixture (4%), and body temperature was maintained at 37±1°C using heating pads. Daily intrathecal injections were administered with a 29-gage needle at L4-5 level to avoid spinal cord injury; successful injections were documented with prominent tail flicks.

Echocardiography and Cardiopulmonary Hemodynamic Measurements

Serial echocardiography (Vevo3100) was performed to monitor cardiopulmonary hemodynamics and the development of PH and RV dysfunction. Direct right heart catheterization (Millar SPR-671) was performed terminally to assess disease severity.

RNA Extraction and qRT-PCR

Real-time quantitative reverse transcription PCR (qRT-PCR) was performed with total RNA extracted from the thoracic and lumbar regions of spinal cord from control, MCT, SuHx, MCT+PBS and MCT+SMTC rats using Trizol (Invitrogen).

RNA Sequencing Analysis

NextSeq400 (Illumina) was performed on rat RV and lung tissue and differential expression analysis was conducted. Differentially expressed genes (DEGs) with false discovery rate (FDR) <0.05 were considered statistically significant. Gene set enrichment analysis was performed and Hallmark[8] gene sets were obtained from molecular signature database (MSigDB)[8]. Enriched pathways considered statistically significant were defined by adjusted p-value <0.05.

Gross Histologic Analysis, Tissue Preparation and Imaging

RV hypertrophy index was calculated as weight ratio of RV/(LV+IVS). Hearts, lungs and spinal cords were fixed and 4–6μm sections were obtained. Heart and lung tissue sections were stained with Masson's trichrome staining. Images were acquired using a confocal microscope (Nikon).

Human Thoracic Spinal Cord Tissue Sections

To validate some of the key findings from rat TSC in human PAH spinal cord we collected autopsy samples from PAH patients (n=3) and controls (n=3) through our collaborators at the UCLA Department of Pathology. Tissues were sectioned at 4–6μm for immunostainings.

Immunofluorescence Staining and Quantification

Thoracic spinal cord sections were stained with the primary antibodies against neuronal nitric oxide synthase-1 (Anti-NOS1), microtubule-associated protein 2 (Anti-MAP2), NMDA2R (Anti-GRIN2D), Cx3Cl1 (Anti-Cx3Cl1), microglia (Anti-IBA1), astrocytes (Anti-

GFAP), neurons (Anti-NeuN) and Cleaved Caspase-3 (Asp175). RV and lung sections were stained with the primary antibodies against transient receptor potential vanilloid 1 (Anti-TRPV1), substance P (Anti-SP), anti-vWF and Anti-αSMA. Quantifications were performed using ImageJ.

TUNEL Staining

Thoracic spinal cord sections were stained with the terminal deoxynucleotidyl transferase dUTP nick end labeling (TUNEL) Assay Kit-BrdU-Red (Abcam, ab66110) and the $TUNEL^+$ cells were calculated as integrated optical density using ImageJ (1.45p, NIH, Bethesda, MD).

Plasma Norepinephrine Assays

Plasma norepinephrine level was quantified using an enzyme-linked immunosorbent assay (ELISA) kit (Abnova, KA1877) following the manufacturer's protocols.

NOS Activity Assays

TSC NOS activity levels were quantified using a fluorometric assay (Nitric Oxide Synthase Activity Assay) kit (Abcam, ab211084) following the manufacturer's protocols.

Statistical Analysis

Unpaired t-test and one-way ANOVA tests were used to compare between groups using GraphPad Prism. When significant differences were detected, individual mean values were compared by post-hoc tests that allowed for multiple comparisons. $P<0.05$ was considered statistically significant. Values are expressed as mean±SD. For RNA-seq, differential expression analysis was conducted using the R-program DeSeq2 correcting for multiple hypothesis testing using the Benjamini Hochberg method.

Results

Increased Signature of Glutamatergic and NOS1 Signaling in the TSC of MCT and SuHx Rats and PAH patients

RNA-seq was performed to investigate the transcriptomic remodeling of the TSC of MCT- and SuHx-induced PH rats (Figure 1). Hierarchical clustering of top DEGs (FDR<0.05) from TSC RNASeq of MCT and SuHx rats demonstrated increased expression of multiple N-methyl-D-aspartate receptor (NMDAR) subunit genes, neuronal nitric oxide synthase (NOS1) and it's adaptor protein (NOS1AP) as well as endothelial nitric oxide synthase (NOS3), whereas inducible nitric oxide synthase (NOS2) was unchanged (Figure 1B). Increased NMDAR subunit Grin2D immunoreactivity was confirmed in the TSC of both MCT and SuHx rats (Figure 1C). PCR validation confirmed preferential and significant increase of NOS1 in the TSC, but not lumbar spinal cord (Figure 1D,E). NOS specific activity assay demonstrated significantly increased NOS activity in the TSC of both rat models (Figure 1F). Increased NOS1 expression was also confirmed in the TSC of PAH patients (Figure 1G). Immunostaining demonstrated increased NOS1 localization in neurons as well as activated astrocytes and microglia in the TSC of MCT, SuHx rats and PAH patients (Figure 1G,J, S1). To investigate the NOS1 expression levels as a function of PH and RVF development, a time-course experiment was performed in MCT rats (Figure 1H). Interestingly, there was no significant increase in NOS1 transcription and immunoreactivity in the TSC at day-7, however, significantly increased NOS1 transcription and immunoreactivity was observed at day-14 (Figure 1H,I). This coincided with a significant increase in RVSP, Fulton Index and neuroinflammation at day-14[8].

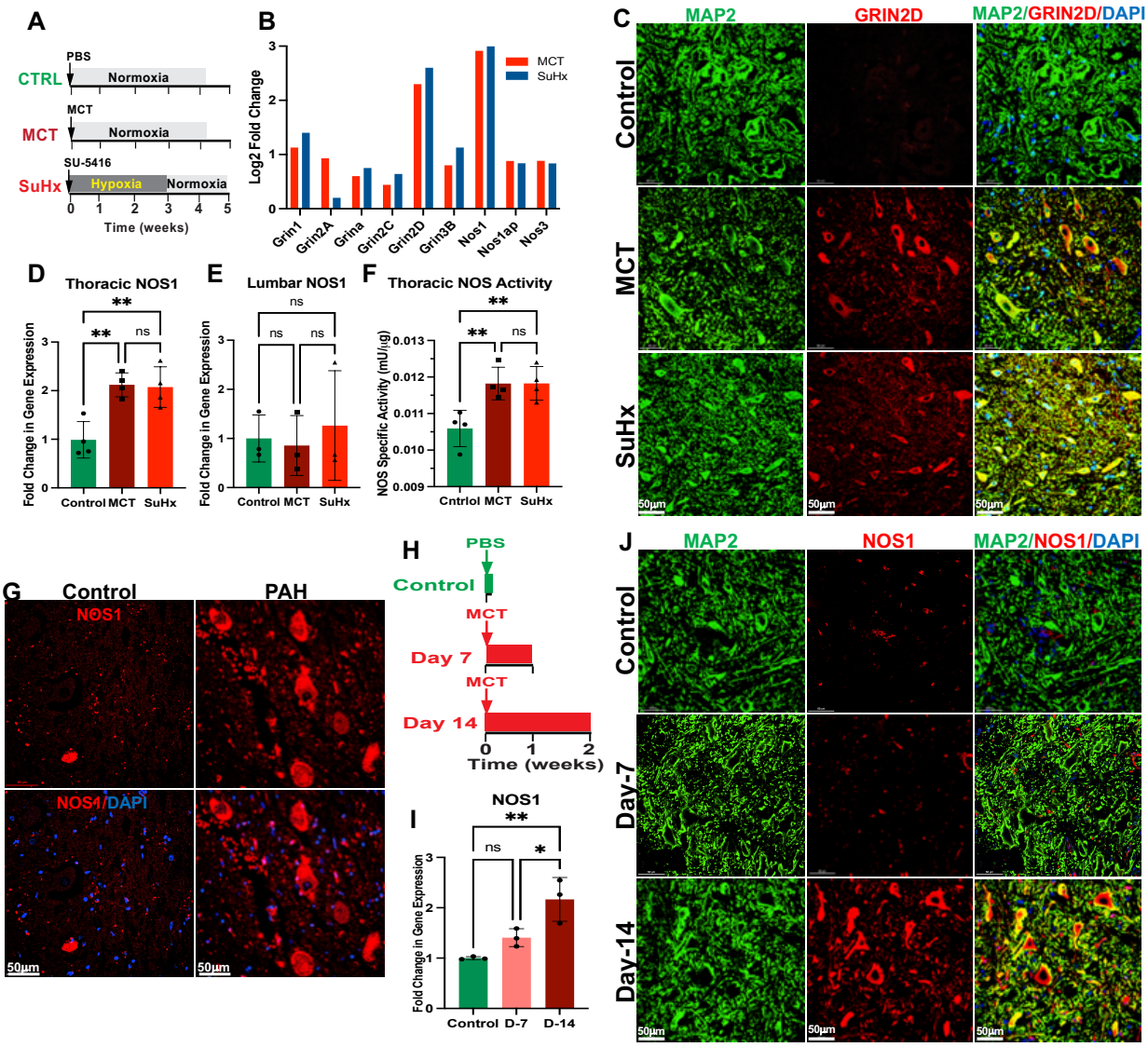

Figure 1. Increased Signature of Glutamatergic and NOS1 Signaling in the TSC of MCT and SuHx Rats and PAH patients (**A**) Experimental protocol. (**B**) Top common significantly upregulated DEGs from the TSC RNA-Seq of MCT (red) and SuHx (blue). (**C**) Representative images of immunofluorescence staining with anti-MAP2 (Green), anti-GRIN2D (Red), and DAPI (DNA; blue) from the TSC of Control, MCT and SuHx rats. N=3 per group. (**D**) Normalized qRT-PCR data of NOS1 gene expression in the TSC of Control, MCT and SuHx. N=4 per group. ***p*<0.01. (**E**) Normalized qRT-PCR data of NOS1 gene expression in the lumbar spinal cord of Control, MCT and SuHx. N=3 per group. (**F**) TSC NOS specific activity (mU/µg) of Control, MCT and SuHx. N=4 per group. ***p*<0.01. (**G**) Representative immunofluorescence images of NOS1

(Red), and DAPI (blue) in controls and PAH patients. N=4 per group. (**H**) Time course experimental protocol. (**I**) Normalized qRT-PCR data of NOS1 gene expression in the TSC of Control, Day-7 and Day-14 MCT rats. N=3 per group. *p<0.05, **p<0.01. (**J**) Representative images of immunofluorescence staining with anti-MAP2 (Green), anti-NOS1 (Red), and DAPI (blue) from the TSC of Control, Day-7 and Day-14 MCT rats. N=3 per group.

TSC NOS1 activation is NMDAR-dependent in PH-RVF

To investigate whether NOS1 activation in the TSC in PH rats is NMDAR-dependent, pharmacologic inhibition of NMDAR was performed using daily intrathecal injections of AP-5 (30μg/day/rat in 30μl PBS, at L4-5) in MCT rats from day 14-28 (Figure 2A). AP-5 significantly attenuated PH severity as demonstrated by decreased RVSP and rescued RVF as shown by increased RVFAC and decreased Fulton index of RV hypertrophy but did not affect LV pressure and LVEF (Figure 2B, C). Importantly, AP-5 significantly reduced plasma norepinephrine and lung arteriolar wall thickness in the MCT rats (Figure 2B,C). Further, AP-5 resulted in a significant decrease in total microglial count, microglial percent activation, astrogliosis and expression of NMDAR subunit GRIN2D, NOS1, fractalkine CX3CL1 as well as pro-apoptotic, transforming growth factor-β1 (TGFβ1) in the TSC (Figure 2C-F, S2). These hemodynamics and histological data suggest an important regulatory role of NMDAR in TSC NOS1 activation and associated neuroinflammation, apoptosis as well as sympathoexcitation in PH-RVF.

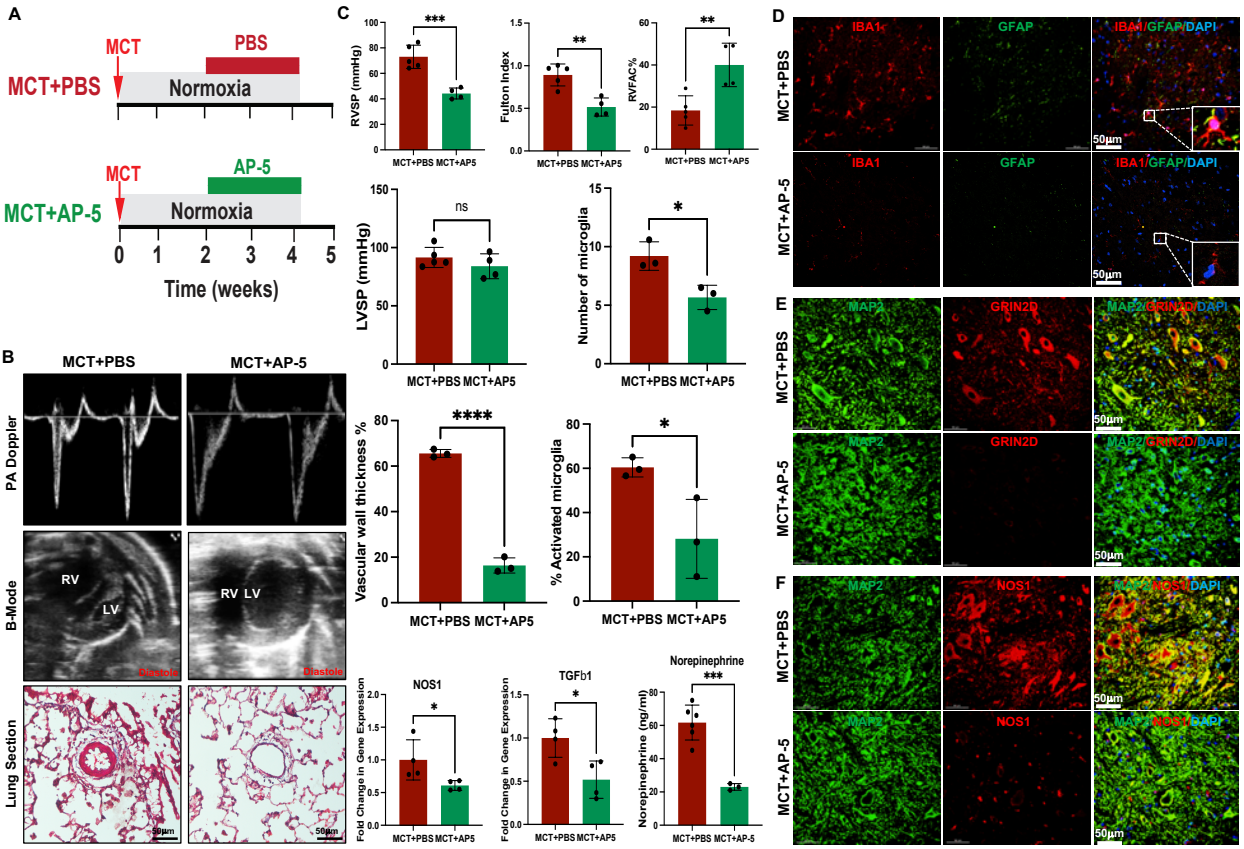

Figure 2. AP5 attenuates MCT induced PH and RVF by reducing TSC NOS1, neuroinflammation and associated sympathoexcitation. (**A**) Experimental Protocol. (**B**) PA Doppler, B-Mode echo and cross section from lung in PBS and AP5 treated MCT rats. (**C**) RVSP, Fulton index, RVFAC, LVSP, LVEF, quantification of pulmonary vascular (arteriolar) wall thickness, quantification of number of microglia/HPF and percent activated microglia/HPF, normalized qRT-PCR data of NOS1 and apoptotic gene TGFβ1 expression in the TSC of PBS and AP5 treated MCT rats. Plasma norepinephrine level measured by ELISA in PBS and AP5 treated MCT rats. N=3-6 per group. *p<0.05, **p<0.01, ***p<0.001 ****p<0.0001. (**D**) Representative images of immunofluorescence staining with microglial marker anti-Iba1 (Red), astrocytic marker anti-GFAP (Green) and DNA marker DAPI (Blue) in the TSC of PBS and Minocycline treated MCT rats. N=3 per group. (**E**) Representative images of immunofluorescence staining with anti-MAP2 (Green), anti-GRIN2D (Red), and DAPI (DNA; blue) from the TSC of Control, MCT and SuHx rats. N=3 per group. (**F**) Representative images of immunofluorescence staining with anti-MAP2 (Green), anti-

NOS1 (Red), and DAPI (blue) from the TSC of Control, Day-7 and Day-14 MCT rats. N=3 per group.

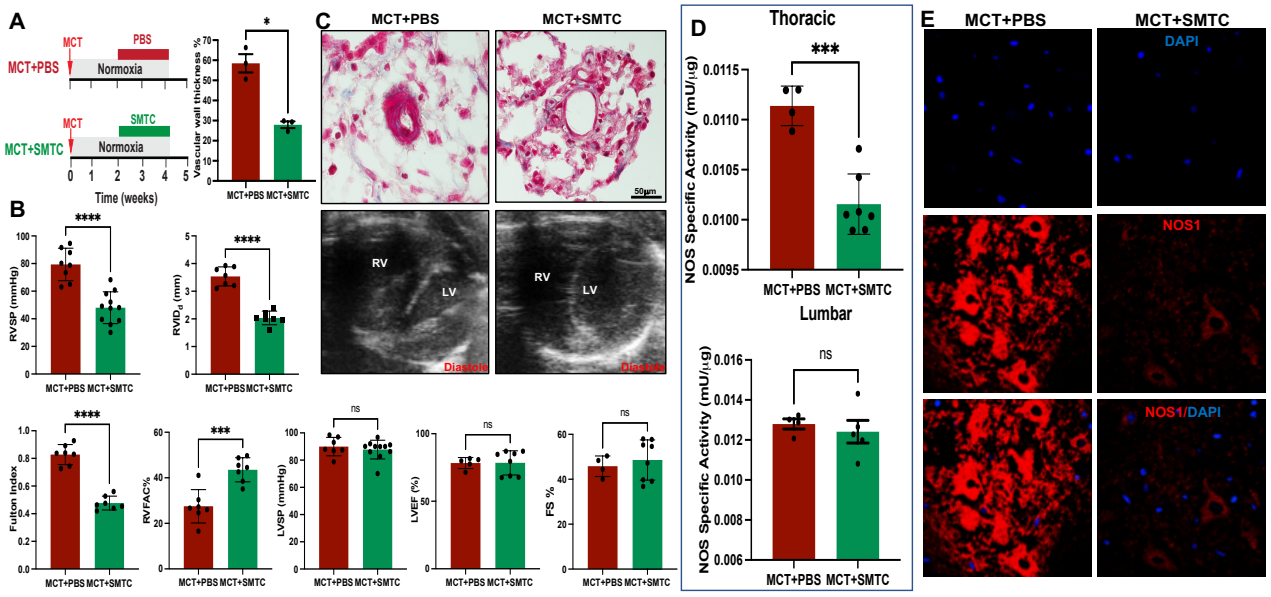

Figure 3. NOS1 inhibition attenuates MCT induced PH and RVF. (**A**) Experimental Protocol. (**B**) RVSP, Fulton index, $RVID_d$, RVFAC, LVSP, LVEF, FS%, and quantification of pulmonary vascular (arteriolar) wall thickness of PBS and SMTC treated MCT rats. N=3-11 per group. *p<0.05, **p<0.01, ***p<0.001, ****p<0.0001. (**C**) Lung cross section and B-Mode echo from PBS and SMTC treated MCT rats. (**D**) TSC and LSC NOS specific activity (mU/μg) of PBS and SMTC-treated MCT rats. N=4-7 per group. ***p<0.001. (**E**) Representative images of immunofluorescence staining with anti-NOS1 (Red), and DAPI (blue) from the TSC of PBS and SMTC-treated MCT rats. N=3 per group.

TSC NOS1 inhibition rescues PH and RVF in MCT rats

To investigate the role of increased TSC NOS1 in PH rats, pharmacologic inhibition of NOS1 was performed using daily intrathecal injections of S-Methyl-L-thiocitrulline (SMTC, 0.5mg/kg in 30μl PBS, at L4-5) in MCT rats from day 14-28 (Figure 3A). SMTC significantly attenuated PH severity as demonstrated by decreased RVSP and rescued

RVF as shown by decreased Fulton index and RVID as well as increased RVFAC (Figure 3B, C). However, SMTC did not affect LV pressure, LVEF and FS% (Figure 3B, C). Importantly, SMTC significantly reduced lung arteriolar wall thickness in the MCT rats (Figure 3B, C). Immunostaining confirmed significantly decreased NOS1 expression in the TSC of SMTC treated rats (Figure 3E). NOS specific activity assay demonstrated significantly decreased NOS activity in the TSC of MCT rats, but lumbar NOS activity was unchanged (Figure 3D). These hemodynamics data suggest an important regulatory role of TSC NOS1 in PH-RVF.

NOS1 inhibition attenuates TSC neuroinflammation and apoptosis and decreases sympathoexcitation

Intrathecal SMTC treatment resulted in a significant decrease in total microglial count, microglial percent activation, astrogliosis and expression of the fractalkine, CX3CL1 in the TSC of MCT-treated rats (Figure 4A-C). Moreover, significantly decreased apoptosis in the TSC of SMTC-treated rats was validated by TUNEL staining and reduced transcription of TGFβ1 (Figure 5A, B). Interestingly, decreased cleaved Caspase-3 immunoreactivity and it's colocalization with NeuN in the TSC of SMTC-treated rats confirmed reduced neuronal apoptosis in this region (Figure 5C). Importantly, SMTC significantly reduced sympathetic activation marker, plasma norepinephrine levels in the MCT rats (Figure 4D). These data suggest an important regulatory role of NOS1 in TSC neuroinflammation, apoptosis and associated sympathoexcitation in PH.

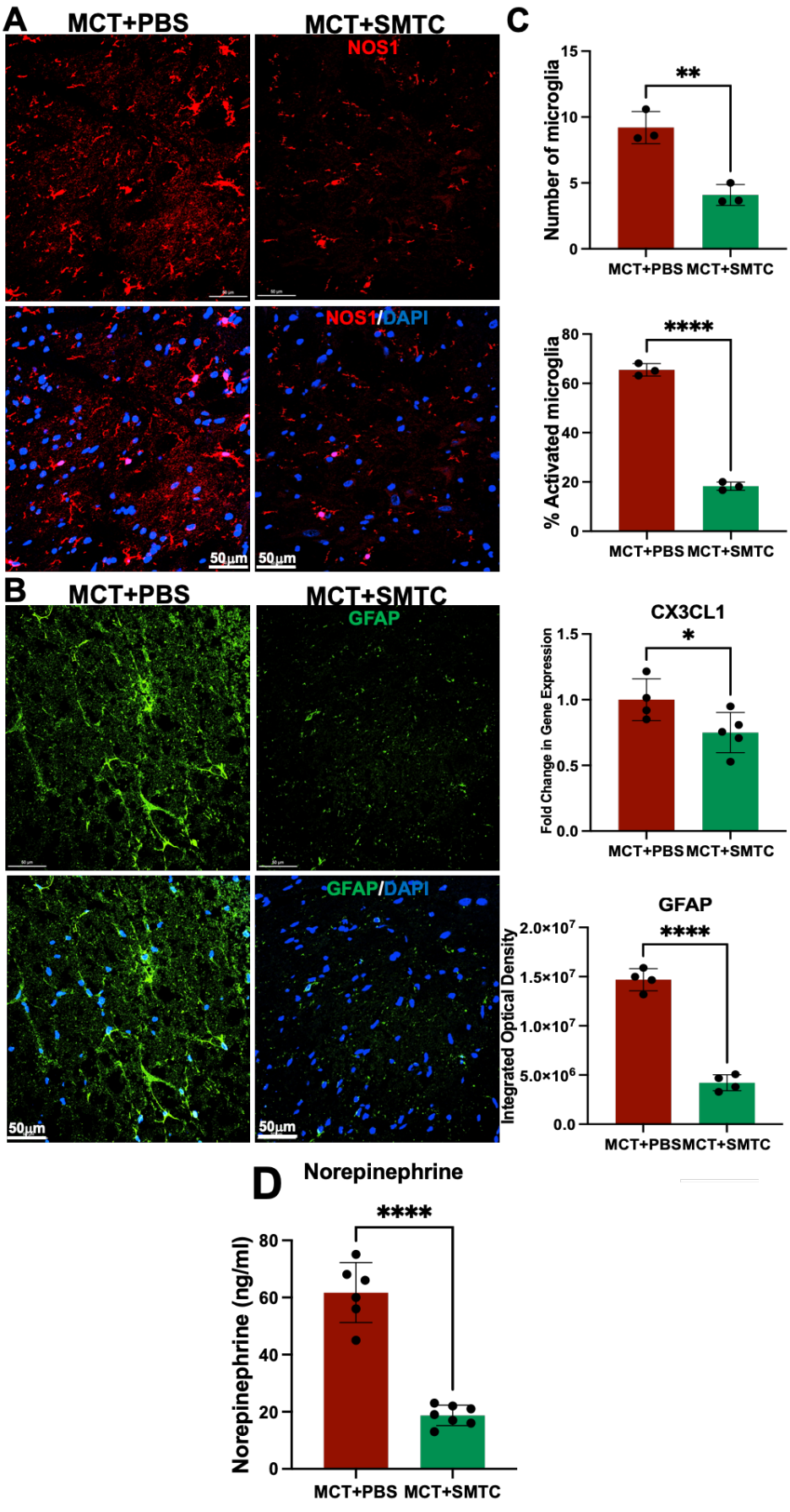
A
MCT+PBS
MCT+SMTC
NOS1
NOS1/DAPI
50μm
B
GFAP
GFAP/DAPI
C
Number of microglia
% Activated microglia
CX3CL1
Fold Change in Gene Expression
GFAP
Integrated Optical Density
MCT+PBS MCT+SMTC
D
Norepinephrine
Norepinephrine (ng/ml)

Figure 4. NOS1 inhibition attenuates TSC neuroinflammation and decreases sympathoexcitation in MCT induced PH rats. (**A**) Representative images of immunofluorescence staining with Iba1 (Red) and DAPI (Blue) in the TSC of PBS and SMTC-treated MCT rats. (**B**) Representative images of immunofluorescence staining with GFAP (Green) and DAPI (blue) from the TSC of PBS and SMTC-treated MCT rats. (**C**) Quantification of number of microglia/HPF and percent activated microglia/HPF, normalized qRT-PCR data of Cx3Cl1 gene expression and GFAP quantification in the TSC of PBS and SMTC-treated MCT rats. N=3-5 per group. *p<0.05, **p<0.01, ***p<0.001 ****p<0.0001. (**D**) Plasma norepinephrine level measured by ELISA in PBS and SMTC treated MCT rats. N=6-7 per group. ****p<0.0001.

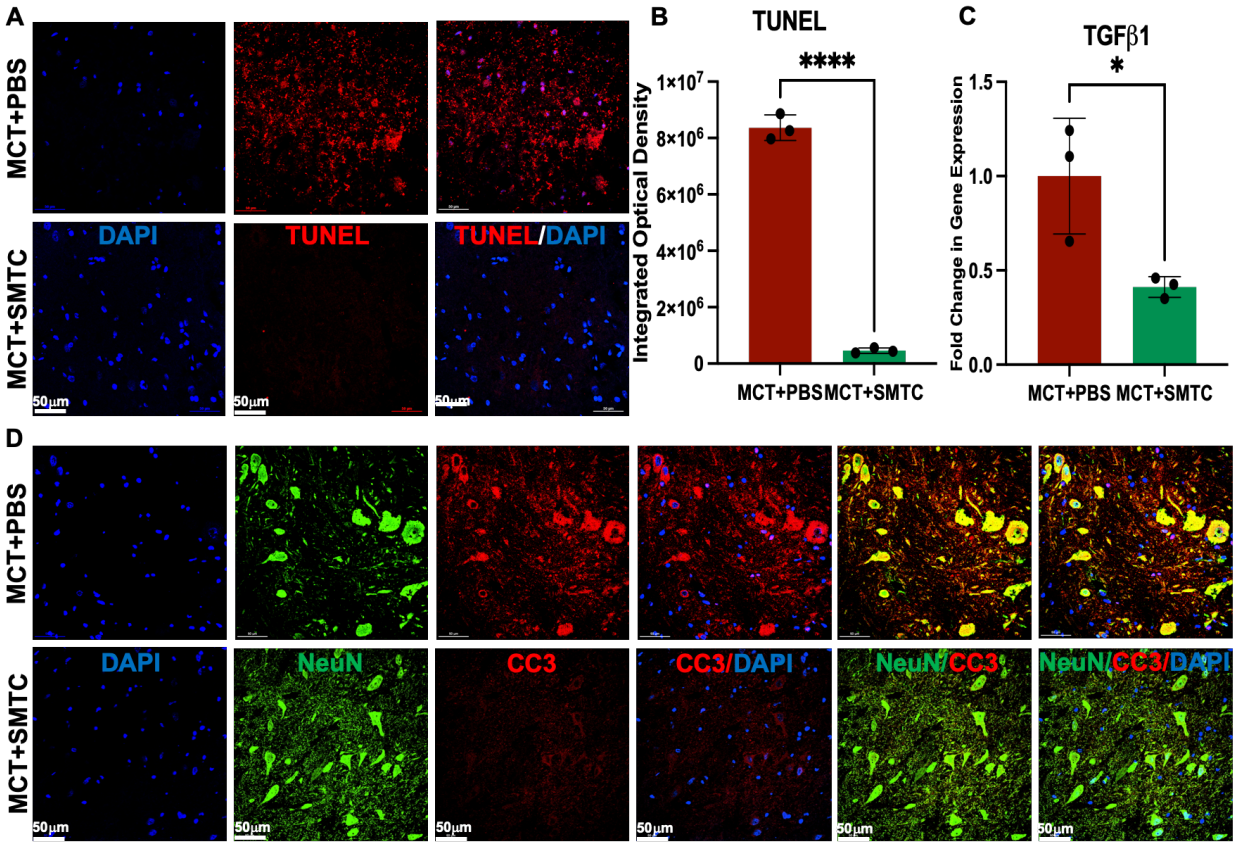

Figure 5. NOS1 inhibition attenuates neuronal apoptosis in the TSC of MCT induced PH rats. (**A**) TUNEL staining showing DAPI (Blue) and BRDU (Red) validating increased

apoptosis in the TSC of PBS and SMTC-treated MCT rats. (**B**) Quantification of TUNEL positive cells (integrated optical density). N=4 per group. ****p<0.0001. (**C**) Normalized qRT-PCR data of pro-apoptotic TGFβ1 gene expression in the TSC of PBS and SMTC-treated MCT rats. N=3 per group. *p<0.05. (**D**) Representative images of immunofluorescence staining with DAPI (blue), anti-NeuN (Green), anti-Cleaved Caspase-3 (CC3; Red), CC3 and DAPI colocalization, NeuN and CC3 colocalization (Yellow) and merged images from the TSC of PBS and SMTC-treated MCT rats. N=3 per group.

TSC NOS1 inhibition results in reversal of RV transcriptomic signature in MCT rats

To investigate the therapeutic effects of intrathecal SMTC treatment on RV, RNASeq on RV tissue was performed from MCT+PBS vs. MCT+SMTC rats (Figures 6, Table 1). Hierarchical clustering of top DEGs (FDR<0.05) from RV RNASeq revealed 716 differentially expressed genes that were either up- or down-regulated in the SMTC treated group compared to MCT rats (Figure 6A, Table 1). Gene Set Enrichment Analysis revealed 29 hallmark pathways significantly enriched (FDR<0.05) in SMTC-treated group compared to MCT rats (Figure 6B). Hallmark analysis demonstrated significant down-regulation (FDR<0.05) of pro-inflammatory pathways such as Hypoxia, IL2 STAT5 signaling, and KRAS signaling in SMTC-treated group (Figure 6B). Many significantly downregulated pro-inflammatory genes, such as, CCND2, MAPK1, NOTCH3 were enriched in these pathways (Table 1). Moreover, RV RNASeq revealed epithelial mesenchymal transition and TGFβ-signaling as some of the top down-regulated pro-fibrotic pathways along with downregulation of pro-fibrotic genes such as COL4a3,

COL14a1, ITGB5 and MMP2 in SMTC-treated group (Figure 6B, Table 1). Similarly, several down-regulated pro-apoptotic genes such as FOXO3, TGFβR2, BCL2L2 and MMP2 were enriched in down-regulated apoptosis pathway in the RV of SMTC-treated group (Figure 6B, Table 1). Interestingly, many SNS, RAAS and arrhythmia related genes, such as CAMK2D, ADRA1A, ADRA2A, ACE2, KCNJ2, RYR2, GJA1 and DBH were significantly down-regulated in the SMTC-treated rats compared to MCT group (Table 1).

EMT/EndMT, fibrosis, inflammation and apoptosis play important regulatory role in the development and progression of PH[23-25] and RVF[26]. Decreased vWF and αSMA coimmunolocalization in the RV arteriolar endothelial cells validated decreased EMT/EndMT in SMTC-treated MCT rats compared to PBS-treated MCT group (Figure 6C). Moreover, decreased RV fibrosis in the SMTC-treated MCT rats was validated by trichrome staining (Figure 6C). Substance P[27-32] and norepinephrine[33-46] are known to induce cardiac fibrosis, EMT/EndMT, inflammation and apoptosis during various pathological conditions. To investigate the potential role of SP and NE on RV tissue, human coronary artery endothelial cells (HCAECs), and human cardiac fibroblasts (HCFs) were incubated with SP (150 ug/mL) and NE (10uM) for 48 hours and stained to assess endothelial-to-mesenchymal transition (EndMT) in coronary artery ECs (vWF+αSMA), and fibroblast-to-myofibroblast transdifferentiation (FMT) in HCFs (Vim+αSMA) (Figure S3). Both SP and NE induced increased EndMT and FMT in HCAECs and HCFs respectively (Figure S3). Interestingly, decreased TRPV1 and SP immunoreactivity and their colocalization in the RV tissue was demonstrated in the SMTC-treated MCT rats compared to PBS-treated MCT group (Figure 6C).

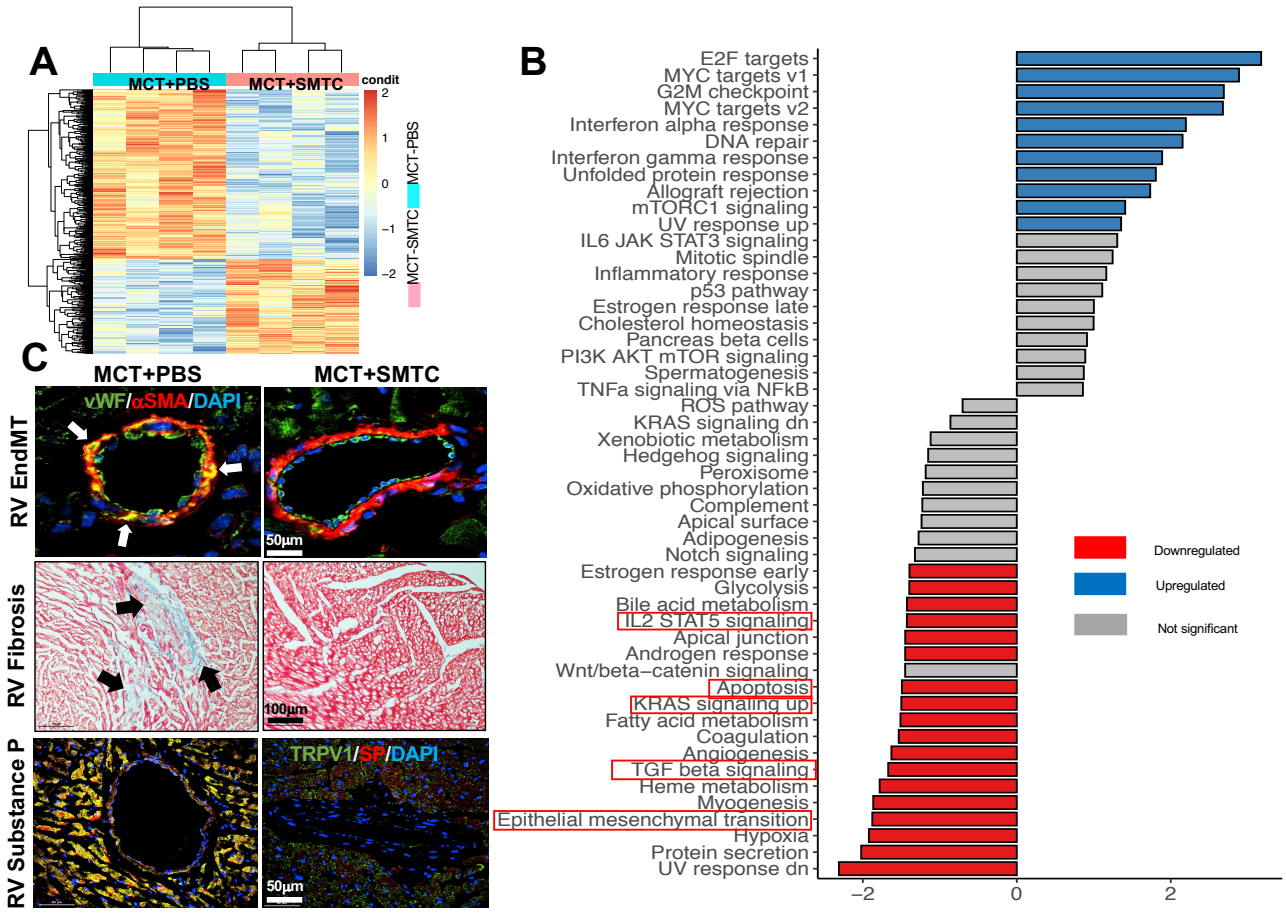

Figure 6. NOS1 inhibition results in reversal of RV transcriptomic signature in MCT-induced PH rats. (**A**) RNA-Seq based heat map showing DEGs from the RV of MCT+PBS (Blue) and MCT+SMTC (Red) groups. (**B**) Bar plot showing normalized enrichment scores (NES) for Hallmark pathways derived from Gene Set Enrichment Analysis (GSEA). For GSEA, differentially expressed genes between MCT+PBS vs. MCT+SMTC were ranked by the Wald statistic derived from DESeq2. Bars in blue and red represent statistically significant (FDR<0.05) pathways in MCT+PBS and MCT+SMTC, respectively, that are either up- or downregulated. N=4 per group. Red boxes in the bar plot indicate downregulation of pro-fibrotic, pro-inflammatory and pro-apoptotic pathways. (**C**) Representative images of immunofluorescence staining with anti-vWR (Green), anti-αSMA (Red), and DAPI (blue) from the RV of PBS and SMTC-treated MCT rats. N=3 per group. Trichrome staining showing interstitial fibrosis (Black arrow) in the RV of PBS and SMTC-

treated MCT rats. N=3 per group. Representative images of immunofluorescence staining with anti-TRPV1 (Green), anti-SP (Red), and DAPI (blue) from the RV of PBS and SMTC-treated MCT rats. N=3 per group.

NOS1 inhibition results in reversal of lung transcriptomic signature in MCT rats

To investigate the therapeutic effects of intrathecal SMTC treatment on lung, RNASeq on lung tissue was performed from MCT+PBS vs. MCT+SMTC rats (Figures 7, Table 1). Hierarchical clustering of top DEGs (FDR<0.05) from lung RNASeq revealed 30 differentially expressed genes, among which 20 were up- and 10 were down-regulated in the SMTC treated group compared to MCT rats (Figure 7A, Table 1). Gene Set Enrichment Analysis revealed 12 hallmark pathways significantly enriched (FDR<0.05) in SMTC-treated group compared to MCT rats (Figure 7B). Hallmark analysis demonstrated significant down-regulation (FDR<0.05) of pro-inflammatory pathways such as Hypoxia, TNFα signaling via NF-κB, mTORC1 signaling, interferon gamma response, IL2 STAT5 signaling, inflammatory response and IL-6 JAK-STAT3 signaling in SMTC-treated group (Figure 7B). Many significantly downregulated pro-inflammatory genes, such as, Ebna1bp2, Fabp4, Itgam, Ctsk, Lgmn and Arntl (Bmal1) were enriched in these pathways (Table 1). Moreover, lung RNASeq revealed epithelial mesenchymal transition as the topmost down-regulated pro-fibrotic pathways along with downregulation of pro-fibrotic genes such as Mfap4, Fabp4, Ctsk, Ltbp2, LGmn and Arntl (Bmal1) in SMTC-treated group (Figure 7B, Table 1).

Interestingly, significantly decreased vWF and αSMA coimmunolocalization in the lung arteriolar endothelium demonstrated decreased EMT/EndMT in the SMTC-treated MCT rats compared to PBS-treated MCT group (Figure 7C). Moreover, decreased lung fibrosis in the SMTC-treated rats was validated by trichrome staining (Figure 3C). Substance P[47,48] and norepinephrine[49,51] are known to induce EMT/EndMT, fibrosis, inflammation and apoptosis in the lung tissue during various pathological conditions. To investigate the potential effects of SP and NE on lung cells, human pulmonary artery endothelial cells (HPAECs) were incubated with SP (150 ug/mL) and NE (10uM) for 48 hrs and stained to assess endothelial-to-mesenchymal transition (EndMT) in pulmonary artery ECs (vWF+αSMA). Both SP and NE induced increased EndMT in HPAECs (Figure S3). Interestingly, decreased TRPV1 and SP immunoreactivity and their colocalization in the lung tissue was demonstrated in the SMTC-treated MCT rats compared to PBS-treated MCT group (Figure 7C).

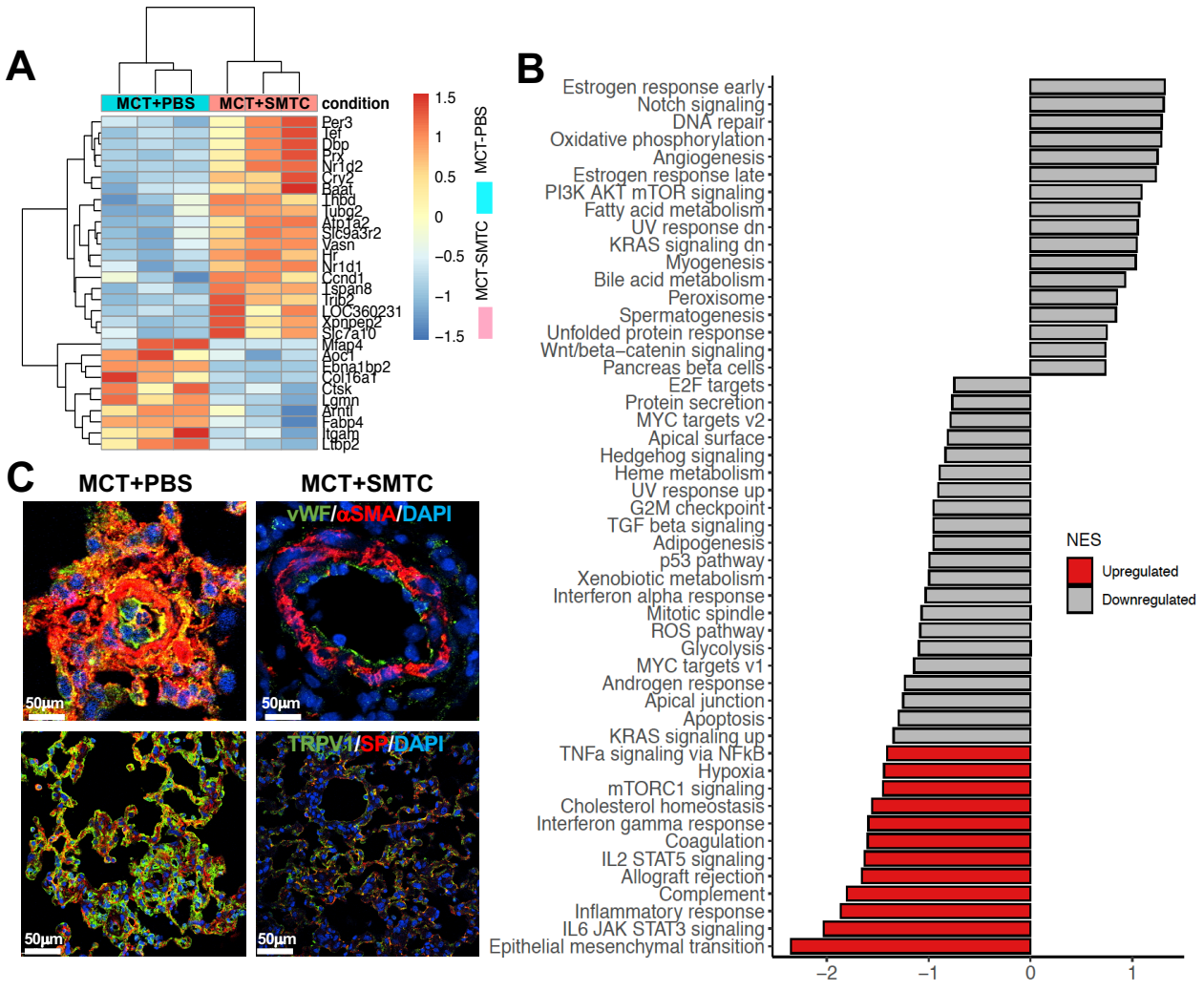

Figure 7. NOS1 inhibition results in reversal of lung transcriptomic signature in MCT-induced PH rats. (**A**) RNA-Seq based heat map showing DEGs from the lung of MCT+PBS (Blue) and MCT+SMTC (Red) groups. (**B**) Bar plot showing normalized enrichment scores (NES) for Hallmark pathways derived from Gene Set Enrichment Analysis (GSEA). For GSEA, differentially expressed genes between MCT+PBS vs. MCT+SMTC were ranked by the Wald statistic derived from DESeq2. Bars in blue and red represent statistically significant (FDR<0.05) pathways in MCT+PBS and MCT+SMTC, respectively, that are either up- or downregulated. N=4 per group. Red boxes in the bar plot indicate downregulation of pro-fibrotic and pro-inflammatory pathways. (**C**) Representative images of immunofluorescence staining with anti-vWR (Green), anti-αSMA

(Red), and DAPI (blue) from the lung of PBS and SMTC-treated MCT rats. N=3 per group. Trichrome staining showing interstitial fibrosis (Black arrow) in the lung of PBS and SMTC-treated MCT rats. N=3 per group. Representative images of immunofluorescence staining with anti-TRPV1 (Green), anti-SP (Red), and DAPI (blue) from the RV of PBS and SMTC-treated MCT rats. N=3 per group.

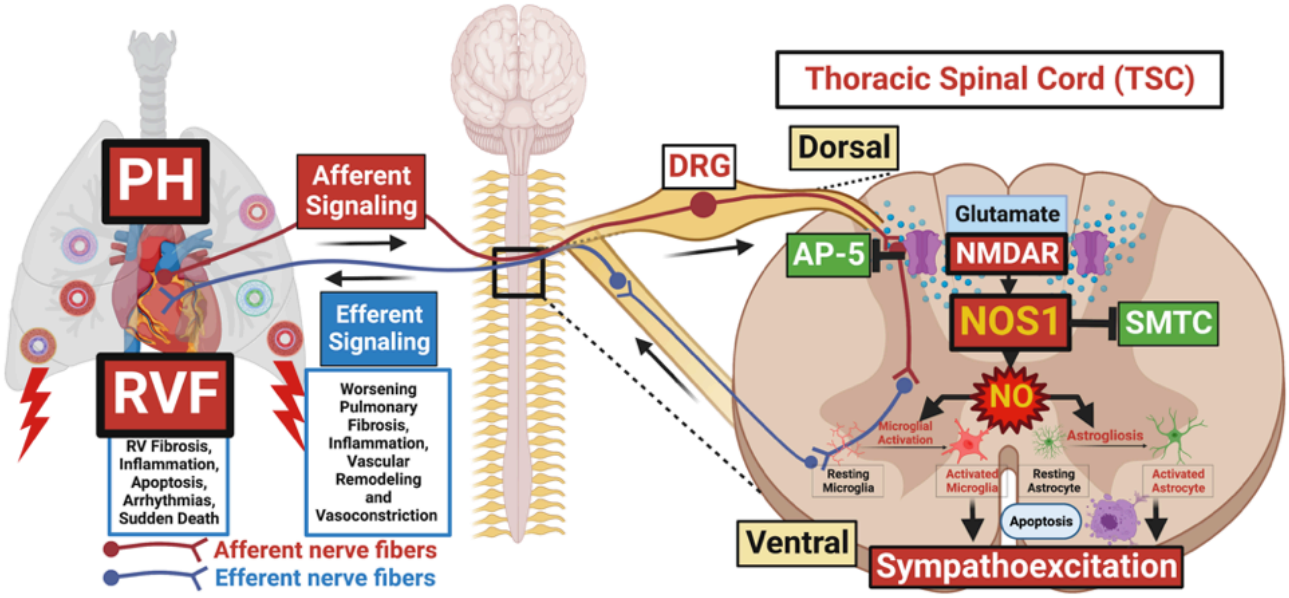

Figure 8. Hypothetical scheme. In PH, cardiopulmonary glutamatergic afferent signaling activates NMDAR-NOS1 axis resulting in TSC neuroinflammation, apoptosis, and associated sympathoexcitation, which leads to further worsening of PH and RVF. Furthermore, targeted intrathecal NOS1 inhibition rescues PH and RVF by attenuating TSC neuroinflammation, apoptosis and associated sympathoexcitation.

Discussion

In this study, using two pre-clinical rat models of severe PH-RVF induced by MCT and SuHx, respectively, we found increased signature of glutamatergic and NOS1 signaling in the TSC (Figure 1). Increased NOS1 expression was also confirmed in the TSC of PAH patients (Figure 1). We found time-dependent increase in NOS1 starting at day-14 after MCT (Figure 1). Mechanistically, NOS1 activation in the TSC was NMDAR-dependent as intrathecal NMDAR specific antagonist AP-5 decreased TSC NOS1 expression, neuroinflammation, neuronal apoptosis and associated sympathoexcitation and rescued PH-RVF in MCT rats (Figure 2). Finally, pharmacological inhibition of NOS1 by intrathecal NOS1 specific inhibitor S-Methyl-L-thiocitrulline (SMTC) attenuated PH and rescued RVF in MCT rats (Figure 3). This rescue was associated with attenuation of TSC neuroinflammation, neuronal apoptosis and reduced markers of sympathoexcitation (Figure 4,5). Moreover, RV-RNA-Seq demonstrated reversal of pro-fibrotic, inflammatory, apoptotic, SNS, RAAS and arrhythmia signatures (Figure 6), whereas, lung-RNA-Seq demonstrated reversal of pro-fibrotic and inflammatory signatures in MCT+SMTC Rats (Figure 7). We validated reduced EndMT, fibrosis and TRPV1-SP expression in RV and lung tissues of MCT+SMTC rats (Figure 6,7). Invitro analysis indicated that norepinephrine and SP may play major role in Lung and RV reversal of EndMT and fibrosis in MCT+SMTC Rats (Figure S4).

Our previous study demonstrated microglial and astrocytic activation mediated neuroinflammation and neuronal apoptosis in the TSC and associated sympathoexcitation in MCT and SuHx PH rats as well as human PAH[8]. However, the precise molecular mechanisms and impact of TSC neuroinflammation and associated SNS activation on cardiopulmonary function in PH and RVF are still unknown. Several pain,

neurodegenerative and cardiovascular studies have indicated that during pathologic conditions primary afferent nerve endings increase glutamate release in the spinal dorsal horn, which can become excitotoxic and has the potential to trigger neurotoxicity[9-17]. Increased glutamate triggers NMDAR activation in the second order spinothalamic neurons, which leads to Ca^{2+} influx and activation of NOS1[9-17,52]. Our current study demonstrated increased expression of several NMDAR subunits, NOS1 and NOS1AP in the TSC of MCT and SuHx rats demonstrating increased excitatory glutamatergic transmission at the level of first synapse in the cardiopulmonary afferent pathway. NOS1AP has been shown to bind with the PDZ domain of NOS1 creating a ternary complex, which interacts between NMDAR and PSD-95 allowing NMDA-induced Ca2+ influx to efficiently activate NOS1[19].

One of our aims of this study is to investigate whether NOS1 activation in the TSC is NMDAR-dependent in PH-RVF. To achieve the first goal, we inhibited NMDAR using daily intrathecal injections of AP-5 in a group of MCT-induced PH-RVF rats (Figure 2A). AP-5 significantly attenuated PH severity and rescued RVF by reducing TSC NOS1 expression, neuroinflammation and associated sympathoexcitation demonstrating an important regulatory role of NMDAR in TSC NOS1 activation and associated neuroinflammation, apoptosis as well as sympathoexcitation in PH-RVF. This data is coherent with many studies demonstrating the essence of NMDAR activation dependent Ca^{2+} influx to activate NOS1 in the CNS[10,52,53].

Activated NOS1 produces ˙NO in the CNS that has been well documented to play a complex dual role, protective and deleterious, depending on the pathophysiological conditions[54-58]. On the one hand, ˙NO activates soluble guanylate cyclase (sGC)-cGMP signal transduction pathway to modulate various physiological effects in the CNS and

cardiovascular system including synaptic plasticity, retrograde signaling, neurodevelopment, vasodilation, inhibition of platelet aggregation and antiapoptotic effects[13,16,20]. On the other hand, during pathological conditions associated with increased oxidative stress and inflammation, excessive ˙NO combines with superoxide ($O_2^{\cdot -}$) to form peroxynitrite ($ONOO^-$), which induces neuroinflammation and neuronal excitotoxicity via protein oxidation and nitration, S-nitrosylation (S-NO), lipid peroxidation and activation of matrix metalloproteinases (MMPs) and cyclooxygenase (COX)[18,20,54-59]. Moreover, peroxynitrite breaks DNA, activating the nuclear enzyme poly(ADP-ribose) polymerase-1 (PARP-1) that causes cell death by rapid depletion of cell energy. Overactivated PARP also facilitates the expression of a variety of inflammatory genes leading to increased inflammation and associated oxidative stress, thus facilitating the progression of cardiovascular dysfunction and heart failure[56-60].

Interestingly, the half-life of ˙NO is less than 5 seconds after its synthesis; therefore, our knowledge of ˙NO in pathophysiology of CNS diseases are based on studies using NOS expression[20]. In several neuropathological and cardiovascular conditions, upregulation of NOS1 in the CNS induces oxidative and nitrosative stress, neuroinflammation, chemokine release, excitotoxicity, and neuronal apoptosis, indicating the involvement of ˙NO, whereas NOS1 inhibition induces neuroprotection[9,10,20]. NOS1 expression plays a complex dual role in sympathoexcitation regulation that depends on the pathophysiological conditions[55-60]. Several studies demonstrated that under physiological conditions, NOS1 has a sympathoinhibitory effect by acting on the paraventricular nucleus (PVN), nucleus of the solitary tract (NST), rostral ventrolateral medulla (RVLM), and carotid body (CB) of the CNS[55-60]. On the other hand, a number of studies demonstrated that during various pathological conditions including hypertension, myocardial infarction, chronic heart failure

and sepsis, NOS1 upregulation plays an essential role in the sympathoexcitatory and pressor action of ˙NO at the RVLM and TSC by increasing systemic arterial pressure, heart rate and sympathetic neurogenic vasomotor tone[54,56,57]. Ji et al demonstrated that i.c.v. administration of adrenomedullin activates ˙NO producing neurons in the PVN, NTS, supraoptic nucleus and nucleus paragigantocelluaris laterialis, causing hypertension and increasing sympathetic outflow, which indicates that central ˙NO may mediate sympathoexcitatory effects of adrenomedullin[63]. In another study microinjection of Nomega-nitro-l-arginine methyl ester (NO synthesis blocker) or carboxy-2-phenyl-4,4,5, 5-tetramethylimidazoline-1-oxyl 3-oxide (Carboxy PTIO, NO trapper) into the NTS decreased arterial pressure, heart rate and renal sympathetic nerve activity (RSNA). Alternatively, microinjection of Et2N[N(O)NO]Na (NO donor) caused increases in arterial pressure, HR and RSNA, which was inhibited by the pre-microinjection of Carboxy PTIO[64]. Moreover, microinjection of L-glutamate or NO donor, sodium nitroprusside or a cyclic GMP agonist, 8-bromocyclic GMP into the RVLM increased arterial pressure, whereas injection of NOS1 inhibitor, Nomega-nitro-L-arginine methyl ester or a soluble guanylate cyclase inhibitor, methylene blue or preinjection of a glutamate receptor antagonist kynurenate decreased arterial pressure[65]. NOS inhibition with L-NAME resulted in a profound decline in renal sympathetic nerve activity (RSNA) and heart rate (HR) in conscious, unrestrained rats on normal (NS), high-(HS), and low-sodium (LS) diets[66]. Increased ˙NO produced by upregulated NOS1 in the TSC has been shown to facilitates bradykinin-induced increase in the cardiac sympathetic afferent reflex by activating glutamatergic neurons[55,58]. Importantly, under physiological conditions, NOS1-derived ˙NO in the TSC modulate sympathetic outflow by exerting a tonic excitatory action on vasomotor tone mediated by norepinephrine released from the sympathetic nerve terminals[57].

Interestingly our time course experiments demonstrated that initial signs of PH coincided with NOS1 upregulation and early phase of TSC neuroinflammation without significant apoptosis and sympathoexcitation observed at day-14 (Figure 1I,J)[8]. As PH progressed, NOS1 upregulation, TSC neuroinflammation and apoptosis increased, leading to aberrant sympathoexcitation and worsening RVF[8]. To understand the role of NOS1 upregulation in TSC neuroinflammation, apoptosis and associated sympathoexcitation in PH-RVF we inhibited NOS1 using daily intrathecal injections of SMTC in a group of MCT-induced PH-RVF rats (Figure 3A). SMTC significantly attenuated PH severity and rescued RVF by reducing TSC NOS1 expression and activity, neuroinflammation, neuronal apoptosis and associated sympathoexcitation demonstrating an important sympathoexcitatory role of TSC NOS1 upregulation in PH-RVF.

RNASeq of RV and lung tissues from SMTC-treated MCT rats demonstrated promising therapeutic potential of intrathecal NOS1 inhibition through reversal of pro-fibrotic, inflammatory, apoptotic and sympathoexcitatory signatures in the RV as well as pro-fibrotic and inflammatory signatures in the lung (Figure 6,7, Table 1). We validated reduced EndMT, fibrosis and TRPV1-SP expression in the RV and lung tissues as well as reduced plasma norepinephrine in SMTC-treated MCT rats (Figure 4,6,7). NE has been shown to enhance cardiac fibrosis through TGFβ signaling and MMP2[37-39]. Our data demonstrated a significant reduction of both TGFβ signaling and MMP2 expression in the RV of SMTC-treated MCT rats leading to reduced fibrosis (Figure 6, Table 1). NE has been shown to induce oxidative stress, cardiomyocyte hypertrophy, fibrosis, activation of MAPK (Mainly p38 and ERK1/2) and AKT as well as NF-κB to release inflammatory cytokines in cultured cardiomyocytes[40,41]. Also, NE has been shown to induce activation of cardiac proinflammatory cytokines IL-6, IL-1β and TNF-α[42-45]. Interestingly, NE has also been

documented to play essential role in tissue repair and formation of extracellular matrix (ECM) during cardiac remodeling process by inducing expression of TGF-β1, TGF-β2, TGF-β3, MMP2, TIMP2 and collagen[37,46]. Moreover, NE is also known to induce apoptosis in cardiac myocytes[36,61]. Several studies have demonstrated that NE induces pulmonary injury with edema and inflammation by increased expression of several cytokines[62]. Studies have also shown that continuous norepinephrine infusion over three days increased mRNA expression of ECM related genes including Coll1, MMP-2, TIMP-2, and all TGF-β isoforms in the rat lung[51]. Elevated plasma norepinephrine leads to severe inflammatory reactions during transition into pulmonary fibrosis leading to the development of acute lung injury and acute respiratory distress syndrome[51]. Therefore, we believe that NOS1 inhibition reverses RV and lung transcriptomics by reducing plasma NE level. Interestingly, SP also plays a key role in inducing cardiac and lung fibrosis, EMT/EndMT, inflammation and apoptosis during various pathological conditions[27-32,47,48].

Our data indicates that reduced SP expression in the RV and lung may also play a major role in the reversal of RV and lung transcriptomics by NOS1 inhibition in MCT rats (Figure 6C, 7C).

Taken together, this study demonstrates upregulated NMDAR-NOS1 axis mediated neuroinflammation and neuronal apoptosis in the TSC and validates increased sympathoexcitation in the clinically relevant MCT and SuHx rat PH-RVF models. We demonstrated that TSC NOS1 specific inhibition by intrathecal SMTC in our MCT rat model reduced NOS activity, neuroinflammation and neuronal cell death in the TSC as well as and significantly attenuated PH-RVF by decreasing SNS activation. Targeting neuroinflammation and associated molecular pathways and genes in the TSC may yield novel therapeutic strategies for PH and RVF.

Supplementary Figures

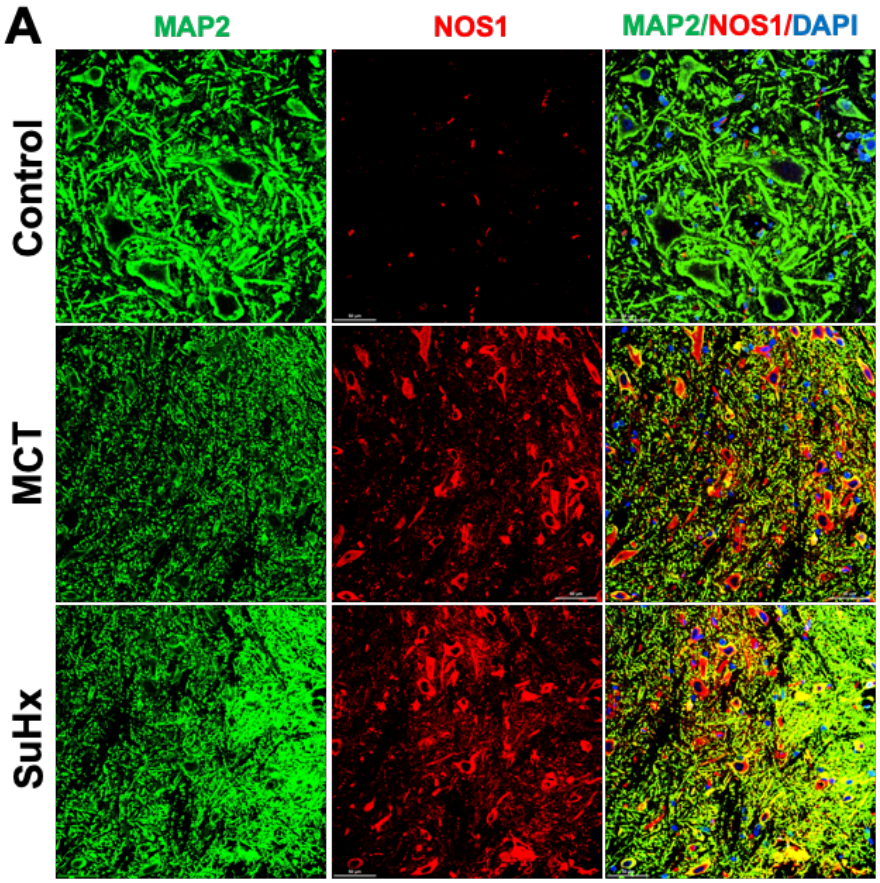

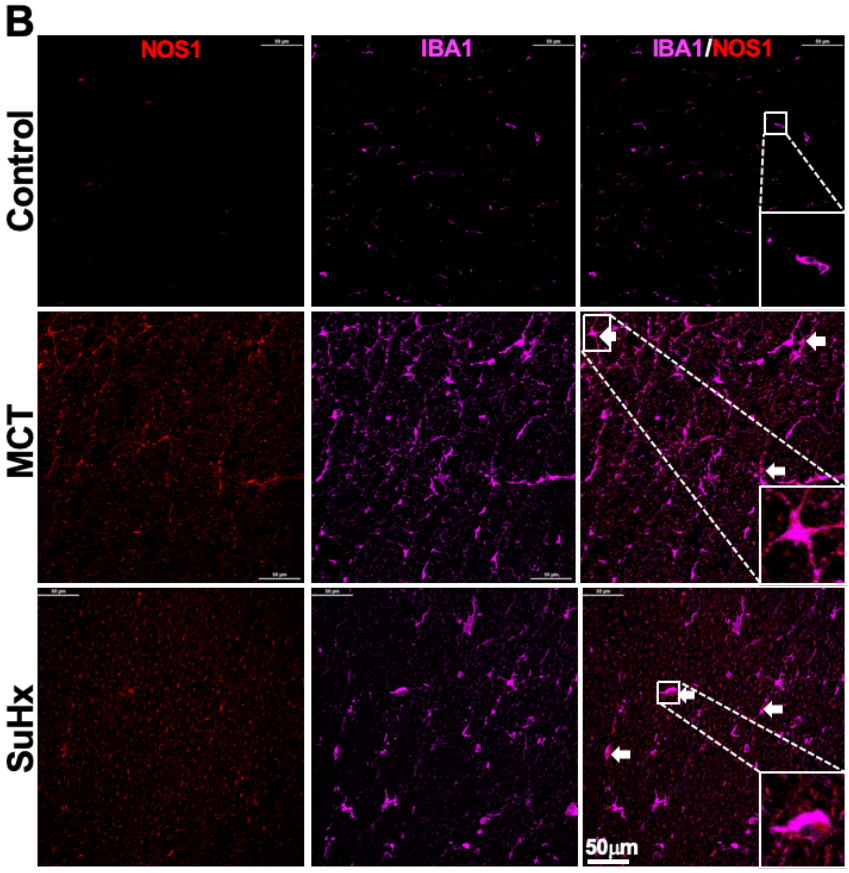
B
NOS1
IBA1
IBA1/NOS1
Control
MCT
SuHx
50μm

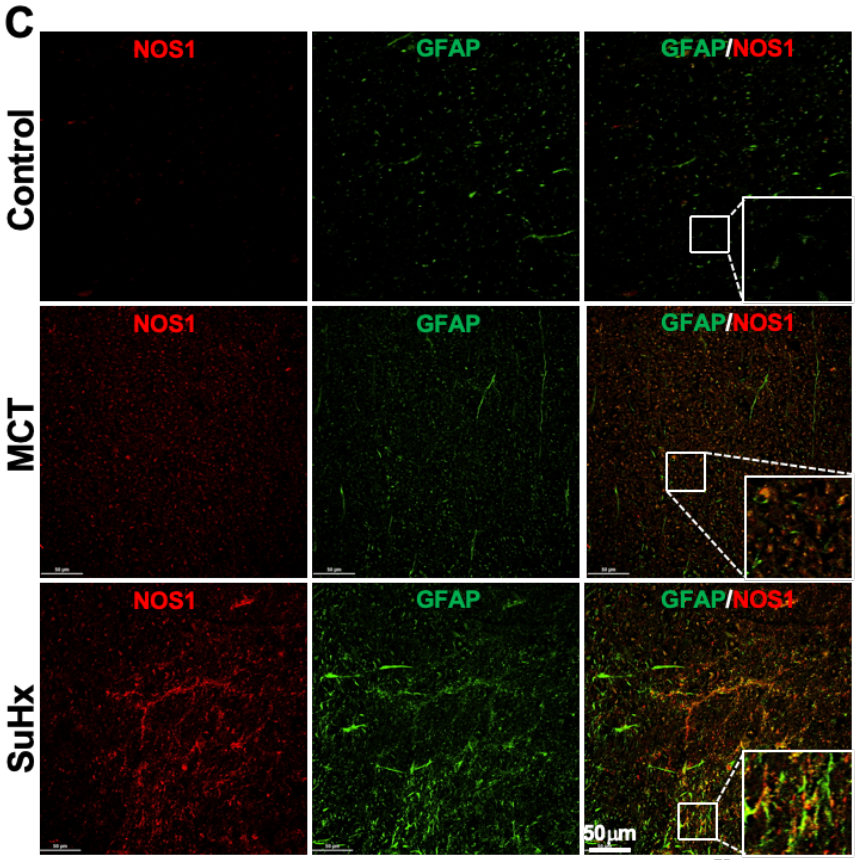
C
NOS1
GFAP
GFAP/NOS1
Control
MCT
SuHx
50μm

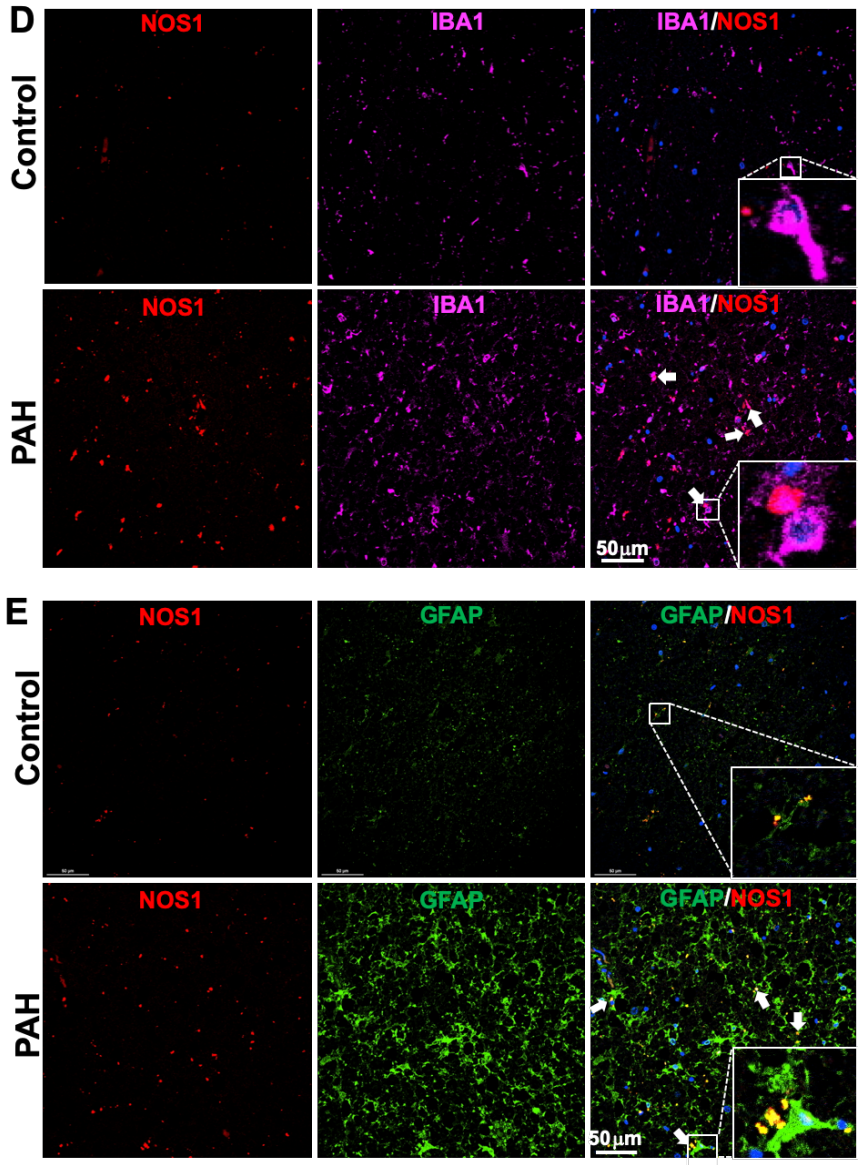

Figure S1. Increased NOS1 Expression in the TSC of MCT and SuHx Rats and PAH patients. (**A**) Represetative images of immunofluorescence staining with anti-MAP2 (Green), anti-NOS1 (Red), and DAPI (blue) from the TSC of Control, MCT and SuHx rats. N=3 per group. (**B**) Represetative images of immunofluorescence staining with anti-NOS1 (Red), anti-IBA1 (microglial marker; purple), along with their colocalization (right) in the TSC of Control, MCT and SuHx rats. N=3 per group. (**C**) Represetative images of immunofluorescence staining with anti-NOS1 (Red), anti-GFAP (astrocytic marker; green)

and their colocalization (right) in the TSC of Control, MCT and SuHx rats. N=3 per group. (**D**) Representative immunofluorescence images of Iba1 (purple), NOS1(red), and DAPI (DNA; blue) in control and PAH patients. White arrows indicate colocalization of NOS1+Iba1. N=4 per group. (**E**) Representative immunofluorescence images of GFAP (green), NOS1(red), and DAPI (DNA; blue) in control and PAH patients. White arrows indicate colocalization of NOS1+GFAP (yellow). N=4 per group.

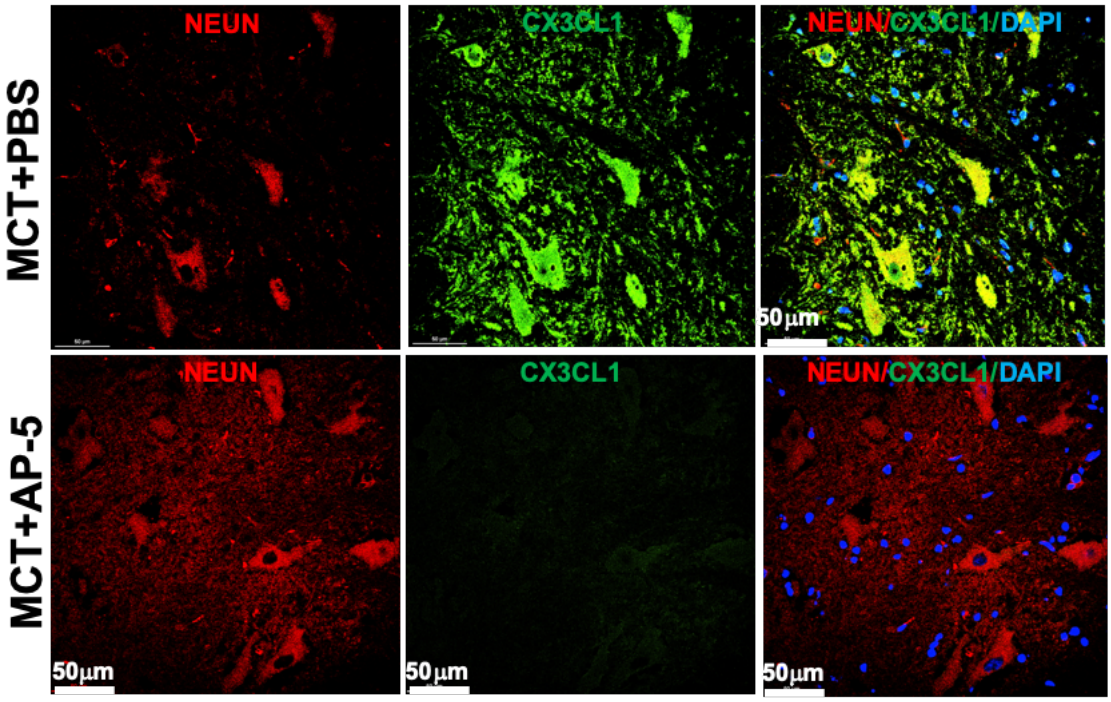

Figure S2. AP-5 reduced Cx3Cl1 expression in the TSC of MCT Rats. Representative images of immunofluorescence staining with neuronal marker NeuN (Red), Cx3Cl1 (Green) and DAPI (Blue) in the TSC of PBS and AP-5 treated MCT rats. N=3 per group.

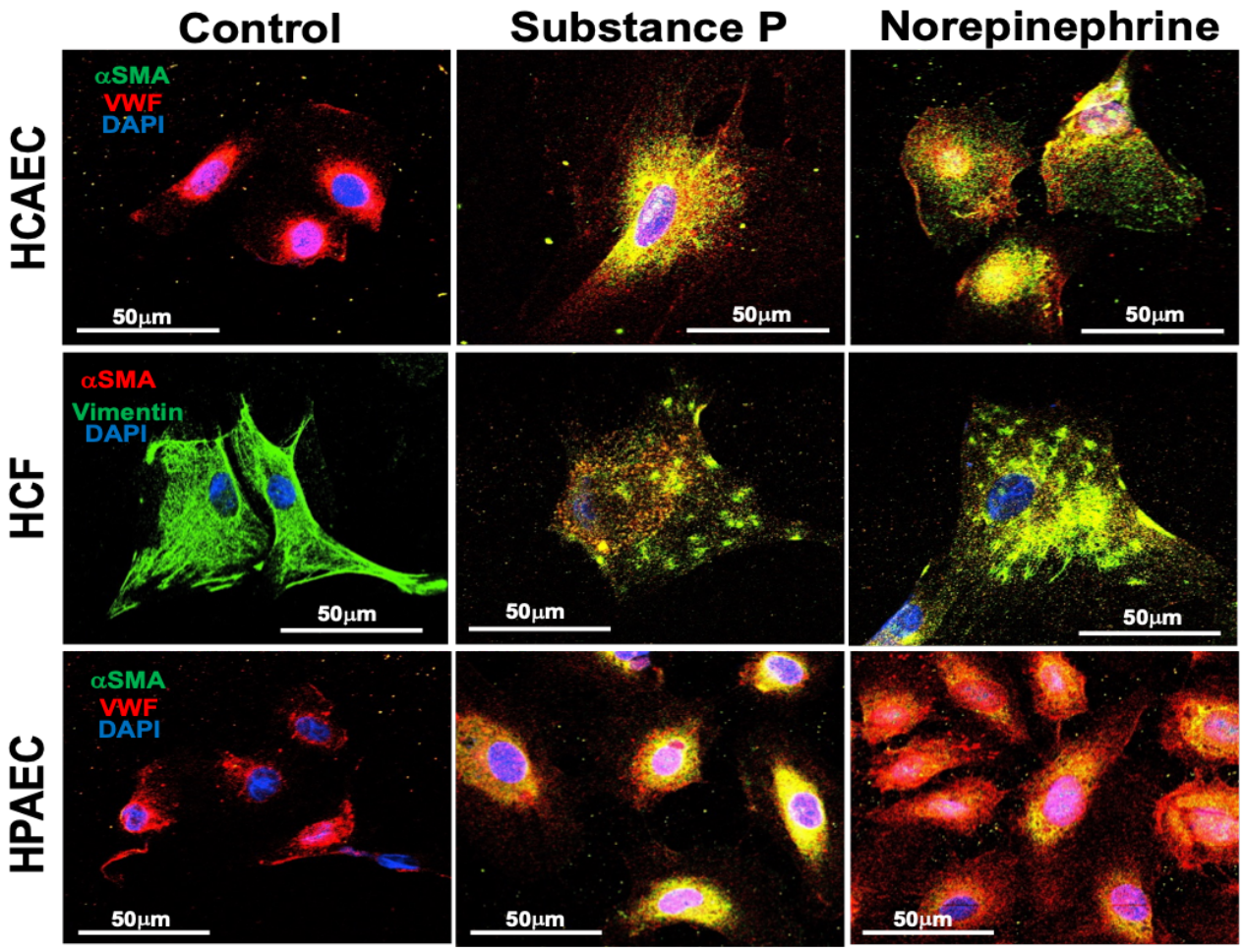

Figure S3. Substance P and Norepinephrine induce EndMT in HCAECs and HPAECs and Myofibroblast Transition in HCF *in vitro*. HCAEC, HPAEC and HCF were incubated with Substance P (SP) (150 ug/mL)[62-64] and NE (10uM)[65-68] for 48 hrs and stained to assess endothelial-to-mesenchymal transition (EndMT) or Fibroblast to Myofibroblast transition. N=3 per group.

Supplementary Tables

Table S1: Leading edge down-regulated RV genes from SMTC-treated MCT vs. PBS-treated MCT rats

Gene	Full Name	Expression	Log2Fold Change	Padj Value
Pro-fibrotic Genes				
COL4a3 SMTC vs PBS	Collagen type IV alpha 3 chain	Decreased	-1.3084067	0.0013715
COL14a1 SMTC vs PBS	Collagen type XIV alpha 1 chain	Decreased	-0.9204674	0.00595681
ITGB5 SMTC vs PBS	Integrin subunit beta 5	Decreased	-0.78599	0.00210762
MMP2 SMTC vs PBS	Matrix metallopeptidase 2	Decreased	-0.7625847	0.00617871
SERPINE2 SMTC vs PBS	Serpin family E member 2	Decreased	-0.9982296	0.02134555
SMAD6 SMTC vs PBS	SMAD family member 6	Decreased	-0.40505146	0.00177887
TGFβR3 SMTC vs PBS	Transforming growth factor, beta receptor 3	Decreased	-1.5047972	0.01477763
BMPR2 SMTC vs PBS	Bone morphogenetic protein receptor type 2	Decreased	-0.483927	0.01175912
BMP6 SMTC vs PBS	Bone morphogenetic protein 6	Decreased	-1.0681964	0.00665441
Pro-inflammatory Genes				
CCND2 SMTC vs PBS	Cyclin D2	Decreased	-1.4604008	3.64E-08
MAPK1 SMTC vs PBS	Mitogen activated protein kinase 1	Decreased	-0.3284388	0.01309412
NOTCH3 SMTC vs PBS	Notch receptor 3	Decreased	-0.6143453	0.00414546
CARD6 SMTC vs PBS	Caspase recruitment domain family, member 6	Decreased	-0.6403424	0.01166342

Gene	Full Name	Expression	Log2Fold Change	Padj Value
Pro-apoptotic Genes				
FOXO3 SMTC vs PBS	Forkhead box O3	Decreased	-0.7743993	0.04733615
TGFβR2 SMTC vs PBS	Transforming growth factor, beta receptor 2	Decreased	-0.5767913	0.00235379
BCL2L2 SMTC vs PBS	Bcl2-like 2	Decreased	-0.3711533	0.04505631
MMP2 SMTC vs PBS	Matrix metallopeptidase 2	Decreased	-0.7625847	0.00617871
SNS, RAAS and Arrhythmia Genes				
CAMK2D SMTC vs PBS	Calcium/calmodulin-dependent protein kinase II delta	Decreased	-0.8535827	0.00272177
ADRA1A SMTC vs PBS	Alpha 1-A adrenergic receptor	Decreased	-1.1067306	1.85E-06
ADRA2A SMTC vs PBS	Alpha 2-A adrenergic receptor	Decreased	-1.2453222	0.02615252
ACE2 SMTC vs PBS	Angiotensin I converting enzyme 2	Decreased	-2.9606068	0.00285297
KCNJ2 SMTC vs PBS	Potassium inwardly-rectifying channel, subfamily J, member 2	Decreased	-1.010301	0.01240958
RYR2 SMTC vs PBS	Ryanodine receptor 2	Decreased	-0.350844	0.00034011
GJA1 SMTC vs PBS	Gap junction protein, alpha 1	Decreased	-0.5378049	0.00323351
DBH SMTC vs PBS	Dopamine β hydroxylase	Decreased	-0.9003486	1.85E-06

Table S2: Leading edge down-regulated lung genes from SMTC-treated MCT vs. PBS-treated MCT rats

Gene	Full Name	Expression	Log2Fold Change	Padj Value
Pro-inflammatory Genes				
Ebna1bp2 SMTC VS PBS	EBNA1 binding protein 2	Decreased	-11.4289648	1.3080E-17
Fabp4 SMTC VS PBS	Fatty Acid Binding Protein 4	Decreased	-1.03148513	1.4021E-05
Itgam SMTC VS PBS	Integrin Subunit Alpha M	Decreased	-1.79574228	0.0002570
Ctsk SMTC VS PBS	Cathepsin K	Decreased	-1.38510519	0.00025700
Lgmn SMTC VS PBS	Legumain	Decreased	-0.52589126	0.00305565
Arntl (Bmal1) SMTC VS PBS	Brain And Muscle ARNT-Like 1	Decreased	-1.52390920	0.03277429
Pro-fibrotic Genes				
Mfap4 SMTC VS PBS	Microfibril Associated Protein 4	Decreased	-30	5.3484E-11
Fabp4 SMTC VS PBS	Fatty Acid Binding Protein 4	Decreased	-1.03148513	1.4021E-05
Ctsk SMTC VS PBS	Cathepsin K	Decreased	-1.38510519	0.00025700
Ltbp2 SMTC VS PBS	Latent Transforming Growth Factor Beta Binding Protein 2	Decreased	-0.65748919	0.00203278 0981294
Lgmn SMTC VS PBS	Legumain	Decreased	-0.52589126	0.00305565
Arntl (Bmal1) SMTC VS PBS	Brain And Muscle ARNT-Like 1	Decreased	-1.52390920	0.03277429

References

1. Umar S, Lee JH, de Lange E, Iorga A, Partow-Navid R, Bapat A, van der Laarse A, Saggar R, Saggar R, Ypey DL, Karagueuzian HS, Eghbali M. Spontaneous ventricular fibrillation in right ventricular failure secondary to chronic pulmonary hypertension. Circ Arrhythm Electrophysiol. 2012 Feb;5(1):181-90. doi: 10.1161/CIRCEP.111.967265. Epub 2011 Dec 22. PMID: 22199010; PMCID: PMC3319685.

2. Vaillancourt, M., Chia, P., Sarji, S., Nguyen, J., Hoftman, N., Ruffenach, G., et al. Autonomic nervous system involvement in pulmonary arterial hypertension. Respir. Res. 2017;18:201.

3. Ciarka, A., Doan, V., Velez-Roa, S., Naeije, R., and van de Borne, P. Prognostic significance of sympathetic nervous system activation in pulmonary arterial hypertension. Am. J. Respir. Crit. Care Med. 2010;181:1269–1275.

4. Saddic LA, Howard-Quijano K, Kipke J, Kubo Y, Dale EA, Hoover D, Shivkumar K, Eghbali M, Mahajan A. Progression of myocardial ischemia leads to unique changes in immediate-early gene expression in the spinal cord dorsal horn. Am J Physiol Heart Circ Physiol. 2018 Dec 1;315(6):H1592-H1601. doi: 10.1152/ajpheart.00337.2018. Epub 2018 Sep 14. PMID: 30216122; PMCID: PMC6336975.

5. Gao C, Howard-Quijano K, Rau C, Takamiya T, Song Y, Shivkumar K, Wang Y, Mahajan A. Inflammatory and apoptotic remodeling in autonomic nervous system following myocardial infarction. PLoS One. 2017 May 18;12(5):e0177750. doi: 10.1371/journal.pone.0177750. PMID: 28542617; PMCID: PMC5436752.

6. Sharma RK, Oliveira AC, Kim S, et al. Involvement of Neuroinflammation in the Pathogenesis of Monocrotaline-Induced Pulmonary Hypertension. Hypertension. 2018;71(6):1156-1163.

7. Milanez MIO, Nishi EE, Bergamaschi CT, Campos RR. Role of spinal neurons in the maintenance of elevated sympathetic activity: a novel therapeutic target? Am J Physiol Regul Integr Comp Physiol. 2020 Sep 1;319(3):R282-R287. doi: 10.1152/ajpregu.00122.2020. Epub 2020 Jun 24. PMID: 32579387.

8. Razee A, Banerjee S, Hong J, Magaki S, Fishbein G, Ajijola OA, Umar S. Thoracic Spinal Cord Neuroinflammation as a Novel Therapeutic Target in Pulmonary Hypertension. Hypertension. 2023 Jun;80(6):1297-1310. doi: 10.1161/HYPERTENSIONAHA.122.20782. Epub 2023 Apr 24. PMID: 37092338; PMCID: PMC10192067.

9. Ahlawat A, Rana A, Goyal N, Sharma S. Potential role of nitric oxide synthase isoforms in pathophysiology of neuropathic pain. Inflammopharmacology. 2014 Oct;22(5):269-78. doi: 10.1007/s10787-014-0213-0. Epub 2014 Aug 6. PMID: 25095760.

10. Rameau GA, Chiu LY, Ziff EB. NMDA receptor regulation of nNOS phosphorylation and induction of neuron death. Neurobiol Aging. 2003 Dec;24(8):1123-33. doi: 10.1016/j.neurobiolaging.2003.07.002. PMID: 14643384.

11. Freire MA, Guimarães JS, Leal WG, Pereira A. Pain modulation by nitric oxide in the spinal cord. Front Neurosci. 2009 Sep 15;3(2):175-81. doi: 10.3389/neuro.01.024.2009. PMID: 20011139; PMCID: PMC2751623.

12. Esplugues JV. NO as a signaling molecule in the nervous system. Br J Pharmacol. 2002 Mar;135(5):1079-95. doi: 10.1038/sj.bjp.0704569. PMID: 11877313; PMCID: PMC1573233.

13. Cury Y, Picolo G, Gutierrez VP, Ferreira SH. Pain and analgesia: The dual effect of nitric oxide in the nociceptive system. Nitric Oxide. 2011 Oct 30;25(3):243-54. doi: 10.1016/j.niox.2011.06.004. Epub 2011 Jun 24. PMID: 21723953.

14. Yuste JE, Tarragon E, Campuzano CM, Ros-Bernal F. Implications of glial nitric oxide in neurodegenerative diseases. Front Cell Neurosci. 2015 Aug 17;9:322. doi: 10.3389/fncel.2015.00322. PMID: 26347610; PMCID: PMC4538301.

15. Liñares D, Taconis M, Maña P, Correcha M, Fordham S, Staykova M, Willenborg DO. Neuronal nitric oxide synthase plays a key role in CNS demyelination. J Neurosci. 2006 Dec 6;26(49):12672-81. doi: 10.1523/JNEUROSCI.0294-06.2006. PMID: 17151270; PMCID: PMC6674851.

16. Reis PA, de Albuquerque CFG, Gutierrez TM, Silva AR, de Castro Faria Neto HC. Role of nitric oxide synthase in the function of the central nervous system under normal and infectious conditions. In: Saravi SSS, editor. Nitric Oxide Synthase – Simple Enzyme-Complex Roles. London: InTech (2017). p. 55–70.

17. Komers R, Oyama TT, Chapman JG, Allison KM, Anderson S. Effects of systemic inhibition of neuronal nitric oxide synthase in diabetic rats. Hypertension. 2000 Feb;35(2):655-61. doi: 10.1161/01.hyp.35.2.655. PMID: 10679513.

18. Janes K, Neumann WL, Salvemini D. Anti-superoxide and anti-peroxynitrite strategies in pain suppression. Biochim Biophys Acta. 2012 May;1822(5):815-21. doi: 10.1016/j.bbadis.2011.12.008. Epub 2011 Dec 19. PMID: 22200449; PMCID: PMC3478755.

19. O'Toole, Eileen, et al. "Novel targets in the glutamate and nitric oxide neurotransmitter systems for the treatment of depression." Systems neuroscience in depression. Academic Press, 2016. 81-113.

20. Pacher P, Beckman JS, Liaudet L. Nitric oxide and peroxynitrite in health and disease. Physiol Rev. 2007 Jan;87(1):315-424. doi: 10.1152/physrev.00029.2006. PMID: 17237348; PMCID: PMC2248324.

21. Nazarian A, Gu G, Gracias NG, Wilkinson K, Hua XY, Vasko MR, Yaksh TL. Spinal N-methyl-D-aspartate receptors and nociception-evoked release of primary afferent substance P. Neuroscience. 2008 Mar 3;152(1):119-27. doi: 10.1016/j.neuroscience.2007.11.037. PMID: 18222611; PMCID: PMC2730522.

22. Nishiyama T. Interaction between intrathecal morphine and glutamate receptor antagonists in formalin test. Eur J Pharmacol. 2000 May 3;395(3):203-10. doi: 10.1016/s0014-2999(00)00268-5. PMID: 10812050.

23. Ranchoux B, Antigny F, Rucker-Martin C, Hautefort A, Péchoux C, Bogaard HJ, Dorfmüller P, Remy S, Lecerf F, Planté S, Chat S, Fadel E, Houssaini A, Anegon I, Adnot S, Simonneau G, Humbert M, Cohen-Kaminsky S, Perros F. Endothelial-to-mesenchymal transition in pulmonary hypertension. Circulation. 2015 Mar 17;131(11):1006-18. doi: 10.1161/CIRCULATIONAHA.114.008750. Epub 2015 Jan 15. PMID: 25593290.

24. Sydykov A, Mamazhakypov A, Petrovic A, Kosanovic D, Sarybaev AS, Weissmann N, Ghofrani HA, Schermuly RT. Inflammatory Mediators Drive Adverse Right Ventricular Remodeling and Dysfunction and Serve as Potential Biomarkers. Front Physiol. 2018 May 23;9:609. doi: 10.3389/fphys.2018.00609. PMID: 29875701; PMCID: PMC5974151.

25. Michelakis ED. Spatio-temporal diversity of apoptosis within the vascular wall in pulmonary arterial hypertension: heterogeneous BMP signaling may have therapeutic implications. Circ Res. 2006 Feb 3;98(2):172-5. doi: 10.1161/01.RES.0000204572.65400.a5. PMID: 16456109.

26. Park JF, Clark VR, Banerjee S, Hong J, Razee A, Williams T, Fishbein G, Saddic L, Umar S. Transcriptomic Analysis of Right Ventricular Remodeling in Two Rat Models of Pulmonary Hypertension: Identification and Validation of EMT in Human Right Ventricular

Failure. Circ Heart Fail. 2021 Feb 5:CIRCHEARTFAILURE120007058. doi: 10.1161/CIRCHEARTFAILURE.120.007058. Online ahead of print. PMID: 33541093.

27. Villablanca AC, Murphy CJ, Reid TW. Growth-promoting effects of substance P on endothelial cells in vitro. Synergism with calcitonin gene-related peptide, insulin, and plasma factors. Circ Res. 1994 Dec;75(6):1113-20. doi: 10.1161/01.res.75.6.1113. PMID: 7525104.

28. Słoniecka M, Danielson P. Substance P induces fibrotic changes through activation of the RhoA/ROCK pathway in an in vitro human corneal fibrosis model. J Mol Med (Berl). 2019 Oct;97(10):1477-1489. doi: 10.1007/s00109-019-01827-4. Epub 2019 Aug 9. PMID: 31399750; PMCID: PMC6746877.

29. Kähler CM, Sitte BA, Reinisch N, Wiedermann CJ. Stimulation of the chemotactic migration of human fibroblasts by substance P. Eur J Pharmacol. 1993 Nov 16;249(3):281-6. doi: 10.1016/0014-2999(93)90523-k. PMID: 7507058.

30. Peng L, Agogo GO, Guo J, Yan M. Substance P and fibrotic diseases. Neuropeptides. 2019 Aug;76:101941. doi: 10.1016/j.npep.2019.101941. Epub 2019 Jun 24. PMID: 31256921.

31. Xu Y, Gu Q, Qu C. Capsaicin pretreatment reversed pulmonary arterial hypertension by alleviating inflammation via p38MAPK pathway. Exp Lung Res. 2017 Feb;43(1):8-18. doi: 10.1080/01902148.2016.1271481. Epub 2017 Mar 10. PMID: 28281854.

32. O'Connor TM, O'Connell J, O'Brien DI, Goode T, Bredin CP, Shanahan F. The role of substance P in inflammatory disease. J Cell Physiol. 2004 Nov;201(2):167-80. doi: 10.1002/jcp.20061. PMID: 15334652.

33. Shan T, Cui X, Li W, Lin W, Li Y, Chen X, Wu T. Novel regulatory program for norepinephrine-induced epithelial-mesenchymal transition in gastric adenocarcinoma cell

lines. Cancer Sci. 2014 Jul;105(7):847-56. doi: 10.1111/cas.12438. Epub 2014 Jun 18. PMID: 24815301; PMCID: PMC4317918.

34. Guo K, Ma Q, Wang L, Hu H, Li J, Zhang D, Zhang M. Norepinephrine-induced invasion by pancreatic cancer cells is inhibited by propranolol. Oncol Rep. 2009 Oct;22(4):825-30. doi: 10.3892/or_00000505. PMID: 19724861.

35. Zhang J, Deng YT, Liu J, Wang YQ, Yi TW, Huang BY, He SS, Zheng B, Jiang Y. Norepinephrine induced epithelial-mesenchymal transition in HT-29 and A549 cells in vitro. J Cancer Res Clin Oncol. 2016 Feb;142(2):423-35. doi: 10.1007/s00432-015-2044-9. Epub 2015 Sep 10. PMID: 26358081.

36. Fu YC, Chi CS, Yin SC, Hwang B, Chiu YT, Hsu SL. Norepinephrine induces apoptosis in neonatal rat endothelial cells via down-regulation of Bcl-2 and activation of beta-adrenergic and caspase-2 pathways. Cardiovasc Res. 2004 Jan 1;61(1):143-51. doi: 10.1016/j.car

37. Akiyama-Uchida Y, Ashizawa N, Ohtsuru A, Seto S, Tsukazaki T, Kikuchi H, Yamashita S, Yano K. Norepinephrine enhances fibrosis mediated by TGF-beta in cardiac fibroblasts. Hypertension. 2002 Aug;40(2):148-54. doi: 10.1161/01.hyp.0000025443.61926.12. PMID: 12154105.

38. Tian CJ, Pang X. Ca2+-calcineurin signaling is involved in norepinephrine-induced cardiac fibroblasts activation. Int J Clin Exp Pathol. 2015 May 1;8(5):5210-6. PMID: 26191219; PMCID: PMC4503091.

39. Dincer HE, Gangopadhyay N, Wang R, Uhal BD. Norepinephrine induces alveolar epithelial apoptosis mediated by alpha-, beta-, and angiotensin receptor activation. Am J Physiol Lung Cell Mol Physiol. 2001 Sep;281(3):L624-30. doi: 10.1152/ajplung.2001.281.3.L624. PMID: 11504689.

40. Tang K, Zhong B, Luo Q, Liu Q, Chen X, Cao D, Li X, Yang S. Phillyrin attenuates norepinephrine-induced cardiac hypertrophy and inflammatory response by suppressing p38/ERK1/2 MAPK and AKT/NF-kappaB pathways. Eur J Pharmacol. 2022 Jul 15;927:175022. doi: 10.1016/j.ejphar.2022.175022. Epub 2022 May 13. PMID: 35569549.

41. Briest W, Hölzl A, Rassler B, Deten A, Leicht M, Baba HA, Zimmer HG. Cardiac remodeling after long term norepinephrine treatment in rats. Cardiovasc Res. 2001 Nov;52(2):265-73. doi: 10.1016/s0008-6363(01)00398-4. PMID: 11684074.

42. Briest W, Elsner C, Hemker J, Müller-Strahl G, Zimmer HG. Norepinephrine-induced expression of cytokines in isolated biventricular working rat hearts. Mol Cell Biochem. 2003 Mar;245(1-2):69-76. doi: 10.1023/a:1022861609896. PMID: 12708746.

43. Barth W, Deten A, Bauer M, Reinohs M, Leicht M, Zimmer HG. Differential remodeling of the left and right heart after norepinephrine treatment in rats: studies on cytokines and collagen. J Mol Cell Cardiol. 2000 Feb;32(2):273-84. doi: 10.1006/jmcc.1999.1075. PMID: 10722803.

44. Leicht M, Briest W, Zimmer HG. Regulation of norepinephrine-induced proliferation in cardiac fibroblasts by interleukin-6 and p42/p44 mitogen activated protein kinase. Mol Cell Biochem. 2003 Jan;243(1-2):65-72. doi: 10.1023/a:1021655023870. PMID: 12619890.

45. Briest W, Rassler B, Deten A, Leicht M, Morwinski R, Neichel D, Wallukat G, Ziegelhöffer T, Zimmer HG. Norepinephrine-induced interleukin-6 increase in rat hearts: differential signal transduction in myocytes and non-myocytes. Pflugers Arch. 2003 Jul;446(4):437-46. doi: 10.1007/s00424-003-1043-x. Epub 2003 May 6. PMID: 12733076.

46. Briest W, Homagk L, Rassler B, Ziegelhöffer-Mihalovicová B, Meier H, Tannapfel A, Leiblein S, Saalbach A, Deten A, Zimmer HG. Norepinephrine-induced changes in cardiac transforming growth factor-beta isoform expression pattern of female and male rats.

Hypertension. 2004 Oct;44(4):410-8. doi: 10.1161/01.HYP.0000141414.87026.4d. Epub 2004 Aug 23. PMID: 15326086.

47. Lo CCW, Moosavi SM, Bubb KJ. The Regulation of Pulmonary Vascular Tone by Neuropeptides and the Implications for Pulmonary Hypertension. Front Physiol. 2018 Aug 23;9:1167. doi: 10.3389/fphys.2018.01167. PMID: 30190678; PMCID: PMC6116211.

48. Yaraee R, Ghazanfari T. Substance P potentiates TGFbeta-1 production in lung epithelial cell lines. Iran J Allergy Asthma Immunol. 2009 Mar;8(1):19-24. PMID: 19279355.

49. Liu R, Zhang Q, Luo Q, Qiao H, Wang P, Yu J, Cao Y, Lu B, Qu L. Norepinephrine stimulation of alpha1D-adrenoceptor promotes proliferation of pulmonary artery smooth muscle cells via ERK-1/2 signaling. Int J Biochem Cell Biol. 2017 Jul;88:100-112. doi: 10.1016/j.biocel.2017.05.001. Epub 2017 May 2. PMID: 28476501.

50. Xiao X, Zhang Y, Tian S, Wang X, Zhang Q, Zhang L, Yu X, Ma C, Zheng X, Li Y, Zhang J, Qu L. Alpha1B-adreneroceptor is involved in norepinephrine-induced pulmonary artery smooth muscle cell proliferation via p38 signaling. Eur J Pharmacol. 2022 Sep 15;931:175159. doi: 10.1016/j.ejphar.2022.175159. Epub 2022 Jul 30. PMID: 35917901.

51. Rassler B, Marx G, Schierle K, Zimmer HG. Catecholamines can induce pulmonary remodeling in rats. Cell Physiol Biochem. 2012;30(5):1134-47. doi: 10.1159/000343304. Epub 2012 Oct 5. PMID: 23171784.

52. Ally A, Powell I, Ally MM, Chaitoff K, Nauli SM. Role of neuronal nitric oxide synthase on cardiovascular functions in physiological and pathophysiological states. Nitric Oxide. 2020 Sep 1;102:52-73. doi: 10.1016/j.niox.2020.06.004. Epub 2020 Jun 23. PMID: 32590118; PMCID: PMC7375925.

53. Cury Y, Picolo G, Gutierrez VP, Ferreira SH. Pain and analgesia: The dual effect of nitric oxide in the nociceptive system. Nitric Oxide. 2011 Oct 30;25(3):243-54. doi: 10.1016/j.niox.2011.06.004. Epub 2011 Jun 24. PMID: 21723953.

54. Chan SH, Wang LL, Wang SH, Chan JY. Differential cardiovascular responses to blockade of nNOS or iNOS in rostral ventrolateral medulla of the rat. Br J Pharmacol. 2001 Jun;133(4):606-14. doi: 10.1038/sj.bjp.0704105. PMID: 11399678; PMCID: PMC1572812.

55. Wang Y, Golledge J. Neuronal nitric oxide synthase and sympathetic nerve activity in neurovascular and metabolic systems. Curr Neurovasc Res. 2013 Feb;10(1):81-9. doi: 10.2174/156720213804805963. PMID: 23151079.

56. Vayssettes-Courchay C, Bouysset F, Verbeuren TJ. Involvement of COX and NOS induction in the sympatho-activation during sepsis. Auton Neurosci. 2002 Jun 28;98(1-2):33-6. doi: 10.1016/s1566-0702(02)00027-9. PMID: 12144036.

57. Poon YY, Tsai CY, Cheng CD, Chang AY, Chan SH. Endogenous nitric oxide derived from NOS I or II in thoracic spinal cord exerts opposing tonic modulation on sympathetic vasomotor tone via disparate mechanisms in anesthetized rats. Am J Physiol Heart Circ Physiol. 2016 Sep 1;311(3):H555-62. doi: 10.1152/ajpheart.00246.2016. Epub 2016 Jul 1. PMID: 27371683.

58. Guo ZL, Moazzami AR, Longhurst JC. Stimulation of cardiac sympathetic afferents activates glutamatergic neurons in the parabrachial nucleus: relation to neurons containing nNOS. Brain Res. 2005 Aug 16;1053(1-2):97-107. doi: 10.1016/j.brainres.2005.06.051. PMID: 16054113.

59. Vayssettes-Courchay C, Bouysset F, Verbeuren TJ. Involvement of COX and NOS induction in the sympatho-activation during sepsis. Auton Neurosci. 2002 Jun 28;98(1-2):33-6. doi: 10.1016/s1566-0702(02)00027-9. PMID: 12144036.

60. Calabrese V, Mancuso C, Calvani M, Rizzarelli E, Butterfield DA, Stella AM. Nitric oxide in the central nervous system: neuroprotection versus neurotoxicity. Nat Rev Neurosci. 2007 Oct;8(10):766-75. doi: 10.1038/nrn2214. PMID: 17882254.

61. Lai KB, Sanderson JE, Yu CM. High dose norepinephrine-induced apoptosis in cultured rat cardiac fibroblast. Int J Cardiol. 2009 Jul 24;136(1):33-9. doi: 10.1016/j.ijcard.2008.04.022. PMID: 18675472.

62. Rassler B, Rohling MA, Reissig C, Briest W, Tannapfel A, Zimmer HG. Involvement of cytokines and inflammation in catecholamine-induced pulmonary injury in rats. Vascular Disease Prevention. 2005 Jan 1;2(1):1-9.

63. Ji SM, Wang ZM, Li XP, He RR. Intracerebroventricular administration of adrenomedullin increases the expression of c-fos and activates nitric oxide-producing neurons in rat cardiovascular related brain nuclei. Sheng Li Xue Bao. 2004 Jun 25;56(3):328-34. PMID: 15224145.

64. Matsumura K, Tsuchihashi T, Kagiyama S, Abe I, Fujishima M. Role of nitric oxide in the nucleus of the solitary tract of rats. Brain Res. 1998 Jul 6;798(1-2):232-8. doi: 10.1016/s0006-8993(98)00420-x. PMID: 9666137.

65. Morimoto S, Sasaki S, Miki S, Kawa T, Nakamura K, Itoh H, Nakata T, Takeda K, Nakagawa M, Fushiki S. Nitric oxide is an excitatory modulator in the rostral ventrolateral medulla in rats. Am J Hypertens. 2000 Oct;13(10):1125-34. doi: 10.1016/s0895-7061(00)01182-1. PMID: 11041168.

66. McKeogh DF, O'Donaughy TL, Brooks VL. NO and endogenous angiotensin II interact in the generation of renal sympathetic nerve activity in conscious rats. Am J Physiol Heart Circ Physiol. 2004 Apr;286(4):H1258-65. doi: 10.1152/ajpheart.00791.2003. Epub 2003 Dec 4. PMID: 14656704.

Chapter 5: Conclusions and Future Directions

Conclusions

PH is a progressive and fatal disease characterized by persistent elevation of pulmonary arterial pressure, which is caused by pulmonary vascular remodeling due to endothelial dysfunction, excessive smooth muscle cell proliferation, migration, arteriolar muscularization, fibrosis, extracellular matrix deposition, thrombosis and inflammatory cell recruitment[1]. These factors result in persistent increase in PVR, vasoconstriction, loss of distal pulmonary arteries, pressure overload, RVH, RVF, arrhythmias and ultimately, death[1,2]. Although the dysregulation of vasomotor pathways, for example, upregulation of endothelin and downregulation of nitric oxide and prostacyclin pathways have been identified as the main causes, growing body of evidence demonstrates the contribution of autonomic imbalance in the pathophysiology of PAH, strengthening the hypothesis for the role of SNS activation in PAH progession[3-7]. Progressive increase in PVR and RV afterload activates SNS and RAAS to compensate for low cardiac output with relatively fixed stroke volume in PAH, however, chronic SNS hyperactivity leads to arrhythmias, RVF and sudden death[3,6,8]. In fact, numerous studies have indicated that continuous sympathoexcitation is one of the main contributors of pathological cardiac remodeling including hypertrophy, ventricular dysfunction and arrhythmia in various cardiovascular diseases, hence, strategies to reduce sympathetic vasomotor overactivity in cardiovascular diseases can be beneficial[9-13]. Although RVF is the major cause of death among patients with PAH, none of the currently FDA approved therapies directly target right heart failure[14]. This necessitates further investigation in understanding the cellular and molecular mechanisms of SNS hyperactivity beyond the vasomotor pathways in PH progression to identify novel therapeutic targets.

A complex interplay of mechanical, neurohumoral, and inflammatory stresses has been

suggested as an underpinning cellular and molecular mechanism involved in sympathetic activation in PAH[15]. Recently, neuroinflammation in the CNS has been implicated in sympathetic activation leading to arrhythmias and RVF in experimental PH[8,16-18]. Microglial activation mediated cytokine release in the PVN has been shown to increase RAS components, sympathetic drive and plasma NE in MCT-induced PH rats, whereas ICV infusion of minocycline attenuated microglial activation and proinflammatory cytokines in the PVN, reduced sympathoexcitation and prevented PH-RVF[16], suggesting that microglial activation-mediated neuroinflammation and a dysregulated brain RAS is involved in the pathogenesis of PH-RVF. Furthermore, Oliveira et al demonstrated that chronic hypoxia-induced microglial activation in the PVN resulted in a fivefold increase in the sympathetic/vagal balance (low frequency/high frequency ratio), suggesting an increase in sympathetic activity in PH mice. However, CX3CR1$^{GFP/GFP}$ mice were protected from hypoxia-induced microglial activation in the PVN and sympathoexcitation[17]. We recently reported for the first time significantly increased GFAP, pro-inflammatory marker chemokine (C-C motif) ligand 3 (CCL3) and angiogenesis marker adhesion molecule CD31 expression in the TSC indicating severe neuroinflammation in MCT-induced PH rats[18]. Although, in line with the previous reports on various cardiovascular diseases[19-23] and pain[24-26], we postulated that peripheral sensitization of cardiopulmonary sensory afferents in response to local tissue injury or inflammation leads the sensory neurons to release increased neurotransmitters such as SP and CGRP in the dorsal horn causing sustained astrocyte activation and neuroinflammation in the TSC of PH rats in our study, however, the precise molecular mechanisms and impact of TSC neuroinflammation and associated SNS activation on cardiopulmonary function in PH and RVF still remained elusive. The work included in this dissertation focuses on a novel approach to study the

new concept of integration between neuroinflammation and sympathoexcitation in the pathogenesis of PH. We aim to better understand the neuroimmune crosstalk around cardiovascular autonomic neural circuits within the CNS, particularly in the TSC that regulate sympathetic activity and introduce the hypothesis of a mechanistic role of neuroinflammation mediated sympathoexcitation in PH and RVF.

We investigated cardiopulmonary afferent signaling in the TSC in PH-RVF and discovered through histological and functional evidence that TRPV1 expressing afferent nerve endings in thoracic dorsal horn release increased SP in PH-RVF to mediate cardiopulmonary sympathoexcitatory reflex in MCT- and SuHx-induced PH as well as patients with PAH. Moreover, we demonstrated that sensitizing TRPV1 receptors with bradykinin in the cardiac sympathetic afferent nerve endings elicits autonomic reflex characterized by increased RVSP and heart rate in MCT-induced PH-RVF rats demonstrating that TRPV1 expressing afferent nerve endings in the thoracic dorsal horn may be responsible for sympathoexcitatory signal transmission in PH. We then performed first-ever transcriptomic analysis on TSC of MCT and SuHx rats to determine the impact of PH and RVF on TRPV1-mediated TSC gene expression. RNASeq delineated common dysregulated genes and pathways between the two rat models highlighting neuroinflammation and apoptosis within the remodeled TSC. Many inflammatory genes such as ALOX15, CX3CL1, EDN1, mTOR, NOTCH3, NF-κB-1, STAT3, ICAM-1 and NOS1 were significantly enriched in several upregulated proinflammatory pathways including IL-6 JAK-STAT3 signaling, IL-2 STAT5 signaling, TNF-α signaling via NF-κB, hypoxia and KRAS signaling in both rat models (**Chapter 2**). In fact, CX3CL1 has been implicated in classical microglial activation-mediated sympathoexcitation in the brain of MCT-treated rats and hypoxic mice[16,17,27,28]. Previous studies demonstrated that TRPV1 activation in

sensory nerve endings releases CGRP, glutamate, and SP, which modulate microglial activation via NF-κB[29]. NF-κB-mediated microglial activation is also regulated by notch signaling[30] and mTOR[31]. Activated microglia express several proinflammatory factors, such as TNF-α, IL-6, MCP-1, ICAM-1, and VCAM-1, which mediate neuroinflammation and excitotoxic neuronal damage[21–23]. Interestingly, no significant changes in inflammation-related gene expression were seen in lumbar spinal cords of MCT- and SuHx-treated rats suggesting TSC-specific neuroinflammation is likely due to direct cardiopulmonary neural connections (**Chapter 2**).

We observed microgliosis- and astrogliosis-mediated neuroinflammation and increased fractalkine, Cx3Cl1 expression in the TSC of both rat models and patients with PAH. TSC RNASeq revealed a number of pro-apoptotic genes including TP53, PRF1, FOXO3, TGFβ1, and NCOR2 that were enriched in several apoptotic pathways. Moreover, increased neuronal apoptosis in the TSC was validated by TUNEL and CC3 staining in both rat models. Significantly elevated glutamatergic signaling and NPY expression in the TSC and plasma norepinephrine in both rat models confirmed increased sympathoexcitation. However, our time-course experiments demonstrated that initial signs of PH coincided with early phase of TSC neuroinflammation without significant apoptosis and sympathoexcitation in the MCT rats. Interestingly, intrathecal microglial activation inhibitor, minocycline administration decreased microgliosis, astrogliosis and expression of proinflammatory cytokines in the TSC and reduced sympathoexcitation resulting in rescue of PH-RVF. These studies demonstrated the regulatory role of microglial and astrocytic activation-mediated TSC neuroinflammation and SNS activation in the progression of experimental PH and RVF. However, the role of TRPV1 activation in TSC neuroinflammation, sympathoexcitation and cardiopulmonary function in PH still remained

unknown (**chapter 2**).

TRPV1 activation has been implicated in NMDAR mediated NOS1 activation and ˙NO production leading to oxidative and nitrosative stress, neuroinflammation, chemokine release, excitotoxicity, and neuronal apoptosis in the CNS[32-35]. Moreover, TRPV1 activation in the thoracic dorsal horn has been shown to promote microglial activation mediated release of inflammatory cytokines and ROS as well as regulate NF-κB pathway mediated neuroinflammation[36-39]. Intrathecal administration of RTX was demonstrated to abolish TRPV1 expression in the dorsal horn, which resulted in reduction of pain, inflammation, thermal hypersensitivity and over-activated CSAR, thereby preventing myocardial hypertrophy, fibrosis, and apoptosis[40-45]. Hence, we administered RTX intrathecally to ablate the TRPV1+ cardiopulmonary sensory nerve endings to determine the role of TRPV1 in TSC NOS1 expression, neuroinflammation, sympathoexcitation and cardiopulmonary function in MCT and SuHx rats. Consequently, we observed that intrathecal RTX administration selectively abolished TRPV1 expression in the thoracic dorsal horn, attenuated PH severity and prevented RVF by decreasing cardiac sympathetic tone in both rat models. We also revealed that mechanistically, NMDAR-NOS1 mediated neuroinflammation and neuronal apoptosis in the TSC in PH is dependent on TRPV1 activation, as intrathecal RTX reduced NMDAR and NOS1 expression, microglial and astrocytic activation and apoptosis in the TSC of MCT rats (**Chapter 3**). Importantly, intrathecal RTX administration prevented PH-induced RV remodeling, including RV hypertrophy, fibrosis, inflammation and apoptosis. Similarly, RTX prevented MCT-induced lung remodeling, including pulmonary arteriolar wall thickness, fibrosis, inflammation and apoptosis. RNASeq of lung and RV tissues from RTX-treated MCT rats demonstrated reversal of several pro-fibrotic (epithelial

mesenchymal transition and TGFβ-signaling), inflammatory (mTORC1, IL2 STAT5, IL6 JAK STAT3 and TNFα-signaling via NFk-B) and apoptotic (p53 pathway) pathways. Several down-regulated pro-fibrotic genes including Vim, Ctsk and Serpine2 in lung and TGFβ1 and SMAD6 in RV, pro-inflammatory genes IL6, CxCl1 and TNF in lung and CxCr4, Ccr4 and STAT3 in RV as well as pro-apoptotic genes IER3, BAK1 and GM2A in lung and TGFβ1, PERP and RRAD in RV were enriched in the aforementioned downregulated pathways (**Chapter 3**). NE has been shown to enhance cardiac fibrosis through TGFβ signaling[46-48]. Moreover, NE was shown to induce oxidative stress, cardiomyocyte hypertrophy, fibrosis, activation of MAPK (Mainly p38 and ERK1/2) and AKT as well as NF-κB to release inflammatory cytokines in cultured cardiomyocytes[49,50]. Further, NE is implicated in the activation of cardiac proinflammatory cytokines IL-6, IL-1β and TNF-α[51-54] and induce apoptosis in rat cardiomyocytes[55,56]. Several studies have demonstrated that NE induces pulmonary injury with edema and inflammation by increased expression of several cytokines[57]. Elevated plasma NE leads to severe inflammatory reactions during transition into pulmonary fibrosis leading to the development of acute lung injury and acute respiratory distress syndrome[58]. Therefore, we believe that the reversal of fibrotic, inflammatory and apoptotic signatures in the lung and RV in RTX-treated MCT rats were due to reduced NE release from the sympathetic nerve terminals, which was evident from reduced plasma NE (**Chapter 3**).

We further investigated downstream of TRPV1 gene and found increased signature of glutamatergic and NOS1 signaling in the TSC of MCT and SuHx rats and patients with PAH. Several pain, neurodegenerative and cardiovascular studies have indicated that during pathologic conditions primary afferent nerve endings increase glutamate release in the spinal dorsal horn, which can become excitotoxic and has the potential to trigger

neurotoxicity[59-67]. Increased glutamate triggers NMDAR activation in the second order spinothalamic neurons, which leads to Ca^{2+} influx and activation of NOS1[59-68]. We demonstrated that mechanistically, NOS1 activation in the TSC is NMDAR-dependent as intrathecal NMDAR specific antagonist AP-5 decreased TSC NOS1 expression, neuroinflammation, neuronal apoptosis and associated sympathoexcitation and rescued PH-RVF in MCT rats. To decipher the role of TSC NOS1 upregulation in neuroinflammation and sympathoexcitation in cardiopulmonary function in PH, we inhibited NOS1 by intrathecal NOS1 specific inhibitor S-Methyl-L-thiocitrulline (SMTC) that attenuated PH and rescued RVF in MCT rats. This rescue was associated with attenuation of TSC neuroinflammation, neuronal apoptosis and reduced markers of sympathoexcitation. Moreover, RV-RNA-Seq demonstrated reversal of pro-fibrotic, inflammatory, apoptotic, SNS, RAAS and arrhythmia signatures, whereas, lung-RNA-Seq demonstrated reversal of pro-fibrotic and inflammatory signatures in SMTC-treated MCT Rats (**Chapter 4**). EMT/EndMT, fibrosis, inflammation and apoptosis play important regulatory role in the development and progression of PH[69-71] and RVF[72]. We validated reduced EndMT, fibrosis and TRPV1-SP expression in RV and lung tissues as well as reduced plasma NE in SMTC-treated MCT rats. NE has been shown to enhance cardiac fibrosis and apoptosis through TGFβ signaling and MMP2[46-48,55,73]. Moreover, NE also plays essential role in tissue repair and formation of extracellular matrix (ECM) during cardiac remodeling process by inducing expression of TGF-β1, TGF-β2, TGF-β3, MMP2, TIMP2 and collagen[46,74]. Our data demonstrated a significant reduction of both TGFβ signaling and MMP2 expression in the RV of SMTC-treated MCT rats leading to reduced fibrosis (**Chapter 4**). Studies have shown that continuous norepinephrine infusion over three days increased mRNA expression of ECM related genes including Coll1, MMP-2,

TIMP-2, and all TGF-β isoforms in the rat lung[58]. Elevated plasma NE leads to severe inflammatory reactions during transition into pulmonary fibrosis leading to the development of acute lung injury and acute respiratory distress syndrome[58]. Moreover, our invitro experiments demonstrated that NE induces increased EndMT in HCAECs and HPAECs and FMT in HCFs. Therefore, we believe that NOS1 inhibition reverses RV and lung transcriptomics through NE as evident by reduced plasma NE level in SMTC-treated MCT rats. Interestingly, SP also plays a key role in inducing cardiac and lung fibrosis, EMT/EndMT, inflammation and apoptosis during various pathological conditions[75-80]. Our invitro experiments demonstrated that SP induces increased EndMT in HCAECs and HPAECs and FMT in HCFs (**Chapter 4**). Consequently, we believe that reduced SP expression in the RV and lung may also play a major role in the reversal of RV and lung transcriptomics in SMTC-treated MCT rats.

Taken together, this dissertation provides compelling evidence that in PH, cardiopulmonary afferent signaling mediated by TRPV1-SP-Glutamate activates NMDAR-NOS1 axis resulting in microglial and astrocytic activation mediated neuroinflammation and neuronal apoptosis in the TSC, which lead to further worsening of PH and RVF by increasing sympathoexcitation. Furthermore, targeted intrathecal inhibition of NOS1 in the TSC may serve as a novel therapeutic strategy for PH and RVF (**Figure 1**). While the studies presented here provide the first insight into the role of TSC neuroinflammation in PH, they also provide a foundation for further investigation into the molecular mechanisms of downstream pathways and genes that will likely lead to even greater understanding of the disease pathophysiology. These future studies are outlined in the following section.

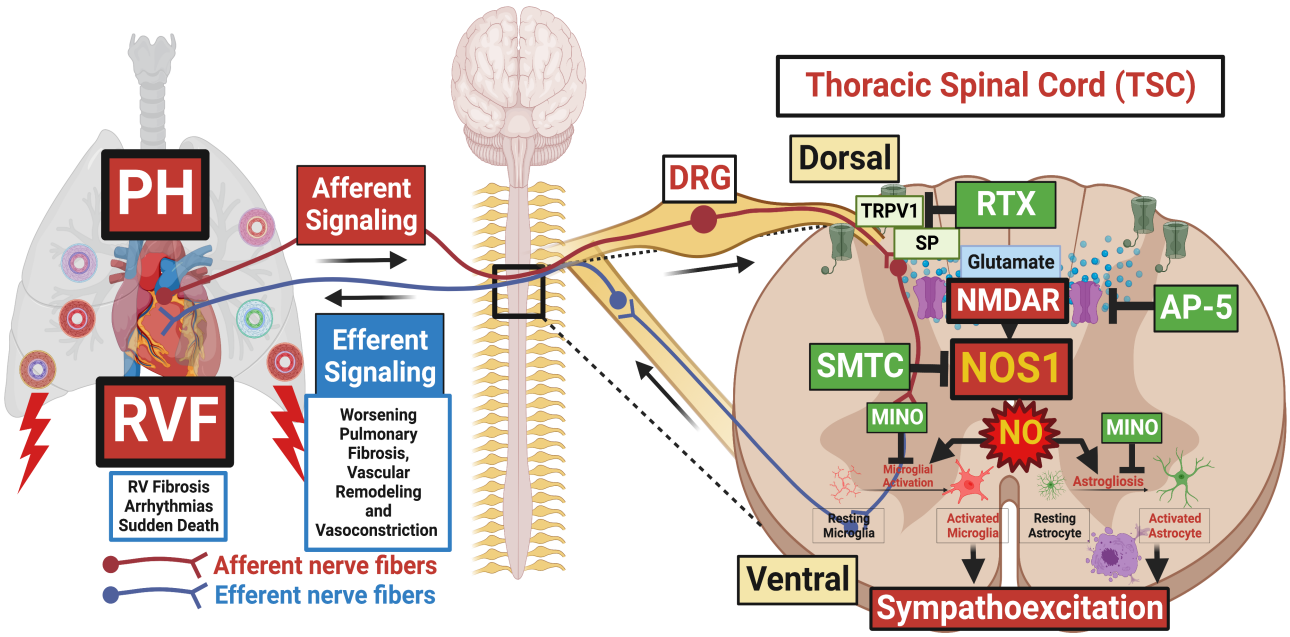

Fig. 1. Schematic of proposed mechanism of TSC neuroinflammation through TRPV1 activation and downstream NOS1 upregulation in PH and potential therapeutic targets. In PH, cardiopulmonary afferent signaling mediated by TRPV1-SP-Glutamate activates NMDAR-NOS1 axis resulting in microglial and astrocytic activation mediated neuroinflammation and neuronal apoptosis in the TSC, which lead to further worsening of PH and RVF by increasing sympathoexcitation. Furthermore, targeted intrathecal inhibition of NOS1 in the TSC may serve as a novel therapeutic strategy for PH and RVF.

Future Directions

Our investigation of TSC neuroinflammation included terminal or endpoint RNASeq analysis of MCT (4-weeks) and SuHx (5-weeks) rat models. Although we performed a timecourse experiment that indicated time dependent progression of TSC neuroinflammation, key gene expression (NOS1, Cx3Cl1), apoptosis and sympathoexcitation in MCT rats, we would perform TSC RNASeq analysis in MCT rats from day-7, day-14 and day-21 to compare TSC transcriptomic remodeling progression with the terminal data point. This will advance our understanding of any potential comparison between early vs. late gene expression. Similarly we would assess TSC transcriptomic remodeling of SuHx rats from day-21 and day-28 and compare with terminal terminal data point.

To better understand the role of microglial and astrocytic activation in TSC neuroinflammation, we would perform RNAScope for key inflammatory genes specific to microglia and astrocytes coupled with their specific respective markers using immunofluorescence at different timepoints as mentioned above. We inhibited microglial activation by intrathecal minocycline administration that demonstrated the regulatory function of TSC microglial activation and production of cytokines in sympathoexcitation in MCT rats. However, to understand the contribution of TSC astrocytic activation in PH, we would perform astrocytic activation inhibition by intrathecal Fluorocitrate[81,82] (after dose response experiments) in MCT and SuHx rats using protocols similar to Minocycline (**Chapter 2**). We will also assess the effect of combined intrathecal Minocycline+Fluorocitrate treatment in MCT and SuHx rats. Besides all the hemodynamics and molecular assessents already described in chapter 2, we would also perform RNAScope+immunofluorescence in TSC vs. lumbar SC after Minocycline and/or

Fluorocitrate treatment.

In our pilot data, we validate some of the key findings from rat TSC in human PAH spinal cord autopsy samples, adding valuable translational relevance. Obtaining fresh human spinal cord samples from PAH patients is extremely challenging, therefore we have used human PAH autopsy samples. Currently, we have a total of 8 human TSC autopsy samples for Group I PH patients and 4 samples for Controls. We recognize the importance of careful human tissue phenotyping and would continue to collect more tissue from Group I PAH patients through our collaborators at UCLA Pathology and Pulmonary Critical Care.

We would confirm time dependent changes of cardiopulmonary afferent signaling in PH by PGP9.5+NOS1 co-immunolabeling in the thoracic DRG and TRPV1+SP co-immunolabeling in the thoracic dorsal horn neurons in MCT and SuHx rats and PAH patients. We would also measure glutamate levels in the TSC at various timepoints. Although chemical ablation of TRPV1+ sensory nerve endings in our MCT and SuHx rats prevented PH-RVF by reducing neuroinflammation, neuronal apoptosis and sympathoexcitation, we would test whether TRPV1 knock-out rat (TRPV1-/-) develops PH-RVF by MCT or SuHx.

We would validate cell type specific NOS1, inflammatory and apoptotic gene expression patterns using RNAScope technology coupled with immunofluorescence for neuronal, microglial and astrocytic markers. As NOS1 is known to be activated by glutamatergic signaling, we would measure glutamate levels in the TSC and compare them to lumbar spinal cord (LSC) in MCT and SuHx rats in a time-dependent fashion and assess if there is any correlation with NOS1 levels. Moreover, NOS1 activation leads to nitrosative stress, therefore we would assess for nitrosative stress markers (e.g. Ap1B1, Ap1M1) with PCR, and measure peroxynitrite levels in TSC *vs.* LSC in PH rats in a time-dependent manner.

We are cognizant of potential off-target effects of intrathecal injections of drugs. Our data showed normal LV pressures and LV function in the SMTC group ruling out off-target effects (**Chapter 4**). However, we would investigate diaphragm and intercostal muscle function to rule out potential off-target effects[83,84]. An alternate approach for NOS1 knockdown could involve the use of siRNA against NOS1 instead of SMTC delivered *via* intrathecal injections. As SMTC is dissolved in PBS, is not lipophilic in nature and is delivered *via* intrathecal route, it is highly unlikely that it will be absorbed in the systemic circulation in any significant proportions. In fact, we did not find any change in lung or RV NOS1 expression or hypotension after 2 weeks of daily intrathecal SMTC administration.

Interestingly, our data strongly suggest attenuation of key EndMT, pro-inflammatory and pro-fibrotic genes and pathways in both lungs and RV of SMTC treated rats (**Chapter 4**). These key pathways involved in lung and RV remodeling associated with SNS activation in PH and RVF[11,72,85-87] are likely mediated *via* norepinephrine and Substance P (**Chapter 4**). The principal neurotransmitter released by postganglionic sympathetic neurons is norepinephrine[11], whereas neuropeptide substance P is released by sensory afferent C fiber nerve endings[88]. Substance P can directly regulate vascular tone, tends to act as a vasoconstrictor in the pulmonary circulation and increases in the lungs during experimental PH[88]. Further delineation of these pathways would help us understand the mechanisms of regression of lung and RV remodeling by SMTC. Specifically, we will assess lung, RV and plasma norepinephrine (ELISA) and Substance P (ELISA+IF) and validate inflammation (ELISA for cytokines and immunofluorescence for inflammatory cell markers) and EMT/EndMT (α-SMA+CD31 co-immunolabeling, EMT transcription factors and EMT genes by PCR and WB) in lung and RV[72].

Investigating afferent signaling, neuroinflammation and apoptosis in the thoracic DRGs would be instrumental in MCT and SuHx rats, since the sympathetic ganglia within the DRG controls cardiopulmonary sympathetic output. Therefore, we would perform RNASeq analysis of the thoracic DRGs from MCT and SuHx rats as well as assess microglial and astrocytic activation at different time points.

Finally, we are aware of the disruption of blood spinal cord barrier (BSCB) as an additional source of recruitment of inflammatory and immune cells to the TSC[89]. As an alternative approach, we will consider investigating the contributory role of disrupted BSCB in TSC neuroinflammation in PH. However, our main hypothesis revolves around cardiopulmonary afferent signaling-induced activation of NMDAR-NOS1 axis as the main source for TSC neuroinflammation and apoptosis as strongly demonstrated by our data.

Final remarks from the author

PAH is a rare but terminal pulmonary vascular disease that lead to right heart failure. The current treatments for this devastating disease are largely inadequate, and research into novel therapeutic strategies is pivotal to increase patient survival. It has been a privilege to study this disease, provide novel insight into its pathogenesis and extend hope to affected patients. I strongly believe that the preclinical therapies reported in this work will get to clinical trials someday, given that the intrathecal drug delivery is an already approved mode of treatment for patients in the hospitals. Finally, I hope that this dissertation will encourage researchers to investigate into PH pathophysiology beyond the vasomotor pathways of the lung.

References

1. Simonneau G, Montani D, Celermajer DS, Denton CP, Gatzoulis MA, Krowka M, Williams PG, Souza R. Hemodynamic definitions and updated clinical classification of pulmonary hypertension. Eur Respir J2019; 53:doi: 10.1183/13993003.01913-2018.
2. Dandel M, et al. Assessment of right ventricular adaptability to loading conditions can improve the timing of listing to transplantation in patients with pulmonary arterial hypertension. J Heart Lung Transplant. 2015;3:319-28. doi: 10.1016/j.healun.2014.11.012.
3. Vaillancourt M, Chia P, Sarji S, Nguyen J, Hoftman N, Ruffenach G, Eghbali M, Mahajan A, Umar S. Autonomic nervous system involvement in pulmonary arterial hypertension. Respir Res. 2017 Dec 4;18(1):201. doi: 10.1186/s12931-017-0679-6. PMID: 29202826; PMCID: PMC5715548.
4. Wensel R, Jilek C, Dörr M, Francis DP, Stadler H, Lange T, Blumberg F, Opitz C, Pfeifer M, and Ewert R. Impaired cardiac autonomic control relates to disease severity in pulmonary hypertension. Eur Respir J 34: 895–901, 2009.
5. Velez-Roa S, Ciarka A, Najem B, Vachiery JL, Naeije R, and van de Borne P. Increased sympathetic nerve activity in pulmonary artery hypertension. Circulation 110: 1308–1312, 2004.
6. Ciarka A, Doan V, Velez-Roa S, Naeije R, and van de Borne P. Prognostic significance of sympathetic nervous system activation in pulmonary arterial hypertension. Am J Respir Crit Care Med 181: 1269–1275, 2010.
7. Oliveira AC, Richards EM, Raizada MK. Pulmonary hypertension: Pathophysiology beyond the lung. Pharmacol Res. 2020 Jan;151:104518. doi:

10.1016/j.phrs.2019.104518. Epub 2019 Nov 13. PMID: 31730803; PMCID: PMC6981289.

8. Razee A, Banerjee S, Hong J, Magaki S, Fishbein G, Ajijola OA, Umar S. Thoracic Spinal Cord Neuroinflammation as a Novel Therapeutic Target in Pulmonary Hypertension. Hypertension. 2023 Jun;80(6):1297-1310. doi: 10.1161/HYPERTENSIONAHA.122.20782. Epub 2023 Apr 24. PMID: 37092338; PMCID: PMC10192067.
9. Fonkoue IT, Le NA, Kankam ML, DaCosta D, Jones TN, Marvar PJ, Park J. Sympathoexcitation and impaired arterial baroreflex sensitivity are linked to vascular inflammation in individuals with elevated resting blood pressure. Physiol Rep. 2019 Apr;7(7):e14057. doi: 10.14814/phy2.14057. PMID: 30968587; PMCID: PMC6456445.
10. Veiga AC, Milanez MIO, Ferreira GR, Lopes NR, Santos CP, De Angelis K, Garcia ML, Oyama LM, Gomes GN, Nogueira FN, Carvalho PM, Campos RR, Bergamaschi CT, Nishi EE. Selective afferent renal denervation mitigates renal and splanchnic sympathetic nerve overactivity and renal function in chronic kidney disease-induced hypertension. J Hypertens 38: 765–773, 2020. doi:10.1097/HJH.0000000000002304.
11. Vaillancourt, M., Chia, P., Sarji, S. et al. Autonomic nervous system involvement in pulmonary arterial hypertension. Respir Res 18, 201 (2017). https://doi.org/10.1186/s12931-017-0679-6.
12. Wang M, Li S, Zhou X, et al. Increased inflammation promotes ventricular arrhythmia through aggravating left stellate ganglion remodeling in a canine ischemia model. Int J Cardiol. 2017;248:286–293. doi: 10.1016/j.ijcard.2017.08.011
13. Wang Y, Jiang W, Chen H, et al. Sympathetic nervous system mediates cardiac

remodeling after myocardial infarction in a circadian disruption model. Front Cardiovasc Med. 2021;**8**:668387. doi: 10.3389/fcvm.2021.668387.

14. Rosenkranz S, Howard LS, Gomberg-Maitland M, Hoeper MM. Systemic Consequences of Pulmonary Hypertension and Right-Sided Heart Failure. Circulation. 2020 Feb 25;141(8):678-693. doi: 10.1161/CIRCULATIONAHA.116.022362. Epub 2020 Feb 24. PMID: 32091921.
15. Yoshida K, Saku K, Kamada K, Abe K, Tanaka-Ishikawa M, Tohyama T, Nishikawa T, Kishi T, Sunagawa K, Tsutsui H. Electrical Vagal Nerve Stimulation Ameliorates Pulmonary Vascular Remodeling and Improves Survival in Rats With Severe Pulmonary Arterial Hypertension. JACC Basic Transl Sci. 2018 Nov 12;3(5):657-671. doi: 10.1016/j.jacbts.2018.07.007. PMID: 30456337; PMCID: PMC6234524.
16. Sharma RK, Oliveira AC, Kim S, Rigatto K, Zubcevic J, Rathinasabapathy A, Kumar A, Lebowitz JJ, Khoshbouei H, Lobaton G, Aquino V, Richards EM, Katovich MJ, Shenoy V, and Raizada MK. Involvement of Neuroinflammation in the Pathogenesis of Monocrotaline-Induced Pulmonary Hypertension. Hypertension 71: 1156–1163, 2018.
17. Oliveira AC, Sharma RK, Aquino V, Lobaton G, Bryant AJ, Harrison JK, Richards EM, and Raizada MK. Involvement of Microglial Cells in Hypoxia-induced Pulmonary Hypertension. Am J Respir Cell Mol Biol 59: 271–273, 2018.
18. Vaillancourt M, Chia P, Medzikovic L, Cao N, Ruffenach G, Younessi D, Umar S. Experimental Pulmonary Hypertension Is Associated With Neuroinflammation in the Spinal Cord. Front Physiol. 2019 Sep 20;10:1186. doi: 10.3389/fphys.2019.01186. PMID: 31616310; PMCID: PMC6764190.
19. Saddic LA, Howard-Quijano K, Kipke J, Kubo Y, Dale EA, Hoover D, Shivkumar K,

Eghbali M, Mahajan A. Progression of myocardial ischemia leads to unique changes in immediate-early gene expression in the spinal cord dorsal horn. Am J Physiol Heart Circ Physiol. 2018 Dec 1;315(6):H1592-H1601. doi: 10.1152/ajpheart.00337.2018.

20. Wang HJ, Rozanski GJ, Zucker IH. Cardiac sympathetic afferent reflex control of cardiac function in normal and chronic heart failure states. J Physiol. 2017 Apr 15;595(8):2519-2534. doi: 10.1113/JP273764. Epub 2017 Feb 27. PMID: 28116751; PMCID: PMC5390865.
21. Steagall RJ, Sipe AL, Williams CA, Joyner WL, Singh K. Substance P release in response to cardiac ischemia from rat thoracic spinal dorsal horn is mediated by TRPV1. Neuroscience. 2012 Jul 12;214:106-19. doi: 10.1016/j.neuroscience.2012.04.023. Epub 2012 Apr 21. PMID: 22525132.
22. Zahner MR, Li DP, Chen SR, Pan HL. Cardiac vanilloid receptor 1-expressing afferent nerves and their role in the cardiogenic sympathetic reflex in rats. J Physiol. 2003 Sep 1;551(Pt 2):515-23. doi: 10.1113/jphysiol.2003.048207. Epub 2003 Jun 26. PMID: 12829722; PMCID: PMC2343227.
23. Kong WL, Peng YY, Peng BW. Modulation of neuroinflammation: Role and therapeutic potential of TRPV1 in the neuro-immune axis. Brain Behav Immun. 2017 Aug;64:354-366. doi: 10.1016/j.bbi.2017.03.007. Epub 2017 Mar 22. PMID: 28342781.
24. Iyengar, S., Ossipov, M. H., and Johnson, K. W. (2017). The role of calcitonin gene-related peptide in peripheral and central pain mechanisms including migraine. Pain 158, 543–559. doi: 10.1097/j.pain.0000000000000831.
25. Pan XQ, Gonzalez JA, Chang S, et al. Experimental colitis triggers the release of

substance P and calcitonin gene-related peptide in the urinary bladder via TRPV1 signaling pathways. Exp Neurol. 2010;225:262–273.

26. Old EA, Malcangio M. Chemokine mediated neuron-glia communication and aberrant signalling in neuropathic pain states. Curr Opin Pharmacol. 2012;12(1):67–73. doi: 10.1016/j.coph.2011.10.015.
27. Liu Y, Wu XM, Luo QQ, Huang S, Yang QW, Wang FX, Ke Y, Qian ZM. CX3CL1/CX3CR1-mediated microglia activation plays a detrimental role in ischemic mice brain via p38MAPK/PKC pathway. J Cereb Blood Flow Metab. 2015 Oct;35(10):1623-31. doi: 10.1038/jcbfm.2015.97. Epub 2015 May 13. PMID: 25966946; PMCID: PMC4640309.
28. Milior G, Lecours C, Samson L, Bisht K, Poggini S, Pagani F, Deflorio C, Lauro C, Alboni S, Limatola C et al. Fractalkine receptor deficiency impairs microglial and neuronal responsiveness to chronic stress. Brain Behav Immun. 2016 Jul;55:114-125. doi: 10.1016/j.bbi.2015.07.024.
29. Zhang X, Ye L, Huang Y, Ding X, Wang L. The potential role of TRPV1 in pulmonary hypertension: Angel or demon? Channels (Austin). 2019 Dec;13(1):235-246. doi: 10.1080/19336950.2019.1631106. PMID: 31189399; PMCID: PMC6602577.
30. Yao L, Kan EM, Kaur C, Dheen ST, Hao A, Lu J, Ling EA. Notch-1 signaling regulates microglia activation via NF-κB pathway after hypoxic exposure in vivo and in vitro. PLoS One. 2013 Nov 6;8(11):e78439. doi: 10.1371/journal.pone.0078439. PMID: 24223152; PMCID: PMC3819391.
31. Xu T, Liu J, Li XR, Yu Y, Luo X, Zheng X, Cheng Y, Yu PQ, Liu Y. The mTOR/NF-κB Pathway Mediates Neuroinflammation and Synaptic Plasticity in Diabetic

Encephalopathy. Mol Neurobiol. 2021 Aug;58(8):3848-3862. doi: 10.1007/s12035-021-02390-1. Epub 2021 Apr 15. PMID: 33860440.

32. Carletti F, Gambino G, Rizzo V, Ferraro G, Sardo P. Neuronal nitric oxide synthase is involved in CB/TRPV1 signalling: Focus on control of hippocampal hyperexcitability. Epilepsy Res. 2017 Dec;138:18-25. doi: 10.1016/j.eplepsyres.2017.09.018. Epub 2017 Oct 3. PMID: 29035821.
33. Chen Y, Willcockson HH, Valtschanoff JG. Influence of the vanilloid receptor TRPV1 on the activation of spinal cord glia in mouse models of pain. Exp Neurol. 2009 Dec;220(2):383-90. doi: 10.1016/j.expneurol.2009.09.030. Epub 2009 Oct 6. PMID: 19815011; PMCID: PMC2784271.
34. Hwang SJ, Burette A, Rustioni A, Valtschanoff JG. Vanilloid receptor VR1-positive primary afferents are glutamatergic and contact spinal neurons that co-express neurokinin receptor NK1 and glutamate receptors. J Neurocytol. 2004 May;33(3):321-9. doi: 10.1023/B:NEUR.0000044193.31523.a1. PMID: 15475687.
35. Peters JH, McDougall SJ, Fawley JA, Smith SM, Andresen MC. Primary afferent activation of thermosensitive TRPV1 triggers asynchronous glutamate release at central neurons. Neuron. 2010 Mar 11;65(5):657-69. doi: 10.1016/j.neuron.2010.02.017. PMID: 20223201; PMCID: PMC2837850.
36. Talbot S, Dias JP, Lahjouji K, Bogo MR, Campos MM, Gaudreau P, Couture R. Activation of TRPV1 by capsaicin induces functional kinin B(1) receptor in rat spinal cord microglia. J Neuroinflammation. 2012 Jan 20;9:16. doi: 10.1186/1742-2094-9-16. PMID: 22264228; PMCID: PMC3282640.
37. Chen Y, Willcockson HH, Valtschanoff JG. Influence of the vanilloid receptor TRPV1 on the activation of spinal cord glia in mouse models of pain. Exp Neurol. 2009

Dec;220(2):383-90. doi: 10.1016/j.expneurol.2009.09.030. Epub 2009 Oct 6. PMID: 19815011; PMCID: PMC2784271.

38. Hassan S, Eldeeb K, Millns PJ, Bennett AJ, Alexander SP, Kendall DA. Cannabidiol enhances microglial phagocytosis via transient receptor potential (TRP) channel activation. Br J Pharmacol. 2014 May;171(9):2426-39. doi: 10.1111/bph.12615. PMID: 24641282; PMCID: PMC3997281.
39. Doly S, Fischer J, Salio C, Conrath M. The vanilloid receptor-1 is expressed in rat spinal dorsal horn astrocytes. Neurosci Lett. 2004 Mar 4;357(2):123-6. doi: 10.1016/j.neulet.2003.12.051. PMID: 15036590.
40. Wang D., Wu Y., Chen Y., Wang A., Lv K., Kong X., et al. (2019). Focal Selective Chemo-Ablation of Spinal Cardiac Afferent Nerve by Resiniferatoxin Protects the Heart from Pressure Overload-Induced Hypertrophy. Biomed. Pharmacother. 109, 377–385. 10.1016/j.biopha.2018.10.156
41. M. Bishnoi, C.A. Bosgraaf, L.S. Premkumar, Preservation of acute pain and efferent functions following intrathecal resiniferatoxin-induced analgesia in rats, J. Pain 12 (2011) 991–1003.
42. M. Leo, M. Schulte, L.I. Schmitt, M. Schafers, C. Kleinschnitz, T. Hagenacker, Intrathecal resiniferatoxin modulates TRPV1 in DRG neurons and reduces TNF-induced pain-related behavior, Mediat. Inflamm. 2017 (2017) 2786427.
43. L. Karai, D.C. Brown, A.J. Mannes, S.T. Connelly, J. Brown, M. Gandal, et al., Deletion of vanilloid receptor 1-expressing primary afferent neurons for pain con-trol, J. Clin. Invest. 113 (2004) 1344–1352.
44. Horton J. S., Shiraishi T., Alfulaij N., Small-Howard A. L., Turner H. C., Kurokawa T., et al. (2019). TRPV1 Is a Component of the Atrial Natriuretic Signaling Complex, and

Using Orally Delivered Antagonists, Presents a Valid Therapeutic Target in the Longitudinal Reversal and Treatment of Cardiac Hypertrophy and Heart Failure. Channels 13, 1–16. 10.1080/19336950.2018.1547611

45. M.R. Sapio, J.K. Neubert, D.M. LaPaglia, D. Maric, J.M. Keller, S.J. Raithel, et al., Pain control through selective chemo-axotomy of centrally projecting TRPV1+ sensory neurons, J. Clin. Invest. 128 (April (4)) (2018) 1657–1670.
46. Akiyama-Uchida Y, Ashizawa N, Ohtsuru A, Seto S, Tsukazaki T, Kikuchi H, Yamashita S, Yano K. Norepinephrine enhances fibrosis mediated by TGF-beta in cardiac fibroblasts. Hypertension. 2002 Aug;40(2):148-54. doi: 10.1161/01.hyp.0000025443.61926.12. PMID: 12154105.
47. Tian CJ, Pang X. Ca2+-calcineurin signaling is involved in norepinephrine-induced cardiac fibroblasts activation. Int J Clin Exp Pathol. 2015 May 1;8(5):5210-6. PMID: 26191219; PMCID: PMC4503091.
48. Dincer HE, Gangopadhyay N, Wang R, Uhal BD. Norepinephrine induces alveolar epithelial apoptosis mediated by alpha-, beta-, and angiotensin receptor activation. Am J Physiol Lung Cell Mol Physiol. 2001 Sep;281(3):L624-30. doi: 10.1152/ajplung.2001.281.3.L624. PMID: 11504689.
49. Tang K, Zhong B, Luo Q, Liu Q, Chen X, Cao D, Li X, Yang S. Phillyrin attenuates norepinephrine-induced cardiac hypertrophy and inflammatory response by suppressing p38/ERK1/2 MAPK and AKT/NF-kappaB pathways. Eur J Pharmacol. 2022 Jul 15;927:175022. doi: 10.1016/j.ejphar.2022.175022. Epub 2022 May 13. PMID: 35569549.
50. Briest W, Hölzl A, Rassler B, Deten A, Leicht M, Baba HA, Zimmer HG. Cardiac remodeling after long term norepinephrine treatment in rats. Cardiovasc Res. 2001

Nov;52(2):265-73. doi: 10.1016/s0008-6363(01)00398-4. PMID: 11684074.

51. Briest W, Elsner C, Hemker J, Müller-Strahl G, Zimmer HG. Norepinephrine-induced expression of cytokines in isolated biventricular working rat hearts. Mol Cell Biochem. 2003 Mar;245(1-2):69-76. doi: 10.1023/a:1022861609896. PMID: 12708746.
52. Barth W, Deten A, Bauer M, Reinohs M, Leicht M, Zimmer HG. Differential remodeling of the left and right heart after norepinephrine treatment in rats: studies on cytokines and collagen. J Mol Cell Cardiol. 2000 Feb;32(2):273-84. doi: 10.1006/jmcc.1999.1075. PMID: 10722803.
53. Leicht M, Briest W, Zimmer HG. Regulation of norepinephrine-induced proliferation in cardiac fibroblasts by interleukin-6 and p42/p44 mitogen activated protein kinase. Mol Cell Biochem. 2003 Jan;243(1-2):65-72. doi: 10.1023/a:1021655023870. PMID: 12619890.
54. Briest W, Rassler B, Deten A, Leicht M, Morwinski R, Neichel D, Wallukat G, Ziegelhöffer T, Zimmer HG. Norepinephrine-induced interleukin-6 increase in rat hearts: differential signal transduction in myocytes and non-myocytes. Pflugers Arch. 2003 Jul;446(4):437-46. doi: 10.1007/s00424-003-1043-x. Epub 2003 May 6. PMID: 12733076.
55. Fu YC, Chi CS, Yin SC, Hwang B, Chiu YT, Hsu SL. Norepinephrine induces apoptosis in neonatal rat endothelial cells via down-regulation of Bcl-2 and activation of beta-adrenergic and caspase-2 pathways. Cardiovasc Res. 2004 Jan 1;61(1):143-51. doi: 10.1016/j.car
56. Fu YC, Chi CS, Yin SC, Hwang B, Chiu YT, Hsu SL. Norepinephrine induces apoptosis in neonatal rat cardiomyocytes through a reactive oxygen species-TNF

alpha-caspase signaling pathway. Cardiovasc Res. 2004 Jun 1;62(3):558-67. doi: 10.1016/j.cardiores.2004.01.039. PMID: 15158148.

57. Rassler B, Rohling MA, Reissig C, Briest W, Tannapfel A, Zimmer HG. Involvement of cytokines and inflammation in catecholamine-induced pulmonary injury in rats. Vascular Disease Prevention. 2005 Jan 1;2(1):1-9.
58. Rassler B, Marx G, Schierle K, Zimmer HG. Catecholamines can induce pulmonary remodeling in rats. Cell Physiol Biochem. 2012;30(5):1134-47. doi: 10.1159/000343304. Epub 2012 Oct 5. PMID: 23171784.
59. Ahlawat A, Rana A, Goyal N, Sharma S. Potential role of nitric oxide synthase isoforms in pathophysiology of neuropathic pain. Inflammopharmacology. 2014 Oct;22(5):269-78. doi: 10.1007/s10787-014-0213-0. Epub 2014 Aug 6. PMID: 25095760.
60. Rameau GA, Chiu LY, Ziff EB. NMDA receptor regulation of nNOS phosphorylation and induction of neuron death. Neurobiol Aging. 2003 Dec;24(8):1123-33. doi: 10.1016/j.neurobiolaging.2003.07.002. PMID: 14643384.
61. Freire MA, Guimarães JS, Leal WG, Pereira A. Pain modulation by nitric oxide in the spinal cord. Front Neurosci. 2009 Sep 15;3(2):175-81. doi: 10.3389/neuro.01.024.2009. PMID: 20011139; PMCID: PMC2751623.
62. Esplugues JV. NO as a signaling molecule in the nervous system. Br J Pharmacol. 2002 Mar;135(5):1079-95. doi: 10.1038/sj.bjp.0704569. PMID: 11877313; PMCID: PMC1573233.
63. Cury Y, Picolo G, Gutierrez VP, Ferreira SH. Pain and analgesia: The dual effect of nitric oxide in the nociceptive system. Nitric Oxide. 2011 Oct 30;25(3):243-54. doi: 10.1016/j.niox.2011.06.004. Epub 2011 Jun 24. PMID: 21723953.

64. Yuste JE, Tarragon E, Campuzano CM, Ros-Bernal F. Implications of glial nitric oxide in neurodegenerative diseases. Front Cell Neurosci. 2015 Aug 17;9:322. doi: 10.3389/fncel.2015.00322. PMID: 26347610; PMCID: PMC4538301.
65. Liñares D, Taconis M, Maña P, Correcha M, Fordham S, Staykova M, Willenborg DO. Neuronal nitric oxide synthase plays a key role in CNS demyelination. J Neurosci. 2006 Dec 6;26(49):12672-81. doi: 10.1523/JNEUROSCI.0294-06.2006. PMID: 17151270; PMCID: PMC6674851.
66. Reis PA, de Albuquerque CFG, Gutierrez TM, Silva AR, de Castro Faria Neto HC. Role of nitric oxide synthase in the function of the central nervous system under normal and infectious conditions. In: Saravi SSS, editor. Nitric Oxide Synthase – Simple Enzyme-Complex Roles. London: InTech (2017). p. 55–70.
67. Komers R, Oyama TT, Chapman JG, Allison KM, Anderson S. Effects of systemic inhibition of neuronal nitric oxide synthase in diabetic rats. Hypertension. 2000 Feb;35(2):655-61. doi: 10.1161/01.hyp.35.2.655. PMID: 10679513.
68. Ally A, Powell I, Ally MM, Chaitoff K, Nauli SM. Role of neuronal nitric oxide synthase on cardiovascular functions in physiological and pathophysiological states. Nitric Oxide. 2020 Sep 1;102:52-73. doi: 10.1016/j.niox.2020.06.004. Epub 2020 Jun 23. PMID: 32590118; PMCID: PMC7375925.
69. Ranchoux B, Antigny F, Rucker-Martin C, Hautefort A, Péchoux C, Bogaard HJ, Dorfmüller P, Remy S, Lecerf F, Planté S, Chat S, Fadel E, Houssaini A, Anegon I, Adnot S, Simonneau G, Humbert M, Cohen-Kaminsky S, Perros F. Endothelial-to-mesenchymal transition in pulmonary hypertension. Circulation. 2015 Mar 17;131(11):1006-18. doi: 10.1161/CIRCULATIONAHA.114.008750. Epub 2015 Jan 15. PMID: 25593290.

70. Sydykov A, Mamazhakypov A, Petrovic A, Kosanovic D, Sarybaev AS, Weissmann N, Ghofrani HA, Schermuly RT. Inflammatory Mediators Drive Adverse Right Ventricular Remodeling and Dysfunction and Serve as Potential Biomarkers. Front Physiol. 2018 May 23;9:609. doi: 10.3389/fphys.2018.00609. PMID: 29875701; PMCID: PMC5974151.
71. Michelakis ED. Spatio-temporal diversity of apoptosis within the vascular wall in pulmonary arterial hypertension: heterogeneous BMP signaling may have therapeutic implications. Circ Res. 2006 Feb 3;98(2):172-5. doi: 10.1161/01.RES.0000204572.65400.a5. PMID: 16456109.
72. Park JF, Clark VR, Banerjee S, Hong J, Razee A, Williams T, Fishbein G, Saddic L, Umar S. Transcriptomic Analysis of Right Ventricular Remodeling in Two Rat Models of Pulmonary Hypertension: Identification and Validation of EMT in Human Right Ventricular Failure. Circ Heart Fail. 2021 Feb 5:CIRCHEARTFAILURE120007058. doi: 10.1161/CIRCHEARTFAILURE.120.007058. Online ahead of print. PMID: 33541093.
73. Lai KB, Sanderson JE, Yu CM. High dose norepinephrine-induced apoptosis in cultured rat cardiac fibroblast. Int J Cardiol. 2009 Jul 24;136(1):33-9. doi: 10.1016/j.ijcard.2008.04.022. PMID: 18675472.
74. Briest W, Homagk L, Rassler B, Ziegelhöffer-Mihalovicová B, Meier H, Tannapfel A, Leiblein S, Saalbach A, Deten A, Zimmer HG. Norepinephrine-induced changes in cardiac transforming growth factor-beta isoform expression pattern of female and male rats. Hypertension. 2004 Oct;44(4):410-8. doi: 10.1161/01.HYP.0000141414.87026.4d. Epub 2004 Aug 23. PMID: 15326086.

75. Villablanca AC, Murphy CJ, Reid TW. Growth-promoting effects of substance P on endothelial cells in vitro. Synergism with calcitonin gene-related peptide, insulin, and plasma factors. Circ Res. 1994 Dec;75(6):1113-20. doi: 10.1161/01.res.75.6.1113. PMID: 7525104.
76. Słoniecka M, Danielson P. Substance P induces fibrotic changes through activation of the RhoA/ROCK pathway in an in vitro human corneal fibrosis model. J Mol Med (Berl). 2019 Oct;97(10):1477-1489. doi: 10.1007/s00109-019-01827-4. Epub 2019 Aug 9. PMID: 31399750; PMCID: PMC6746877.
77. Kähler CM, Sitte BA, Reinisch N, Wiedermann CJ. Stimulation of the chemotactic migration of human fibroblasts by substance P. Eur J Pharmacol. 1993 Nov 16;249(3):281-6. doi: 10.1016/0014-2999(93)90523-k. PMID: 7507058.
78. Peng L, Agogo GO, Guo J, Yan M. Substance P and fibrotic diseases. Neuropeptides. 2019 Aug;76:101941. doi: 10.1016/j.npep.2019.101941. Epub 2019 Jun 24. PMID: 31256921.
79. Xu Y, Gu Q, Qu C. Capsaicin pretreatment reversed pulmonary arterial hypertension by alleviating inflammation via p38MAPK pathway. Exp Lung Res. 2017 Feb;43(1):8-18. doi: 10.1080/01902148.2016.1271481. Epub 2017 Mar 10. PMID: 28281854.
80. O'Connor TM, O'Connell J, O'Brien DI, Goode T, Bredin CP, Shanahan F. The role of substance P in inflammatory disease. J Cell Physiol. 2004 Nov;201(2):167-80. doi: 10.1002/jcp.20061. PMID: 15334652.
81. Nakagawa T, Wakamatsu K, Zhang N, Maeda S, Minami M, Satoh M, Kaneko S. Intrathecal administration of ATP produces long-lasting allodynia in rats: differential mechanisms in the phase of the induction and maintenance. Neuroscience. 2007 Jun

29;147(2):445-55. doi: 10.1016/j.neuroscience.2007.03.045. Epub 2007 Jun 1. PMID: 17543465.

82. Xu Y, Cheng G, Zhu Y, Zhang X, Pu S, Wu J, Lv Y, Du D. Anti-nociceptive roles of the glia-specific metabolic inhibitor fluorocitrate in paclitaxel-evoked neuropathic pain. Acta Biochim Biophys Sin (Shanghai). 2016 Oct;48(10):902-908. doi: 10.1093/abbs/gmw083. Epub 2016 Aug 25. PMID: 27563006.
83. Martin M, Li K, Wright MC, Lepore AC. Functional and morphological assessment of diaphragm innervation by phrenic motor neurons. J Vis Exp. 2015 May 25;(99):e52605. doi: 10.3791/52605. PMID: 26066371; PMCID: PMC4542903.
84. Fayssoil A, Michel-Flutot P, Lofaso F, Carlier R, El Hajjam M, Vinit S, Mansart A. Analysis of inspiratory and expiratory muscles using ultrasound in rats: A reproducible and non-invasive tool to study respiratory function. Respir Physiol Neurobiol. 2021 Mar;285:103596. doi: 10.1016/j.resp.2020.103596. Epub 2020 Dec 7. PMID: 33301966.
85. Bogaard HJ, Natarajan R, Mizuno S, Abbate A, Chang PJ, Chau VQ, et al. Adrenergic receptor blockade reverses right heart remodeling and dysfunction in pulmonary hypertensive rats. Am J Respir Crit Care Med. 2010;182(5):652–60.
86. Maron BA, Zhang Y-Y, White K, Chan SY, Handy DE, Mahoney CE, et al. Aldosterone inactivates the endothelin-B receptor via a cysteinyl thiol redox switch to decrease pulmonary endothelial nitric oxide levels and modulate pulmonary arterial hypertension. Circulation. 2012;126(8):963–74.
87. Ranchoux B, Antigny F, Rucker-Martin C, Hautefort A, Péchoux C, Bogaard HJ, Dorfmüller P, Remy S, Lecerf F, Planté S, Chat S, Fadel E, Houssaini A, Anegon I, Adnot S, Simonneau G, Humbert M, Cohen-Kaminsky S, Perros F. Endothelial-to-

mesenchymal transition in pulmonary hypertension. Circulation. 2015 Mar 17;131(11):1006-18. doi: 10.1161/CIRCULATIONAHA.114.008750. Epub 2015 Jan 15. PMID: 25593290.

88. Lo CCW, Moosavi SM, Bubb KJ. The Regulation of Pulmonary Vascular Tone by Neuropeptides and the Implications for Pulmonary Hypertension. Front Physiol. 2018 Aug 23;9:1167. doi: 10.3389/fphys.2018.01167. PMID: 30190678; PMCID: PMC6116211.

89. Montague-Cardoso K, Malcangio M. Changes in blood-spinal cord barrier permeability and neuroimmune interactions in the underlying mechanisms of chronic pain. Pain Rep. 2021 Mar 9;6(1):e879. doi: 10.1097/PR9.0000000000000879. PMID: 33981925; PMCID: PMC8108584.